Faculty of Resource Science and Technology

Characterisation of the Interaction Between A Subset of Ribosomal Proteins and their Putative Co-Acting Factors in Nasopharyngeal Carcinoma

Ng Kher Lee

Doctor of Philosophy
2020

Characterisation of the Interaction Between A Subset of Ribosomal Proteins and their Putative Co-Acting Factors in Nasopharyngeal Carcinoma

Ng Kher Lee

A thesis submitted

In fulfillment of the requirements for the degree of Doctor of Philosophy

(Molecular Biology)

Faculty of Resource Science and Technology
UNIVERSITI MALAYSIA SARAWAK
2020

DECLARATION

I declare that the work in this thesis was carried out in accordance with the regulations of Universiti Malaysia Sarawak. Except where due acknowledgements have been made, the work is that of the author alone. The thesis has not been accepted for any degree and is not concurrently submitted in candidature of any other degree.

……

Signature

Name: Ng Kher Lee

Matric No.: 14010065

Faculty of Resource Science and Technology

Universiti Malaysia Sarawak

Date:

ACKNOWLEDGEMENT

The seemingly never-ending journey heretofore has been nothing short of a roller coaster ride. As it finally comes to the end, I would like to take this opportunity to express my sincerest gratitude and appreciation to those without whom, this achievement would have not been possible. First and foremost, I would like to thank my supervisor, Prof. Dr. Edmund Sim for his unending guidance, wisdom, support, and encouragement, in and out of lab, all these years. His time and vision have always been available throughout the course of this project, and for that, I am eternally grateful.

I would also like to extend my gratitude to the current and past members of the Immunology Lab for their camaraderie and support that made life in lab so much more colourful and tolerable. Special thank you to the members of the lab, Felicia Kavita Thomas, Yew Keh Li, Cassandra Chee and Sonia Sim and may our friendship stay steadfast for the years to come.

I would also like to acknowledge and appreciate the financial assistance and grants that made this project a possibility, such as the MyBrain PhD scholarship from the Ministry of Education, the Universiti Malaysia of Sarawak Postgraduate Research Grant (F04(DPP08)/1160/2014(08)) and the Fundamental Research Grant Scheme (FRGS) from the Ministry of Higher Education (E14099-F07-69-962/2013(03)).

To my dearest family, husband and friends, who are my biggest source of strength and inspiration, thank you very much for always believing in and supporting me, through good and bad times. Thank you.

ABSTRACT

Ribosomal proteins (RPs) are a family of proteins that, together with rRNAs, constitute the ribosomal subunits involved in protein biosynthesis. As it was traditionally believed to only play a role in ribosomal biogenesis, RPs have remained largely unexplored until studies from the past few decades revealed the extra-ribosomal roles of RPs, particularly in the tumorigenesis of various cancers. Relative to other well-studied cancers such as breast, lung and colorectal carcinomas, RP research on nasopharyngeal carcinoma (NPC), in particular, received a lesser extent of global attention and interest due to its exclusive geographical and racial affiliation. To date, the expression of only a handful of RPs had been implicated in NPC progression and none of those reported were functionally investigated. Therefore, this study aims to characterise the interaction of a subset of ribosomal proteins and their putative co-acting factor in NPC cells. Differential expression of eight RP genes (*uS4 (S9), eS8 (S8), eS31 (S27a), eL6 (L6), uL14 (L23), eL18 (L18), eL24 (L24), eL30 (L30))* and three possible target proteins (*NPM1, BTF3* and *UBA52)* was determine in six different NPC cell lines (HONE-1, SUNE-1, HK1, TW01, TW04 and C666-1) compared to an immortalized nasopharyngeal epithelial cell line (NP69). Of the eight RP genes, four RPs (*uS4 (S9), eS8 (S8), eS31 (S27a)* and *uL14 (L23)*) and a potential binding partner, *NPM1,* were significantly dysregulated in their transcript and protein levels in NPC cell lines. On the other hand, this study also demonstrated the insignificant correlation in terms of the expression levels of eL6 (L6), eL18 (L18), eL24 (L24), eL30 (L30), BTF3, and UBA52, in the progression of NPC. Additionally, sequence analyses revealed missense mutations on *uS4 (S9)* and *uL14 (L*23). Subsequent *in vitro* and *in vivo* protein-protein interaction assay demonstrated the direct association of uS4 (S9) and uL14 (L23) to NPM1. The central domain of uS4 (S9) was able

to interact with the N- and C-terminal domains of NPM1, while the centre motif of uL14 (L23) interacted with the N-terminal oligomerization domain of NPM1. Both RPs were identified as positive regulators of MDM2 by sequestering NPM1, while uL14 (L23) also played a dual-role as negative regulator of NPM1. Overall, this study has revealed the over-expression of uS4 (S9) and uL14 (L23) in NPC cells induced the translocation of NPM1 from the nucleolus to the nucleoplasm and cytoplasm, which in turn, transactivated MDM2 and its associated effector pathways in promoting tumorigenicity of NPC.

Keywords: Ribosomal proteins, nasopharyngeal carcinoma, protein-protein interaction, NPM1

Pencirian Interaksi antara Subset Protein Ribosom dan Faktor-faktor yang Berinteraksi dalam Karsinoma Nasofaring

ABSTRAK

Protein ribosom (RP) adalah keluarga protein yang, bersama-sama dengan rRNA, membentuk subunit ribosom yang terlibat dalam biosintesis protein dan ia secara tradisinya dipercayai hanya memainkan peranan dalam biogenesis ribosom, RP masih jarang diterokai sehingga kajian dari beberapa dekad yang lalu menunjukkan peranan tambahan-ribosom RP, terutamanya dalam tumorigenesis pelbagai jenis kanser. Berbanding dengan kanser lain yang dikaji dengan baik seperti karsinoma payudara, paru-paru dan kolorektal, penyelidikan RP dalam kes karsinoma nasofaring (NPC), khususnya, mendapat sedikit perhatian dan kepentingan global disebabkan oleh hubungan geografi dan perkaumannya yang eksklusif. Setakat ini, hanya segelintir RP yang telah dilaporkan terlibat dalam perkembangan NPC dan daripada kajian tersebut, tiada yang mengkaji aspek kefungsiannya. Oleh itu, kajian ini bertujuan untuk mencirikan interaksi subset protein ribosomal dan faktor co-actative mereka dalam sel karsinoma nasofaring (NPC). Perbezaan ekspresi untuk lapan gen RP (uS4 (S9), eS8 (S8), eS31 (S27a), eL6 (L6), uL14 (L23), eL18 (L18), eL24 (L24), eL30 (L30)) dan tiga protein target (NPM1, BTF3 and UBA52) telah ditentukan dalam enam kultur sel NPC (HONE-1, SUNE-1, HK1, TW01, TW04 and C666-1) berbanding dengan kul sel epitelium nasofaring yang normal (NP69). Daripada lapan RPs, hanya empat RPs (uS4 (S9), eS8 (S8), eS31 (S27a) and uL14 (L23)) dan satu protein sasaran ramalan, NPM1, telah menunjukkan perbezaan ekspresi yang signifikan, dalam tahap transkrip dan proteinnya. Di samping itu, kajian ini juga menunjukkan korelasi yang tidak ketara dari segi tahap espresi eL6 (L6), eL18 (L18), eL24 (L24), eL30 (L30), BTF3, dan UBA52, dalam perkembangan NPC. Selain itu, analisis turut mendedahkan mutasi 'missense' pada uS4 (S9) dan uL14 (L23). Pendekatan in vitro *dan* in vivo *seterusnya telah*

menentukan interaksi langsung antara uS4 (S9) dan uL14 (L23) dengan NPM1 dalam sel NPC. Domain tengah uS4 (S9) dapat berinteraksi dengan domain N- dan C-terminal NPM1, manakala motif tengah uL14 (L23) berinteraksi dengan domain oligomerisasi N-terminal NPM1. Kedua-dua RP adalah pengawal selia positif MDM2 dengan menghadkan aktiviti NPM1, manakala uL14 (L23) juga memainkan peranan dwi-ganda sebagai pengawal selia negatif NPM1. Secara keseluruhannya, kajian ini telah mendedahkan peningkatan ekspresi uS4 (S9) dan uL14 (L23) dalam sel-sel NPC yang menyebabkan penukaran lokasi NPM1 dari nukleolus ke nukleoplasma dan sitoplasma, dan juga mengaktifkan MDM2 dan laluan efektor yang berkaitan dalam perkembangan karsinogenesis NPC.

Kata kunci: *Protein ribosom, karsinoma nasofaring, protein-protein interaksi, NPM1*

TABLE OF CONTENTS

LIST OF TABLES

LIST OF FIGURES

LIST OF ABBREVIATIONS

µg	Microgram
µL	Microliter
µM	Micromolar
5-FU	5-fluorouracil
ACTB	Beta-actin
AF	Assembly factors
AGE	Agarose gel electrophoresis
AJCC	American Joint Committee on Cancer
AL	Acute leukaemia
ARF	Alternate reading frame tumour suppressor protein
ASIR	Age-standardized incidence rate
BART	Bam H1-A region rightward transcripts
BL	Burkitt's lymphoma
BSA	Bovine serum albumin
cDNA	Complementary DNA
CDS	Coding region
CML	Chronic myeloid leukaemia
CRC	Colorectal cancer
CT	Computerized tomography scan
DBA	Diamond-Blackfan anaemia
D-EA	IgA diffuse early antigen
DMSO	Dimethyl sulphoxide

dNTP	Deoxynucleotide triphosphate
EBER	EBV-encoded small RNAs
EBNA1	EBV nuclear antigen 1
EBV	Epstein-Barr virus
EDTA	Ethylenediaminetetraacetic acid
EGFR	Epidermal growth factor receptor
EMT	Epithelial-mesenchymal transition
EtBr	Ethidium bromide
ETS	External transcribed spacer
FBS	Fetal bovine serum
FD	Fold difference/ Fold change
FDG-PET	Fluorodeoxyglucose positron emission tomography
GAPDH	Glyceraldehyde-3-phosphate dehydrogenase
GOI	Genes of interest
GSTM1	Glutathione S-transferase M1
HCC	Hepatocellular carcinoma
HHV-4	Human herpesvirus 4
HIV	Human immunodeficiency virus
HLA	Human leucocyte antigen
IARC	International Agency for Research on Cancer
IGSF4	Immunoglobulin superfamily member 4
IHC	Immunohistochemistry
IMRT	Intensity-modulated radiotherapy
LMP	Latent membrane protein

LOH	Loss of heterozygosity
MDM2	Mouse double minute 2 homolog
MDS	Myelodysplastic syndrome
mg	Milligram
MHC	Major histocompatibility complex
mL	Millilitre
mM	Millimolar
M-MLV RT	Moloney Murine Leukemia Virus Reverse Transcriptase
MRI	Magnetic resonance imaging
mRNA	Messenger RNA
NES	Nuclear export signal
ng	Nanogram
NK-κB	Nuclear factor kappa-light chain enhancer of activated B cells
NLS	Nuclear localization signal
NMD	Nonsense-mediated decay
NoLS	Nucleolar localization signal
NPC	Nasopharyngeal carcinoma
NPM1	Nucleophosmin/B23
NRD	Non-functional rRNA decay pathway
nt	nucleotide
NTC	Non-template control
OS	Overall survival rate
PBS	Phosphate-buffered saline
PTC	Peptidyl-transferase centre

qPCR	Quantitative real-time polymerase chain reaction
RASSF1A	Ras-association domain family 1A
rDNA	Ribosomal DNA
RE	Restriction enzyme
RIPA	Radioimmunoprecipitation assay
RNP	Ribonucleoprotein
RP	Ribosomal protein
RPM	Rotation per minute
rRNA	Ribosomal RNA
RT	Radiation therapy
RT	Reverse transcription
SCCHN	Squamous cell carcinoma of the head and neck
SD	Standard deviation
SDS	Schwachmann-Diamond syndrome
SDS-PAGE	Sodium dodecyl sulphate polyacrylamide gel electrophoresis
siRNA	Small-interfering RNA
snoRNA	Small nucleolar RNA
TNM	Tumour-node-metastasis classification
TRAF2	Tumour necrosis factor-associated factor 2
tRNA	Transfer RNA
TSG	Tumour suppressor genes
UICC	Union for International Cancer Control
VCA	Viral capsid antigen
WHO	World Health Organization

CHAPTER 1

INTRODUCTION

Nasopharyngeal carcinoma (NPC), a highly malignant tumour originating from the epithelial mucosal lining of the nasopharynx, is distinctively distinguishable from other cancers of the head and neck in terms of its epidemiology, etiological factors, clinical behaviour as well as therapy and treatment response. Though relatively rare worldwide with a gender-combined age-standardized incidence rate (ASIR) of only 1.5 per 100,000, in Malaysia, NPC was the fifth most common cancer overall and the third highest contributor of new cancer cases in 2018, revealing a worrying trend (National Cancer Registry, 2017; Bray et al., 2018). NPC can be histologically grouped into three types, namely keratinizing squamous cell carcinoma, non-keratinizing carcinoma (differentiated and non-differentiated) and basaloid squamous cell carcinoma (Stelow & Wenig, 2017). This classification allows for better representation of variants in high- and low-incidence regions as well as for better prediction in terms of the lymph node metastasis predisposition, therapy responsiveness and prognosis estimation, although it does not guarantee treatment efficiency due to the heterogeneity of the cancer.

Ribosomal proteins (RPs) are small individual RNA-binding proteins that were once thought to be exclusively involved in protein synthesis, specifically in ribosome biogenesis. However, this is not the entire picture as evidence from studies since the last two decades have demonstrated the active involvement of RPs in a diverse range of extra-ribosomal (ribosome-independent) cellular processes such as DNA repair, cell growth and apoptosis regulation, RNA processing and transcription regulation and many others (Wool, Chan, & Glück, 1995; Lindström & Nistér, 2010; Wang et al., 2015). In cancer, the expression of

several RP genes has been shown to be dysregulated, with close association to cancer detection, diagnosis, treatment response and prognosis.

Although studies on the dysregulation of RP genes in cancer have been going on for many years, studies on the association of RP genes and NPC remain in its infancy. To date, only the expression levels of ribosomal protein genes have been reported in NPC cases, though no further functional investigations were conducted (Yang et al., 2005; Sim, Chan, Ng, Lee, & Narayanan, 2016; Sim, Ng, Lee, & Narayanan, 2017). As such, examining novel ribosomal protein genes that are differentially expressed in NPC cells and validating the direct target co-factors will further the current understanding of the roles of ribosomal proteins in cancer progression. Thus, the objectives of this study are:

i. To investigate the nucleotide sequence aberrancy and differential expression of a subset of ribosomal protein genes and their putative co-acting factors in nasopharyngeal carcinoma cells and select for transcriptionally dysregulated genes for further studies.
ii. To identify the differential expression of selected ribosomal proteins and potential interacting partners in nasopharyngeal carcinoma cells and select for translationally dysregulated proteins for further studies.
iii. To investigate the presence of protein-protein interaction between a subset of ribosomal proteins and their putative protein partners *in vitro* and *in vivo*.
iv. To investigate the mode of interaction between ribosomal protein and target protein *in vivo* in order to delineate the potential signalling network regulated by the selected ribosomal protein in the oncogenesis of NPC.

CHAPTER 2

LITERATURE REVIEW

2.1 Nasopharyngeal Carcinoma (NPC)

Nasopharyngeal carcinoma (NPC) is the most common highly malignant tumour arising from the epithelium of the nasopharynx and is distinguished from other cancers of the head and neck by its distinct histopathology, racial and geographical distributions, clinical behaviour and treatment.

2.1.1 The Nasopharynx

2.1.1.1 Anatomy of the Nasopharynx

The nasopharynx, the uppermost extent of the aerodigestive tract, is a musculofascial tubular passage located superiorly to the other two subsections of the pharynx, namely the oropharynx and the laryngopharynx, also known as hypopharynx. Anteriorly, the nasopharynx is an extension of the posterior openings of the nasal cavity through the posterior end of the nasal septum and the choanae. The sloping roof of the soft palate creates the junction between the nasopharynx and the oropharynx and together with the hard palate, form the inferior border of the nasopharynx. The posterior and superior walls of the nasopharynx, adjacently located at the base of the skull, are formed by the clivus, pharyngeal adenoid pad and the first two cervical vertebrae: the atlas and the axis. The nasopharynx is connected to the middle ear cavity via the auditory eustachian tubes, which descend medially and opens into the lateral wall of the nasopharynx. The posterior orifices of the eustachian tubes form comma-shaped cartilaginous protrusion called the torus tubarius. Posterior to the torus tubarius lies fossa of Rosenmüller, or the pharyngeal recess, which is the uppermost

part of the lateral recess formed by the junction of the posterior and lateral walls of the nasopharynx. The lateral wall of the nasopharynx, including the fossa of Rosenmüller, is the most frequent site of origin of nasopharyngeal cancer (Figure 2.1) (Donner, Bosma, & Robertson, 1985).

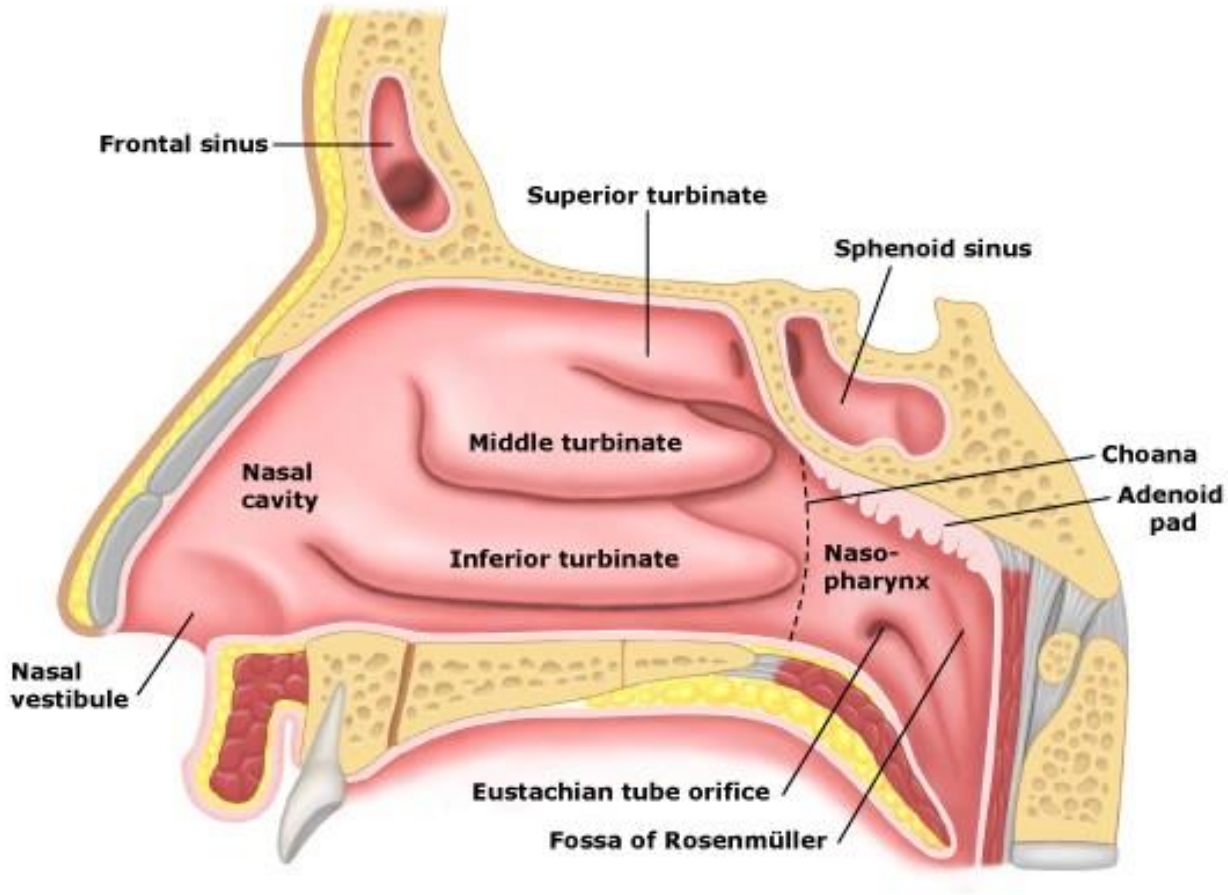

Figure 2.1: Anatomic diagram of the nasopharynx. (Digital image. *Online Wiring Library. http://4.criptoaldia.co/nasal-diagram.html*)

2.1.1.2 Histology of the Nasopharynx

The nasopharyngeal mucosal cavity is primarily lined by two types of epithelia: stratified squamous epithelium covering approximately 60% of the nasopharyngeal epithelium, pseudostratified columnar respiratory epithelium and a small percentage of intermediate epithelium makes up the remaining 40% (Ali, 1965). Stratified squamous epithelium comprises of flattened epithelial cells arranged in layers, which also covers the surfaces of the oral cavity and the oesophagus. Absent in the oropharynx and laryngopharynx, the pseudostratified columnar ciliated respiratory epithelium overlays a nasopharyngeal submucosa that is made up of mucus-secreting goblet cells, ciliated cells and basal cells (Dungworth, 1993). As a transitional interphase between stratified squamous epithelium and columnar respiratory epithelium, the intermediate epithelium exhibits similar stratified characteristic to that of squamous epithelium while its nuclei showed vertical alignment similar to that of ciliated epithelium, revealing a gradation of epithelium transformation from columnar to squamous epithelium (Ali, 1965).

2.1.2 Histopathology of NPC

NPC was first histologically confirmed and described in 1845 as a "skull base cancer" by Michaux in his examination of a 45-year-old male with "Carcinome de base du crâne" (Michaux, 1845). An earlier report by Durand- Fardel in 1837 on the detection of a nasopharyngeal neoplasm failed to receive credit as the earliest discovery of NPC as the diagnosis was not supported by histological examination of the tumour (Durand, 1837). In 1911, Trotter characterized NPC as "endothelioma", indicative of benign or malignant tumours originating from the endothelial tissue of blood vessels or lymphatic channels; a decade later, Regaud and Schmincke coined the term "lymphoepithelial carcinoma" (Trotter

1911; Regaud, 1921). Ewing, in 1929, histopathologically classified NPC into five subtypes, which were lymphoepithelial carcinoma, transitional cell carcinoma, squamous cell carcinoma, malignant adenoma and cystic adenoid basal cell carcinoma (Ewing, 1929).

During the 1967 NPC Symposium of the UICC (Union for International Cancer Control), it was proposed that NPC histopathology was to be divided into seven subtypes: lymphoepithelial carcinoma, transitional cell carcinoma, typical epidermoid carcinoma, clear cell carcinoma, pleomorphic carcinoma and mixed cell carcinoma. Subsequently, Shanmugaratnam classified NPC into two major types: squamous cell carcinoma, which was further categorized as typical carcinoma, clear cell carcinoma and spindle cell carcinoma, and undifferentiated carcinoma, which included vesicular nucleus cell carcinoma, fused type and mixed type (Muir, 1967).

In 1978, the first edition of WHO (World Health Organization) NPC histological classification divided NPC into three major types: type I (squamous cell carcinoma), type II (non-keratinizing carcinoma) and type III (undifferentiated carcinoma) (Shanmugaratnam & Sobin, 1978). However, in 1982, a report by the WHO regional office on its suggestion to reconstruct NPC histopathology was received with vehement disagreements from high-incidence endemic regions, China in particular. The report proposed not only to consolidate type II and type III NPC, but also to redefine "NPC" to include only nasopharyngeal neoplasm based ultrastructural evidence of squamous differentiation, thereby excluding lymphomas, sarcomas, adenocarcinomas and salivary gland-type carcinomas from the histopathology of NPC (Pacific., 1982). Therefore, for its second edition published in 1991, WHO modified the NPC histopathological classification by re-dividing it into two major

types, namely, keratinizing squamous cell carcinoma and non-keratinizing carcinoma. The former included well-, moderately- and poorly-differentiated squamous cell carcinoma and the latter included differentiated carcinoma and undifferentiated carcinoma (Shanmugaratnam, Sobin & Barnes, 1991). Subsequently, the 3rd edition of WHO NPC histopathological classification in 2005 included basaloid squamous cell carcinoma as one of three NPC types. The current 4th edition of WHO NPC classification published in 2017 maintained the classification system in line with the previous (3rd) edition (Stelow & Wenig, 2017). Table 2.1 summarizes and compares the evolvement of NPC histopathological classification according to well-acclaimed WHO standards (Shanmugaratnam & Sobin, 1978; Shanmugaratnam, Sobin, & Barnes, 1991; Chan, 2005; Stelow & Wenig, 2017).

Table 2.1: WHO NPC histopathology classifications.

WHO NPC histopathological classification			
1st edition (1978)	2nd edition (1991)	3rd edition (2005)	4th edition (2017)
Type I: Squamous cell carcinoma	Type I: Keratinizing squamous cell carcinoma	Type I: Keratinizing squamous cell carcinoma	Type I: Keratinizing squamous cell carcinoma
Type II: Non-keratinizing carcinoma	Type II: Non-keratinizing carcinoma a. Differentiated b. Undifferentiated	Type II: Non-keratinizing carcinoma a. Differentiated b. Undifferentiated	Type II: Non-keratinizing carcinoma a. Differentiated b. Undifferentiated
Type III: Undifferentiated carcinoma	N/A	Type III: Basaloid squamous cell carcinoma	Type III: Basaloid squamous cell carcinoma

Type I keratinizing squamous cell carcinoma is characterized as differentiated squamous carcinoma with histologically visible intercellular bridges, variable degree of keratinization, and invasive growth. Type I cells exhibited higher locally advanced tumour growth rate, lower lymph node metastatic rate, lower responsiveness to radiation therapy and poorer prognosis (Hoppe, Williams, Warnke, Goffinet, & Bagshaw, 1978; Shanmugaratnam et al., 1979; Reddy, Raslan, Gooneratne, Kathuria, & Marks, 1995).

Type II non-keratinizing NPC contributes to approximately 95% of NPC cases in highly endemic areas and about 80% in low incidence areas and is frequently associated with Epstein-Barr virus (EBV) (Marks, Phillips, & Menck, 1998). The differentiated carcinoma (type IIa), accounting for only about 7-12% of NPC cases in southern China, displays cellular stratification and pavementing with distinct cell borders, inconspicuous nucleoli and intercellular bridges (Chan, 2005). In contrast, undifferentiated carcinoma (type IIb), also known as lymphoepithelial carcinoma, is characterized by comparably larger tumour cells with indistinct cell borders and rounded nuclei with dominant central nucleoli. Due to heavy infiltration of lymphocytes and plasma cells that disrupts the epithelial nature of the tumour, Type IIb cells tend to appear as isolated clusters of tumour islands in an overlapping manner (Wenig, 2015). This undifferentiated subtype of NPC accounts for over 90% of NPCs in high incidence areas, and it is the most common NPC subtype in the paediatric age group (Ayan, Kaytan, & Ayan, 2003; Jeyakumar, Brickman, & Doerr, 2006). Type III NPC, basaloid squamous cell carcinoma, is characterized as small cells with hyperchromatic nuclei, low nuclear-cytoplasmic ratio and the absence of nucleoli. It is the most uncommon NPC type as it only represents less than 0.2% of NPC cases in southern China (Chan & McCarron, 2005).

2.1.3 Epidemiology of NPC

NPC is a relatively rare malignancy of the head and neck. According to a 2018 cancer statistic report by the International Agency for Research on Cancer (IARC), the age-standardized incidence rate (ASIR) of NPC is 1.5 per 100,000 (2.2 for males and 0.8 for females). Cumulatively, NPC contributed to approximately 0.7% of new cancer cases and 0.8% of global mortality cases (Bray et al., 2018). Independent of race and ethnicity, NPC incidence is 2- to 3-fold higher in males than in females. In high-risk groups, the rate of incidence peaks around ages of 50 to 59 after which declines considerably as well as a minor peak during adolescence (Lee et al., 2003). In contrast, NPC incidence in low-risk group increases uniformly with age (Lee & Ko, 2005).

Intermediate to highly endemic regions for NPC such as Southern China, Southeast Asia, Arctic and North Africa record ASR incidence rates ranging from 3.6 to 31.5/ 100,000 per year (Devi, Pisani, Tang, & Parkin, 2004; Hamdi Cherif et al., 2014; Ben Ayoub Hizem Wided & Mansour, 2015; Lindsey et al., 2015). Curiously, in the highly endemic province of Guangdong in southeast China where the overall ASIR for males is 27.2/100,000, the NPC incidence rate among the Cantonese descent is almost twice as high as those belonging to other dialect groups such as Hokkien, Hakka and Chiu Chau (Li, Yu, & Henderson, 1985; Zhang & Kong, 2007). Due to this striking ethnic association to the Cantonese people, NPC has also been known universally as a “Cantonese Cancer” (Hepeng, 2008). Even in low incidence countries such as the United States, a similar racial tendency has been reported, wherein the highest NPC rate is observed among the American Chinese, followed by American Filipinos, American Japanese, African Americans, Hispanics or Latinos and lastly, the Caucasian (Burt, Vaughan, & McKnight, 1992).

In Malaysia, IARC reported that NPC is the third highest contributor to new cancer cases in 2018, irrespective of age and sex (Bray et al., 2018). In addition to that, the Malaysian Ministry of Health's most recent cancer registry report for 2007-2011 published in 2017 places NPC as the fifth most common cancer overall and the third most common cancer in men. The NPC incidence in men increased drastically from the age of 45, peaking at the 65-69 age gap (National Cancer Registry, 2017). Likewise, in the state of Selangor, the Cantonese Chinese recorded the highest NPC incidence rate, followed distantly by the Khek people and lowest among the Teochews and Hokkiens (Armstrong, Kannan Kutty, Dharmalingam, & Ponnudurai, 1979). In light of the highly irrefutable association of NPC incidence and the Chinese Cantonese, it came as a surprise when a rather obscure population-based study by Devi reported that the Bidayuh population, one of the largest native communities in the Borneo island of Sarawak, recorded a dramatically elevated ASIR of 31.5/100,000 and 29.4/100,000 for Bidayuh male and female respectively, surpassing that of Hong Kong and Guangdong, China (Devi et al., 2004). To date, the exact mechanism underlying this curious geographical distribution and NPC genetic risk inquiry remains to be elucidated although it has been proposed that a genetic lesion originating in Bai-Yue-speaking ("proto-Tai Kadai" or "proto-Zhuang") aborigines who were scattered by Sundaland submersion following the last glacial maximum, gave rise to the current population pattern of NPC occurrence (Wee, Ha, Loong, & Qian, 2010).

2.1.4 Aetiology of NPC

As previously described, NPC presents an unusual epidemiological dependency on geographic and racial distribution. As such, the aetiology of NPC is complicated and multifactorial involving various risk factors such as EBV infection, genetic susceptibility, lifestyle and environmental influences.

2.1.4.1 Epstein-Barr Virus (EBV) Infection

A strong correlation between NPC pathogenesis and EBV infection is a unique distinguishing feature of NPC from the other head and neck cancers (Licitra et al., 2003; Lung et al., 2014). Besides NPC, particularly Type IIb NPC, EBV has also been associated with the development of other various forms of cancer, such as Burkitt's lymphoma (BL), Hodgkin's lymphoma, a subset (~10%) of gastric cancer, certain autoimmune diseases as well as conditions associated with human immunodeficiency virus (HIV) (van Beek et al., 2004; Toussirot & Roudier, 2008; Bibas & Antinori, 2009; Küppers, 2009; Rowe, Fitzsimmons, & Bell, 2014).

EBV, also known as human herpesvirus 4 (HHV-4), is one of the commonest viruses found in human with over 90-95% of the world population expressing antibodies against EBV proteins. In regions of high NPC incidence such as Hong Kong, China and Taiwan, approximately 60% of children have been infected with EBV by the age of 2, 80% by the age of 6 and almost 100% by the age of 10 (Hjalgrim, 2007). The ubiquity of EBV infection is largely due to its highly evolved ability to infect and establish lifelong latency with sporadic reactivation accompanied by asymptomatic clinical indicators within most of the infected individuals. The detection of monoclonal EBV genome in almost all tumour cells

indicates that the progenitor tumour cell was infected with EBV before clonal expansion, suggesting that EBV infection plays a role in the early stages of tumorigenesis. In addition to that, the presence of EBV viral capsid antigen (VCA) antibody titer was identified in healthy individuals living in high-incidence areas and in NPC patients months or years before the onset of NPC (Pagano et al., 2004). As such, EBV infection is believed to be a dominant risk factor of NPC development as not all EBV infection leads to malignancies, but almost all NPC scenarios begin with EBV infection.

Following EBV primary infection of B lymphocytes or epithelial cells, its viral genome remains in the nucleus in the form of monoclonal episomes without undergoing viral replication or host-cell integration. EBV latency is characterized by the three stages of latency programs (Latency I, II and III)- each program represents a specific stage within the viral life cycle that involves the expression of distinct subsets of EBV latent genes, viral protein and viral RNAs. In the case of NPC, upon primary infection, EBV adopts latency II, which is characterized by the expression of EBV nuclear antigen 1 (EBNA1), latent membrane protein 1, 2A and 2B (LMPs), small non-polyadenylated EBV-encoded small RNAs (EBERs) and Bam H1-A region rightward transcripts (BARTs). LMP1 was found to be expressed in almost all NPC tissues while LMP2 was detected in about 50% of primary NPC tissues examined (Tsao, Tramoutanis, Dawson, Lo, & Huang, 2002; Kong, 2010).

Since the discovery of EBV in 1964, the exact mechanism in which EBV infection subsequently leads to the development and progression of NPC epithelial cells after achieving latency remains poorly understood. This is in contrast with the established role of EBV in the pathogenesis of B cells-EBV-related malignancies. However, a recent study has

reported on the elevated levels of lytic phase proteins such as BALF1, BCRF1 and BHRF1 in NPC patients (Hu et al., 2016). This highlights the involvement of EBV lytic cycle reactivation in the presence of cellular stress in NPC oncogenesis by promoting oxidative stress, inflammation, angiogenesis, invasiveness and genome instability (Young, Yap, & Murray, 2016).

Recently, a major large-scale genome sequencing study identified two non-synonymous EBV variants within *BALF2*, an EBV gene that encodes a DNA-binding protein that regulates the lytic phase of EBV DNA replication, and its strong association with NPC risk. Following that, phylogenetic investigation on the gene variants shows an unique origin in Asia, thus providing novel insights into the regional specificity of NPC (Xu et al., 2019).

In short, EBV infection itself is not a sufficient factor for NPC tumorigenesis as EBV genome can be detected in almost all human population worldwide, and yet only a minor percentage develops NPC. Thus, NPC development and progression can be attributed to other risk factors such as genetic and/or environmental influences.

2.1.4.2 Genetic Susceptibility

High NPC incidence amongst the Chinese (native and migrant) population points to a strong correlation between genetic susceptibility and the risk of developing NPC. In 1974, the association between Human Leucocyte Antigen (HLA) and increased NPC risk was first observed (Simons et al., 1974). HLA, the protein complex encoded by the major histocompatibility complex (MHC) class I and II genes, is the hallmark of a highly evolutionary adaptive immunity rendered by the diversity of allelic polymorphism of HLA

genes. HLA complexes are responsible for foreign antigen presentation, including viral peptides, to the immune system for targeted lysis. In the case of NPC in which almost all infected cells contain EBV, individuals who inherit HLA haplotypes with reduced affinity to EBV antigens would have higher risks for NPC as viral antigens are not being effectively presented on the cell surface for the action of EBV-specific T lymphocytes, thus escaping the immunity's surveillance system (Salek-Ardakani, Arrand, & Mackett, 2002).

Genetic association studies have consistently confirmed the implication of HLA class I allele variations in NPC development across geographical regions such as Taiwan, China and the United States (Jing, Louie, Henderson, & Terasaki, 1977; Chan, Day, Kunaratnam, Chia, & Simons, 1983; Moore, Pearson, Neel, & Weiland, 1983; Pimtanothai, Kangwanshiratada, & Charoenwongse, 2003; Lu et al., 2003; Lu et al., 2005). A subsequent meta-analysis study expanding that of the study done in 1974 substantiated that HLA-A2/ -B46 and B17 increased the risk of NPC 2- to 3-fold higher in Chinese and other high-risk Asian populations while HLA-B5 increased the risk in Caucasians. On the other hand, HLA-A11 lowers the risk of about 30% to 50% across all races, HLA-B13 in Tunisians and Chinese and HLA-A2 in non-Chinese (Goldsmith, West, & Morton, 2002). However, how exactly the variation of specific HLA haplotypes affect NPC susceptibility remains poorly understood even though the association of HLA polymorphism and NPC predisposition is indisputable, either by playing a functional role in coordinating an adaptive immune response against EBV infection or as an early detection marker for NPC.

Besides HLA haplotypes, NPC tumorigenesis has also been attributed to genetic polymorphisms and chromosomal abnormalities. In China and Taiwan, there is a 2- to 5-

fold increase in NPC risk in association with polymorphisms in cytochrome P450 2E1I (*CYP2A6)* and the absence of glutathione S-transferase M1 (*GSTM1*) (Hildesheim et al., 1995; Hildesheim et al., 1997; Kongruttanachok et al., 2001). High frequency of allelic loss on chromosomes 3p, 9p, 11q and 14q as well as inactivation of tumour-suppressor genes such as Ras-association domain family 1A *(RASSF1A)* and immunoglobulin superfamily member 4 (*IGSF4*) by promoter methylation have been detected in NPC tumours (Hu et al., 1996; Lo et al., 2001; Kwong et al., 2002; Lung et al., 2004; Li et al., 2006).

Besides that, whole-exome sequencing (WES) and whole-genome sequencing (WGS) analyses on micro-dissected EBV-positive NPCs reveal the mutational aberrations of several negative regulators of the constitutively activated NF-κB pathway, such as CYLD, TRAF3, NFKBIA and NLRC5 and the mutual exclusivity of these mutations and LMP1 overexpression, thus indicating that the activation of the NF-κB pathway is dependent on both somatic and viral events during NPC oncogenesis (Li et al., 2017). In addition, to further understand the genetic factors that predispose to EBV-induced carcinogenesis of NPC, a study conducted in Taiwan with the utility of whole-exome sequencing on primary NPC tissues has reported the involvement of genes responsible for the following pathways: magnesium transport (NIPAL1), EBV cell entry (ITGB6), telomere biology (CLPTM1L, BRD2, HNRNPU), regulation of cAMP pathway (RAPGEF3), DNA repair (PRKDC, MLH1), Notch signalling (NOTCH1, DLL3) as well as regulation of EBV infection (BCL2L12, NEDD4L) (Yu et al., 2019).

2.1.4.3 Dietary and Environmental Factors

Besides genetic susceptibility, unbalanced NPC incidence with specific ethnic and

geographical patterns could be ascribed to the unique lifestyle, dietary preference and exposure to certain environmental factors of the population in endemic areas.

The non-viral risk factor most strongly associated with NPC is the consumption of salt-preserved fish- a traditional staple for the Cantonese and the Bidayuh communities. For the Chinese, the relative risk of NPC for weekly consumption of salt-preserved fish compared to no or rare consumption is within the approximate range of 1.4- to 3.2-times higher while the relative risk for daily consumption hits a soaring upper range of 1.8- to 7.5-times higher (Yu, Ho, Lai, & Henderson, 1986; Armstrong et al., 1998; Yuan et al., 2000) . Besides salt-preserved fish, relative risk for NPC has been observed in association with the continuous consumption of other preserved food items such as meat, eggs, fruits and vegetables in Southern China, Southeast Asia, North Africa, Arctic and United States (Yu, Huang, & Henderson, 1989; Sriamporn, Vatanasapt, Pisani, Yongchaiyudha, & Rungpitarangsri, 1992; Farrow et al., 1998; Gallicchio et al., 2006).

As such, this dietary pattern of salted preserved food consumption may play a role in addressing the distinctive distribution of NPC incidence. In studies with rat models, malignant nasal and nasopharyngeal tumour formation was observed in rats that were on Chinese salted fish diet (Huang, Ho, Saw, & Teoh, 1978; Zheng, Luo, Christensson, & Drettner, 1994). Due to ineffective traditional salt preservation techniques, fish and other food were not monitored properly and left to be partially putrefied, resulting in an accumulation of carcinogenic nitrosamines (IARC., 1993; Zou, Lu, & Liu, 1994).

Besides the over-consumption of salted preserved food, cigarette smoking has been arguably

associated with NPC in a dose-dependent manner with an increased risk of 2- to 6-times higher in smokers compared to non-smokers (Nam, McLaughlin, & Blot, 1992; Zhu, Levine, Brann, Gnepp, & Baum, 1997). On the other hand, some studies reported no association (Li et al., 1985; Ng, 1986; Sriamporn et al., 1992).

Occupational exposures to fumes, smokes, wood and cotton dusts or chemicals such as phenoxy acid and chlorophenol are also one of the risk factors of NPC development (Henderson, Louie, SooHoo Jing, Buell, & Gardner, 1976; Hardell, 1982; Yu, Garabrant, Huang, & Henderson, 1990; West, Hildesheim, & Dosemeci, 1993; Hildesheim et al., 2001). An evaluation by the International Agency for Research on Cancer (IARC) in 2005 showed an increased NPC risk and mortality with the cumulative exposure to formaldehyde (Cogliano, 2005).

2.1.5 Clinical Presentation, Diagnosis and Treatment

2.1.5.1 Signs and Symptoms

In its early stages, NPC may be asymptomatic though with possible noticeable symptoms, which include, but not limited to, nasal blockage or stuffiness, sore throat, nosebleeds, headache, hearing loss or ringing in the ears, frequent ear infections, facial pain or numbness, and blurred or double vision. Due to the similarity of these symptoms with that of other diseases, including the common cold, the accurate diagnosis of NPC at an early stage is a challenge. Later stage symptoms include the appearance of a solid and painful neck lump or mass localized to the posterior cervical region (Grammatica, Achille, Piepoli, & Paradiso, 1999). As a consequence of its hidden locality and confusing early symptoms, NPC remains one of the most misdiagnosed carcinomas with most of diagnosed NPC cases are of

advanced stage with poorer prognosis.

2.1.5.2 Detection and Diagnosis of NPC

Due to the non-specificity of the symptoms, detection and diagnosis of NPC during the initial stages are alarmingly few, with most of the cases detected at later stages for both sexes (63% for men; 60% in female) (National Cancer Registry, 2017). Regardless of sex, only 9% of NPC cases are detected during Stage I, followed by 83% during Stage II and III, and 39% during Stage IV (Society., 2017).

Preliminary screening tests are performed with either a nasal or nasopharyngeal swab. The latter involves the insertion of the swab deep into the nasopharynx. A higher percentage of EBV DNA can be detected on nasopharyngeal swabs as compared to nasal swabs (Coghill et al., 2018). Apart from this, EBV-based serological assays that detect the elevated titre levels of EBV-specific IgA antibodies (IgA viral capsid protein (VCA), IgA diffuse early antigen (D-EA) and EBV DNase) are also adapted to predict subsequent NPC symptomatic development (Chang & Adami, 2006; Zhou et al., 2007).

Besides that, the common techniques used for NPC diagnosis include clinical examinations and imaging studies such as computerized tomography (CT), magnetic resonance imaging (MRI) and more recently, fluorodeoxyglucose- positron emission tomography (FDG-PET) scans. Subsequently, for patients with detected cervical lymphadenopathy, fine needle aspiration cytological examination of the nodes will be performed for biopsy samples for NPC diagnosis and histopathological confirmation.

Despite the advancement in radiotherapy techniques and concurrent treatment protocols, the survival rates of NPC patients remain relatively low as most NPC cases are only diagnosed in the advanced stages due to the regular presentation of unspecific early symptoms of NPC.

2.1.5.3 Cancer Staging of NPC

NPC tumour staging is founded on the tumour-node-metastasis (TNM) classification by The American Joint Committee on Cancer (AJCC) first developed in 1977 and after seven revisions later, the current eighth edition published in 2017 (Amin et al., 2017) is adopted worldwide. 'T' refers to tumour size, 'N' denotes the invasion of regional lymph nodes while 'M' describes the metastasis extensiveness. Relying on tumour examinations, biopsies and imaging scans, each of the T, N and M stages are individually scored and subsequently combined for stage grouping (Stage 0, I, II, III, IVA and IVB). Further details on the stages of NPC are outlined in Table 2.2.

Table 2.2: Stages of nasopharyngeal carcinoma. Adapted from Amin et al. (2017).

AJCC Stage	Grouping	Stage Description
0	Tis, N0 M0	Tumour confined to nasopharynx with no invasion and metastasis.
I	T1 N0 M0	Tumour extends to the soft tissue of oropharynx and/or nasal cavity with no further invasion and metastasis.
II	T1 N1 M0	Tumour extends to the soft tissue of oropharynx and/or nasal cavity, and lymph nodes in the neck, with EBV-positive titres but no distant metastasis.
	T2 N0/N1 M0	Tumour growth into tissues of the sides of the upper part of the throat, with or without lymph nodes invasion, and no distant metastasis.
III	T1 N2 M0	Tumour extends to the soft tissue of oropharynx and/or nasal cavity, and invasion to lymph nodes on both sides of the neck, with no distant metastasis.
	T2 N2 M0	Tumour growth into tissues of the sides of the upper part of the throat, and invasions to lymph nodes on both sides of the neck, with no distant metastasis.
	T3 N0 to N2 M0	Tumour growth into sinuses and/or nearby bones, with or without lymph nodes invasion, and no distant metastasis.
IVA	T4 N0 to N2 M0	Tumour growth into the skull and/or cranial nerves and nearby tissues, with or without lymph nodes invasion, and no distant metastasis.
	Any T N3 M0	Varying growth of the tumour, confirmed lymph nodes invasion, and no distant metastasis.
IVB	Any T Any N M1	Varying growth of the tumour, varying lymph nodes invasion with confirmed distant metastasis.

2.1.5.4 Treatment and Management of NPC

NPC treatment depends on the location and the invasiveness of the tumour as well as the patient's overall health status. Due to the elusive location of NPC, surgery is not the main treatment. Instead, radiation therapy (RT) is the main prescription for early stages of NPC: Stage 0 and I, in which there is no spreading of the cancer. Intensity-modulated radiotherapy (IMRT) allows for better radiation control for *in-situ* NPC tumours while minimizing both the side effects of conventional RT and the damage to surrounding healthy tissues (Kam et al., 2007). Advanced stages such as Stage II, III, IVA and IVB are treated with a combination of radiotherapy and chemotherapy (chemoradiotherapy) with biological drugs such as docetaxel, cisplatin and 5-fluorouracil (5-FU) (Ekenel et al., 2011).

Subsequent to a randomized phase III trial, Chan reported the significant increase in the 5-year overall survival (OS) rate in patients diagnosed with stage II and III NPC treated with concurrent chemoradiotherapy with cisplatin (70.3%) compared to patients treated with radiation alone (58.6%) (Chan et al., 2005). Similarly, a study demonstrated the improvements in 5-year OS rate in patients treated with concurrent chemoradiotherapy with cisplatin and 5-FU (72.3%) as compared to those treated with radiation alone (54.2%) (Lin et al., 2003). However, it is important to note that several other large, randomized trials demonstrated no significant improvement in OS rate of patients subjected to chemoradiation in comparison to patients subjected to radiation therapy alone (Chan et al., 2005; Ma & Chan, 2005). These conflicting reports further confound inter-study comparison and interpretation. The OS rate disparity between these trials could be attributed to the disproportionate representation of the three types of NPC, each with different degrees of radio-sensitivity, within each trial. Besides that, different combinations of chemotherapeutic drugs were tested

within each trial with different delivery schedules (neoadjuvant, concurrent and adjuvant). Nevertheless, it remains a consensus that concomitant chemoradiotherapy is the current standard of care for locally advanced NPC.

Apart from surgery, radiotherapy and chemotherapy, another form of NPC treatment that is currently gaining interest is molecular-based targeted therapy such as the use of cetuximab. Cetuximab, an engineered chimeric monoclonal antibody, targets and inhibits epidermal growth factor receptor (EGFR), in which its expression was found to be significantly over-expressed in most cases of NPC (Leong, Loh, Putti, Goh, & Tan, 2004). When cetuximab was delivered concurrently with induction cisplatin-based chemoradiotherapy, an increased OS rate of 94.0% was observed among the patients when compared 87.9% of those without the provision of cetuximab (Peng et al., 2018).

As NPC treatment efficacy, patient survival and prognosis decline drastically in the advanced stages, early diagnosis and proper disease management are of the highest importance. When diagnosed at Stage I, the 5-year survival rate is 72% and declines to 64% when diagnosed at Stage II and III, and eventually hits the lowest survival rate of 38% when diagnosed at Stage IV (Society., 2017). Therefore, the development of a comprehensive primary NPC screening and detection approach could greatly contribute to the early detection and improvement of treatment outcome.

2.1.6 Early Detection of NPC

One of the routine practices for early detection of NPC is the detection of viral capsid antigen (VCA)/IgA and early antigen (EA)/IgA antibody titers against EBV as EBV infection is an early event during tumorigenesis and its genome and gene products can be detected in almost all type III NPC tumours (Pagano et al., 2004). The seropositivity of another form of EBV-associated product, EBV nuclear antigen-1 (EBNA1)/IgA, is the most strongly associated EBV marker to the risk of NPC susceptibility (Yu et al., 2011). Although the detection of antibodies against EBV is a valuable early detection tool for NPC and is widely adopted, this method presents certain drawbacks in its implementation, especially in high incidence populations. Firstly, with a false positive rate of 2 to 18 percent, EBV-associated antibody serological testing does not represent a comprehensive and definitive early detection method for NPC screening (Rickinson & Kieff, 2001). Secondly, elevated antibody titers against EBV could also be attributed to psychological or physical stress in normal individuals thus decreasing its specificity (Stowe, 2001). With these limitations, alternative detection systems with higher sensitivity and specificity are necessary.

Molecular studies, such as expression and pathway analysis of NPC, are therefore undertaken in order to explore novel and reliable biomarkers for early detection and markers that correlate NPC with clinical staging, metastasis and prognosis. For instance, both genetic and protein expressions of Galectin-1 are much more elevated in NPC tissues compared to normal nasopharyngeal epithelial tissues, intimating its probable role in NPC tumorigenesis and as a potential diagnostic marker (Tang et al., 2010). The overexpression of SOX4 was found to be strongly associated with poorer prognosis and cancer progression in terms of cellular proliferation, invasiveness, and epithelial-mesenchymal transition (EMT) (Shi et al.,

2015). In addition to these molecular factors, the up-regulations of CXC chemokine receptor type 7 (CXCR7), hypoxia up-regulated 1 (HYOU1), Kelch Domain Containing 4 (KLHDC4), aldo-keto-reductase 1B10 (AKR1B10) and prohibtin-1 (PHB1) were also shown to be closely associated with cellular proliferation, tumour differentiation and metastasis and poor disease prognosis (Liao et al., 2013; Zhu et al., 2015; He et al., 2016; Lian et al., 2016; Zhou et al., 2016). Moreover, a recent study attempted to integrated both serological and genetic profiling proposed the detection of chemokine CCL27 as a complementary approach to conventional EBV markers in primary screening of NPC. This study demonstrated that plasma expression of chemokine CCL27 was able to distinguish NPC patients within a VCA/IgA-positive population thereby suggesting its role in predicting NPC susceptibility in healthy individuals with seropositive VCA/IgA titres and increasing early detection accuracy by eliminating false-positives (Mao et al., 2018). These molecular targets, together with many more, have also been identified as potential biomarkers that are vital for early diagnosis and staging of NPC. In 2017, a clinical investigation involving over 20,000 Hong Kong Chinese participants has demonstrated the highly specific and sensitive analysis of measuring circulating cell-free EBV DNA in plasma samples to screen for NPC in asymptomatic persons (Chan et al., 2017). An even recent genome-wide pilot study conducted in Nanjing, China, reported the potential of circulating salivary microRNAs (miRNAs) as biomarkers for NPC detection and prognosis prediction (Wu et al., 2019).

Apart from genetic and protein expression profiling, other advances in NPC early detection technology include measurement of EBV copy number and detection of promoter methylation from biopsy tissues, plasma and brushing samples collected from the nasopharynx (Chan et al., 2017). However, the degree of reliability and accuracy of these

methods as a diagnostic test on a larger and randomized sample size have not been properly evaluated.

2.2 Molecular Pathogenesis of NPC

The onset of NPC is multifactorial in origin and multistep in progression. It involves an intricate and complex play of various genetic, epigenetic and molecular factors.

2.2.1 Molecular Onset of NPC

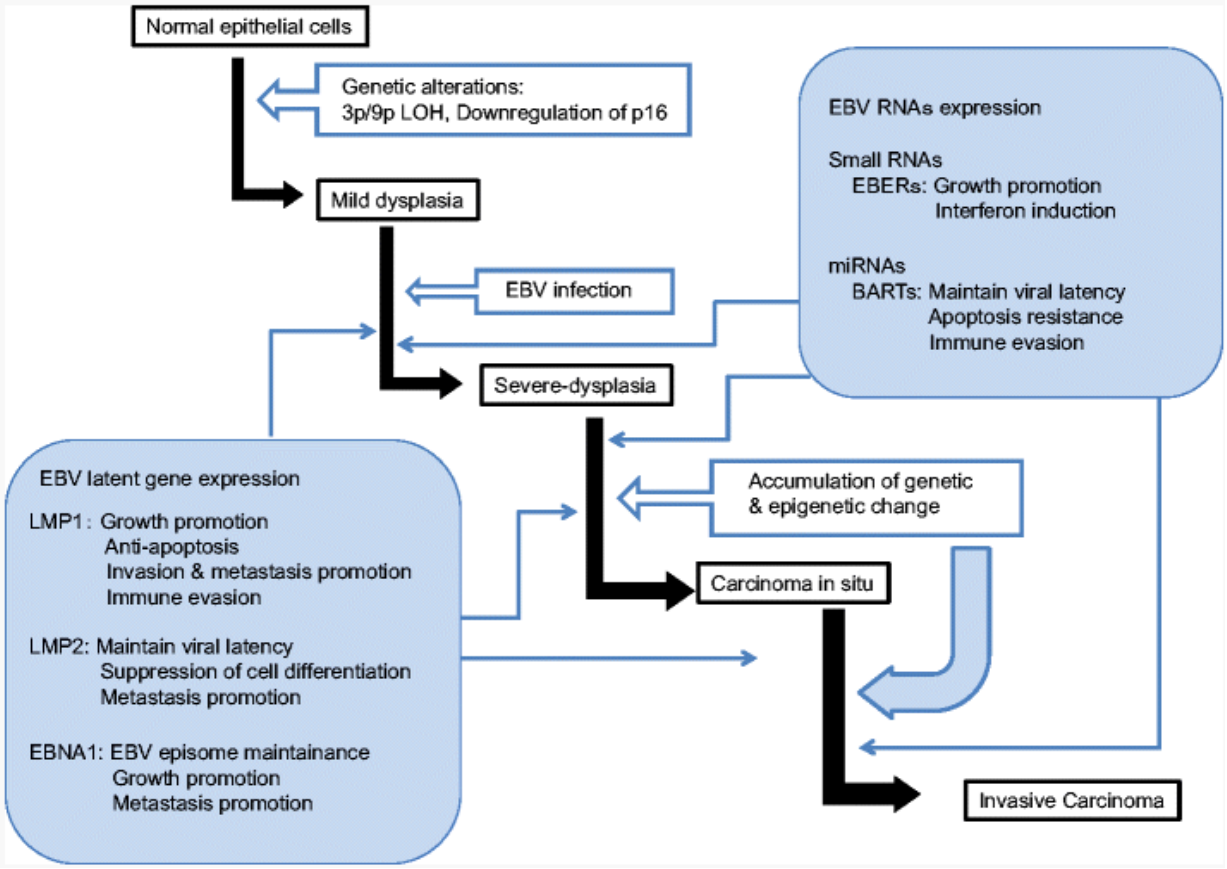

Figure 2.2: The roles genetic aberration and EBV infection in the stepwise development of NPC. The molecular transition of a normal nasopharyngeal epithelial cell to an invasive carcinoma involves a series of genetic and epigenetic alterations and the intricate interplay of various EBV-encoded RNAs and proteins (taken from Nakanishi et al., 2017).

The onset of NPC is initiated by the transition of a normal nasopharyngeal epithelial cell into

a mildly hyperplastic cell, driven by specific genetic alternations as depicted in Figure 2.2. Pioneering genome-wide studies have discovered the loss of heterozygosity (LOH) on chromosomes 3p, 9p, 11q, 13q, 14q and 16q in primary NPC tissues, confirming the role of genetic deletions in the development of NPC, though the exact molecular mechanisms remain poorly understood (Hui et al., 1999; Lo et al., 2000). LOH is defined as the scenario when one parental allele copy of a polymorphic heterozygous locus is lost resulting in a homozygous or hemizygous region. However, there is no phenotypic change as the remaining functional allele on the other locus compensates the loss of the other allele. In the landscape of cancer genetics, when this compensating mechanism fails due to deletion or promoter methylation of the remaining functional allele, especially that of tumour suppressor genes, cancer is likely to occur.

In the case of NPC, further studies have detected LOH on chromosome 3p and 9p in histologically normal nasopharyngeal epithelial and mildly dysplastic (premalignant) tissues, hence demonstrating that genetic alterations such as LOH are early events in NPC pathogenesis prior to EBV latent infection (Chan et al., 2000; Chan et al., 2002).

2.2.1.1 Chromosome 3p LOH

Deletion of the short arm of chromosome 3 was detected in almost all (81-100%) NPC samples from both high- and low-risk regions and in 75% of dysplastic nasopharyngeal lesions (Chan et al., 2000). 3p21.3, an important critical region (CR) along chromosome 3p, houses multiple tumour suppressor genes implicated in NPC tumorigenesis (Chow et al., 2004). One such gene, *RASSF1A*, Ras-associated domain-containing protein 1, encodes for a protein with similar homology to resistance to audiogenic seizures (Ras) effector protein,

Nore1, thereby implying its role in the Ras signalling pathway. It has been shown that RASSF1A exerts its tumour suppressive effect by either activating pro-apoptotic MST2 kinase or by inhibiting cyclin D1 accumulation, in which both scenarios would subsequently lead to cellular apoptosis (Shivakumar, Minna, Sakamaki, Pestell, & White, 2002; Matallanas et al., 2007). Due to the high frequency of somatic mutations and promoter hypermethylation, the expression of RASSF1A is significantly down-regulated in NPC and thus resulting in a cascade of molecular events leading to NPC development (Lo et al., 2001; Pan et al., 2005).

Besides *RASSF1A*, zinc-finger MYND-type containing 10 (*ZMYD10)* or more commonly known as *BLU*, has been mapped to chromosome 3p21.3 and its expression has been found to be commonly down-regulated in NPC due to promoter hypermethylation (Lerman & Minna, 2000; Qiu et al., 2004). Cheng and his team reported that 84.2% of all NPC primary biopsies and 93.5% of early-stage (Stage I and II) primary NPC tumours exhibited down-regulated *BLU* expression and is correlated with angiogenesis (Cheng et al., 2015). *In vitro* and *in vivo* studies both showed that the anti-proliferative and anti-migratory effects of *BLU* and when injected with exogenous BLU, up to 70-90% of tumour cells underwent apoptosis in animal models (Cheng et al., 2015). These reports on the crucial roles of genes located on chromosome 3p, and the lack thereof, associates chromosomal LOH of the genome to the genetic landscape of NPC.

2.2.1.2 Chromosome 9p LOH

9p LOH was detected in almost 77.8% of invasive NPC tissues from high-risk region, 63.6% of NPC from low-risk region, and 66.7% of dysplastic nasopharyngeal lesions (Chan et al.,

2002). Due to the allelic loss on chromosome 9p, a tumour suppressor protein p16 (encoded by cyclin-dependent kinase inhibitor 2A gene, *CDKN2A*) located at 9p21.3 was found to be frequently deleted, hypermethylated or mutated in NPC xenografts and primary tumours (Kamb et al., 1994; Kwong et al., 2002; Mäkitie et al., 2003). p16 protein plays a vital role in the regulation of cell cycle progression by binding to both CDK4 and CDK6, thereby sequestering the cyclin D/CDK complex from catalysing the phosphorylation of the retinoblastoma protein (pRB) required for the transition from G1 to S phase (Hara et al., 1996). The decreased p16 expression as the result of homozygous deletion, gene inactivation or transcription repression, compromises G1/S checkpoint security, leading to the uninhibition of cellular progression and growth and eventually, tumour formation (Baba et al., 2001).

The subsequent progression from mild to severe dysplasia is triggered by the activation and expression of both EBV latent genes and RNAs following EBV infection of epithelial cells (Figure 2.2). The molecular mechanism in which EBV infects target cells, achieve latency and eventually re-activated, has been previously described in Chapter 2.1.4.1. The expression of EBV latent genes such as LMP1, LMP2 and EBNA1 and EBV RNAs such as small EBER RNAs and miRNA BARTs collectively maintains viral episome in infected epithelial cell while suppressing cell differentiation and promoting cellular proliferation (transition into carcinoma *in situ*) and metastasis (irreversible and rapid transition into invasive carcinoma). As summarized in Figure 2.3, EBV proteins and RNAs are fully capable of interacting and inducing downstream intracellular proteins leading to the dysregulation of various signalling pathways involved in cellular behaviour such as angiogenesis (IL-8), metastasis (E-cadherin and MMPs), transformation (TERT),

proliferation (β-catenin, NF-κB and AP-1) and apoptosis (Bcl-2 and p53) (Tulalamba & Janvilisri, 2012). Taken together, the disruption of critical signalling pathways in cell survival, growth and metastasis mediates the biological behaviour of NPC.

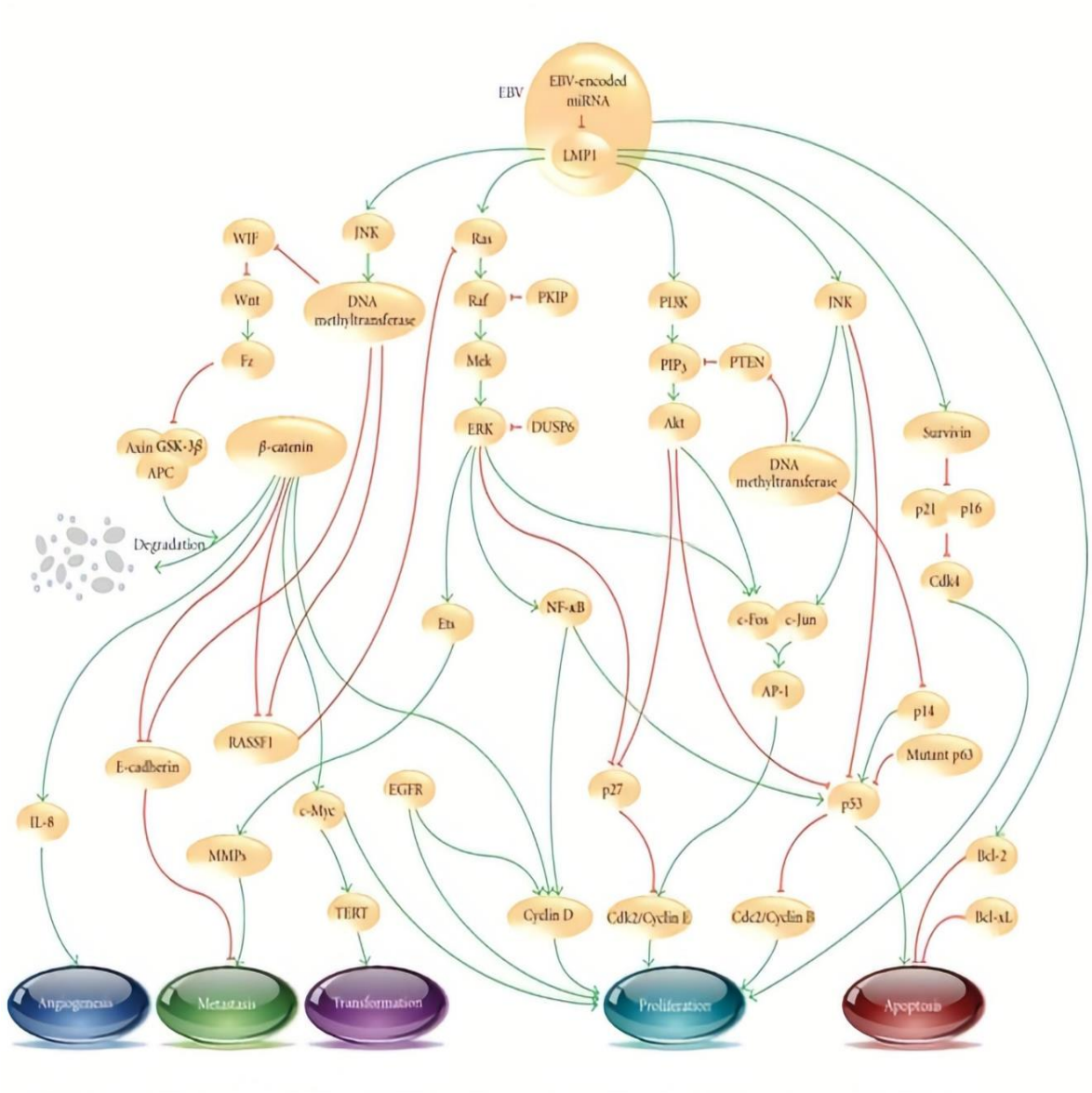

Figure 2.3: LMP1 downstream intracellular signalling pathways in the development of NPC. Schematic overview of the cascade of interactions leading to cellular angiogenesis, metastasis, transformation, proliferation and apoptosis begins with EBV-encoded latent gene products. Arrows and blunt-end arrows represent induction and inhibition, respectively. Adapted from Tulalamba & Janvilisri (2012).

2.2.2 Tumour Suppressor Genes (TSGs) and Oncogenes in NPC

Besides EBV infection, the progression from dysplastic lesion to carcinoma (*in situ* and invasive) is also aided by the accumulation of genetic modifications and epigenetic changes on pivotal group of genes, known as tumour suppressor genes (TSGs) and oncogenes. Even the slightest aberration in the expression or functionality of these genes could potentially disrupt major cellular surveillance systems such as cell cycle checkpoints, DNA repair and apoptosis. As such, TSGs and oncogenes are often the focus of cancer genetics and therapeutics studies due to their indispensable contribution in cancer progression.

2.2.2.1 Tumour Suppressor Genes (TSGs)

A tumour suppressor gene (TSG) is defined as a gene that encodes for a protein vital in regulating cell growth and the loss or reduction in its expression would result in the dysregulation of DNA repair mechanism and cell cycle checkpoints, eventually leading to unrestrained cellular growth. Tumour suppressor genes are inactivated in cases of germline mutation, somatic mutation, LOH and promoter hypermethylation. In hereditary cancer cases, the expression of TSG is compromised when mutation in one of the two copies of a TSG allele is inherited from germinal cells while the other mutation on the second allele is acquired somatically (Frebourg, Malkin, & Friend, 1991). On the other hand, in non-hereditary cancer, both alleles of a TSG undergo sequential somatic mutation resulting in the repression of the TSG. Table 2.3 summarizes the list of known tumour suppressor genes involved in NPC development and the modifications detected individually (W. Dai, Zheng, Cheung, & Lung, 2016). These abnormalities in TSGs would negatively affect multiple signalling processes and cellular regulatory pathways that would contribute to NPC pathogenesis.

Table 2.3: Tumour suppressor genes frequently modified via genetic and/or epigenetic mechanisms in NPC. Adapted from Dai et al. (2016).

Gene	Full Name	Location	Genetic/ Epigenetic Modification	Function
TP73	Tumour suppressor p73	1p36.3	Hypermethylation	Cell cycle, DNA damage
CASP8	Caspase 8	2q33	Hypermethylation	Apoptosis
ZMYND10	Zinc finger, MYND-type containing 10	3p21.3	Hypermethylation	Angiogenesis
RASSF1	Ras association domain family member 1	3p21.3	Hypermethylation	Cell growth, proliferation
DLEC1	Deleted in lung and oesophageal cancer 1	3p21.3	Hypermethylation	Cell communication
LARS2	Leucyl-tRNA synthetase 2	3p21.3	Hypermethylation & allelic deletion	Aminoacyl-tRNA synthetase
PTPRG	Protein tyrosine phosphatase, receptor type G	3p21	Hypermethylation	Cell cycle
RARB	Retinoic acid receptor, beta	3p24.2	Hypermethylation	Hormone receptor, transcriptional regulator
FBLN1	Fibulin 2	3p25.1	Hypermethylation & allelic deletion	Cell growth, angiogenesis, migration
UCHL1	Ubiquitin carboxyl-terminal esterase L1	4p14	Hypermethylation	De-ubiquitination
IED3	Immediate early response 3	6p21.3	Hypermethylation	DNA damage and repair, apoptosis
SFRP1	Secreted frizzled-related protein 1	8p11.21	Hypermethylation	Inhibitor of Wnt/ β-catenin pathway
DLC1	DLC1 Rho GTPase activating protein	8p22	Hypermethylation & allelic deletion	Cytoskeleton organization, GTPase activator, cell adhesion

Table 2.3 continued

CDKN2A	Cyclin-dependent kinase inhibitor 2A	9p21	Hypermethylation & allelic deletion	Cell cycle
CDKN2B	Cyclin-dependent kinase inhibitor 2B	9p21	Hypermethylation & allelic deletion	Cell cycle
DAPK1	Death-associated protein kinase 1	9p21.33	Hypermethylation	Cell cycle
MGMT	O-6-methylguanine-DNA methyltransferase	10q26	Hypermethylation	DNA repair, cell cycle
CRYAB	Crystallin, alpha B	11q22.3	Hypermethylation & allelic deletion	Epithelial-mesenchymal transition (EMT)
CADM1	Cell adhesion molecule 1	11q23.2	Hypermethylation	Cell growth, apoptosis
THY1	Thy-1 cell surface antigen	11q23.3	Hypermethylation	Cell invasion, cell growth
MMP19	Matrix metallopeptidase 19	12q14	Hypermethylation & allelic deletion	Angiogenesis
WF1	WNT inhibitor factor 1	12q14.3	Hypermethylation	Inhibitor of Wnt pathway
DUSP6	Dual specificity phosphatase 6	12q22	Hypermethylation & allelic deletion	Migration, invasion, cell growth, EMT
CHFR	Checkpoint with fork head and ring finger domain	12q24.33	Hypermethylation	Cell cycle
LTBP2	Latent transforming growth factor beta binding protein 2	14q24	Hypermethylation & histone deacetylation	Cell mobility, cell invasion

2.2.2.1.1 *p53*

In NPC, interestingly, the genetic alterations of a well-established TSG, *TP53*, which encodes for p53 protein, is comparatively infrequent in NPC biopsies and cell lines when compared to other carcinomas (Effert et al., 1992; Spruck et al., 1992; Sun, Hegamyer, & Colburn, 1993). The rarity of p53 mutations observed in primary NPC tissues and cell lines suggests that there is minimal selection for genetic inactivation of p53 in NPC development. Despite this, the overexpression of p53 protein has been detected in several cases via immunohistochemistry (IHC) of NPC biopsy samples obtained from various high and low endemic regions and of distinct histopathological types (Kurniawan & Leong, 2000; Agaoglu et al., 2004; Taweevisit, 2007; Hoe, Lee, Khoo, & Peh, 2009). Collectively, these data have shown that the oncogenic role of p53 is due not to the inactivating genetic aberrations of p53, as observed in various other carcinomas, but on the post-transcription mechanism regulation of p53.

In the context of NPC, the up-regulation of p53 is in close association with EBV infection and the high levels of LMP1 (Figure 2.3). EBV-encoded oncoprotein LMP1 regulates and promotes the transcription and translation activity of p53 by means of phosphorylation and ubiquitination (Li et al., 2007). This is achieved when LMP1 suppresses the K48-linked ubiquitination of p53 by inhibiting MDM2 (Li et al., 2008). Mouse double minute 2 homolog (MDM2) is an E3 ubiquitin ligase that negatively regulates p53 by ubiquitinating p53. p53 and MDM2 form an autoregulatory negative feedback loop, in which p53 stimulates the expression of MDM2 and in turn, MDM2 represses p53 activity (Picksley & Lane, 1993). Besides that, the accumulation of p53 is attributed to the binding competition between MDM2 and the increasing levels of MDMX, a MDM2 homologue without the E3 ligase

domain, to the N-terminus of p53 thereby inhibiting MDM2-mediated p53 ubiquitination (Figure 2.4) (Jackson & Berberich, 2000; Stad et al., 2000).

Besides MDM2, the interaction between LMP1 and tumour necrosis factor receptor-associated factor 2 (TRAF2) up-regulates the expression of nuclear factor kappa-light-chain-enhancer of activated B cells (NF-κB), resulting in the activation of downstream effector proteins in the cellular viability and proliferative pathways, such as p53, thereby further expanding the accumulating pool of p53 (Mainou, Everly, & Raab-Traub, 2005; Li et al., 2008).

Apart from the EBV-related pathway, the up-regulation of p53 has been linked to the impairment of ribosome biogenesis due to nucleolar or ribosomal distress (discussed in Section 2.3.1.2) (Teng, Thomas, & Mercer, 2013). It was proposed that due to the disruption in ribosome synthesis mechanism, unassembled trimeric ribosomal 5S ribonucleoprotein (RNP) particle, a ribosomal subcomplex of the large ribosomal subunit consisting of the 5S rRNA, uL18 (RPL5) and uL5 (RPL11), accumulates freely in the nucleoplasm (Bursać et al., 2012; Donati, Peddigari, Mercer, & Thomas, 2013; Sloan, Bohnsack, & Watkins, 2013). Instead of functioning individually, all three of the 5S RNP components have been demonstrated to be fully capable of binding and inhibiting the ubiquitin activity of MDM2 and therefore stabilizing p53 in HEK283 and U2OS cells (Elenbaas, Dobbelstein, Roth, Shenk, & Levine, 1996; Sloan et al., 2013).

However, the high level of p53 is not sufficient to induce cellular apoptosis, though the exact justification remains unclear (Yoshizaki et al., 2012). Having mentioned that, a hypothesis

has been brought forward based on the current data standing regarding this conundrum, and that is the mutation of p63. p63, a known structural homolog to p53, consists of a conserved DNA binding domain similar to that of p53 and possesses similar functionality in inducing cellular apoptosis (Yang et al., 1998). Crook and colleagues reported the high expression of p63 in all tumour specimens via IHC and subsequent sequencing revealed a truncated ΔN-terminal transactivating domain isotype that was capable of blocking p53-mediated transactivation and inhibiting apoptosis (Crook, Nicholls, Brooks, O'Nions, & Allday, 2000). Taken together, these findings reveal the unique oncological landscape of NPC compared to that of other cancers in terms of p53 accumulation and the complicated precursor pathways leading to it.

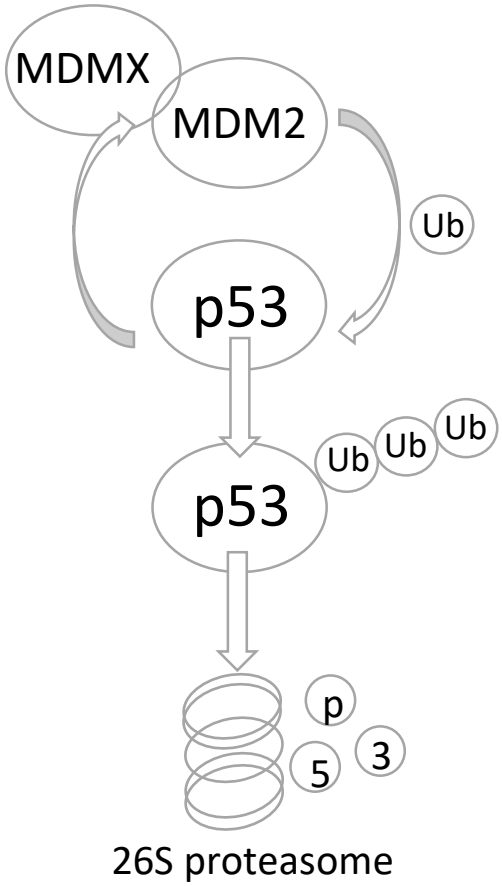

Figure 2.4: The MDM2-p53 signalling pathway. Under normal conditions, p53 expression levels are kept at a basal level by MDM2 and MDMX. The dimerization of MDM2 and MDMX stabilizes MDM2 by inhibiting MDM2 auto-ubiquitination, therefore enhances the E3 ubiquitin ligase activity of MDM2 on p53 resulting in p53 degradation by the 26S proteasome. Under nucleolar stress, the decrease in MDM2 leads to p53 stabilization, which in turn, in a negative feedback loop fashion, activates MDM2 (Vogelstein, Lane, & Levine, 2000; Gu et al., 2002).

2.2.2.2 Oncogenes

An oncogene is defined as a gene that initiates cancer progression by inducing uncontrolled cellular growth, proliferation and survival. In tumour cells, oncogenes are usually mutated in a gain-of-function manner and detected with high expression levels.

Complementing its virally-motivated role in the transformation of dysplastic lesions to carcinoma, LMP1 has been shown to demonstrate oncogenicity by promoting cell transformation, survival and invasion (Dawson, Port, & Young, 2012). In NPC tumours, mutations were detected in oncogenes such as phosphatidylinositol-4,5-biphosphate 3-kinase catalytic subunit alpha (*PIK3CA)*, neuroblastoma RAS viral oncogene homolog (*NRAS)*, receptor tyrosine kinase (*KIT)*, platelet-derived growth factor receptor alpha (*PDGFRA)*, Abelson murine leukaemia viral homolog 1 (*ABL)*, transforming protein p21 encoding gene (*HRAS)*, epidermal growth factor receptor (*EGFR)* and v-Raf murine sarcoma viral oncogene homolog B (*BRAF)*, and are closely associated with tumour metastasis and patient relapse (Zhang et al., 2014). Recently, a study on NPC tissues reported the potential oncogenic role of AIMP2-DX2, an isoform of the aminoacyl-tRNA synthetase-interacting multifunctional protein, in promoting cell viability, cell proliferation, migration and invasion, *in vitro* and *in vivo* (Cao, Zhang, & Zhang, 2018).

Due to the complex and intricate inter-dependence framework involving oncogenes and tumour suppressor genes in nasopharyngeal cancer genetics, in which much of it remains to be elusive, much work remains to be done in hopes of painting a clearer picture on the precise molecular oncogenic landscape of NPC for improved disease management and cancer therapeutics.

2.3. The Ribosome and Ribosomal Proteins (RPs)

The main machinery of cellular protein biosynthesis, the ribosome comprises of an inner rRNA core and a periphery of ribosomal proteins. Due to its central role in protein translation, impairment in ribosome biogenesis and its functionality can severely affect cell viability, growth, proliferation, differentiation and organism development.

2.3.1 An Overview of the Ribosome

Though a relatively tiny organelle, a ribosome is a complex macromolecular machinery responsible for a key cellular process: protein biosynthesis. Present in large numbers within all living cells, ribosomes are found either as freely floating particles in the cytosol or bound to membranes of the rough endoplasmic reticulum (ER) or that of the nuclear envelope.

These small particles were first observed and described in 1955 by a Romanian-American biologist George Emil Palade as “dense particles or granules” in eukaryotic cells using an electron microscope (Palade, 1955). A few years later in 1958, the term “ribosome” was coined by Richard B. Roberts to define a group of ribonucleoprotein particles that are involved in protein synthesis in the cytoplasm (Roberts, 1958).

Protein synthesis by the ribosome is initiated when the small ribosomal subunit, bound to an aminoacyl-tRNA attached to amino acid methionine, binds to an AUG start codon on the 5’ end of the template mRNA and engage the large ribosomal subunit. This process is followed by the scanning and reading of messenger RNA (mRNA) coding triplets for ‘translation instructions’ and the recruitment of successive corresponding amino acids to the ribosomes by transfer RNAs (tRNAs). The tRNA binding site on the ribosome is made up of three

distinct sections: an aminoacyl binding site for incoming tRNA molecule attached to a subsequent amino acid, a peptidyl binding site to contain a peptidyl-tRNA bound to the growing peptide chain, and an exit binding site to release free tRNA from the ribosome. Peptide bond linkages at the peptidyl-transferase centre (PTC) on the large ribosomal subunit is formed by a nucleophilic attack of the α-amino group on the aminoacyl-tRNA onto the carbonyl carbon on the peptidyl-tRNA.

2.3.1.1 Eukaryotic Ribosome Structure

A ribosome, also known as a ribonucleoprotein (RNP), is made up of complexes of 4 ribosomal RNAs (rRNAs) and approximately 80 ribosomal proteins (RPs) and it is divided into two subunits: a smaller subunit that binds to the mRNA coding strand and a larger subunit that catalyses the peptidyl transferase reaction. The RNA sequence, ribosome structure and size, ratio of protein to RNA content and the translation efficiency of ribosomes vary from bacteria, archaea and eukaryotes (Lafontaine & Tollervey, 2001).

Advances in three-dimensional crystallographic work have demonstrated that eukaryotic ribosomes, also known as 80S ribosomes, are made up of a small 40S subunit, containing an 18S RNA and 33 proteins, and a large 60S subunit consisting of three RNAs (28S, 5.8S and 5S) and 47 proteins (Wool, 1979; Ben-Shem et al., 2011; Khatter, Myasnikov, Natchiar, & Klaholz, 2015). Despite the differences across domains, ribosomes share a highly similar core, made up of distinctly organized RNAs and folded in tertiary structural motifs, that is the centre for all catalytic activity of the ribosome. Moreover, high-resolution images on the catalytic centre of a ribosome highlight the absence of ribosomal proteins in that region accordingly suggesting that ribosomal proteins are not directly involved in peptide bond

formation reactions but instead these proteins endow protection and stabilization to the RNA core (Ben-Shem et al., 2011; Klinge, Voigts-Hoffmann, Leibundgut, Arpagaus, & Ban, 2011; Yusupova & Yusupov, 2014).

2.3.1.2 Ribosome Biogenesis

Ribosome biogenesis refers to the multifaceted process of ribosome synthesis within a cell. For eukaryotic ribosomes, this process involving the transcription of rRNAs and the assembly of four rRNAs and ribosomal proteins happens in the nucleolus and the cytoplasm. Deemed to be the most energy-demanding cellular process, ribosome biogenesis involves a strict regulation of various assembly and maturation factors (Warner, Vilardell, & Sohn, 2001; Goodfellow & Zomerdijk, 2013).

In the nucleolus of eukaryotic cells, the 47S precursor rRNA comprising of the 18S, 5.8S and 28S rRNA strands are co-transcribed as a single transcript from tandemly arranged ribosomal DNA (rDNA) by RNA polymerase I (Pol I) (Figure 2.5). In contrast, the 5S rRNA is independently transcribed in the nucleoplasm by RNA polymerase III from multiple copies of the 5S rDNA gene located at several loci on chromosome I. Upon successful transcription, 5S rRNA is packaged with ribosomal proteins uL18 (RPL5) and uL5 (RPL11) to form 5S RNP complex and is subsequently imported into the nucleolus for further processing (Lee & Nazar, 2003). The third component of a ribosome, ribosomal proteins, are transcribed by RNA polymerase II, translated in the cytoplasm and eventually translocated into the nucleolus for pre-ribosomal assembly via multiple transport receptors such as karyopherins or importins (Jäkel & Görlich, 1998; Plafker & Macara, 2002). In the nucleolus, the 90S pre-ribosomes are assembled with the assistance of non-ribosomal factors

and small nucleolar RNAs (snoRNA), and are re-modelled and subsequently separated into the nascent pre-60S and pre-40S particles (Tschochner & Hurt, 2003). The individual subunit particles, 66S (precursor to 60S large subunit) and 43S (precursor to the 40S small subunit) are subjected to distinct maturation pathways, each with its unique sets of biogenesis factors, and upon proper assembly and maturation, will be exported out of the nucleolus to the cytoplasm via the exportin 1 nuclear export pathway (Nissan, Bassler, Petfalski, Tollervey, & Hurt, 2002; Thomas & Kutay, 2003; Tschochner & Hurt, 2003). Once in the cytoplasm, the pre-60S and pre-40S subunits undergo additional processing and eventually combining, via inter-subunit bridges, to form active and functional 80S ribosomes (Pestova et al., 2001; Gao & Frank, 2006).

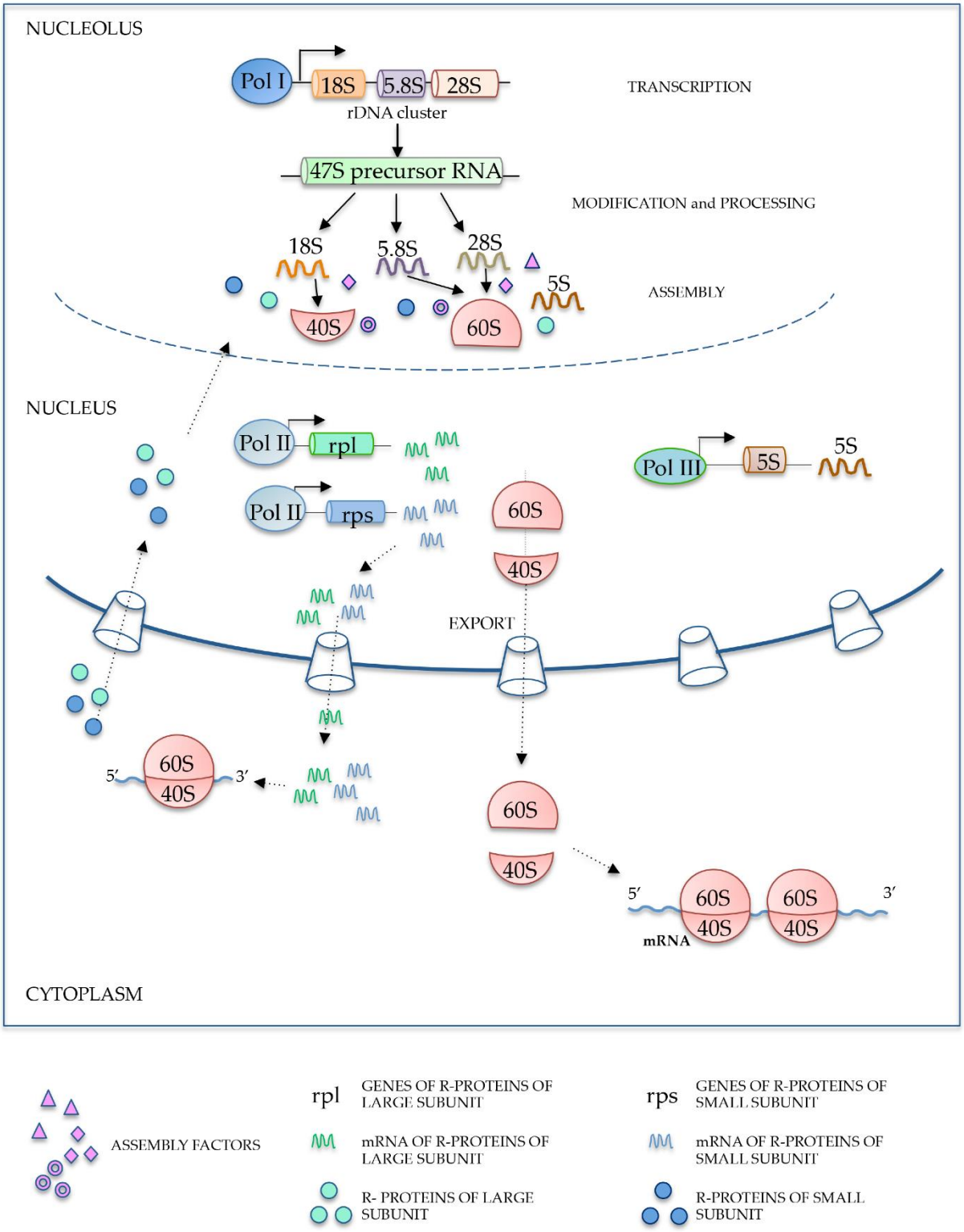

Figure 2.5: Ribosome biogenesis and maturation process. Schematic representation of the step-wise process and compartmentalisation of ribosome biogenesis and maturation (Russo & Russo, 2017).

2.3.1.3 Quality Control and Related Human Diseases

Ribosome biogenesis is a tightly regulated process due to its importance in cell metabolism and growth. Therefore, it is necessary that several quality control measures are put into place to prevent wastage of cellular energy and resources that go into synthesizing non-functional or less-efficient defective ribosomes.

Besides being seminal components of the ribosome synthesis machinery, assembly factors (AF) act as a surveillance system that also regulates and controls the very process they assist. Assembly factors are able to prevent premature translation by blocking the assembly of ribosomal proteins to form pre-40S subunit and by blocking the assembly of the 60S and 40S to form the translation initiation complex (Gartmann et al., 2010; Strunk et al., 2011). Secondly, the TRAMP (Trf4/Air2/Mtr4p Polyadenylation) complex identifies and marks defectively transcribed pre-rRNAs and unassembled rRNAs in the nucleolus for degradation by exosomes, thus ensuring that ribosome assembly intermediates are functional and timely assembled (LaCava et al., 2005; Houseley, LaCava, & Tollervey, 2006). Even if defective pre-ribosomal subunits escape degradation within the nucleolus, the ribosomal surveillance system continues in the cytoplasm. When a ribosome stalls inappropriately at a sense codon during translation due to faulty 60S and/or 40S subunits with mutations within the peptidyl transfer centre (PTC) and decoding centre, respectively, the defective ribosome subunits are eliminated via a non-functional rRNA decay (NRD) pathway that eventually recruits cytoplasmic exosome for rRNA degradation (Cole, LaRiviere, Merrikh, & Moore, 2009).

Faulty quality control over the mechanism of ribosome biogenesis would result in ribosomopathy genetic diseases such as skeletal muscular dystrophy, Diamond-Blackfan

anaemia (DBA), Treacher Collins Syndrome (TCS) and Schwachman-Diamond syndrome (SDS), and an increased susceptibility to cancer (Nakhoul et al., 2014). Mutations within the *SBDS* gene (encodes for ribosome maturation protein SBDS), resulting in dysregulated RNA metabolism, are associated with the onset of Schwachman-Diamond syndrome. Additionally, defects in a few ribosomal protein genes such as *eS19* (*RPS19*), *eS26* (*RPS26*), *uL18* (*RPL5*) and *uL5* (*RPL11*) have been implicated in Diamond-Blackfan anaemia. Furthermore, haploinsufficiency due to hemizygous deletions in *uS11 (RPS14)* has been identified as a risk factor for myelodysplastic syndrome (MDS) and $5q^-$ syndrome, characterized by erythroid differentiation defects and acquired myelodysplasia (Ebert et al., 2008; Ebert, 2009). Taken together, these genetic diseases showcase the importance of a well-orchestrated and well-controlled ribosome biogenesis machinery in disease and cancer prevention.

2.3.2 Ribosomal Proteins (RPs)

Ribosomal proteins (RPs) are small individual RNA-binding proteins that are the fundamental building blocks of the ribosomal subunits, playing vital roles in the concerted assembly and structure of ribosomes and in the initiation, elongation and termination phases of protein synthesis.

2.3.2.1 Primary Progression on Ribosomal Proteins

Much of the earliest work on the purification and characterisation of ribosomal proteins was conducted with the ribosomes of *Escherichia coli* (*E. coli*). In 1968, Traub and Nomura were the first to partially fractionate ribosomal proteins and successfully reconstituted

functionally active 30S ribosomal particles from isolated RNAs and ribosomal proteins *in vitro* (Traub & Nomura, 1968a, 1968b). Following single protein addition and omission studies as well as structural and biochemical analyses, an ordered assembly map was constructed that divulged the positions of known ribosomal proteins, albeit not fully comprehensive, and putative protein-protein and RNA-protein interactions (Mizushima, 1970). Around this time, due to the lack of consensus of an established naming system for ribosomal proteins, Wittmann and her group published a standard experimental protocol for identification and characterisation of ribosomal proteins and at the same time, put forth a naming system based on the arrangement of respective protein bands on a 2-dimensional polyacrylamide gel, which was then universally adopted (Wittmann et al., 1971).

However, in the intervening years, protein-naming complexities arose with the influx of ribosomal protein sequence and atomic resolution crystal structure studies on other eubacterial species such as *Thermus thermophilus* and *Deinococcus radiodurans*, archaeal *Haloarcula marismortui*, yeast and rats, due to sequence homology and structural differences of ribosomal proteins across domain boundaries (Wittmann-Liebold et al., 1990; Wool et al., 1995; Yusupov et al., 2001; Harms et al., 2001; Ben-Shem et al., 2011; Klinge et al., 2011; Rabl, Leibundgut, Ataide, Haag, & Ban, 2011;). Consequently, a novel naming system was proposed by Ban and his team that homologous ribosomal proteins are assigned a similar name, regardless of domain. Proteins that are found in all three domains are given the prefix ‘u’ (for universal) followed by the assigned name; archaeal proteins without any bacterial or eukaryotic homologues are identified by the prefix ‘a’ (for archaeal), though none has been reported so far; proteins exclusively found in bacteria are designated with the prefix ‘b’ (for bacterial); and eukaryotic ribosomal proteins are given the prefix ‘e’ (for

eukaryotic) (Table 2.4 and Table 2.5) (Ban et al., 2014). For the purpose of ribosomal protein naming and identification in this thesis, the current naming system will be adopted followed by the old name in parenthesis, for example, uL18 (RPL5).

Table 2.4: New nomenclature for ribosomal proteins from the small subunit. Universal ribosomal proteins that are present across all domains are highlighted in grey. Adapted from Ban et al. (2014).
* b: bacteria, e: eukaryotic, u: universal

New name*	Bacteria name	Yeast name	Human name	New name*	Bacteria name	Yeast name	Human name
bS1	S1	-	-	**uS14**	S14	S29	S29
eS1	-	S1	S3a	**uS15**	S15	S13	S13
uS2	S2	S0	Sa	**bS16**	S16	-	-
uS3	S3	S3	S3	**uS17**	S17	S11	S11
uS4	S4	S9	S9	**eS17**	-	S17	S17
eS4	-	S4	S4	**bS18**	S18	-	-
uS5	S5	S2	S2	**uS19**	S19	S15	S15
bS6	S6	-	-	**eS19**	-	S19	S19
eS6	-	S6	S6	**bS20**	S20	-	-
uS7	S7	S5	S5	**bS21**	S21	-	-
eS7	-	S7	S7	**bTHX**	THX	-	-
uS8	S8	S22	S15a	**eS21**	-	S21	S21
eS8	-	S8	S8	**eS24**	-	S24	S24
uS9	S9	S16	S16	**eS25**	-	S25	S25
uS10	S10	S20	S20	**eS26**	-	S26	S26
eS10	-	S10	S10	**eS27**	-	S27	S27
uS11	S11	S14	S14	**eS28**	-	S28	S28
uS12	S12	S23	S23	**eS30**	-	S30	S30
eS12	-	S12	S12	**eS31**	-	S31	S27a
uS13	S13	S18	S18	**RACK1**	-	Asc1	RACK1

Table 2.5: New nomenclature for ribosomal proteins from the large subunit. Universal ribosomal proteins that are present across all domains are highlighted in grey. Adapted from (Ban et al., 2014).
* b: bacteria, e: eukaryotic, u: universal

New name*	Bacteria name	Yeast name	Human name	New name*	Bacteria name	Yeast name	Human name
uL1	L1	L1	L10a	**uL24**	L24	L26	L26
uL2	L2	L2	L8	**eL24**	-	L24	L24
uL3	L3	L3	L3	**bL25**	L25	-	-
uL4	L4	L4	L4	**bL27**	L27	-	-
uL5	L5	L11	L11	**eL27**	-	L27	L27
uL6	L6	L9	L9	**bL28**	L28	-	0
eL6	-	L6	L6	**eL28**	-	-	L28
eL8	-	L8	L7a	**uL29**	L29	L35	L35
bL9	L9	-	-	**eL29**	-	L29	L29
uL10	L10	P0	P0	**uL30**	L30	L7	L7
uL11	L11	L12	L12	**eL30**	-	L30	L30
bL12	L7/L12	-	-	**bL31**	L31	-	-
uL13	L13	L16	L13a	**eL31**	-	L31	L31
eL13	-	L13	L13	**bL32**	L32	-	-
uL14	L14	L23	L23	**eL32**	-	L32	L32
eL14	-	L14	L14	**bL33**	L33	-	-
uL15	L15	L28	L27a	**eL33**	-	L33	L35a
eL15	-	L15	L15	**bL34**	L34	-	-
eL16	L16	L10	L10	**eL34**	-	L34	L34
bL17	L17	-	-	**bL35**	L35	-	-
uL18	L18	L5	L5	**bL36**	L36	-	-
eL18	-	L18	L18	**eL36**	-	L36	L36
bL19	L19	-	-	**eL37**	-	L37	L37
eL19	-	L19	L19	**eL38**	-	L38	L38
bL20	L20	-	-	**eL39**	-	L39	L39
eL20	-	L20	L18a	**eL40**	-	L40	L40
bL21	L21	-	-	**eL41**	-	L41	L41
eL21	-	L21	L21	**eL42**	-	L42	L36a
uL22	L22	L17	L17	**eL43**	-	L43	L37a

Table 2.5 continued

eL22	-	L22	L22	**P1/P2**	-	P1/P2	P1/P2
uL23	L23	L25	L23a			(AB)	(αβ)

2.3.2.2 Diversity and Conservation of Ribosomal Proteins

The diversity of ribosomal proteins was first discovered more than 50 years ago when more than 20 ribosomal polypeptides were isolated from bacterial ribosome of *E. coli* (Waller & Harris, 1961). The interest boost in ribosomal protein sequences and primary structures in *E. coli* and other organisms promoted extensive comparative genomics and structural analysis of ribosomal proteins from other domains of life. The first attempt was undertaken by Wool and his group in 1995, in which they revealed a total of 31 ribosomal proteins present in ribosomes from members of all domain of life (Wool et al., 1995). By 2002, with the advent of whole genome sequence technology, Lecompte and his colleagues conducted a large-scale comparative study on ribosomal protein genes from sixty-six genomes of different species and domains. The group detected 34 universal ribosomal proteins that were present in all genomes under study hence, indicating the diversity, evolution and conservativeness of sequence, structure and function of ribosomal proteins across all domains of life (Lecompte, Ripp, Thierry, Moras, & Poch, 2002). By the end of 2004, a Ribosomal Protein Gene database was set up to contain detailed information on sequences (genomic, cDNA and amino acid sequences), genomic locations, intron/exon junctions and orthology of ribosomal proteins of human and other organisms (Nakao, Yoshihama, & Kenmochi, 2004).

Taken together, ribosomal proteins have highly conserved sequences and structures across

all life forms. Among the 40 ribosomal proteins belonging to the small ribosomal subunit of all taxonomic range, 15 proteins are universally conserved across prokaryotes to eukaryotes while 7 proteins are exclusively found in bacteria (bS1, bS6, bS16, bS18, bS29, bS21 and bTHX) and 18 proteins are found in both archaea and eukaryotes, but not in bacteria (Ban et al., 2014) (Table 2.4). Interestingly, all known eukaryotic ribosomal proteins of the small subunit are homologous to their corresponding archaeal protein subunit, and vice versa, substantiating the long-standing idea that archaeal organisms are more closely related, evolutionarily, to eukaryotes than to bacteria (Ban et al., 2014).

Among the 62 ribosomal proteins of the large subunit, 18 proteins are universally present, 15 proteins are exclusively found in bacteria, 28 proteins are found in both archaea and eukaryotes and one ribosomal protein, eL28, has only been identified in eukaryotes (Table 2.5). Similar to that of the ribosomal proteins of the small subunit, all eukaryotic proteins of the large subunit, except eL28, are homologous to their corresponding counterparts in archaea (Ban et al., 2014).

Due to the existence of overlapping homologous sequence of ribosomal proteins of the small and large subunits across all domains, it was proposed that the primitive version of ribosomal proteins was present in proto-ribosomes before the phylogenetic divergence into archaea, eubacteria and eukaryotes. Furthermore, extensive comparative analysis of the primary structures of ribosomal proteins revealed the lack of non-conserved sequences in that of universal proteins, such as, uS4 (S9), uS17 (S11), uS15 (S13), uL18 (L5) and uL5 (L11), which are believed to be involved in the catalytic site formation of the ribosome (Hartman, Favaretto, & Smith, 2006).

2.3.2.3 Ribosomal Proteins and Their Ribosomal Function

Within the ribosome, a specific subset of ribosomal proteins, usually the universal proteins, carries more weight in the functioning of the ribosome when compared to the rest. Nevertheless, the primary role of ribosomal proteins within the ribosome is in the hierarchical ribosomal assembly and sequential stabilization of subdomains (Yusupova & Yusupov, 2014).

In terms of the regulation of pre-18S rRNA, siRNA (small-interfering RNA) knockdown of 31 out of the 33 human ribosomal proteins of the small subunit resulted in the impairment of pre-rRNA maturation of the 18S rRNA. Specifically, the ablation of 16 ribosomal proteins, out of the 31 proteins under study, lead to the accumulation of 30S and 45S pre-rRNAs, demonstrating the failure of all rRNAs processing steps in the cleavage of 5'-external transcribed spacer (ETS) and 5'- internal transcribed spacer1 (ITS1) necessary for 18S rRNA maturation and export (O'Donohue, Choesmel, Faubladier, Fichant, & Gleizes, 2010). Not only that, the RACK1 ribosomal protein of the small subunit proves to be a necessary factor in the final processing of the 3' end of 18S-E-pre rRNA (following nuclear export). The knockdown of RACK1 induced the accumulation of 18S-E pre-rRNA in the cytoplasm but did not significantly affect the depletion of mature 18S rRNA, in this case, suggests the role of RACK1 protein in retarding, not blocking, the kinetics of endonucleolytic cleavage of its 3'end to generate a mature 18S rRNA (Larburu et al., 2016). Similarly, the knockdown of ribosomal protein uL18 (RPL5) has been cited in the significant accumulation of 18S pre-rRNA in the nucleus, a testament to a failed nuclear export system (Larburu et al., 2016). In addition to that, mutations in *eS24 (RPS24)* have been linked to defective 18S pre-rRNA maturation as eS24 (RPS24) was found to be a necessary factor for

the endonucleolytic cleavage of the 5'-ETS (Choesmel et al., 2008). Though its exact mechanism remains unclear, the depletion of eS19 (RPS19) showed a significant decrease in small 40S subunits and mature 80S ribosomes but an increase in large 60S subunit, implying its role the 18S rRNA processing and maturation pathway (Idol et al., 2007). Ribosomal proteins uL18 (RPL5) and uL5 (RPL11) have been shown to be co-recruited with 5S rRNA particle prior to being imported into the nucleolus for subsequent integration into pre-ribosome complex (Lee & Nazar, 2003).

Apart from rRNA processing and pre-ribosome transport, ribosomal proteins also have pivotal roles in other processes in relation to ribosomal assembly and translation activity. uS9 (S16), eL15 (L15), and eL24 (L24) are involved in the formation of inter-subunit bridges that holds ribosomal sub-particles together by interacting with one or more domains of rRNAs (Gao & Frank, 2006). Besides that, eL24 (L24) maintains proper functioning of ribosome exit 'E' section, where emerging polypeptides are released after translation (Thomson, Ferreira-Cerca, & Hurt, 2013).

2.3.2.4 Extra-Ribosomal Functions of Ribosomal Proteins

Shelving the long-held notion that ribosomal proteins only play roles exclusively in the synthesis, modification, and assembly of ribosomes and protein biosynthesis, numerous studies have demonstrated the active involvement of ribosomal proteins in a diverse range of cellular processes, such as cell growth, proliferation and differentiation, apoptosis and DNA repair, that are independent of their ribosomal capacity (Wool et al., 1995; Lindström, 2009; Warner & McIntosh, 2009). In 2010, the term 'moonlight proteins' was coined in reference to these multitasking polypeptide chains (Huberts & van der Klei, 2010).

In the review by Warner and McIntosh, it was proposed that at least one of the three qualifying criteria had to be met in the validation of an extra-ribosomal function of a ribosomal protein. The three criteria suggested were: (i) RP interacts specifically with non-ribosomal component (RNA or protein) of the cell; (ii) such interaction to have a physiological effect on the cell; (iii) such effect to occur away from the ribosome. A list of moonlighting ribosomal proteins with their reported extra-ribosomal functions is summarized in Table 2.6 (Warner & McIntosh, 2009). It should also be noted that numerous haploinsufficiency studies of RPs are excluded due to the inconclusive direct correlation between ribosomal proteins and altered phenotype, which could be a result of cellular pathways downstream of that of the ribosomes.

Table 2.6: Ribosomal proteins and their respective extra-ribosomal functions (adapted from Wang et al. (2015)).

Ribosomal Protein	Extra-ribosomal Function(s)	Reference
	Ribosomal Proteins of the Small Subunit	
uS3 (S3)	Interacts with both MDM2 and p53	Yadavilli et al. (2009)
	Interacts with DNA base excision repair proteins	Lee et al. (2010)
	Induces apoptosis via NF-κB pathway	Jang, Kim, & Kim (2012)
	Knockdown decreases migration and invasion of osteosarcoma cells via interaction with glioma-associated oncogene homolog (GLI)	Nagao-Kitamoto et al. (2015)
uS4 (S9)	Silencing inhibits cell growth via p53 pathway	Lindström & Nistér (2010)
eS4 (S4)	Blocks cell proliferation via cysteine protease activity	Yadaiah et al. (2013)
eS6 (S6)	Depletion attenuates cell proliferation and induces apoptosis via p53 pathway	Volarevic et al. (2000) Narla, Hurst, & Ebert (2011)
uS7 (S5)	Induces cell cycle arrest and differentiation by downregulating CDK-2/4/6 levels	Matragkou et al. (2008)
eS7 (S7)	Induces cell cycle arrest and apoptosis by interacting with MDM2 via p53-dependent and p53-independent pathways	Chen et al. (2007) Gao et al. (2013)
eS8 (S8)	Increases sensitivity to Fas ligand-induced apoptosis via interaction with CDK11p46	Hao et al. (2011)
uS10 (S20)	Induces cell cycle arrest and apoptosis by interacting with MDM2	Daftuar, Zhu, Jacq, & Prives (2013)

Table 2.6 continued

uS11 (S14)	Induces cell cycle arrest and apoptosis by interacting with MDM2 and by negatively regulating c-Myc activity Attenuates cell cycle progression by inhibiting CDK4/6	Zhou, Hao, Liao, Zhang, & Lu (2013) Lessard, Brakier-Gingras, & Ferbeyre (2019)
uS14 (S29)	Induces apoptosis by regulating the expressions of apoptotic inducers and inhibitors	Khanna, Sen, Sharma, & Singh (2003) Khanna, Reddy, Tuteja, & Singh (2000)
uS15 (S13)	Induces cell growth by negatively regulating p27 expression and CDK2 kinase activity	Guo et al. (2011)
uS19 (S15)	Induces cell cycle arrest and apoptosis by interacting with MDM2	Daftuar et al. (2013)
eS19 (S19)	Silencing disrupts erythropoiesis via p53-dependent cell cycle arrest Dysregulates immunoregulation by negatively regulating macrophage migration inhibitory factor (MIF)	Moniz et al. (2012) Filip et al. (2009)
eS25 (S25)	Induces cell cycle arrest and apoptosis by interacting with MDM2	Zhang et al. (2013)
eS26 (S26)	Induces cell cycle arrest and apoptosis by interacting with MDM2	Cui et al. (2014)
eS27 (S27)	Induces cell cycle arrest and apoptosis by interacting with MDM2 Regulates NF-κB apoptosis pathway Regulates cellular invasiveness and migration via integrin β4 expression	Xiong, Zhao, He, & Sun (2011) Yang et al. (2012) Yang et al. (2013)
eS31 (S27a)	Induces cell cycle arrest and apoptosis by interacting with MDM2	Sun, DeVine, Challagundla, & Dai (2011)

Table 2.6 continued

Ribosomal Proteins of the Large Subunit		
uL3 (L3)	Induces cell cycle arrest and apoptosis by regulating p53-independent p21 expression	Russo et al. (2013) Russo & Russo (2017)
uL5 (L11)	Induces cell cycle arrest and apoptosis by interacting with MDM2 and negatively regulating c-Myc expression and activity	Zhang et al. (2003) Dai, Arnold, Sun, Sears, & Lu (2007)
eL6 (L6)	Induces cell cycle arrest and apoptosis by interacting with MDM2 Induces cell growth and cell cycle progression by up-regulation of cyclin E in gastric cancer	Bai, Zhang, Xiao, & Zheng (2014) Gou et al. (2010) Wu et al. (2011)
uL13 (L13a)	Regulates immunoregulation by inhibiting the expression of inflammatory chemokines in macrophages and leukemic cells	Mukhopadhyay et al. (2008) Poddar et al. (2013)
uL14 (L23)	Induces cell cycle arrest and apoptosis by interacting with MDM2 Positively regulates cell cycle progression by sequestering nucleophosmin, NPM1	Dai et al. (2004) Wanzel et al. (2008)
eL15 (L15)	Ablation in gastric cancer decreased cellular growth due to disruption in its interaction with interferon (IFN)-stimulated antiviral protein, p56	Hsu et al. (2011)
uL18 (L5)	Induces cell cycle arrest and apoptosis by interacting with MDM2	Dai & Lu (2004) Horn & Vousden (2008)
uL22 (L17)	Inhibits vascular smooth muscle growth	Smolock et al. (2012)

Table 2.6 continued

eL22 (L22)	Depletion in αβ T cells resulted in cycle cell arrest and apoptosis due to induction of p53 expression	Anderson et al. (2007)
	Inactivation promotes transformation potential of T-lineage progenitors by induction of stemness factor, Lin28B	Rao et al. (2012)
	Mutation in cancers retards cell survival by blocking p53-MDM2 pathway	Cao et al. (2017)
uL24 (L26)	Induces cell cycle arrest and apoptosis by interacting with MDM2	Ofir-Rosenfeld, Boggs, Michael, Kastan, & Oren (2008)
eL29 (L29)	Silencing in mice decreased VEGF-stimulated tumour angiogenesis	Jones et al. (2013)
	Depletion in pancreatic cancer cells leads to cellular proliferation inhibition	Li, Ge, Yin, Luo, & Chen (2012)
eL33 (L35a)	Depletion results in cell cycle arrest in a p53-dependent manner	Llanos & Serrano (2010)
eL37 (L37)	Induces cell cycle arrest and apoptosis by interacting with MDM2	Daftuar et al. (2013)
eL41 (L41)	Silencing in NIH3T3 cells induced transformation and tumour growth and resulted in mitosis and centrosome disruption	Wang et al. (2010)
P1 (P1)	Induces cell proliferation by up-regulating transcription factor E2F1 and cyclin E	Artero-Castro et al. (2009)

2.3.2.5 Ribosomal Proteins in Cancers

According to Table 2.6, ribosomal proteins are involved in various ribosome-independent functions that affects a cell's biochemical, physiological and cellular well-being. By exerting their respective indispensable roles in multiple cellular processes such as cell cycle progression, cellular growth, proliferation, differentiation, DNA damage repair and nucleolar stress response, it does not come as a surprise that the post-transcription and translation dysregulation of ribosomal proteins triggers the onset of tissue-specific malignancies (Ruggero & Pandolfi, 2003). Even though clinical studies on the association of ribosomal protein expression and human cancers are still in its infancy, a remarkable number of molecular and animal studies have implicated the up- or down-regulation of specific RPs in various carcinomas. Table 2.7 summarizes the dysregulation of ribosomal protein expression according to the type of cancer.

Table 2.7: Ribosomal protein expressions in human cancers.

Cancer Type	Ribosomal Protein(s)	Altered Expression	Mechanism	References
Liver cancer (HCC)	uS8 (S15a) eS8 (S8) uL11 (L12) uL23 (L23a) eL27 (L27) eL30 (L30) eL36 (L36) eL42 (L36a)	Up-regulation	Associated with increased tumour cell proliferation	Kim et al. (2004) Kondoh et al. (2001) Song et al. (2011) Guo et al. (2018)
Gastric cancer	uS15 (S13) eL6 (L6) eL13 (L13) eL15 (L15) eL34 (L34)	Up-regulation	Associated with enhanced proliferation, transformation and tumour growth	Guo et al. (2011) Gou et al. (2010) Wang et al. (2006) Kobayashi et al. (2006) Liu et al. (2015)
Colorectal cancer (CRC)	uS3 (S3) eS6 (S6) uS8 (S15a) eS8 (S8)	Up-regulation	Associated with cell differentiation and growth	Chester et al. (1989) Pogue-Geile et al. (1991) Kondoh, Schweinfest, Henderson, & Papas (1992)

Table 2.7 continued

	uS17 (S11) eS19 (S19) eS31 (S27a) uL10 (P0) uL18 (L5) eL19 (L19) uL30 (L7) eL31 (L31)			Wong et al. (1993) Kasai et al. (2003) Huang et al. (2008) Chen et al. (2016)
	eS7 (S7) eL6 (L6) eL15 (L15) uL18 (L5) eL29 (L29) eL31 (L31) eL39 (L39)	Down-regulation	Associated with increased growth, proliferation and glycolysis of CRC cells	Bertucci et al. (2004) Zhang et al. (2016)
Prostate cancer	uS5 (S2) eS19 (S19) eS21 (S21) eS24 (S24) eL19 (L19)	Up-regulation	Associated with increased tumour growth	Bee et al. (2006) Wang, Hu, & Stearns (2009) Bee et al. (2011) Arthurs et al. (2017)

Table 2.7 continued

Oesophageal cancer	eS6 (S6) eL15 (L15) eL23 (L34)	Up-regulation	Associated with increased cell viability, migration and invasion and shorter survival	Wang et al. (2001) Kim, Jang, Chau, Pyo, & Um (2013) Fan et al. (2017)
	eL14 (L14)	Down-regulation	Associated with earlier event in tumorigenesis	Huang et al. (2006)
Lung cancer	peS6 (pS6) uS8 (S15a)	Up-regulation	Associated with increased proliferation and shorter metastasis-free survival	McDonald et al. (2008) Zhao et al. (2015)
	uL3 (L3) uL10 (P0) eL22 (L22) uL30 (L7)	Down-regulation	Associated to reduced apoptosis and enhanced cell migration and invasion	Yang et al. (2013) Nigro et al. (2015) Russo et al. (2016)
Breast cancer	eL24 (L24)	Up-regulation	Associated to induced growth and viability	Wilson-Edell et al. (2014)
	uS4 (S9) eL41 (L41)	Down-regulation	Related to malignant transformation	Bin Amer et al. (2008) Wang et al. (2010)
Osteosarcoma	uS3 (S3) uS8 (S15a) eL34 (L34)	Up-regulation	Associated to increased migration and invasion	Nagao-Kitamoto et al. (2015) Zhang et al. (2014) Luo et al. (2016)

Table 2.7 continued

	eL8 (L7a)	Down-regulation	Related to poor survival	Zheng et al. (2009)
Leukemic Lymphoma	eS6 (S6) uL14 (L23)	Up-regulation	Related to enhanced cell transformation and lower survival rates	Hagner et al. (2011) Wu et al. (2012)
	eL22 (L22)	Down-regulation	Associated with cell transformation and poor survival	Rao et al. (2016)
Ovarian cancer	eS7 (S7) uS13 (S18)	Up-regulation	Not known	Luo, Herrera, Soosaipillai, & Diamandis (2002) Wang et al. (2013)
	eS4 (S4)	Down-regulation	Associated with tumour stage	Tsofack et al. (2013)
Pancreatic cancer	uL24 (L26) eL29 (L29) eL39 (L39)	Up-regulation	Associated with increased proliferation and cell cycle progression	Li et al. (2012) Li, Chen, Luo, Ge, & Zhu (2014)
Nasopharyngeal cancer	uS4 (S9) eS8 (S8) uL14 (L23) eL27 (L27) eL43 (L37a) eL41 (L41)	Up-regulation	Not known	Sim et al. (2016) Sim et al. (2017)

2.3.2.5.1 Ribosomal Proteins as Cancer Biomarkers and Targets for Therapy

The differential expression of several ribosomal proteins has been implicated in an array of disorders and cancers (Table 2.7). Regrettably, it is still unclear if the differential expression of RPs is the causative factor or the by-product of stimulated cell proliferation in the context of individual cancer model. Despite this uncertainty, it is well-established that the differential expression of genes or proteins in a treated sample (or in a broader sense, disease or cancer model) in comparison to an untreated (normal) sample suggests their involvement in the development and progression of a certain phenotype, regardless if its favourable or unfavourable. In disease and cancer genetics, the differential expression of a subset of RPs have been strongly correlated not only to the development and progression, but also to the staging and prognosis of a disease or cancer, hereby making them reliable therapeutic targets and early detection and prognosis biomarkers.

In hepatocellular carcinoma (HCC), differential display analysis revealed that ribosomal proteins eS8 (S8), uL11 (L12), uL23 (L23a), eL27 (L27) and eL30 (L30) mRNAs were up-regulated in HCC tissues and cell lines when compared to neighbouring non-tumorous liver tissues and normal liver cell lines, respectively (Kondoh et al., 2001). In a separate study, similar analysis detected the enhanced expression of ribosomal protein eL42 (L36a) mRNA in 85% of HCC specimens and in eight HCC cell lines, leading to activated cell proliferation and colony formation while the knockdown with antisense eL42 (L36a) cDNA reversed these oncogenic phenotypes (Kim et al., 2004). Immunohistochemistry revealed that eL36 (L36) protein is differentially up-regulated in 75% of HCC specimens and no expression is detected in the tumour-adjacent normal tissues. A clear correlation has been noted between the expression of eL36 (L36) and early clinicopathological stages as well as better overall

survival (OS), making it a potential prognostic factor of HCC (Song et al., 2011). Ribosomal protein uS8 (S15a) has been recently identified to be differentially up-regulated in 110 HCC samples relative to the corresponding surrounding normal tissues and linked to poorer survival, increased tumour angiogenesis and growth and its knockdown showed an opposite effect. An additional uS8 (S15a) knockdown study carried out by transducing short hairpin shRPuS8-containing lentivirus showed hepatic cancer cell growth inhibition, colony formation impairment and G_0/G_1 cell cycle arrest (Xu et al., 2014). As such, uS8 (S15a) is deemed to be a potential prognosis biomarker and target for anti-angiogenic therapy for HCC (P. Guo et al., 2018; Xie, Guo, Yu, Wang, & Chen, 2018). Apart from this, a genetically engineered recombinant ribosomal protein uL23 (L23a) and eL31 (L31) clones from giant panda (*Ailuropoda melanoleuca*) have been shown to possess anti-cancer properties in terms of inhibiting cell growth and proliferation of human HCC cells, though its exact molecular mechanism remains poorly understood (Su et al., 2012; Sun et al., 2012).

In gastric cancer tissues and cell lines, ribosome protein eL13 (L13) is significantly up-regulated and is associated, through siRNA knockdown of eL13 (L13), to enhanced cancer cell growth and proliferation, increased cellular chemosensitivity and the progression of clinical staging of gastric cancers (Kobayashi et al., 2006). Likewise, eL15 (L15) expression is dramatically overexpressed in gastric cancer cell lines and tissues and its attenuation with siRNA represses cancer cell growth *in vitro* and tumorigenicity in nude mice *in vivo* (Wang et al., 2006). IHC staining revealed the overexpression of eL6 (L6) and uS15 (S13) proteins in gastric cancer tissues than in normal gastric mucosa and their differential expression is correlated to accelerated growth and colony forming ability and the circumvention of cell cycle arrest of gastric cells *in vitro* (Gou et al., 2010; Guo et al., 2011). The expression of

eL34 (L34) is found to be highly elevated in gastric cancer cell lines and siRNA knockdown reduced cell proliferation, arrested cell cycle progression at S phase and increased apoptosis (Liu et al., 2015). In terms of targeted therapy, adenovirus-mediated delivery of exogenous uL14 (L23) successfully inhibits the growth and proliferation of gastric cancer cells *in vitro* and *in vivo* by inhibiting MDM2-p53 ubiquitination and stabilizing p53 and inducing p53-dependent cell cycle arrest and apoptosis (Zhang, Shi, et al., 2010).

For prostate cancer, ribosomal protein eL19 (L19) mRNA levels are up-regulated 5-fold and 8-fold in malignant cell lines and tissues, respectively, contributing to shorter overall survival (Bee et al., 2006). The knockdown of this gene reduces tumour growth and reverses the malignant phenotype of the cancer (Bee et al., 2011). Ribosomal protein uS5 (S2), eS19 (S19), eS21 (S21) and eS24 (S24) are also up-regulated in prostate cancer cell lines and tumour specimens, suggesting that these genes could be novel diagnostic markers for prostate cancer. Therapeutically, a 'ribozyme-like' motif oligonucleotide, DNAZYM-1P, has been developed to target and decrease uS5 (S2) expression in malignant prostate cells. DNAZYM-1P successfully diminished cell growth and induced apoptosis in prostate cancer cells but had little to no effect on normal prostate cells *in vitro* and inhibited tumour growth and metastasis and eventually eradicated tumours *in vivo*. In a dose-dependent manner, DNAZYM-1P increased disease-free survival rates in tumour-bearing mice (Wang et al., 2009).

Besides those aforementioned cancers, the expression of ribosomal proteins has roles in other cancer types as well and can be referred to in Table 2.6. These findings reveal the diagnostic and prognostic significance of ribosomal proteins in a wide variety of carcinomas

and their potential as novel drug targets.

2.3.2.5.2 Ribosomal Proteins in NPC

The differential expression of ribosomal proteins represents a unique pattern of both down-regulation and up-regulation. Suppression subtractive hybridization (SSH) and reverse northern blot screenings demonstrate the up-regulation of ribosomal proteins eL21 (L21) in a metastatic nasopharyngeal cancer cell line (Yang et al., 2005). In contrast, GeneFishing Differential Expressed Genes (DEG) on NPC biopsy tissues and adjacent non-tumour specimens reveals a conflicting under-expression trend of eS26 (S26), eS27 (S27) and eL32 (L32) (Sim, Toh, & Tiong, 2008). However, our subsequent work with real-time quantitative polymerase chain reaction (qPCR) negates previous findings as no associations were established between transcript expression levels with clinicopathological parameters studied (Ma et al., 2012). In addition to that, microarray analyses conducted in that study reveals six differentially expressed RP genes in primary tissues, which are *uS3 (S3), eS7 (S7), uS19 (S15), eL14 (L14), eL32 (L32),* and *eL34 (L34).* However, further validation analysis with real-time qPCR shows only *uS19 (S15)* is statistically under-expressed in tumour samples. Currently, further work on the functional implication of the dysregulation of *uS19 (S15)* expression in NPC is being conducted in lab. In a subsequent study, ribosomal proteins eL27 (L27), eL41 (L41) and eL43 (L37a) mRNAs and proteins are over-expressed in NPC cell lines compared to normal nasopharyngeal epithelial cell line (Sim et al., 2016). This contradiction puts forth a possible scenario of distinct ribosomal protein expression patterns in regard to the use of cell lines with different NPC histopathological classifications.

2.3.2.6 Ribosomal Proteins in Stress-Induced p53-Dependent and Independent Pathways

The dysregulation of ribosomal proteins has been linked to the onset and progression of various genetic disorders and cancers. As an overall trend, the slightest perturbation of ribosome biogenesis and protein translation results in nucleolar stress that would thereupon affect cell cycle progression and growth, inducing unfavourable malignant transformation. Several intrinsic and extrinsic factors have been identified to be capable of disrupting ribosomal biogenesis and triggering ribosomal stress, such as serum or nutrient deprivation, cell contact inhibition, DNA damage (following UV irradiation or by inhibitory drugs), temperature change, hypoxia, osmotic stress, viral infection, rRNA and RPs transcription alterations (Boulon, Westman, Hutten, Boisvert, & Lamond, 2010).

In response to cellular stress, nuclear composition is altered with the redistribution of nucleolar proteins to the cytoplasm, nuclear architecture is remodelled by nucleolar segregation characterized by the condensation and segregation of the nucleolar fibrillar centre (FC) and the granular component (GC), ribosomal biogenesis is disrupted with the down-regulation of rRNA and RPs transcription, and stress response pathway mediators are activated (Shav-Tal et al., 2005). Many of these stress response pathways that translates stress signals into cellular responses link the nucleolus integrity to the stabilization and activation of the tumour suppressor gene and protein, p53, and induction of p53-dependent cell cycle arrest (Boulon et al., 2010). However, there have been increasing evidence supporting the notion that stress-induced cellular responses are not only triggered exclusively by the highly complex and interconnected p53-dependent pathways, but also by several p53-independent pathways, which will be described in this section (Donati,

Montanaro, & Derenzini, 2012).

2.3.2.6.1 p53-Dependent Pathways

A well-known tumour suppressor and cellular gatekeeper, p53, regulates a myriad of downstream target genes whose protein products mediate cellular growth, proliferation, division, cell cycle arrest, senescence and DNA repair, protecting cells from tumorigenic transformation. Even with the most stringent surveillance system in place, cells are capable of circumventing said system and adopt oncogenic phenotypes by mutations within *TP53*, which encodes for p53, or by the activation of p53-inhibitory proteins.

One of the primary negative regulators of p53 expression is mouse double minute 2 homolog, MDM2 (previously discussed in Chapter 2.2.2.1.1), which forms an autoregulatory negative feedback loop with p53. In normal cells, p53 levels are kept at a basal level by the negative feedback mechanism, in which p53 activates the expression of MDM2, which in turn, targets p53 for ubiquitination and proteasomal degradation (Picksley & Lane, 1993). In response to external or internal stress, the inhibitory action of MDM2 on p53 is relieved by a number of cellular and epigenetic mechanisms. DNA damage, an intrinsic stress perpetrator, stabilizes p53 via the inhibition of MDM2-mediated p53 ubiquitination by the phosphorylation of MDM2 at Ser395 or by the activation of $SCF^{\beta\text{-}TRCP}$ ubiquitin ligase complex that targets phosphorylated MDM2 for destruction (Maya et al., 2001; Inuzuka et al., 2010). Besides site-specific phosphorylation, DNA damage leads to acetylation of lysine residues at the C-terminus of p53, protecting it from MDM2-mediated ubiquitination thus, increasing its half-life *in vivo* (Li, Luo, Brooks, & Gu, 2002). Oncogenic stress, often associated with the up-regulation of oncoproteins such as Ras (resistance to audiogenic seizures) and c-Myc

(cellular myelocytomatosis oncogene), is another example of intrinsic stress that could lead to p53 stabilization. These oncoproteins enhance the expression of alternate reading frame tumour suppressor protein (ARF), which sequesters MDM2 and inhibits its p53 ubiquitination activity (Weber, Taylor, Roussel, Sherr, & Bar-Sagi, 1999). These findings tie the inhibitory effect of MDM2 to the stabilization and activation of p53 in response to cellular or ribosomal stress. The question remains, do ribosomal proteins come into play along the MDM2-p53 mechanism?

Increasing evidence thus far has linked various ribosomal proteins as regulators of the RPs-MDM2-p53 pathway, which represents one of the surveillance systems that monitors nucleolar integrity of ribosome biosynthesis. Ribosomal proteins and p53 are direct site-competitors for the central region of MDM2, which comprises of an acidic domain and a zinc finger domain (Nag, Qin, Srivenugopal, Wang, & Zhang, 2013). With the binding of hydrophilic residues on ribosomal proteins, such as uL5 (L11) to the central acidic portion of MDM2, a tertiary structure conformation change within that region abates its binding capacity to p53 and impairs its ubiquitination activity on p53 (Zhang, Chai, Hoang, & Lu, 2011). As previously described in Chapter 2.3.1.2, ribosomal protein uL18 (L5) and uL5 (L11) complexes with 5S rRNA and other auxiliary cofactors before nucleolus importation. However, due to disrupted ribosome synthesis, the uL18-uL5-5S rRNA complex takes on a secondary role and is redirected from its primary course towards pre-ribosome assembly to being a part of an MDM2 inhibitory complex that stabilizes p53 (Donati et al., 2013). One of those cofactors has been identified to be interacting with both uL18 (L5) and uL5 (L11), individually, is singular protein MDM2 and as a complex with p53 in murine cells, therefore inhibiting MDM2-mediated ubiquitination of p53, which in turn induces G_1 cell cycle arrest

(Dai & Lu, 2004; Marechal, Elenbaas, Piette, Nicolas, & Levine, 1994; Zhang et al., 2003).

Besides those ribosomal proteins mentioned above, other ribosomal proteins have also been found to also modulate this network. Those ribosomal proteins such as uS3 (S3), eS7 (S7), uS10 (S20), uS11 (S14), uS19 (S15), eS25 (S25), eS26 (S26), eS27 (S27), eS31 (S27a), eL6 (L6), uL4 (L4), uL14 (L23), uL24 (L26), eL24 (L24), and eL37 (L37) exhibit similar, but not identical, mechanisms in the regulation of p53 via the MDM2-mediated pathway (Takagi, Absalon, McLure, & Kastan, 2005; Chen et al., 2007; Yadavilli et al., 2009; Wang, et al., 2010; Sun et al., 2011; Xiong et al., 2011; Zhang et al., 2013; Zhang, Daftuar et al., 2013; Zhou, Hao, Liao, Zhang, et al., 2013; Bai et al., 2014; Cui et al., 2014; He, Li, Dai, & Sun, 2016; Meng et al., 2016).

Besides the MDM2-p53 network, ribosomal proteins exert their p53-dependent functionality through other modulators of the p53 pathway, independent of MDM2 binding (Miliani de Marval & Zhang, 2011). Based on a loss-of-function genetic screening, a cluster of ribosomal proteins was shown to directly regulate p53 function via its translational control in the absence of MDM2 (Castro, Leal, Lleonart, Ramon, & Carnero, 2008). Furthermore, uL24 (L26) binds to the 5'-UTR of p53 mRNA and stimulate its translation in response to DNA damage, demonstrating the direct control of ribosomal proteins on p53 translation after the induction of DNA damage (Takagi et al., 2005; Chen, Guo, & Kastan, 2012). In contrast to the established pattern of p53 stabilization due to elevated ribosomal protein expression, eL22 (L22) deficiency stimulates the up-regulation of p53 in αβ-lineage T cells via translational control, suggesting the possibility of cell type-specific, stage-specific and stress-specific functions of ribosomal proteins (Anderson et al., 2007).

2.3.2.6.2 p53-Independent Pathways

The concerted effect on cell growth, proliferation and apoptosis is coordinated by both p53-dependent and p53-independent pathways. Besides being a mediator in the MDM2-p53 pathway, uL5 (L11) plays a secondary role in regulating the expressions of both oncogenic c-Myc and its downstream target genes, such as transcription factor *E2F2* and 5S rRNA during ribosomal stress scenarios. As a response to ribosomal stress, uL5 (L11), co-operatively with uL18 (L5), targets c-Myc mRNA for degradation by RNA-induced silencing complex (RISC) via a feedback mechanism by binding to its 3-UTR and thereby promoting c-Myc mRNA decay and protein turnover (Figure 2.6A) (Dai et al., 2007; Liao, Zhou, Gatignol, & Lu, 2014). On top of that, uL5 (L11) inhibits c-Myc-dependent transcription of target genes by sequestering c-Myc from binding to its co-activator, transformation/ transcription domain-associated protein (TRRAP), in which its recruitment to the promoter region is necessary for the transcription of c-Myc target genes (Figure 2.6B) (Dai, Sun, & Lu, 2010). In a separate study, uS11 (S14) has been shown to function similarly as uL5 (L11) in negatively regulating c-Myc in response to cellular stress (Figure 2.6A) (Zhou, Hao, Liao, Liao, & Lu, 2013). Taken together, a subset of ribosomal proteins is involved in p53-independent pathways via its interaction with c-Myc and its mRNA and as such, decreasing cell proliferation under nucleolar stress.

A potential ribosomal stress sensor, pro-viral integration site for Moloney murine leukaemia virus 1 (PIM1) kinase, has been associated with ribosomal protein eS19 (S19). eS19 (S19) knockdown by RNAi substantially destabilizes PIM1, which in turns activates cyclin-dependent kinase inhibitor $p27^{Kip1}$ and blocks cell cycle progression and cell proliferation in the absence of p53 (Figure 2.6C) (Iadevaia et al., 2010). Addedly, eS7 (S7) has recently been

portrayed to regulate, and to be regulated by, kinase PIM1 via the c-Myc-eS7 (S7) ribosomal stress pathway in reducing cell growth *in vitro* and *in vivo* (Zhang et al., 2018). Activating transcription factor 4 (ATF4) is a stress-induced pro-survival transcription factor that is commonly found to be up-regulated in cancer cells. Under normal physiological conditions, ATF4 regulates an array of adaptive genes that render cells the ability to withstand stressful conditions such as hypoxia or amino acid limitation (Wortel, van der Meer, Kilberg, & van Leeuwen, 2017). However, under extreme duress, eL41 (L41) induces the translocation from nucleus to cytoplasm and the rapid degradation of ATF4 by tagging it via phosphorylation at serine 219, and thus inhibiting proliferation and promoting apoptosis via a p53-independent pathway (Figure 2.6D) (Wang et al., 2011; Geng, Qin, Ren, Xu, & Wang, 2018).

Ribosomal protein uL14 (L23) is a negative regulator of Myc-associated zinc-finger protein, Miz-1 by putatively sequestering its co-activator, nucleophosmin (NPM1). Under ribosomal stress when uL14 (L23) is depleted, Miz-1 is activated and induces the Myc-dependent transcription of cell-cycle inhibitors, p15 and p21, causing arrested cell cycle progression and proliferation (Figure 2.6E) (Wanzel et al., 2008; Wiese et al., 2013). Various ribosomal proteins are capable of interacting and regulating tumour suppressor proteins, other than p53, such as p21 and p73. Ribosomal protein uL3 (L3), with transcription factor Sp1, positively regulates p21 expression and the up-regulated expression of p21 activates G_1/S cell cycle arrest and apoptosis via the mitochondrial apoptosis pathway (Figure 2.6F) (Russo et al., 2013). Moreover, uL24 (L26) stabilizes p73 protein and promotes p73 mRNA translation by binding directly to its 3'-UTR region and recruiting eukaryotic translation initiation factor, eIF4E, consequently inducing p53-independent cell cycle arrest and apoptosis (Figure 2.6G) (Harms & Chen, 2006; Zhang, Zhang, Yan, & Chen, 2016).

Growth arrest and DNA damage-inducible gene 45α (GADD45α) transcript expression is commonly up-regulated in response to ribosomal stress due to stressful growth arrest conditions and treatment with mutagens and is mediated by both p53-dependent and independent mechanisms. Ribosomal protein eS7 (S7) complexes with GADD45α and by doing so, prevents the MDM2-mediated ubiquitination and degradation of GADD45α (Gao et al., 2013). As such, GADD45α induces apoptosis through JNK-dependent and p53-independent pathways (Figure 2.6H) (Salvador, Brown-Clay, & Fornace, 2013; Ueda, Kohama, Kuge, Kido, & Sakurai, 2017). In addition, ribosomal protein eS27 (S27), also known as metallopanstimulin-1 (MPS-1), is a positive regulator of the NF-κB pathway by promoting phosphorylation of p65 at Ser536 and inhibitory protein IκBα at Ser32, both of which are necessary for NF-κB nuclear translocation and transcription of downstream target genes involved in cellular apoptosis, one of which is GADD45β (Figure 2.6I) (Yang et al., 2012).

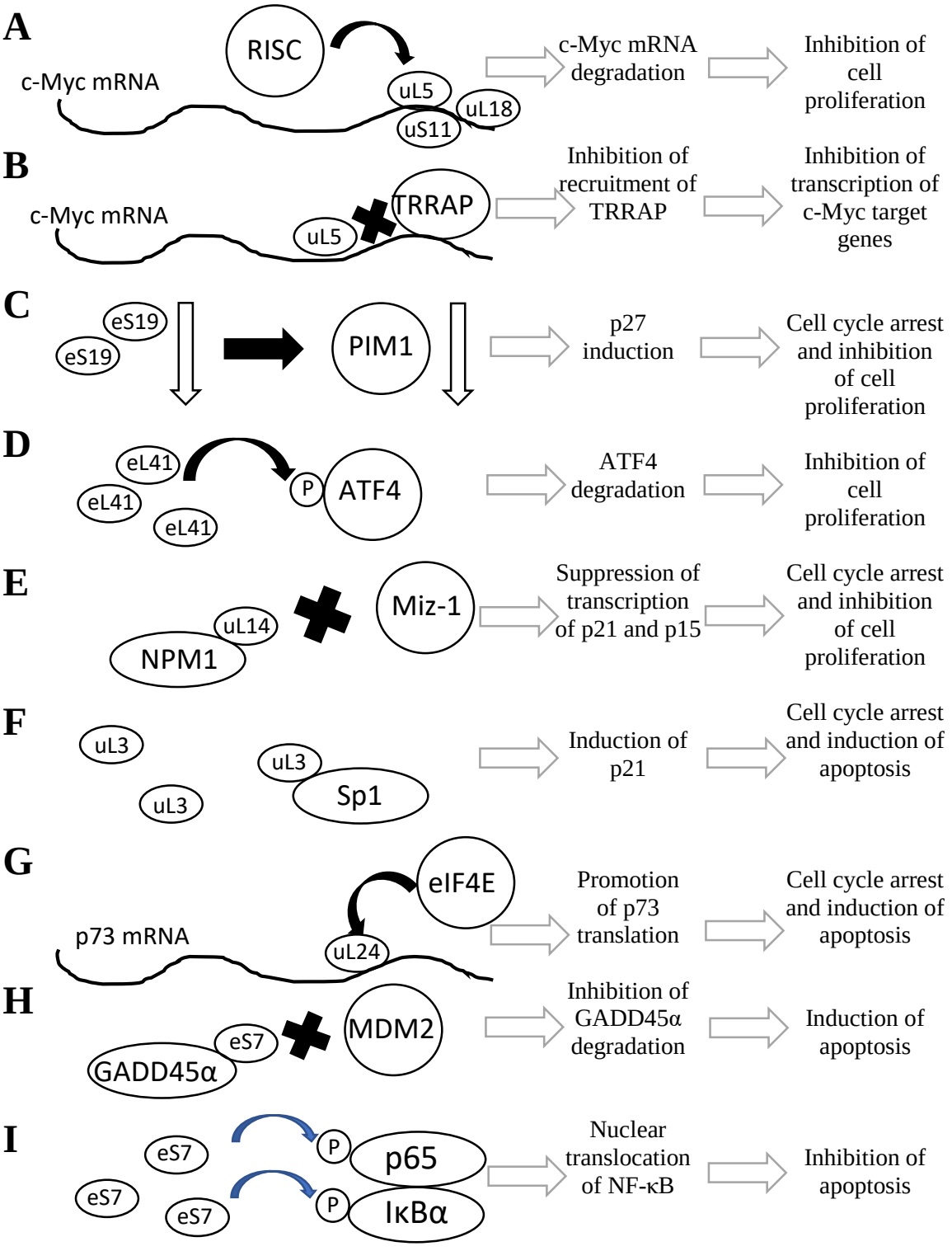

Figure 2.6: p53-independent functions of ribosomal proteins. (A) and (B) c-Myc inhibition pathways. (C) p27 induction via PIM-associated pathway. (D) Degradation of ATF4. (E) Inhibition of Miz-1-dependent transcription. (F) Up-regulation of p21. (G) Stabilization of p73. (H) Inhibition of GADD45α. (I) Activation of NF-κB-mediated pathways.

2.4 Target Proteins of Interest

Below discuss the target proteins of interest in this study, in terms of their respective genomic location, existing transcript variants and protein isoforms, internal ribosomal roles, extra-ribosomal functions as well as their differential expressions in development diseases or cancers.

2.4.1 Ribosomal Protein uS4 (S9)

Ribosomal protein uS4 (S9), a component of the small 40S ribosomal subunit, is encoded by six-exons spanning *RPiS4 (S9)* located on chromosome 19q13.42 (Gene ID: 6203). Due to its highly spliced nature, there are a total of six transcript variants and additional two longer variants with non-coding mRNA introns. A study on the diverse alternatively-spliced *uS4 (S9)* in *Saccharomyces cerevisiae*, *Drosophila melanogaster* and *Homo sapiens* reported the highly conservative *uS4 (S9)* introns within mRNA variants across species and denoted that the introns autoregulate gene expression by means of multiple forms of alternative splicing, thus resulting in numerous transcript variants of *uS4 (S9)* (Plocik & Guthrie, 2012).

In its niche, uS4 (S9) plays a seminal role in the early steps of ribosome assembly as it is one of the first proteins that interact directly with the 18S rRNA (O'Donohue et al., 2010). Silencing of uS4 (S9) results in the accumulation of nucleolar 45S and 30S pre-rRNAs and the subsequent reduction in global protein synthesis. This is due to the impairment in the 18S rRNA processing and maturation pathway as well the induction of p53-mediated G_1 cell cycle arrest and/or apoptosis (Ferreira-Cerca, Poll, Gleizes, Tschochner, & Milkereit, 2005; Lindström & Nistér, 2010). Besides ribosome assembly, uS4 (S9) has been associated in translation elongation and fidelity due to its location at the tip of the small ribosomal subunit,

forming the ‘gate’ into the ribosomal peptidyl transfer centre (PTC) tunnel that leads to the decoding centre, and its ability in mRNA unwinding before entry (Ben-Shem et al., 2011). Apart from its ribosomal responsibilities, uS4 (S9) associates with a multifunctional nucleolar protein, nucleophosmin (NPM1/B23) via an intermediary ARF protein and is involved in various cellular pathways such as ribosomal biogenesis and cell proliferation via interaction with tumour suppressor ARF (Bertwistle, M. Sugimoto, & C.J. Sherr, 2004b).

The under-regulated expression of uS4 (S9) has been observed in primary cells from patients diagnosed with Schwachman Diamond Syndrome (SDS) as well as in invasive breast tumours, anaplastic astrocytoma and pancreatic cancer tissues (Burwick, Shimamura, & Liu, 2011). In contrast, both transcript and protein expression of uS4 (S9) are up-regulated in human osteosarcoma tissues and cell lines and positively correlates with cancer staging and recurrence (Cheng et al., 2017). uS4 (S9) mRNA is also found to be highly expressed in colorectal carcinoma though there is no clear correlation to the severity of the cancer (Frigerio, Dagorn, & Iovanna, 1995). Interestingly, the constitutively consistent expression of uS4 (S9) in adenoid cystic carcinoma and lung adenocarcinoma renders its role as a housekeeping gene (Huang et al., 2003; Li et al., 2014).

The aberrant expression in colon cancer has been translated into a target for cancer therapy. Apigenin, a naturally occurring compound, is known to possess anti-tumour properties and inhibits tumour growth by the induction of G_1 or G_2/M cell cycle arrest. uS4 (S9) is a direct target of apigenin and this interaction induces G_2/M cell cycle arrest via the down-regulation of CDK1 expression (Iizumi et al., 2013).

2.4.2 Ribosomal Protein eS8 (S8)

Ribosomal protein eS8 (S8), a member of the 40S small ribosomal subunit, is encoded by six-exons spanning *RPeS8 (S)* located on chromosome 1p34.1 (Gene ID: 6202). It is co-transcribed with four small nucleolar RNA genes (snoRNAs), *U38A, U38B, U39* and *U40*, which are located on introns four, five, one and two, respectively.

Being a component of the ribosome, eS8 (S8) primary roles are as rRNA-binding proteins and for ribosome stabilization (Davies & Fried, 1993). During ribosome assembly, several residues on eS8 (S8), particularly Glu89, interact with 28S rRNA, forming an inter-subunit bridge (Khatter et al., 2015). Under genotoxic conditions, Glu89 is extensively ADP-ribosylated resulting in possible steric hindrance and/or charge repulsion scenarios that disrupt ribosome assembly (Zhen, Zhang, & Yu, 2017). eS8 (S8) has been reported to associate and synergize with CDK11p46, a key mediator of cell apoptosis, *in vitro* and *in vivo*, to inhibit protein synthesis via the internal ribosomal entry site (IRES) pathway and sensitizes cells to Fas ligand-induced cellular apoptosis (Hao et al., 2011).

Overexpression of eS8 (S8) mRNA has been detected in breast and liver cancer as well as in colon polyps and adenocarcinoma (Pogue-Geile et al., 1991; Kondoh et al., 2001). In contrast, a conflicting under-expression of eS8 (S8) protein expression was detected with IHC on human colorectal mucosa when compared to normal epithelia of human colorectal mucosa and correlates to the maturation of mucosal cells (Kasai et al., 2003). In a large scale gene expression profiling, the under-expression of eS8 (S8) mRNA in meningiomas brain tumours relative to nontumoral meningothelial tissues correlates to malignant progression and recurrence of meningioma (Pérez-Magán et al., 2010).

2.4.3 Ribosomal Protein eS31 (S27a)

Last of the three target ribosomal proteins of the small 40S subunit, eS31 (S27a) is encoded by seven-exons spanning *eS31 (S27a)* on chromosome 2p16.1 (Gene ID: 6233). Three alternatively spliced transcript variants are known to exist and all three encodes for the same protein isoform.

eS31 (S27a), an ubiquitin (Ub) C-terminal extension protein (CEP), is expressed as a fusion protein with ubiquitin at the N-terminus, forming a precursor protein, Uba-S27a, that must be proteolytically processed to produce mature ubiquitin capable of targeting downstream regulatory proteins for degradation by the 26S proteasome (Kirschner & Stratakis, 2000). Working together with three other Ub fusion proteins, Uba-L41, Ubb and Ubc, Ub-S27a makes up the pool of cellular ubiquitin proteins that is vital in a wide variety of regulatory processes, including ribosome biogenesis, cell cycle and proliferation, apoptosis, differentiation and development (Myung, Kim, & Crews, 2001).

Besides that, monomer ribosomal protein eS31 (S27a) interacts with the central acidic domain of MDM2 and represses MDM2-mediated p53 ubiquitination. Knockdown of eS31 (S27a) significantly reduces p53 activation in response to ribosomal stress-inducing agents such as actinomycin-D or 5-FU, suggesting its role as a novel stress sensor in activating cell cycle arrest (Sun et al., 2011). A subsequent study identified eS31 (S27a) as a direct transcriptional target of p53, revealing an autoregulatory loop between eS31 (S27a) and p53 expression levels under stressful conditions (Nosrati, Kapoor, & Kumar, 2015). Besides that, in EBV-infected cells, eS31 (S27a) directly binds to and stabilizes LMP1 *in vitro* and *in vivo* by inhibiting proteasomal ubiquitination of LMP1 and promoting LMP1-mediated

proliferation and invasion (Hong, Kim, Jin, Kim, & Hur, 2017).

eS31 (S27a) is up-regulated in colorectal tumour tissues, rapidly proliferating renal cancer cells and prostate tumours (Kanayama et al., 1991; Wong et al., 1993). eS31 (S27a) has also been found to be drastically over-expressed in advanced-phase chronic myeloid leukaemia (CML) and acute leukaemia (AL) solid tumours as well as established CML cell lines and it is correlated to increased cellular proliferation and cell cycle progression (Wang et al., 2014). One of the most effective target drugs for CML is tyrosine kinase inhibitor (TKI) imatinib though drug resistance to imatinib remains a complication in its clinical application. Interestingly, the up-regulation of eS31 (S27a) is markedly higher in imatinib-resistant CML patients than those who are imatinib responsive, and *in vivo* studies have confirmed that eS31 (S27a), via transactivation by p-STAT3, inhibits the apoptotic effect of imatinib on leukemic cells, making it a potential molecular target for CML therapy (Wang et al., 2016). In breast cancer, the expression of eS31 (S27a) is significantly higher in benign fibroadenomas compared to malignant carcinoma breast tissues, implying the inverse role of eS31 (S27a) in tumour transformation (Adams, Sharp, Walker, Brammar, & Varley, 1992). A similar trend is observed in hepatocellular carcinoma, in which the expression of eS31 (S27a) is higher in liver cirrhosis tissues when compared to malignant hepatocellular tumours (Gunasekaran & Ganeshan, 2014).

2.4.4 Ribosomal Protein eL6 (L6)

A component of the large 60S ribosomal subunit, eL6 (L6) ribosomal protein is encoded by twelve-exons spanning *eL6 (L6)* gene residing on chromosome 12q24.13 (Gene ID: 6128). Due to the considerable number of exon and intron segments, a total of eight different

alternatively spliced transcript variants have been identified, which encode for two slightly similar protein isoforms (288aa and 177aa). The shorter protein isoform (177aa) lacks an N-terminal domain but contains an essential binding site for ribosomal protein eL14 (L14) for ribosomal assembly. Within the ribosome, eL6 (L6) acts as a 'foundational cornerstone' for the architecture of the back cluster of the large subunit and serves to interact and stabilize various RNA expansion segments and ribosomal protein eL14 (L14) (Klinge et al., 2011).

eL6 (L6) has been identified as an intracellular binding partner for basic fibroblast growth factor (FGF-2 or FGF-β), implying its extra-ribosomal roles in cell growth, proliferation and differentiation, angiogenesis and tumour invasion (Shen, Arese, Gualandris, & Rifkin, 1998). eL6 (L6) is also one of the ribosomal protein binding regulators of the MDM2-p53 pathway, whereby eL6 (L6) binds and suppresses the E3 ubiquitin ligase activity of MDM2 resulting in p53-mediated cell cycle arrest and cell growth inhibition (Bai et al., 2014). Recently, a study reveals a novel role of eL6 (L6) in immunosurveillance, in which the knockdown of eL6 (L6) decreases ubiquitin-dependent peptide presentation on MHC class I antigen presenting cells, thus decreasing T cell targeting and elimination of tumour cells (Wei et al., 2019). In addition to that, another recent report unveils yet another extra-ribosomal function of eL6 (L6) in DNA damage response pathway via its interaction, tested *in vitro* and *in vivo*, to histone H2A, a histone protein mainly involved in DNA folding into chromatin in the nucleosome. The ablation of eL6 (L6) reduces the subsequent recruitment and accumulation of downstream repair proteins at DNA damage sites, resulting in a faulty G_2/M cell cycle arrest, DNA damage repair and cellular survival (Yang et al., 2019).

In Schwachman-Diamond Syndrome, eL6 (L6) is under-expressed in bone marrow cells

from patients diagnosed with SDS, implicating dysregulated ribosome biogenesis and RNA processing in SDS progression (Rujkijyanont, Adams, Beyene, & Dror, 2009). In contrast, eL6 (L6) transcript and protein levels are up-regulated in gastric cancer tissues relative to normal gastric mucosa and positively correlates to the acceleration of tumour growth, enhancement of colony forming ability and induction of cell cycle progression (Gou et al., 2010). Similarly, the overexpression of eL6 (L6) in multi-drug resistant gastric cancer cell lines is associated with enhanced resistance to anticancer drugs and drug-induced apoptosis (Du et al., 2005). A study to investigate differentially expressed genes in penile cancer reported the overexpression of eL6 (L6) in high-risk human papillomavirus (HPV) positive penile carcinoma but no significant overexpression was observed between penile squamous cell carcinoma with respect to normal penile tissues, suggesting the role of eL6 (L6) in association with HPV-induced penile cancer progression (Calmon et al., 2013).

2.4.5 Ribosomal protein uL14 (L23)

Also a component of the large 60S ribosomal subunit, ribosomal protein uL14 (L23) is encoded by five-exons spanning *uL14 (L23)* gene located on chromosome 17q12 (Gene ID: 9349). Due to the lack of transcript variants, *uL14 (L23)* is expressed as a single protein isoform. Crystallographic structure of the eukaryotic large 60S subunit reveals the pivotal role of uL14 (L23) in its association with translation initiation factor, ElF6, that functions as a ribosome anti-association factor when it is in complex with pre-60S ribosomal subunit. Defects within uL14 (L23) destabilizes 60S subunit biogenesis, attenuates ribosomal subunit shuttling from the nucleolus to the cytoplasm and subsequently decreases mature ribosome assembly and maturation (Benelli et al., 2009; Klinge et al., 2011).

Ribosomal protein uL14 (L23) has been found to exert its extra-ribosomal function by regulating the expression of Miz-1, a mediator in Myc-dependent tumorigenesis. Under nucleolar stress, the depletion of uL14 (L23) fails to sequester nucleophosmin, a co-activator of Miz-1, thereby activating Miz-1 and Myc-dependent transcription of cell cycle inhibitors, p15 and p21, resulting in blocked cell cycle progression and cell proliferation in osteosarcoma cells (Wanzel et al., 2008; Wiese et al., 2013).

uL14 (L23) up-regulation associates with higher-risk apoptotic-resistant myelodysplastic syndrome (MDS) and its knockdown reduced cell viability, increased G_1/S cell cycle arrest and apoptosis via the Miz-1/c-Myc regulatory circuit (Qi et al., 2017). Similarly, uL14 (L23) is up-regulated in squamous cell carcinoma of the head and neck (SCCHN) tissues and cell lines and the exogenous over-expression of uL14 (L23) in non-malignant cell results in carcinogenic transformation, making it a potential biomarker for SCCHN (Russo et al., 2013). uL14 (L23) is also identified as an up-regulated factor in multidrug-resistance gastric cancer cells, demonstrating the role of uL14 (L23) in suppressing drug-induced apoptosis and cell transformation (Shi et al., 2004). On the other hand, a large-scale microarray identification of differentially expressed genes in serous epithelial ovarian cancer (SEOC) relative to normal ovarian tissues reports on the down-regulation of uL14 (L23) (Grisaru et al., 2007).

uL14 (L23) has been the attention of several studies to delineate potential therapeutic targets in various cancers. For instance, adenovirus-mediated delivery of exogenous uL14 (L23) into cultured human colorectal carcinoma cells stimulates the accumulation of wild-type p53 protein and as a result, suppresses tumour cell growth and induces cell cycle arrest and

apoptosis (Fang et al., 2015). A similar study on human gastric cancer shows comparable results to that done on colorectal carcinoma, suggesting the prospect of uL14 (L23) as a novel therapeutic molecular target in cancer treatment (Zhang et al., 2013).

2.4.6 Ribosomal Protein eL18 (L18)

Another component of the 60S large ribosomal subunit of interest is eL18 (L18) that is encoded by seven-exons spanning *eL18 (L18)* gene located on chromosome 19q13.33 (Gene ID: 6141). Alternative splicing results in three distinct transcript variants encoding multiple protein isoforms. eL18 (L18) facilitates the release of uL4 (L4) from its nuclear import chaperone protein and its incorporation into pre-60S ribosome subunit and mutations within the hydrophobic interacting domain of eL18 (L18) delays pre-60S ribosome assembly (Stelter et al., 2015).

eL18 (L18) is under-regulated in Diamond-Blackfan Anaemia (DBA) specimens containing *uS4 (S9)* mutation, which is found in 25% of DBA cases, thereby associating eL18 (L18) in oncogenic pathways in DBA (Gazda et al., 2006). A reverse expression trend is observed in colorectal carcinoma whereby the expression of eL18 (L18) mRNA has been reported to be overexpressed but it is not correlated to CLC cancer staging while no differential expression of eL18 (L18) is observed in gastric and hepatocellular carcinomas (Barnard et al., 1993; Kitahara et al., 2001). However, a subsequent study on the protein expression level of eL18 (L18) via IHC reports the under-expression this protein in colorectal carcinoma cells in respect to normal colorectal mucosa and its expression is observed to be relatively higher, though not significantly, in well-differentiated carcinoma than in moderately differentiated carcinoma (Kasai et al., 2003). On the other hand, genome-wide transcriptomics study on

lymphoblastoid cell lines validates the use of eL18 (L18) as an internal reference for expression studies in LCLs due to its constitutively enhanced expression levels with minimal variations across independent LCL specimens and cell lines (Vincent et al., 2012).

2.4.7 Ribosomal Protein eL24 (L24)

Another component of the large 60S ribosome subunit, eL24 (L24) is encoded by six-exons spanning *eL24 (L24)* gene located on chromosome 3q12.3 (Gene ID: 6152). Since there have been no multiple transcript variants detected, eL24 (L24) is expressed as a single protein isoform. Similar to uL14 (L23), ribosomal protein eL24 (L24) is topologically in close association with eukaryotic translation initiation factor, EIF6 and its depletion results in failure of ribosome assembly and inefficient cap-dependent mRNA translation (Zhou, Roy, & von Arnim, 2010; Klinge et al., 2011).

Not only does its association with EIF6 ties the role of eL24 (L24) to the tightly regulated ribosomal assembly and its functionality, but also implicates it in cellular pathways such as cell proliferation, survival and genome repair and integrity via cyclin D1, survivin and nibrin (NBS1), respectively (Wilson-Edell et al., 2014).

The transcription of eL24 (L24) is found to be higher in a drug-resistant liver carcinoma cell line, granting a possibility of the involvement of eL24 (L24) in drug resistance mechanisms in the progression of HCC (Guo, Kong, Liu, & Tan, 2014). Following a similar trend, the up-regulation of eL24 (L24) in human breast cancers compared to normal mammary tissue could be a possible therapeutic target as its depletion or acetylation suppresses polysome assembly and cancer cell growth and proliferation (Wilson-Edell et al., 2014).

2.4.8 Ribosomal Protein eL30 (L30)

Last of the RPs belongs to the large 60S subunit, single protein isoform eL30 (L30) is encoded by five-exons spanning *eL30 (L30)* gene located on chromosome 8q22.2 (Gene ID: 6156). Within the 60S subunit, eL30 (L30) interacts with both ribosomal protein eL43 (L37a) and 25S rRNA at the inter-subunit interface and actively engages in the formation of two inter-subunit bridges, eB9 and B4 (Halic, Becker, Frank, Spahn, & Beckmann, 2005). Interestingly, eL30 (L30) is self-autoregulated during translation by binding of eL30 (L30) protein to its own transcript and inhibiting splicing *in vitro* (Li, Vilardell, & Warner, 1996). Subsequent X-ray crystallography and nuclear magnetic resonance (NMR) studies further confirms this self-protein-transcript interaction (Chao & Williamson, 2004).

In contrast to previously described RPs and their direct interactions with MDM2, eL30 (L30) do not bind to MDM2 and therefore, do not inhibit MDM2-mediated p53 ubiquitination and degradation, establishing that the RPs-MDM2-p53 feedback loop is specific to certain ribosomal proteins, and not all. However, the knockdown of eL30 (L30) markedly activates p53 and the subsequent p53-dependent cell cycle arrest by stabilizing the interaction between uL5 (L11) and uL18 (L5) and MDM2. This shows that eL30 (L30) indirectly regulates the MDM2-p53 pathway in response to perturbation of ribosomal biosynthesis (Sun, Wang, Xirodimas, & Dai, 2010). Besides that, another link between ribosome biogenesis and cell proliferation could be the interaction of eL30 (L30) and ErbB-3-binding protein (EBP1), which is part of the ribonucleoprotein (RNP) complex and functions as a growth-regulating protein (Squatrito, Mancino, Donzelli, Areces, & Draetta, 2004).

In the case of medulloblastoma, various chromosomal alteration has been identified and gain

of chromosome 8q attributes to the worst overall patient survival. Using comparative genomic hybridization (CGH), primary medulloblastoma specimens are analysed for chromosomal copy number to identify differentially expressed genes associated with survival. One of the up-regulated 8q-mapped target genes is eL30 (L30) and it is associated with tumorigenicity in medulloblastoma tumours (De Bortoli et al., 2006). On the other hand, the expression of eL30 (L30) has been validated to be highly constitutively and stably expressed across tumours and matched normal samples of not only head and neck squamous cell carcinoma, but also breast cancer biopsy and oral squamous cell carcinoma samples, making it a suitable internal control for gene expression studies (Martin, 2016; El Hadi et al., 2017; Palve et al., 2018).

2.4.9 Nucleophosmin (NPM1/ B23/ Numatrin)

Nucleophosmin (NPM1), also known as B23 or Numatrin, is encoded by thirteen-exons spanning *NPM1* gene located on chromosome 5q35.1 (Gene ID: 4869). *NPM1* is alternatively spliced into seven known transcript variants that encode for three protein isoforms. NPM1.1 (or B23.1), corresponding to the full-length transcript, is translated into 35-40kDa proteins (294aa in length), are found most abundantly in all tissues (Figure 2.7). In comparison, the translation product of NPM1.3 (or B23.2) excludes the last 35 amino acids constituting the C-terminus of NPM1, in which the nucleolar localization signal (NoLS) is situated. A third isoform without the N-terminal of NPM1 has been identified, though with insufficient biological information. All isoforms contain a highly conserved N-terminal core domain, an acidic domain and a nuclear localization signal (NLS), but only NPM1.1 possesses additional nucleolar localization signal (NoLS) and nuclear export signal (NES) (Lim & Wang, 2006; Platonova, Akey, Head, & Akey, 2011). The N-terminal of

NPM1, which is highly conserved across all isoforms of the nucleophosmin family, mediates the oligomerization of NPM1 and intermolecular binding to interacting proteins. The highly disordered, negatively charged, acidic central domain of NPM1 is responsible for its binding to histone proteins while the basic, positively charged C-terminal contains a DNA/RNA binding domain (Hingorani, Szebeni, & Olson, 2000).

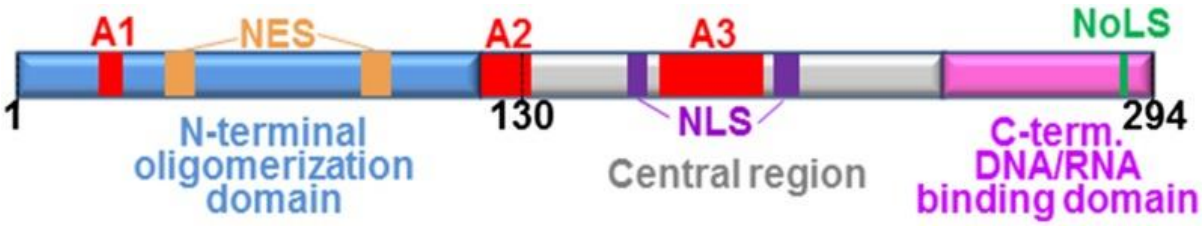

Figure 2.7: Domain structure of NPM1. The three functional regions of NPM1 consist of an N-terminal oligomerization domain with two nuclear export signals (NES) (blue), a central unstructured section with two nuclear localization signals (NLS) (grey), and a C-terminal DNA/RNA binding domain containing a nucleolar localization signal (NoLS) (purple). Three highly conserved acidic regions are denoted in red. Adapted from Mitrea et al. (2014).

NPM1, a member of a histone chaperone family, is primarily detected in the nucleolus though this phosphoprotein chaperones ribosomal proteins and core histones from the nucleus to the cytoplasm, therefore constantly shuttling in and out the nucleolus, nucleoplasm and cytoplasm (Lim & Wang, 2006). The localization of NPM1, leading to its varied functional repertoire, has been attributed to the structural polymorphism in the N-terminal oligomerization domain, switching conformation from highly organized, folded multimeric pentamer to highly unstable, unfolded monomers. The delicate pentamer-monomer equilibrium is regulated by post-translational modification, whereupon phosphorylation disrupts NPM1 oligomerization and leads to the accumulation of monomers, and the scale is reversely tipped towards the native folded state by its binding to its interacting partners (Mitrea et al., 2014).

NPM1 has been implicated in various pathways dictating cellular processes such as histone chaperones, ribosome biosynthesis and transport, DNA repair and genomic integrity and mediating ARF-MDM2-p53 tumour suppressor pathway (Box et al., 2016). The localization of NPM1 dictates its biological function. In its oligomeric form, NPM1 is localized within the nucleolus, which is the site of rRNA transcription, processing, and together with RPs, assembly into pre-ribosomal subunits. Specifically, NPM1 plays a role in the processing of rRNAs, chaperoning the nucleolus importation of ribosomal proteins, sequestering ARF tumour suppressor protein and shuttling of precursor 60S and 40S subunits of the ribosome from the nucleolus to the cytoplasm for subsequent processing and maturation (Bertwistle, M. Sugimoto, & Sherr, 2004a; Maggi et al., 2008; Li & Hann, 2009; Lindström, 2011).

A number of interacting protein partners of NPM1 has been identified. The oligomerization of NPM1 results in its nucleolar localization and hence, the activation of cellular proliferation due to the inability of ARF proteins to bind to MDM2 in the cytoplasm, and by doing so (or the lack of) frees MDM2 to catalyse MDM2-mediated p53 ubiquitination (Koike et al., 2010). Besides that, oligomerization of NPM1 is important for chaperoning the nucleolar import of ribosomal proteins for ribosome assembly. The association of NPM1 and ribosomal protein uS4 (S9) in osteosarcoma cells stimulate nucleolar influx and storage of uS4 (S9) and the depletion of either partner diminishes the level of nucleolar uS4 (S9) (Lindström & Zhang, 2008). On the other hand, the monomeric form of NPM1 dictates its role in apoptosis and DNA damage response by binding to DNA lesions and activating distinct downstream repair pathways corresponding to the nature of damage: homologous recombination for DNA double-strand breaks (DSB), homologous recombination, trans-lesion synthesis or nucleotide excision repair pathways for UV-induced DNA lesions, and

base excision repair pathway for oxidation damage (Wu & Yung, 2002; Lee et al., 2005; Vascotto et al., 2009; Ziv et al., 2014; Jansen, Tsaalbi-Shtylik, & de Wind, 2015).

As described above, the expression of NPM1 is capable of being tumour-suppressive or growth-inducing, therefore it is not surprising that the aberrant expression of NPM1 has been implicated in various diseases and cancers. Genomic perturbation of *NPM1* by mutations, heterozygous deletion, or chromosomal translocation has been associated with hematopoietic disorders, such as acute promyelocytic leukaemia (APL), anaplastic large cell lymphoma (ALCL), and MDS (Naoe, Suzuki, Kiyoi, & Urano, 2006; Qiu, Wan, Wang, & Wang, 2017). In general, NPM1 is always been found to be overexpressed in several solid tumours. In glioblastoma, ovarian cancer and hepatocellular carcinoma (HCC), NPM1 up-regulation is correlated to high-grade tumours and increased resistance to apoptosis (Liu et al., 2012; Londero et al., 2014; Holmberg Olausson, Elsir, Moazemi Goudarzi, Nistér, & Lindström, 2015). Similarly, overexpression of NPM1 in oral squamous cell carcinoma, prostate cancer, salivary gland adenoid cystic carcinoma and colorectal carcinoma (CLC) enhances migration and proliferation of tumour cells, decreases disease-free survival rate and is deemed a potential prognostic marker (Coutinho-Camillo, Lourenço, Nishimoto, Kowalski, & Soares, 2010; Liu et al., 2012; Loubeau et al., 2014; Li, Zhang, Zhou, Huang, & Liu, 2017). In contrast, down-regulation of NPM1 has been observed in gastric cancer compared to non-tumorous adjacent tissues, and in breast cancer, where NPM1 low expression is associated with poor prognosis (Karhemo et al., 2011; Leal et al., 2014).

2.4.10 Basic Transcription Factor 3 (BTF3)

Basic Transcription Factor 3 (BTF3), an essential component required for transcription

initiation of RNA polymerase IIb, is encoded by six-exons spanning *BTF3* gene located on chromosome 5q13.2 (Gene ID: 689). This gene has two transcript variants that encode for two corresponding protein isoforms. The shorter among the two, which is 162aa in length, is transcriptionally inactive. Both isoforms of BTF3 are capable of interacting with protein kinase CK2 *in vitro* and *in vivo*, hence denoting its role in cell cycle control and DNA repair (Grein & Pyerin, 1999). Also, BTF3 acts as one of the intermediary effectors for the target genes transcription of estrogen receptor (ER) via its transactivation function, AF-1, inducing cell proliferation (Green, Thompson, Johnston, & El-Tanani, 2007).

BTF3 is overexpressed in glioblastoma multiforme, a highly invasive and aggressive form of brain astrocytoma, representing its role in the malignant progression and as a potential marker for tumour staging of this cancer (Odreman et al., 2005). Additionally, BTF3's potential as an early stage marker is reported in CRC (Wang et al., 2013). Moreover, BTF3 overexpression has been found in pancreatic ductal adenocarcinoma and prostate cancer (Kusumawidjaja et al., 2007; Wang, Lu, Fang, & Yao, 2007; Symes et al., 2013). The significant up-regulation of BTF3 mRNA and protein has been detected in gastric tumour samples and cell lines. Interestingly, BTF3 ablation decreases cell percentages arrested at G_1 phase but increases cell percentages arrested at S and G_2/M phases, thereby reducing cell cycle progression (Liu et al., 2013). A subsequent study substantiates the up-regulation of BTF3 in tumour samples and cell lines and its knockdown inhibits epithelial-mesenchymal transition (EMT) and dysregulates the JAK2/STAT3 signalling pathway, though the exact mechanism remains to be explored (Zhang et al., 2017).

2.4.11 Ubiquitin A-52 Residue Ribosomal Protein Fusion Product 1 (UBA52)

Ubiquitin A-52 Residue Ribosomal Protein Fusion Product 1 (UBA52), also known as ubiquitin-60S ribosomal protein L40, is encoded by seven-exons spanning *UBA52* gene located on chromosome 19p13.11 (Gene ID: 7311). This gene encodes for a fusion protein comprising of polyubiquitin or single ubiquitin moiety at the N-terminus and ribosomal protein eL40 (L40) at the C-terminus as a C-terminal extension protein (CEP). Alternative splicing results in eight transcript variants, which encode for three protein isoforms with length variation in the N-terminus ubiquitin component.

Cellular ubiquitin proteins are encoded by four genes, *UBB*, *UBC*, *UBA52,* and *UBA80,* whereby UBB and UBC are composed of polymer chains of ubiquitin while UBA52 and UBA80 are precursor fusion proteins comprising of a single ubiquitin fused at its C-terminal to ribosomal protein eL40 (L40) and eS31 (S27a), respectively (Redman & Rechsteiner, 1989; Baker & Board, 1991). As such. UBA52 and UBA80 undergo post-translational modification to 'release' ubiquitin from its conjugated form via the action of deubiquitinases (DUBs) *de novo*, thereby sustaining the pool of free cellular ubiquitin that regulates ubiquitin-proteasome system (Grou, Pinto, Mendes, Domingues, & Azevedo, 2015).

It has been shown that the deficiency of *UBA52* in mice results in death during embryogenesis and *UBA52* deficiency in cells leads to decreased total protein synthesis and cell cycle arrest. Simultaneously, the same study reveals a novel role of 'freed' ubiquitin from UBA52 precursor protein in regulating ribosomal protein complex ubiquitination of misfolded proteins during translation, by demonstrating the dual roles of UBA52's ubiquitin domain (Kobayashi et al., 2016). Recently, a study published its intriguing data on the

synergistic co-operation of both ubiquitin and eL40 (L40) after being cleaved apart from the precursor UBA52 fusion protein. After cleavage, eL40 (L40) functions to regulate the MDM2-p53 pathway, while ubiquitin functions to regulate the stability of MDM2 by ubiquitination (Zhou et al., 2019).

UBA52 transcript and protein levels are substantially up-regulated in rapidly proliferating primary renal cancer cells and cell lines as well as in blood of breast cancer patients, and colorectal carcinoma, but not in gastric cancer (Kanayama et al., 1991; Barnard et al., 1995; Aarøe et al., 2010).

CHAPTER 3

MATERIALS AND METHODS

3.1 Cell culture and maintenance

Six NPC-derived cell lines (HONE-1, SUNE-1, HK1, TW01, TW04 and C666-1) and an immortalized non-malignant nasopharyngeal epithelial cell line (NP69) were used in this study. All cell lines were derived from epithelial cells originating from the nasopharyngeal region. The NPC cell lines (HONE-1, SUNE-1, HK1, TW01 and TW04) were cultured in RPMI-1640 (Gibco, USA) containing 10% (v/v) heat-inactivated fetal bovine serum (FBS) (Gibco, USA), 2 mM L-glutamine (Gibco, USA) and 100 U/mL penicillin-streptomycin (Gibco, USA). The EBV-positive cell line, C666-1, was cultured on fibronectin-coated cell culture flask containing pre-warmed (37^{o}C) RPMI-1640 medium. The culture flask was pre-coated and incubated in 10 ng/mL human plasma-derived fibronectin (Sigma-Aldrich, USA) in sterile PBS at 4^{o}C overnight. NP69 cells were cultured in defined keratinocyte serum-free medium (D-KSFM) (Invitrogen, USA) supplemented with 0.2 ng/mL recombinant epidermal growth factor (Invitrogen, USA), 5% heat-inactivated dialyzed FBS and 100 U/mL penicillin-streptomycin. All cells were maintained at 37^{o}C in a humidified environment containing 5% CO_2. Cells were harvested when a 70-80% confluence was reached.

Three NPC cell lines (HONE-1, SUNE-1 and HK1) were provided by Dr. Ching-Ching Ng, NPC Research Laboratory in University of Malaya. TW01, TW04 and NP69 cell lines were obtained from Dr. Samirah Abdullah, Faculty of Medicine and Health Sciences, Universiti

Malaysia Sarawak. The EBV-positive cell line, C666-1, were given by Dr. Paul Neilsen, Swinburne University of Technology, Sarawak.

Based on the WHO classification, TW01 and HK1 are categorized as Type I NPC. HONE-1 and SUNE-1 are categorized as Type IIa NPC while TW04 and C666-1 are classified as Type IIb NPC. NP69 cell line is derived from normal nasopharyngeal epithelial cells. Most of the cell lines were found to be EBV-negative, except SUNE-1 with unknown EBV status and C666-1 that consistently harbours EBV in long-term cultures (Table 3.1).

Table 3.1: WHO classification of NPC cell lines used (Stelow & Wenig, 2017).

Cell line	**Origin of cell line**	**NPC WHO classification**		**EBV status**	**Reference on establishment**
		Type	**Characteristic**		
NP69	Epithelial	Normal	Normal nasopharyngeal epithelial	Negative	Tsao, Wang, et al. (2002)
TW01	Epithelial	I	Keratinised, differentiated	Negative	Lin et al. (1993)
HONE-1	Epithelial	IIa	Non-keratinised, poorly-differentiated	Negative	Glaser et al. (1989)
SUNE-1	Epithelial	IIa	Non-keratinised, poorly-differentiated	Unknown	Teng, Ooka, Huang, & Zeng (1996)
HK1	Epithelial	I	Keratinised, differentiated	Negative	Huang et al. (1980)
TW04	Epithelial	IIb	Non-keratinised, undifferentiated	Negative	Lin et al. (1993)
C666-1	Epithelial	IIb	Non-keratinised, undifferentiated	Positive	Cheung et al. (1999)

3.1.1 Cell culture sub-cultivation

Each cell line was passaged after three to four days when approximately 70-80% confluency was achieved in the cell culture flask. The spent culture media was first aspirated and discarded followed by the rinsing of the cell monolayer on the surface of the flask with sterile cold phosphate-buffered saline (PBS) (Nacalai Tesque, USA) to remove any traces of the cell culture medium. After discarding the PBS, 0.25% trypsin enzyme solution (Gibco, USA) with 0.53 mM ethylenediaminetetraacetic acid (EDTA) (Gibco, USA) was added to the flask and placed in a CO_2 incubator at 37°C for 5 minutes for bond dissociation between cells of the monolayer and with the surface of the flask. After the content of the flask was viewed under an IBS100 inverted microscope (RaxVision, USA) to ensure sufficient cellular detachment from each other and from the surface, an equal volume of complete culture medium was added to inactivate further trypsinization. The content from the flask was then transferred to a sterile 15 mL screw cap tube for centrifugation at 1500rpm in a Rotanta 460R benchtop centrifuge (Hettich, Germany) to pellet the cells. After the supernatant was carefully aspirated and discarded, the cell pellet was resuspended with 1mL of complete culture medium with gentle pipetting. The cell suspension was then either re-plated and re-passaged or counted and plated in multi-well cell culture plates for further experimental purposes.

3.1.2 Cryopreservation of cell lines

When cells achieved confluency of 70-80%, the cells were trypsinized and pelleted as described above. After centrifugation and removal of the supernatant, the pellet was resuspended in 1 mL pre-chilled freezing medium consisting of 50% complete culture medium, 40% FBS and 10% dimethyl sulphoxide (DMSO) (Sigma-Aldrich, USA). The

suspension was transferred to Nunc cryovials (Sigma-Aldrich, USA), placed in a freezing container (Thermo Scientific, USA) containing isopropyl alcohol (Mallinckrodt, USA) and stored at -80^{o}C for optimal gradual freezing rate. The next day, the cryovials were transferred to a liquid nitrogen storage tank (-140^{o}C) for long term storage.

For cell culture revival after cryopreservation, the content of the cryovial was thawed rapidly in a 37^{o}C water bath and transferred to a sterile 15 mL screw cap tube containing pre-warmed 10 mL complete growth medium. The suspension was then centrifuged at 1500rpm for 5 minutes and the supernatant was removed and discarded. The pellet was resuspended in 1 mL complete growth medium by pipetting and subsequently seeded into a tissue culture flask containing pre-warmed 6 mL complete growth medium.

3.2 Selection of ribosomal protein genes and their putative interactors

From an extensive round of literature search on published findings on the differential expression of ribosomal protein genes in carcinomas as well as on bioinformatic predictions on the potential interactors of ribosomal proteins, a bioinformatics paper was selected as a major reference (Choi, Yu, Yoo, & Kim, 2005). This highly cited paper predicted the differential co-expression of certain gene clusters, which made up of individual genes, based on published gene expression datasets from various cancers. Interestingly, ribosomal proteins and their putative factors were reported to be differentially expressed within the tumour co-expression network in comparison to the normal network. Based on this, a list of ribosomal protein genes and their putative interacting partners were selected for gene expression analysis (Figure 3.1).

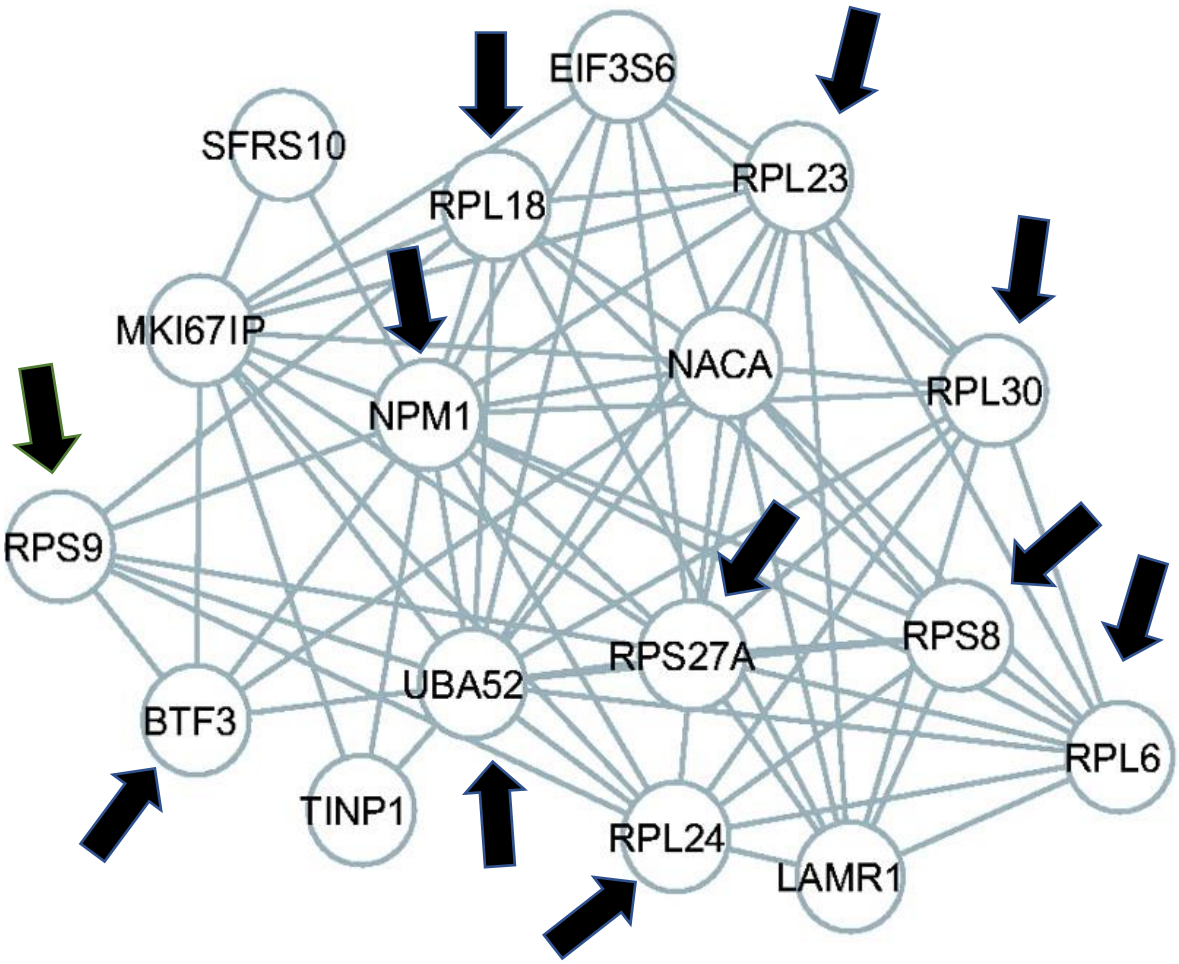

Figure 3.1: Gene co-expression cluster. The protein biosynthesis gene cluster extracted from the tumour specific co-expression network. Darkened arrows mark the genes of interest (GOI) in this study. Adapted from Choi et al. (2005).

3.3 Gene expression analysis

3.3.1 Total RNA extraction

Total cellular RNA was extracted from each cell line using TRizol Reagent (Invitrogen, USA) according to the manufacturer's protocol. Briefly, the media from each flask were discarded and the cell monolayer was washed with ice-cold phosphate buffered saline (PBS) twice. 1 mL of TRizol reagent per 3.5 cm diameter dish was added and the cells were scraped with a cell scraper (Sigma-Aldrich, USA) and incubated for 5 minutes. Cell lysate was transferred to a sterile microcentrifuge tube and 0.2 mL chloroform (Mallinckrodt, USA) per 1 mL of cell lysate was added. After an incubation period of 5 minutes, the samples were centrifuged at 12,000x*g* at 4^{o}C for 15 minutes with a Himac CF15R High-Speed Refrigerated Microcentrifuge (Hitachi, Japan). The upper aqueous layer was transferred into a fresh microcentrifuge tube and 0.5 mL isopropanol (Mallinckrodt, USA) per 1 mL TRizol was added. After 10 minutes of centrifugation at 10,000x*g* at 4^{o}C, the supernatant was discarded. The RNA pellet was washed by adding 1 mL of 70% molecular-grade ethanol (Merck, USA) and centrifuged at 7,500x*g* for 5 minutes at 4^{o}C and air-dried for approximately 5 minutes without total evaporation of the solvent. The pellet was then dissolved in 30 µL of nuclease-free water (Promega, USA) and stored at -80^{o}C. RNA concentration and purity were determined with an ultraviolet (UV)-Vis spectrophotometer (Ultrospec 1100 *pro*, Amersham Biosciences, Germany) at an absorbance of 260nm and 260/280 ratio respectively (Table 3.2).

Table 3.2: RNA quantitation of seven cell lines of three biological replicates.

Cell line	Passage no.	230nm	260nm	280nm	260/280	260/230	µg/ µl
NP69	p68	0.655	0.184	0.068	1.814	0.053	0.513
	p82	3.637	0.616	0.348	1.805	0.166	1.204
	p88	0.065	0.022	0.000	1.968	0.579	0.120
HONE-1	p12	1.029	1.164	0.750	1.899	1.183	1.748
	p13	0.894	0.948	0.732	1.126	1.809	0.964
	p16	1.162	1.100	0.691	1.857	0.938	1.900
SUNE-1	p13	0.957	0.951	0.733	2.030	0.980	0.773
	p16	0.149	0.108	0.058	1.862	0.578	0.218
	p18	0.173	0.224	0.122	1.839	0.972	0.407
HK1	p12	2.954	2.110	1.618	2.065	0.530	1.905
	p14	3.184	2.220	1.672	2.068	0.524	2.121
	p19	0.683	0.591	0.323	1.832	0.865	1.178
TW01	p6	1.038	1.221	0.908	1.942	1.393	1.037
	p8	1.1947	1.146	1.121	1.817	1.403	1.238
	p9	0.658	0.505	0.281	1.888	0.758	0.763
TW04	p16	0.265	0.200	0.117	1.825	0.773	0.371
	p18	0.148	0.130	0.070	2.145	0.866	0.225
	p19	0.103	0.129	0.057	1.975	1.222	0.294
C666-1	p28	1.307	1.759	0.952	1.848	1.346	1.647
	p29	0.791	0.426	0.217	1.996	0.535	0.839
	p30	0.360	0.420	0.253	1.813	1.191	0.595

3.3.2 DNase treatment of RNA samples

Prior to RT-qPCR, the extracted total RNA was firstly DNase treated to remove possible genomic DNA (gDNA) contamination within the RNA samples. This was achieved by using RQ1 RNase-Free DNase kit (Promega, USA) following the manufacturer's protocol. DNase digestion was set up as shown in Table 3.3.

Table 3.3: Components for DNase treatment of RNA samples.

Components	**Volume (µL)**
RNA in water	2 µg (varying volume across samples)
RQ1 RNase-Free DNase 10X Reaction Buffer	1
RQ1 RNase-Free DNase (1 Unit/µL)	2
Total volume	10 µL

The reaction was then incubated at 37ºC for 30 minutes. Following the addition of 1 µL of RQ1 DNase Stop Solution, the reaction was heated at 65ºC for 10 minutes to inactivate the activity of DNase. The entire content of the reaction was then subjected to reverse transcription.

3.3.3 Reverse transcription (RT)

First strand cDNA synthesis from RNA was prepared with Moloney Murine Leukemia Virus Reverse Transcriptase (M-MLV RT) (Promega, USA) following manufacturer's instructions. In a microcentrifuge tube, 1 µg of random primers (Promega, USA) was added to 2 µg of DNase-treated RNA in a total reaction volume of 15 µL. The sample RNA/primer was then denatured at 70ºC for 5 minutes to melt secondary structures within the RNA template. The reaction was then placed immediately on ice to prevent the re-formation of secondary structures. Following that, the reverse transcription master mix was prepared as

detailed in Table 3.4. The mixture was mixed gently by flicking and incubated at 37ºC for 60 minutes and followed by heat inactivation at 70ºC for 15 minutes. The cDNA samples were stored at -20ºC for further use.

Table 3.4: Reverse transcription master mix.

Component	**Volume (µL)**
RNA/primer sample	15
5X M-MLV Reaction Buffer	5
10 mM dNTP Mix (Promega, USA)	1.25
40 U/µL RNasin Plus RNase Inhibitor (Promega, USA)	0.6
200 U/µL M-MLV Reverse Transcriptase	1
Total volume	25 µL

3.3.4 Primer design

Primer sets were designed with NCBI primer-blast program (Ye et al., 2012), which incorporated the Primer3 software, BLAST and global sequence alignment functionalities. As an extra precaution to eliminate false positives amplifications from contaminated RNA, at least one of the primers in each primer set was designed to span an exon-exon junction. Subsequently, selected primer pairs were re-evaluated with OligoCalc to check for self-complementarity in terms of potential hairpin formation, 3' end self-complementarity and self-dimerization sites (Kibbe, 2007). Selected primer pairs were then synthesized by an external vendor, FIRST BASE Laboratories Sdn. Bhd., Malaysia. Primer sequences and corresponding product sizes are listed in Table 3.5.

T**able 3.5:** Primer sequences and product sizes.

Primer	**NCBI Accession No.**	**Sequence (5'-3')**	**Product size (bp)**
GAPDH	NM_002046.5	F: CTGGGCTACACTGAGCACC	101
		R: AAGTGGTCGTTGAGGGCAATG	
uS4 (S9)	NM_001013.3	F: CTGAAGTTGATCGGCGAGTATG	280
		R: ACTTGGCCAAGCCCAGCTTG	
eS8 (S8)	NM_001012.1	F: GCTCAGAGTGTTGTACTCG	106
		R: AGCACGATGCAATTCTTCAC	
eS31 (S27a)	NM_002954.5	F: GCAGCTGGAAGATGGACGTAC	85
		R: ACCACCACGAAGTCTCAAC	
eL6 (L6)	NM_001024662.1	F: GCACGTGAGAACACTGCGAG	139
		R: GAGGACCCGAGCTCCAGTCAC	
uL14 (L23)	NM_000978.4	F: TCCAGCAGTGGTCATTCGAC	117
		R: GCAGAACCTTTCATCTCGCC	
eL18 (L18)	NM_000979.3	F: CTCTGTCCCTTTCCCGGATG	320
		R: GTAGGGTTTGGTGTGGCTG	
eL24 (L24)	NM_000986.3	F: CGAGCTGTGCAGTATTAGCG	117
		R: GAAAGGAAAGCCGACTCGC	
eL30 (L30)	NM_000989.3	F: ATCTTAGTGGCTGCTGTTGG	280
		R: TGCCACTGTACTGATGGACAC	
NPM1	NM_002520.6	F: TTGTTCTCTGGAGCAGCGTTC	231
		R: TTTGCACCAGCCGCTAAAC	
BTF3	NM_001037637.1	F: CAAACTGCAGGCACAAGTGC	311
		R: TCAGACTATCCGCACCAAGC	
UBA52	NM_001033930.1	F: CGCAAGAAGAAGTGTGGTC	126
		R: GGACACTTTATTGAGGCTCC	

3.3.5 Quantitative polymerase chain reaction (qPCR)

Real-time PCR (qPCR) was performed using Rotor-Gene SYBR Green PCR Kit (Qiagen, USA) on a Rotor-Gene 6000 Rotary Analyzer (Qiagen, USA) and monitored with Rotor Gene 6000 software version 2.3.3 (Qiagen, USA). To reduce contamination possibilities, qPCR master mix was prepared on ice without the addition of cDNA template in a ventilated fume hood. cDNA template was added as the last component outside the fume hood. qPCR master mix composition is outlined in Table 3.6.

Table 3.6: qPCR master mix

Component	**Volume (µL)**
2X Rotor-Gene SYBR Green PCR Master Mix	12.5
10 µM Forward primer	1.5
10 µM Reverse primer	1.5
cDNA template after RT reaction	1.4
Nuclease-free water	8.1
Total volume	25.0 µL

qPCR amplifications were performed under the cycling conditions in Table 3.7. At the end of cycle 40, amplicon dissociation analysis (melting curve) was set from 50-99^{o}C with gain optimization before melt.

Table 3.7: qPCR thermal cycler settings.

Step	**Temperature (^{o}C)**	**Duration**	**Number of cycle(s)**
Initial denaturation/ hold	95	5 minutes	1
Denaturation	95	5 seconds	40
Annealing and extension	60	20 seconds	40
Melting curve	50-99	-	1

Glyceraldehyde-3-phosphate dehydrogenase (*GAPDH*) and Beta-actin (*ACTB*) were used as potential endogenous controls. Non-template reaction was used as the negative control. All samples were run with three biologically independent replicates.

3.3.5.1 Validation of qPCR primer efficiencies

The selection of the threshold intensity was set at a fixed intensity on the log-linear phase of the amplification curve for all the samples tested. Validation experiments, which included the generation of standard curves using a series of diluted cDNA samples, were carried out to ensure primer efficiency as well as target and reference gene amplification compatibility.

Samples were run in duplicates for each input amount (4, 0.8, 0.16, 0.032 and 0.0064 ng/µl) and the C_T values were averaged, and standard deviations were obtained. A standard curve for each gene was plotted with the average *threshold cycle* (C_T) values against log input amount (0.602, -0.097, -0.795, -1.495 and -2.194) of HK1 sample. From the standard curve, the amplification efficiency of each gene was calculated with the following formula:

$$Amplification\ efficiency = \left[10^{-\frac{1}{slope}}\right] - 1$$

The ideal amplification range is 0.9-1.1 (90-110%).

The comparative C_T method ($\Delta\Delta C_T$ method) was applied to relatively quantitate the expression levels of the target genes in NPC cell lines compared to that of NP69 (Kenneth & Thomas, 2001). Calculations via means of this method are only valid with comparably similar amplification efficiencies of both target and reference genes, in other words, ideally, the amplification efficiencies of both the target and reference gene must be approximately equal for a valid $\Delta\Delta C_T$ calculation.

From the individual standard curves generated, the amplification efficiencies of the target gene relative to that of the reference gene were evaluated by running standard curves for each amplicon utilizing the same sample. The ΔC_T values ($C_{T\ target} - C_{T\ reference}$) were plotted vs. log input amount (0.602, -0.097, -0.795, -1.495 and -2.194). The slope of the resulting semi-log regression line was used to determine the compatibility of the two PCR efficiencies. The absolute value of the slope of ΔC_T vs. log input should ideally be <0.1.

3.3.5.2 Real-time PCR assay

Real-time PCR assays were performed to determine the differential expressions of eleven genes of interest (GOI) in six NPC cell lines (HONE-1, SUNE-1, HK1, TW01, TW04, and C666-1) compared to NP69. Each final fold difference (FD) was the result of that of three biological replicates, each with two technical replicates.

Subsequent qPCR protocols and data analysis was conducted following the guidelines published by Applied Biosystems (Biosystems, 2008). Melt curve analysis was adopted alongside to verify the presence of a single amplicon. An inter-run calibration scheme was adopted to minimize loading variation and to detect possible contamination with the inclusion of duplicate technical replicates and 'no-template' control (NTC) respectively in each qPCR run. All samples were normalized to GAPDH as the endogenous control and relative fold differences were calculated by the $\Delta\Delta C_T$ method as follow.

$\Delta C_T = C_{T\ target} - C_{T\ reference}$

$s = \sqrt{(s_1^2 + s_2^2)}$, where s is standard deviation.

The standard deviation for $\Delta\Delta C_T$ was carried forward from that for ΔC_T of target genes.

The relative target gene expression to the normal sample (NP69 cell line) was determined

with the following formula:

$\Delta\Delta C_T = \Delta C_{T\ target} - \Delta C_{T\ normal}$

As the fold-differences calculated using the $\Delta\Delta C_T$ method are usually expressed as a range, the standard deviation (SD) was then added and subtracted from respective $\Delta\Delta C_T$ values and converted to log form as the upper and lower $2^{-\Delta\Delta Ct}$ limits to obtain the fold difference (FD) of target gene expression in NPC cell lines in comparison to NP69. The mean of the upper and lower FD was regarded as the final FD output (Biosystems, 2008).

3.3.5.3 Data analysis

For over-expression data (FD >1.0), these values are linear and can be interpreted as such. A fold difference of 2.0 (FD =2.0) would generally mean that the target gene is over-expressed two-fold higher in an NPC cell line compared to NP69. In contrast, extra precaution is necessary when analysing under-expression data as the interpretation for over-expression described above is not valid for fold difference values under 1.0 (FD <1.0) due to the nature of the log-based $2^{-\Delta\Delta C_T}$ method. For instance, FD of 0.5 (FD =0.5) signifies that the target gene is down-regulated by 50% in an NPC cell line compared to NP69.

Statistical analysis was performed to be an indication of differential expression significance of target genes in (1) individual NPC cell lines and (2) in a pooled NPC data, against that of the normal NP69 cell line. The data are presented as mean fold difference± SD. The *p*-value tests the hypothesis that the expected ΔC_T values are zero (no fold change). The difference of ΔC_T values between normal and carcinoma cell lines was evaluated with independent, single-tailed Student's *t*-test with unequal variances. *p*-value of <0.05 was considered to be statistically significant. Error bars represent the standard deviation of the normalized fold

difference (ΔC_T).

3.3.6 Electrophoresis and sequencing

Agarose gel electrophoresis (AGE) was carried out to ensure the usefulness of the primer pairs and the accuracy of PCR amplicons generated. Together with a PageRuler DNA ladder mix (Thermo, USA), qPCR reactions were loaded on a 1.5% agarose gel casted with 0.6 g agarose powder (J. T. Baker, USA) in 40 mL 1X TAE buffer (Vivantis, Malaysia), pre-stained with ethidium bromide (EtBr) (R & M Chemicals, UK). AGE was run at 120 V for 25 minutes. The DNA was then visualized and photographed in an ImageQuant 400 (GE Healthcare, UK) with an ImageQuant Capture software version 1.0.0 (GE Healthcare, UK). Subsequently, the PCR products were then sent for sequencing to FIRST BASE Laboratories Sdn. Bhd., Malaysia.

3.4 Target genes sequence analysis

In order to detect the possible presence of genetic perturbations within the coding region (CDS) of each gene of interest, a separate set of primers were designed to target and amplify the conserved CDS region.

3.4.1 Primer design

The entire repertoire of existing transcript variants of a target gene was obtained from NCBI database and was sequence aligned with NCBI Standard Nucleotide BLAST tool to ascertain the conserved region containing the CDS. Following that, primer sets were designed similarly as the qPCR primers. Primer sequences and corresponding product sizes are listed in Table 3.8.

Table 3.8: Primer sequences and corresponding amplicon sizes for sequence analysis.

Primer	Sequence (5'-3')	Product size (bp)
GAPDH	F: CTGGGCTACACTGAGCACC	101
	R: AAGTGGTCGTTGAGGGCAATG	
uS4 (S9)	F: GCCAACATGCCAGTGGCACG	632
	R: GAAAACGAGACAATCCAGCAGC	
eS8 (S8)	F: TATATATCGCCGAGCGATGATCATC	656
	R: ACAGAACAAGGATTTATTTGCC	
eS31 (S27a)	F: ATGTTGTGGAGCCGCCATTAAAATG	512
	R: CCGTGATGAACTCATACAGTTACTTG	
eL6 (L6)	F: ATGGCGGGTGAACAAGTTGAGAAG	887
	R: CTGAAGACATCTAGAACACCAATCTG	
uL14 (L23)	F: TTACGTTCAAGATGTCGAAGCGAG	450
	R: CAGAGAGACTGGAGAATCATGCAATG	
eL18 (L18)	F: AATTATCAGGAGGCGCCATCATGG	594
	R: TCCAGGGTTAGTTCTTGTAGCCT	
eL24 (L24)	F: GTATCTATCGCCATGAAGGTCG	501
	R: ATCTAATCTGCCAGTTTAGCGTC	
eL30 (L30)	F: TTATACTAATGCAGGCAGATGGTG	377
	R: GGTGACGAGGTTTACTGTTCACC	
NPM1	F: TAATTACGTGCCGCCACTCGATG	942
	R: CGGCGAATGTCTTAACAAATTGC	
BTF3	F: TAGATGAGTAGAGGAAGGCGATG	657
	R: CAGCAGTTGACTCAATTCAGTC	
UBA52	F: GTGCTGGGATTACAGACGCAAAC	434
	R: CTGCCCTTCAAGGAAAGAACCAC	

3.4.2 PCR, AGE and gel extraction

Total RNAs were extracted from TW04 cells with two replicates and reverse-transcribed into cDNAs using M-MLV RT (previously described in Chapter 3.3.3). High fidelity conventional PCR was carried out with *pfu* DNA polymerase (Thermo Scientific, USA) due to its proofreading activity responsible for low error rate per nucleotide. A total of 0.32 ng/µL cDNA was transferred into pre-chilled PCR tubes and the master mix was prepared with the components listed in Table 3.9. GAPDH was used as an endogenous control.

Table 3.9: PCR master mix with *pfu* DNA polymerase.

Component	**Volume (µL)**
2.5 U/µL Recombinant *pfu* DNA polymerase (Thermo Scientific, USA)	1.0
10X *pfu* buffer with $MgSO_4$ (Thermo Scientific, USA)	5.0
10 mM dNTP mix (Promega, USA)	1.0
10 µM Forward primer	2.6
10 µM Reverse primer	2.6
cDNA template after RT reaction and Nuclease-free water	37.9
Total volume	50.0 µL

PCR amplifications were performed under the cycling conditions in Table 3.10.

Table 3.10: PCR cycling conditions for *pfu* DNA polymerase.

Step	**Temperature (ºC)**	**Duration**	**Number of cycle(s)**
Initial denaturation/ hold	95	2 minutes	1
Denaturation	95	30 seconds	35
Annealing	65	30 seconds	
Extension	72	Variable	
Final extension	72	5 minutes	1

Products were separated on 1.5% agarose gel with pre- EtBr staining (running conditions and visualization method described in Materials and methods Chapter 3.2.6). Upon visualization on a BLooK LED transilluminator (GeneDireX, Taiwan), target fragments were excised and extracted with QIAquick Gel Extraction Kit (Qiagen, CA) according to the manufacturer's protocol. Briefly, 6 volumes of Buffer QG was added to 1 volume of gel slice and incubated at 50ºC for 10 minutes with frequent vortex. After the gel was completely dissolved, 1 gel volume of isopropanol was added and the mixture was transferred to a spin column and centrifuged at 13,000rpm for 1 minute. A volume of 0.5 mL Buffer QG was again added and the column was centrifuged for 1 minute and the flow-through was discarded. To wash the pellet, 0.75 mL Buffer PE with added ethanol was added and the column was left to stand for 5 minutes. The column was centrifuged for 1 minute and the flow-through was discarded. The column was centrifuged again for 1 minute to remove residual wash buffer. The column was transferred into a clean 1.5 mL micro-centrifuge tube and 50 µL Buffer EB was added to the centre of the membrane and was left to stand for 4 minutes to increase the yield of purified DNA. The column was centrifuged for 1 minute to elute purified DNA. The amplicons were sent for sequencing to First Base Laboratories Sdn. Bhd., Malaysia.

3.4.3 Sequence analysis

Upon receipt, sequence data of each target gene was pruned by selecting the nucleotide region corresponding to the protein-coding sequence (CDS) and removing unspecific 'Ns' on both the 5' and 3' ends. Multiple sequence alignment was conducted with ClustalW (Thompson, Higgins, & Gibson, 1994) and visualized with MultAlin software (Corpet, 1988).

3.5 Protein expression analysis

Gene expression analysis was not only carried out on the level of transcripts, but also on protein expression. Protein expression analysis was carried out on six candidate genes that exhibited significant differential transcript-level expressions via western blot. Similar to the mRNA expression analysis, 7 different cell lines were included in this part of the study, which were whole cell lysates extracted from NP69, the normal nasopharyngeal epithelial cell line, and 6 NPC cell lines (HONE-1, SUNE-1, HK1, TW01, TW04 and C666-1).

3.5.1 Whole cell lysate extraction

Each cell line was continually cultured and the whole cell lysate was extracted from three different batches of cells of different passage numbers. When a confluency of 70-80% had been achieved, whole cell lysate protein extraction was carried out in a ventilated fume hood. Spent medium was aspirated and discarded. Cells were washed once with ice-cold PBS to remove any leftover culture medium and then lysed in ice-cold RIPA lysis buffer (0.5 mL buffer/ 75 cm^2 flask) containing 10 mM Tris-HCl pH 8.0, 140 mM NaCl, 1 mM EDTA, 0.1% SDS, 1% Triton X-100, 0.1% sodium deoxycholate, supplemented with 1 mM phenylmethanesulfonylfluoride (PMSF) protease inhibitor (Roche Applied Sciences, Switzerland). The adherent cells were scraped off with a chilled plastic cell scraper and the resulting slurry was transferred into a pre-chilled 1.5 mL microcentrifuge tube and left to incubate for 30 minutes with occasional mixing. Cells were then homogenized with a syringe fitted with a 21g needle and centrifuged at 13,000rpm for 5 minutes at 4^oC to pellet cell debris. The tubes were then immediately placed on ice and the supernatants were carefully transferred to new pre-chilled microcentrifuge tubes. Protein concentration was first determined before storing at -80 for future use.

3.5.2 Protein concentration determination

Total protein concentrations in each sample were measured with Bradford Protein Assay. Briefly, five dilutions of BSA (Amresco, USA) standard with concentrations of 0.5, 1.0, 2.0 and 4.0 and 8.0 µg/µL and 4 µL of protein samples at a dilution of 1:250 were added to cuvettes in duplicates. 200 µL of Bradford reagent was then added to each sample at a dilution of 1:5 in distilled water and mixed well. The samples were incubated at room temperature for 5 minutes before absorbance measurements at 595 nm were read on a UV spectrophotometer (Ultrospec 1100 *pro*, Amersham Biosciences, Germany). A standard curve was generated, and the protein concentrations of the samples were determined. The whole cell lysate samples were stored in an -80^{o}C ultra-freezer for further use (Table 3.11).

Table 3.11: Protein concentration determination. Total protein concentration determination of whole cell lysate extracted from NPC cell lines and NP69 with Bradford assay.

Cell Line	Passage No.	Averaged Concentration (µg/µL)	Cell Line	Passage No.	Averaged Concentration (µg/µL)
NP69	p68	1.526	**TW01**	p6	2.481
	p82	1.054		p8	1.812
	p88	1.268		p9	1.760
HONE-1	p12	2.522	**TW04**	p16	2.542
	p13	2.685		p18	3.104
	p16	2.345		p19	1.080
SUNE-1	p13	3.338	**C666-1**	p28	1.987
	p16	3.156		p29	2.284
	p18	2.871		p30	2.351
HK1	p12	2.857			
	p14	2.410			
	p19	2.982			

3.5.3 Sodium Dodecyl Sulphate- Polyacrylamide Gel Electrophoresis (SDS-PAGE) gel preparation

SDS-PAGE was carried out to separate proteins based on their differences in relative molecular mass using electrophoresis. Due to the disruptive properties of sodium dodecyl sulfate (SDS), protein molecules are denatured and carry similar net negative charges, which 'pulls' the proteins toward the positively-charged anode across a discontinuous polyacrylamide gel.

In this study, SDS-PAGE was conducted using the Bio-Rad Mini- PROTEAN system (Bio-Rad Laboratories, USA). A 12% resolving gel was casted into 18cm x 16cm x 1mm gel cassettes (Table 3.12). A layer of isopropanol was added to prevent uneven levelling of the gel as it polymerizes. Once the resolving gel had set for about 30 minutes, the layer of isopropanol was removed with a filter paper. A 4% stacking gel was prepared and poured immediately on top of the resolving gel to the brim of the glass plates (Table 3.12). A 10-well gel comb of 1mm thickness was inserted into the space between the plates without the introduction of air bubbles. After the gel had set for approximately 30 minutes, the gel was placed into the electrophoresis tank filled with 1x running buffer (25 mM Tris, 192 mM glycine, 0.1% SDS in distilled water) and the gel comb was removed.

Table 3.12: Polyacrylamide gel composition.

Ingredients	**Resolving Gel, 12% (mL)**	**Stacking Gel, 4% (mL)**
1.5M Tris-HCl (pH 8.8)	2.000	-
0.5M Tris-HCl (pH 6.8)	-	1.250
30% Bis-acrylamide (Bio-Rad Laboratories, USA)	3.200	0.670
10% SDS	0.080	0.050
10% (w/v) Fresh ammonium persulfate (APS)	0.080	0.050
Tetramethyl-ethylenediamine (TEMED)	0.008	0.005
Distilled water (dH_2O)	2.600	3.000
Total volume	8.000 mL	5.000 mL

3.5.4 Western blot

Western blot, or immunoblot, was carried out to detect specifically targeted proteins in the extracted whole cell lysate samples. Briefly, the western blot protocol involves protein denaturation and gel electrophoresis to separate denatured proteins by their molecular mass. This is followed by an electroblotting of proteins from the gel onto a membrane and an immunostaining method to detect and visualize the targeted protein on the membrane.

3.5.4.1 Sample preparation and SDS-PAGE

Equal amounts of proteins (30 µg) was mixed in 1:1 ratio with 2X Laemmli sample buffer (4% SDS, 10% 2-mercaptoethanol, 20% glycerol, 0.004% bromophenol blue, 0.125M Tris-HCl). The protein-buffer mixtures were boiled at 95^{o}C for 10 minutes and were loaded into the wells with a PageRuler Prestained Protein Ladder (Thermo, USA), which composed of visible coloured bands for convenient estimation of protein migration during electrophoresis. The samples were separated at 50 V for 40 minutes and the voltage was increased to 90 V for another 45 minutes with a MP-2AP Power Supply (Major Science, Taiwan).

3.5.4.2 Protein transfer

Western blot was carried out with Bio-Rad Mini Trans- Blot Cell (Bio-Rad Laboratories, USA). A 0.45 µm PVDF membrane (Immobilon-PSQ, Millipore, USA) was cut out and activated by soaking in methanol (Fisher Scientific, USA) for 10 minutes. After electrophoresis, the gel cassette was pried open and the upper stacking gel was removed and the bottom resolving gel was transferred into a container with 1X transfer buffer (25 mM Tris, 192 mM glycine, 20% methanol in distilled water). The transfer sandwich was assembled, in this order, with the black negative plate at the bottom, followed by a layer of sponge, a pre-soaked thick filter paper (Bio-Rad Laboratories, USA), gel, membrane, filter paper and the last layer of sponge. After each layer was placed, a roller was used to push out any air bubbles that were formed. After the last layer of sponge was placed, the white positive plate was gently fixed in place with the safety cover. The sandwich was then placed into the transfer tank filled with 1X transfer buffer and run at 50 V for 35 minutes with a constant voltage on ice with an EPS-300IIV power supply (C.B.S Scientific, USA).

3.5.4.3 Total protein staining and de-staining

After the transfer was completed, the membrane was removed and stained with 0.1% (w/v) Ponceau S (Sigma-Aldrich, USA) for 3 minutes to check for transfer quality. The membrane was then de-stained with 3 x 5 minutes washes of 1X Tris-buffered Saline-Tween 20 (TBST) buffer (0.2M Tris, 1.5M NaCl, 0.1% Tween-20; pH 7.6) while shaking on a MR-1 mini-rocker shaker (Biosan, Latvia).

3.5.4.4 Blocking and primary antibody incubation

The membrane was then blocked with 3% Bovine Serum Albumin (BSA) in TBST at room

temperature for 2 hours and incubated at 4^{o}C overnight with shaking in optimized dilutions of primary antibodies in 3% BSA in TBST (Table 3.13).

Table 3.13: Primary antibody dilutions for western blot.

Primary Antibody	Species	Dilution	Product Size (kDa)	Manufacturer
ACTB	Mouse monoclonal	1 : 1000	43	Santa Cruz Biotechnology
uS4 (S9)	Goat polyclonal	1 : 500	23	Santa Cruz Biotechnology
eS8 (S8)	Goat polyclonal	1 : 500	24	Santa Cruz Biotechnology
eS31 (S27a)	Rabbit polyclonal	1 : 250	8.5	Thermo Scientific
uL14 (L23)	Goat polyclonal	1 : 500	15	Santa Cruz Biotechnology
eL18 (L18)	Mouse monoclonal	1 : 500	22	Santa Cruz Biotechnology
NPM1	Mouse monoclonal	1: 1000	40	Santa Cruz Biotechnology

3.5.4.5 Secondary antibody incubation

The next day, the primary antibody dilutions were aspirated, and the membrane was washed 3 x 5 minutes with 1X TBST. The membrane was then incubated with corresponding horse-radish peroxidase (HRP)-conjugated secondary antibody diluted in 3% BSA in TBST at room temperature for 2 hours (Table 3.14). The secondary antibody dilutions were aspirated, and the membrane was washed thrice with 1X TBST for 5 minutes per wash.

Table 3.14: Secondary antibody dilutions for western blot.

Secondary Antibody	Dilution	Manufacturer
Goat anti-mouse IgG - HRP	1 : 5000	Santa Cruz Biotechnology
Donkey anti-goat IgG-HRP	1 : 5000	Santa Cruz Biotechnology
Donkey anti-rabbit IgG-HRP	1 : 5000	Santa Cruz Biotechnology

3.5.4.6 Detection and visualization

Protein bands were detected by using SuperSignal West Pico Chemiluminescent Substrate (Thermo, USA) according to the manufacturer's protocol. This kit includes a luminol-based chemiluminescent substrate for the catalytic action of the horseradish peroxide (HRP) enzyme conjugated to the secondary antibodies. This substrate-enzyme reaction results in a chemiluminescent signal that can be detected and visualized with an imaging system.

In short, the peroxide and luminol solutions were mixed in a 1:1 ratio in a total volume of 5mL, added on the membrane and incubated for 1 minute. The membrane was removed from the substrate mixture, drained and subsequently covered with a clear plastic sheet protector before imaging it with ImageQuant 400 (GE Healthcare, UK) with different exposure settings. β-actin antibody was used as a loading control.

3.5.4.7 Data analysis

The intensity of the bands was quantified with ImageJ 1.52a (National Institutes of Health, USA). Pixel intensity was obtained from the area under the peak of the histogram generated. The values were then normalized to that of the loading control (ACTB) of the respective biological replicate. A mean fold difference value of more than 1.0 (>1.0) was considered to be an over-expression data while a fold difference value of less than 1.0 (<1.0) was taken as an indicator of under-expression, provided the FDs were statistically significant.

Statistical analysis was performed to be an indicative of differential expression significance of target protein in (i) individual NPC cell lines and (ii) in an accumulated NPC data, against that of the normal NP69 cell line. The data are presented as fold difference± SE. The *p*-value

tests the hypothesis that the expected fold difference is one (no fold change). The resulting fold difference of target protein in NPC cell line was evaluated against NP69 with independent, single-tailed Student's *t*-test with unequal variances. *p*-value of <0.05 was considered to be statistically significant. Error bars represent the standard error of the normalized mean band intensity.

3.6 Immunoprecipitation assay

Immunoprecipitation assay was performed to 'pull down' or precipitate associated target protein or intact protein complexes using antibody-coupled magnetic beads. This technique involves the immobilization of a target-specific antibody to a solid support such as agarose resin or magnetic particles followed by the addition of cellular protein lysate. Target proteins that are bound to the antibody-beads complex are then precipitated and washed several times to remove any possible contaminants. After dissociation from the antibody-beads support, the proteins could be analysed with SDS-PAGE followed by various methods such as gel staining, protein sequencing or western blot detection with the antibody of interacting protein. The advantages of magnetic beads compared to agarose resin are its high-capacity antibody binding due to its small (1- 4 μm diameter) size, higher yield of target protein as the use of magnetic beads avoids centrifugation steps, which can break weak antibody-antigen binding, and higher reproducibility and purity as supernatants are able to be aspirated completely without disturbing the protein-antibody-beads complexes that are held firmly to the side of the tube with a high-powered magnet.

3.6.1 Dynabeads-antibody linking

In this study, the assay was performed with Dynabeads Protein G (Life Technologies, USA).

The beads were re-suspended in the vial by vortexing for more than 30 seconds. 50 µL of beads were transferred into a 1.5 mL microcentrifuge tube and was placed on a Dynamag magnet (Life Technologies, USA) to separate the beads from the suspension buffer. After the removal of the supernatant, the tube was removed from the magnet rack and 1 µg of primary antibody diluted in 200 µL PBS-Tween (PBS in 0.02% Tween 20, pH 7.4) was added. The antibody-beads slurry was then incubated for 30 minutes at room temperature with constant rotation. The tube was then placed on the magnet rack and supernatant was removed.

3.6.2 Lysate incubation and antibody complexes elution

After the bead-antibody complexes were washed three times with 200 µL PBS-Tween with gentle pipetting, the supernatant was discarded and 100 µL of TW04, C666-1 and NP69 cell lysates were added into separate tubes. After 20 minutes incubation with constant rotation at room temperature, the tube was placed on the magnet rack and supernatant was removed. The Dynabeads complexes were washed three times with 200 µL PBS-Tween with gentle pipetting. 100 µL of PBS-Tween was added for re-suspension and the mixture was transferred into a clean 1.5 mL microcentrifuge tube to prevent co-elution of proteins bound to the wall of the tube.

3.6.3 Protein digestion and SDS-PAGE

After the tube was placed on a magnet rack and the supernatant was removed, 40 µL of 1X Laemlli sample buffer was added. The mixture was then heated at 70^{o}C for 10 minutes for protein denaturation. The tube was placed again on the magnet rack and the supernatant was transferred into two separate tubes, with 20 µL of supernatant in each, and analysed by SDS-

PAGE followed by western blot detection (procedure described in Materials and methods Chapter 3.3.4) with self and targeted primary antibodies respectively to verify the presence of the targeted antigens (Table 3.11). After the removal of the supernatant containing eluted protein samples, the contents of the tube, containing Dynabeads Protein G, was immediately brought to neutral pH with the addition of 0.1M Na-phosphate buffer pH 8.0. The tube was then stored at -20^{o}C and could be recycled.

Table 3.15: Primary antibodies used for immunoprecipitation.

Bead-antibody	**Primary antibodies used for western blot**	
	Self	**Target**
Bead-uS4 (S9)	uS4 (S9)	NPM1
Bead-eS8 (S8)	eS8 (S8)	NPM1
Bead-eS31 (S27a)	eS31 (S27a)	NPM1
Bead-uL14 (L23)	uL14 (L23)	NPM1
Bead-NPM1	NPM1	uS4 (S9)/ eS8 (S8)/ eS31 (S27a)/ uL14 (L23)

Concurrently, a negative control was carried out with un-coupled IgG beads (without antibody coupling) to identify possible non-specific bindings to the antibody as well as 20% input control to determine target protein enrichment and antibodies specificity and sensitivities.

3.7 Expression construct design

Expression constructs were designed by cloning full-length coding sequences (CDS) of target proteins into specific mammalian expression vectors that were compatible with CheckMate Mammalian Two-Hybrid System (Promega, USA).

3.7.1 Primer design and PCR

Forward and reverse primers were designed to target CDS of proteins of interest (Table 3.16). *Bam*HI and *Sal*I restriction enzyme recognition sites were introduced on the forward and reverse primers respectively along with extra sequences on either side of the recognition sites to facilitate efficient cleavage. *Bam*HI and *Sal*I restriction enzymes were selected as they were determined to be non-cutters of all the cloned cDNA (NEBcutter, version 2.0, NEB). A start codon was included in the forward primer following the *Bam*HI restriction site while no stop codon was incorporated in the reverse primer.

Table 3.16: Primer sequences and product lengths for mammalian expression.

Primer	Sequence (5'-3')	Gene product size (bp)	Protein product size (aa)
uS4	F: ATTAGGATCCATGCCAGTGGCCCG	595	194
(S9)	R: CTGGTCGACATCCTCCTCCTCGTCG		
eS31	F: TGCGGATCCATGCAGATTTTCGTGAAAAC	489	156
(S27a)	R: CACGTCGACCTTGTCTTCTGGTTTGTTG		
uL14	F: ATAGGATCCATGTCGAAGCGAGGACGTG	441	140
(L23)	R: ATAGTCGACTGCAATGCTGCCAGCATTG		
NPM1	F: CGTCGGATCCATGGAAGATTCGATGGAC	905	294
	R: GCATGTCGACAAGAGACTTCCTCCACTG		

3.7.2 PCR, AGE and gel extraction

High fidelity conventional PCR was carried out with *pfu* DNA polymerase (Thermo Scientific, USA) as previously described in Chapter 3.4.2 (Materials and Methods). GAPDH was used as an endogenous control. Upon agarose gel separation, visualization and band extraction, products were sent for sequencing to First Base Laboratories Sdn. Bhd.,

Malaysia, to ensure primer specificity and sequence amplification accuracy.

3.7.3 Double digestion of vector and insert

The pACT (Figure 3.3) and pBIND (Figure 3.4) vectors from the CheckMate Mammalian Two-Hybrid System (Promega, USA) were used as reporter vectors for *in vivo* confirmation of protein-protein interactions. Candidate full-length coding sequences were cloned into both pACT and pBIND vectors to reduce possible vector-dependency and directionality.

Using DoubleDigest Calculator (Thermo Scientific, USA), the recommended buffer for optimal double digestion with *Bam*HI and *Sal*I was determined to be Buffer *Bam*HI, in which the restriction enzyme activity of *Bam*HI was reported to be 100% and 50-100% for *Sal*I. For vector digestion, a total of 100 ng of pACT or pBIND vector was added to a final volume of 20 µL consisting of 1X *Bam*HI buffer, 8 Units *Bam*HI and 10 Units *Sal*I. For insert digestion, a total of 100 µg of insert DNA was added to 1X *Bam*HI buffer, 8 Units *Bam*HI and 10 Units *Sal*I in a final volume of 25 µL. The digestion reactions were incubated for an hour at 37^{o}C and heat-inactivated at 68^{o}C for 20 minutes. The digestion products were then separated on 1.5% gel with uncut vector and insert samples as the negative controls.

3.7.4 Phosphatase treatment

Following double digestion, the 5’ and 3’ ends of the digested inserts and expression vectors were dephosphorylated with Antarctic Phosphatase (NEB, UK) to prevent re-ligation of self-fragments and re-circularization respectively. The treatment was set up as shown in Table 3.17. The reaction was incubated at 37^{o}C for 30 minutes and heat-inactivated at 65^{o}C for 20 minutes.

Table 3.17: Phosphatase treatment composition.

Component	Volume (µL)
Double digested sample	10.0
10X Antarctic Phosphatase Reaction Buffer (NEB, UK)	1.5
5 U/µL Antarctic Phosphatase (NEB, UK)	1.0
Nuclease-free water	2.5
Total volume	15.0 µL

3.7.5 Ligation

Ligation reaction was performed in a total volume of 10 µL, containing 100 ng of vector, calculated volume of insert based on a 3:1 molar ratio of insert: vector, 1X Rapid Ligation buffer (Promega, USA) and 3 Units T4 DNA Ligase (Promega, USA). The ligation reaction was left in room temperature for 5 minutes for cohesive-end ligation and heat-inactivated at 70^{o}C for 10 minutes. The products were separated on 1.5% gel with no-insert controls.

3.7.6 Transformation

A total of 300 µL JM109 competent cells (Promega, USA) were thawed and 100 µL of cell stock were transferred into three separate pre-chilled 15 mL tubes. For the positive control, 0.2 ng of undigested vector was added, no DNA was added to the negative control and 1 µL of ligated product was added to the experimental tube. The tubes were placed on ice for 10 minutes, heat shocked at exactly 42^{o}C for 45 seconds and immediately placed on ice for 2 minutes. A volume of 0.9 mL of freshly prepared chilled SOC medium (SOB medium with 20 mM glucose) was added and the samples were incubated in a 37^{o}C water bath for 60 minutes with shaking at 250rpm. For the experimental reaction and negative control, the contents were transferred to 1.5 mL micro-centrifuge tubes and centrifuged at 5000rpm for

60 seconds. Most of the supernatant, all but 100 µL, were discarded and the pellet was re-suspended in the remaining media. Approximately 50 µL of each cell culture was plated on a LB ampicillin plate and the inverted plates were incubated overnight in a 37ºC incubator.

3.7.7 Colony PCR and miniprep of bacterial culture

The next day, white colonies were randomly selected from the experimental and positive control plates with the tip of a sterile toothpick. The tip was then used to scrap the bottom of a 1.5 mL microcentrifuge tube for colony transfer then dropped into the paired culture tube with 4 mL LB ampicillin culture broth. The cultures were incubated overnight in a 37ºC water bath shaker (Labtech, Korea). Colony PCR was carried out with the tubes containing colony DNA along with the master mix ingredients detailed in Table 3.18.

Table 3.18: Colony PCR master mix composition.

Component	**Volume (µL)**
5 U/µL GoTaq DNA Polymerase (Promega, USA)	0.13
5X Green GoTaq Flexi Buffer (Promega, USA)	5.00
10 mM dNTP mix	0.50
$MgCl_2$ solution (Promega, USA)	1.00
10 µM Forward primer	1.30
10 µM Reverse primer	1.30
Nuclease-free water	15.80
Total volume	25.00 µL

Colony PCR was performed with the cycling conditions outlined in Table 3.19.

Table 3.19: Cycling conditions for colony PCR.

Step	Temperature (ºC)	Duration	Number of cycle(s)
Initial denaturation/ hold	95	2 minutes	1
Denaturation	95	30 seconds	35
Annealing	65	30 seconds	
Extension	72	55 seconds	
Final extension	72	5 minutes	1

The PCR products were separated on a 1.5% gel. Specific culture tubes containing the desired insert DNA were identified. The corresponding overnight culture tubes were vortex-ed and 1.5mL of each culture were transferred into a corresponding micro-centrifuge tube. The tubes were centrifuged at 6000rpm for 2 minutes and supernatants were discarded. Plasmid DNA purification was carried out with QIAprep Spin Miniprep Kit (Qiagen, UK) according to the manufacturer's protocol. Briefly, the pellet was re-suspended in 250 µL Buffer PI with added RNase A. For the cell lysis step, 250 µL of Buffer P2 was added and mixed. Without exceeding 5 minutes for the lysis step, 350 µL of Buffer N3 was immediately added, mixed and centrifuged at 13,000rpm for 10 minutes. A volume of 800 µL of supernatant was transferred to the spin column and centrifuged for 1 minute and the flow-through was discarded. For the pellet washing step, 0.75 mL Buffer PE with added ethanol was added to the spin column, centrifuged for 1 minute and flow-through was discarded. The spin column was centrifuged again for 1 minute to remove residual wash buffer. The spin column was transferred into a clean microcentrifuge tube and 60 µL of Buffer EB was added to the centre of the column to elute DNA. The column was left to stand for 1 minute and centrifuged for 1 minute. The miniprep products were then sent for sequencing to the First Base Laboratories Sdn. Bhd., Malaysia. The 5' junction between the vector and insert

were sequenced using T3 promoter primer to ensure proper insert sub-cloning.

3.8 Mammalian two-hybrid system

For *in vivo* protein-protein interaction confirmation, the CheckMate Mammalian Two-Hybrid System (Promega, USA) was used. The basic working principle of this system involves the transcription and expression of a firefly luciferase reporter gene (*luc*$^+$) when two modular domains, encoded on separate plasmids, pACT and pBIND, are closely associated in a mammalian cell environment. The two domains are a pACT VP16 transcriptional activation domain and a pBIND GAL4 DNA-binding domain, which are expressed in fusion with target protein "X" and putative interacting protein "Y" respectively. The close association or direct interaction of protein "X" and protein "Y" will result in the assembly of RNA polymerase II complexes at the TATA box on pG5*luc* vector and results in the transcription of the firefly luciferase gene (*luc*$^+$). In addition to that, the pBIND vector encodes for *Renilla reniformis* luciferase gene, in which its expression is used as a normalization control for transfection efficiency (Figure 3.2).

In this study, candidate full-length coding sequences were cloned into both pACT and pBIND vectors to reduce possible vector-dependency and directionality. pACT-MyoD control vector and pBIND-Id control vectors that encode for two proteins known to interact *in vivo* were included as positive controls. pG5*luc* vector was co-transfected with reporter vectors in each experimental set as an internal control vector.

The maps of these vectors are shown in subsequent pages (Figure 3.3 to Figure 3.7).

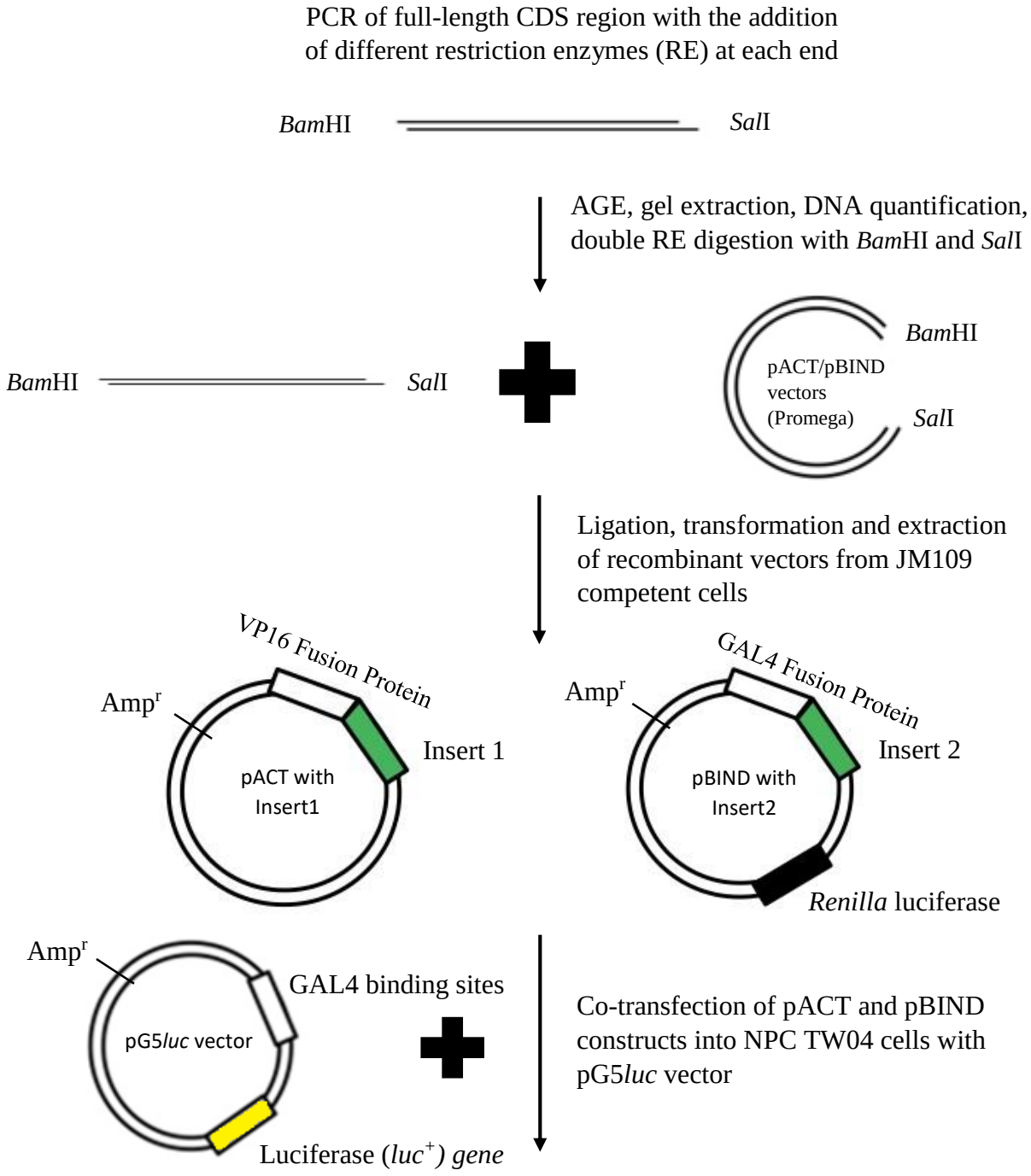

Figure 3.2: General scheme of Mammalian Two-Hybrid System.

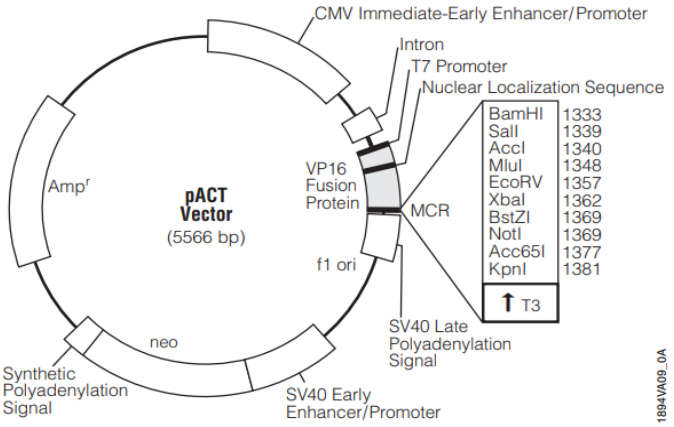

Figure 3.3: pACT Vector circle map.

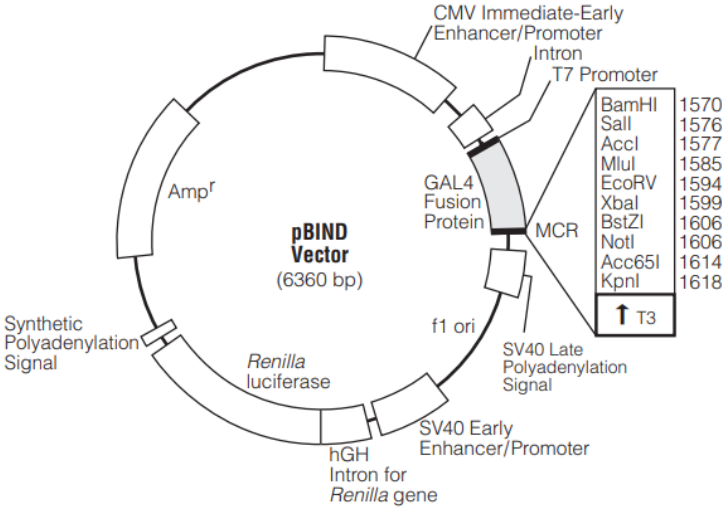

Figure 3.4: pBIND Vector circle map

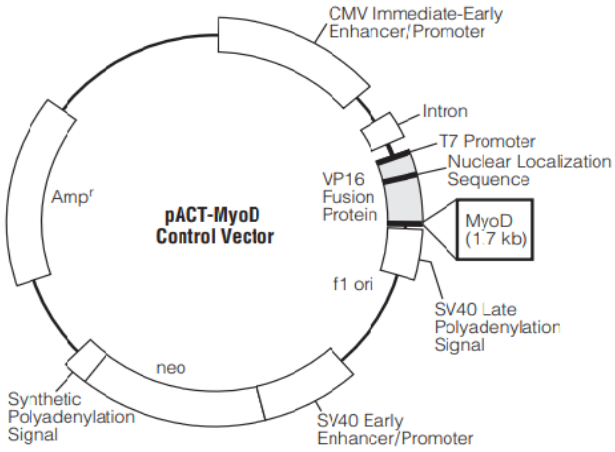

Figure 3.5: pACT-MyoD Control Vector circle map

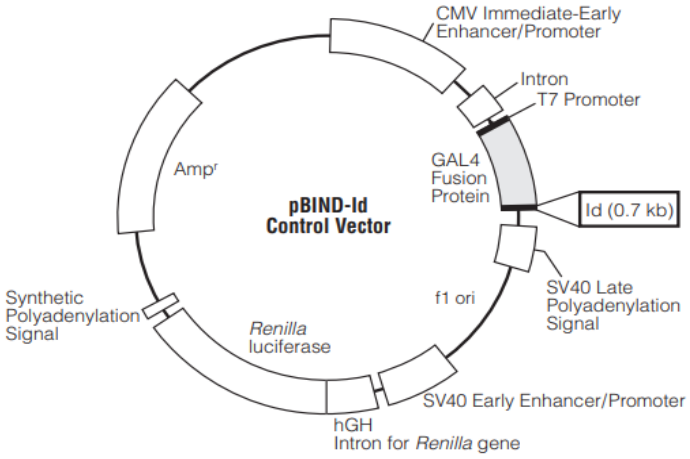

Figure 3.6: pBIND-Id Control Vector circle map

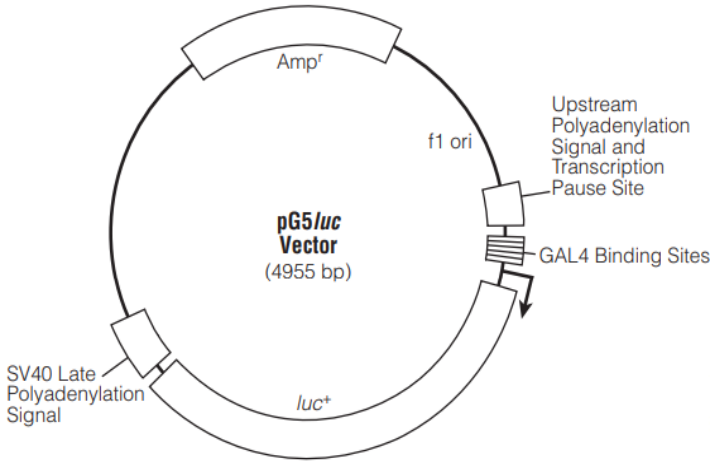

Figure 3.7: pG5*luc* Vector circle map

3.8.1 Cell counting

The cell concentration was calculated with a haemocytometer (Hirschmann Laborgeräte, Germany). After the suspension was gently mixed to ensure even distribution of cells, a 1:1 dilution of cell suspension to 0.08% trypan blue solution (Sigma-Aldrich, USA) for a total volume of 40 µL. The mixture was left at room temperature for 5 minutes to allow the staining of dead cells. After gentle pipetting, 10 µL of the mixture was carefully transferred into the chamber between the haemocytometer and the coverslip without the introduction of

bubbles. Using 100x magnification under an inverted microscope, the cells were ensured to be evenly distributed without any overlapping of cells. The number of viable cells, which were unstained, were counted in the four-square grids at each corner. The total number of viable cells from the four grids were averaged and cell concentration and volume of media to be added to achieve targeted density were calculated as follows:

Cell density (cells/ mL) = Average number of viable cells x Dilution factor x 10^4

Volume of media to be added (mL) = $\frac{Total\ cells}{Target\ density\ (\text{Cells/mL})}$

3.8.2 Transfection of gene constructs into mammalian cells

For transfection, TW04 cell line was used. In a 24-well plate, a density of $1.0x10^5$ cells/ well were seeded in 1 mL complete culture medium in a CO_2 incubator at 37°C for 24 hours or until a confluency of 80% had been achieved. Liposome transfection was carried out with Lipofectamine 2000 Reagent (Invitrogen, USA) following the Lipofectamine 2000 DNA Transfection Reagent Protocol (Invitrogen, USA). Lipofectamine Reagent (optimized at 3 µL) was diluted in 50 µL of serum-free Opti-MEM Reduced Serum Medium (Gibco, USA). Stock solution of DNA comprising of vectors and controls were prepared in 20 µM aliquots. During transfection, 2.5 µL of 20 µM stock solution was diluted in 50 µL Opti-MEM medium. A molar ratio of 1:1:1 for pACT: pBIND: pG5*luc* vectors was routinely used for each experimental set. The diluted DNA and diluted Lipofectamine 2000 Reagent was then mixed in a 1:1 ratio and incubated for 5 minutes at room temperature. The existing spent medium in the 24-well plate was aspirated and discarded and the cell monolayer was washed twice with Opti-MEM medium and added with 1 mL complete growth medium. Following that, appropriate amounts and combinations of vectors and controls were added in a 1:1:1 molar ratio to the assigned wells for transfection and mixed by gentle swirling of well plate.

The plate was then incubated at 37ºC in a 5% CO_2 incubator for approximately 48 hours.

For the synergistic effect of ribosomal proteins on the interaction of NPM1 and MDM2 proteins, full-length CDS region of ribosomal proteins were cloned in-frame into pCI-neo mammalian expression vector (Promega, USA). pCI-RP vectors were subsequently co-transfected with recombinant pACT and pBIND plasmids as indicated at an increasing molar ratio of 1:1:1, 2:1:1 and 3:1:1 in duplicates.

3.8.3 Luciferase reporter assay

Reporter assay was carried out according to the manufacturer's protocol with the Dual-Luciferase Reporter Assay System (Promega, USA), which allowed for the activities of both firefly (*Photinus pyralis*) and *Renilla* (*Renilla reniformis*) luciferases to be selectively and sequentially quantitated in a single sample. Firefly luciferase activity corresponded proportionally to the activity of the reporter of interest while *Renilla* luciferase activity was incorporated as an internal normalizing control for cell viability and transfection efficiency. After 48 hours post-transfection, the spent media in each well were aspirated and the cells were gently washed with 1X PBS. The rinse solution was completed removed from the wells before the addition of 100 µL 1X passive lysis buffer (Promega, USA) and incubated for 15 minutes at room temperature on a rocking platform for cell lysis. Meanwhile, Dual-Glo Luciferase Substrate was resuspended in Dual-Glo Luciferase Buffer to prepare the Dual-Glo Luciferase Reagent required for the assay. After 15 minutes, 100 µL of Dual-Glo Luciferase Reagent was added into each experimental well and the firefly luciferase luminescence activity was measured using a TECAN Infinite 200 Pro Microplate Reader (TECAN, Switzerland) for 10 seconds and recorded. Immediately after that, 50 µL of Dual-

Glo Stop & Glo Reagent was added and mixed briefly in order to quench the firefly luciferase signal and simultaneously to activate *Renilla* luciferase reaction. The *Renilla* luciferase reporter activity was then measured for 10 seconds and recorded as an internal control.

3.8.4 Data Analysis

Adjusted luciferase activity of each well was obtained by subtracting the background activity of the firefly luciferase of the non-transfected control reaction. Subsequently, the relative luciferase activity of each well was calculated by normalising the firefly luciferase activity (RFU) to that of its corresponding *Renilla* RFU, and the duplicate normalized readings were averaged. The averaged firefly/*Renilla* RFU ratio of each experimental set was then normalized against that of the averaged RFU of all negative controls, resulting in a quantified fold-change measurement of the firefly activity in comparison to the background signal. Results were expressed as the mean and standard deviation of duplicate measurements for each experimental set. Student's *t*-test was used to determine statistical significance.

3.8.5 Deletion Mutant Construction

Sequential deletion of deletion mutant ribosomal protein uS4 (S9), uL14 (L23) and NPM1 have been reported in literature (Dai et al., 2004; Lindström, 2012; Shi et al., 2017). For luciferase assay, DNA fragments of mutated target proteins were amplified with the primers outlined in Table 3.20, unless stated otherwise. The 5' junctions between the insert and vector were sequence verified by First Base Laboratories Sdn. Bhd.

Table 3.20: Primer sequences for deletion mutant constructs.

Fragments		Sequence (5'-3')	Gene product size (bp)
uS4 (S9)	uS4$^{1-60}$	F: ATTAGGATCCATGCCAGTGGCCCG	180
		R: ATAGTCGACGTCGTCAAGGGCCCGC	
	uS4$^{1-120}$	F: ATTAGGATCCATGCCAGTGGCCCG	360
		R: CTGGTCGACGAACCGGTTCGGGTCGA	
	uS4$^{121-194}$	Synthesized by First Base Laboratories Sdn. Bhd.	222
uL14 (L23)	uL14$^{1-105}$	F: ATAGGATCCATGTCGAAGCGAGGACGT	315
		R: ATAGTCGACGTGATACTGAGGACGTAA	
	uL14$^{35-105}$	Synthesized by First Base Laboratories Sdn. Bhd.	213
	uL14$^{66-140}$	Synthesized by First Base Laboratories Sdn. Bhd.	225
NPM1	NPM1$^{1-107}$	F: CGTCGGATCCATGGAAGATTCGATGGAC	321
		R: GCATGTCGACACCGGGACTTGGTGTGA	
	NPM1$^{108-188}$	Synthesized by First Base Laboratories Sdn. Bhd.	243
	NPM1$^{189-294}$	Synthesized by First Base Laboratories Sdn. Bhd.	318

3.9 Establishment of uS4 (S9)- and uL14 (L23)- Expressing Cell Line

Similar transfection protocol was utilized as previously described in Section 3.7.2 of Materials and Methods except for a few amendments as stated. NPC TW04 cells were transfected with pCI-uS4 (S9), pCI-uL14 or pCI-neo control vector and incubated at 37ºC in a 5% CO_2 incubator for approximately 24 hours. To select for transfected cells expressing uS4 (S9) or uL14 (L23), sub-confluent cells were seeded at a low cell density and the antibiotic G-418 (Promega, USA) was added to the medium at a concentration of 400 µg/mL. Antibiotic-resistant cells were then selected and re-plated to confluency.

3.10 Cellular Sub-fractionation of NPC Cells

NP69, TW04 and TW04-pCI-uS4 cells were cultured to approximately 80% confluency and the cells were washed thrice with ice-cold PBS (Nacalai Tesque, USA). Cells were then trypsinized with the addition of 0.25% trypsin enzyme solution (Gibco, USA) with 0.53 mM ethylenediaminetetraacetic acid (EDTA) (Gibco, USA) and placed in a CO_2 incubator at 37°C for 5 minutes. The cells were then centrifuged at 1000rpm for 4 minutes. Supernatant was discarded and the pellet was washed with PBS and spun again. The pellet was re-suspended in 5 mL ice-cold Buffer A (10 mM HEPES, pH 7.9, 1.5 mM $MgCl_2$, 10 mM KCl, 0.5mM dithiothreitol (DTT) and supplemented with 1 mM phenylmethanesulfonylfluoride (PMSF) protease inhibitor (Roche Applied Sciences, Switzerland). After incubation on ice for 5 minutes, the sample was subjected to homogenization by passing it through a 27g needle. After centrifugation at 1000rpm, 4^oC for 5 minutes, the supernatant was aspirated and kept as the cytoplasmic fraction. The resulting pellet was re-suspended in 3 mL of Buffer S1 (0.25M sucrose, 10 mM $MgCl_2$) and layered with 3 mL Buffer S2 (0.35M sucrose, 0.5 mM $MgCl_2$). After a 5 minutes incubation and a 5 minutes centrifugation at 2500rpm at 4^oC, the supernatant was discarded while the pellet was re-suspended in 3 mL of Buffer S2 and homogenized with a 25g needle. The homogenized sample was layered with 3mL of Buffer S3 (0.88M sucrose, 0.5 mM $MgCl_2$) and incubated for 5 minutes followed by centrifugation at 3500rpm, 4^oC for 5 minutes. The supernatant was aspirated and kept as the nucleoplasmic fraction while the pellet was resuspended in 500 µL of Buffer S2 and spun for 5 minutes at 4^oC at 3500rpm and kept as the nucleoli fraction. The fractions were kept in a -80^oC ultra-freezer until further use.

CHAPTER 4

DIFFERENTIAL EXPRESSION AND SEQUENCE ANALYSIS OF TARGET GENES IN NPC-DERIVED CELL LINES

4.1 Background

The list of RPs and their putative partners was generated based on a comprehensive meta-analysis of differential genetic datasets across several cancers (Choi et al., 2005). With 10 independent microarray datasets on differential gene expression profiling of 13 human cancers, two gene co-expression networks were generated: a normal and a tumour specific network. This allowed for the exploration of inter-dependable transcription expression in terms of gene interaction instead of individual genes, and the comparison between the two networks to discover cancer-induced modifications. After the exclusion of conserved associations between the normal and tumour networks, subsequent functional grouping and cluster analysis yielded a highly tumour specific network of interconnecting genes related to protein biosynthesis. As such, RPs and their putative co-acting factors were reported to be differentially expressed within the tumour network in comparison to the normal network. These genes were selected for gene expression analysis in nasopharyngeal carcinoma, which was not among the cancer datasets incorporated in the bioinformatics study, granting added advantage to this project[1]. Moreover, this study is the first to report on the differential expression of this subset of RP genes and their putative interacting partners in NPC.

[1] Part of this chapter has been published in Sim, Ng, Lee, & Narayanan. (2017). The *eS8*, *uS4*, *eS31*, and *uL14* Ribosomal Protein Genes Are Dysregulated in Nasopharyngeal Carcinoma Cell Lines. *BioMed Research International*, *2017*, 4876954.

4.2 Methodology Overview

Six NPC-derived cell lines (HONE-1, SUNE-1, HK1, TW01, TW04 and C666-1) of different histopathological subtypes and an immortalized normal nasopharyngeal epithelial cell line, NP69 as listed in Table 3.1 were used in this study. Total RNA was isolated from each cell lines in triplicates. Each of the RNA samples was DNase-treated prior to reverse transcription using M-MLV RT. The differential expression of each target gene was determined with quantitative real-time PCR (qPCR) in nasopharyngeal carcinoma cell lines in comparison to that of NP69.

4.3 Results and Discussion

4.3.1 qPCR relative amplification efficiencies were validated

The efficiencies, *E*%, of each primer set were firstly validated as strictly required by the $2^{-\Delta\Delta C_T}$ relative quantification method used to analyse differential changes in gene expression from real-time quantitative PCR experiments (Livak & Schmittgen, 2001). Standard calibration curves of each primer pair were plotted to determine the slope to calculate for amplification efficiency (Appendix A). The correlation coefficients and PCR efficiencies of each primer set are shown in Table 4.1.

Table 4.1: Correlation coefficients and PCR efficiencies of primers.

Gene	Slope, m	Correlation Coefficient, R^2	Amplification	Efficiency, *E*%
GAPDH	-3.194	0.986	1.037	103.72
Beta Actin	-3.168	0.993	1.068	106.80
uS4 (S9)	-3.448	0.980	0.951	95.11
eS8 (S8)	-3.094	0.986	0.955	95.45
eS31 (S27a)	-3.612	0.993	0.892	89.17
eL6 (L6)	-3.312	0.960	1.013	101.26
uL14 (L23)	-3.430	0.992	0.978	97.83
eL18 (L18)	-3.253	0.999	1.030	102.96
eL24 (L24)	-3.164	0.967	1.069	106.95
eL30 (L30)	-3.083	0.981	1.055	105.54
NPM1	-3.152	0.996	1.076	107.62
BTF3	-3.365	0.987	0.969	96.92
UBA52	-3.378	0.997	0.977	97.67

The efficiency curves for each primer set were found to have $R^2 \geq 0.960$ and *E%* between 89.17 and 107.62%, which were well within the required amplification range of 0.9-1.1 (90%-110%), corresponding to a slope of between -3.1 to -3.6.

In an ideal PCR amplification efficiency of 100%, the number of target sequence should double after each replication cycle. PCR efficiency of less than 100% suggests poor primer design, non-optimal conditions (reagent concentrations and reaction parameters), and potential formation of dimers and hairpins. A generally acceptable range is 90-100%. On the other hand, PCR efficiency of more than 100% indicates polymerase inhibition due to high amounts of template and/or presence of carry-over contaminants, thus prematurely levelling out the amplification plot, decreasing slope and resulting in PCR efficiency of over 100%. An acceptable range is 100-110% (Livak & Schmittgen, 2001).

The selection of a compatible endogenous control was conducted by generating relative primer efficiencies of *glyceraldehyde-3-phosphate dehydrogenase (GAPDH*) or *beta-actin (ACTB)* against that of respective target genes (Appendix B, Parts 1 and 2). The transcript expression of *ACTB* across five template dilutions was observed to be significantly higher than that of *GAPDH*. However, incompatible relative amplification efficiencies of *ACTB* and target genes (absolute value of the slope, m >0.1) were detected after the generation of validation curve (Appendix B, Part 2). As such, the PCR efficiency of GAPDH was determined to be more compatible to that of the target genes, as substantiated by the range of absolute value of slope to be <0.1 (0.0087- 0.0981), with the acceptable exclusion of extreme outlier points as denoted in Table 4.2 as 'N/A'. As the validation experiments demonstrated that the amplification efficiencies of the target and the endogenous control gene (*GAPDH*) were approximately equal (absolute value of slope, m <0.1), the validity of qPCR assay was ascertained and the $\Delta\Delta C_T$ method was employed to calculate the fold-differences of the target genes when compared to the reference gene between various samples (Table 4.2 and Figure 4.1).

Table 4.2: Log input RNA and ΔC_T of targets for validation protocol.

Input amount (ng)	4.000	0.800	0.160	0.032	0.0064	Absolute value
Log input amount	**0.602**	**-0.097**	**-0.795**	**-1.495**	**-2.194**	**of slope**
ΔC_T uS4 (S9)	5.41	N/A	5.59	5.8	5.53	0.075
ΔC_T eS8 (S8)	5.56	5.4	5.55	5.94	5.47	0.052
ΔC_T eS31 (S27a)	3.58	3.72	3.85	3.65	N/A	0.049
ΔC_T eL6 (L6)	9.43	8.96	8.33	8.47	9.87	0.056
ΔC_T uL14 (L23)	3.27	3.42	3.6	3.19	N/A	0.009
ΔC_T eL18 (L18)	0.05	-0.05	-0.3	-0.35	0.26	0.017
ΔC_T eL24 (L24)	4.26	4.24	4.08	2.93	4.67	0.070
ΔC_T eL30 (L30)	0.54	-0.37	-0.69	-0.56	0.50	0.039
ΔC_T NPM1	5.56	5.07	5.04	4.78	5.4	0.087
ΔC_T BTF3	6.67	6.76	6.73	N/A	6.96	0.098
ΔC_T UBA52	0.49	0.58	0.52	0.58	N/A	0.030

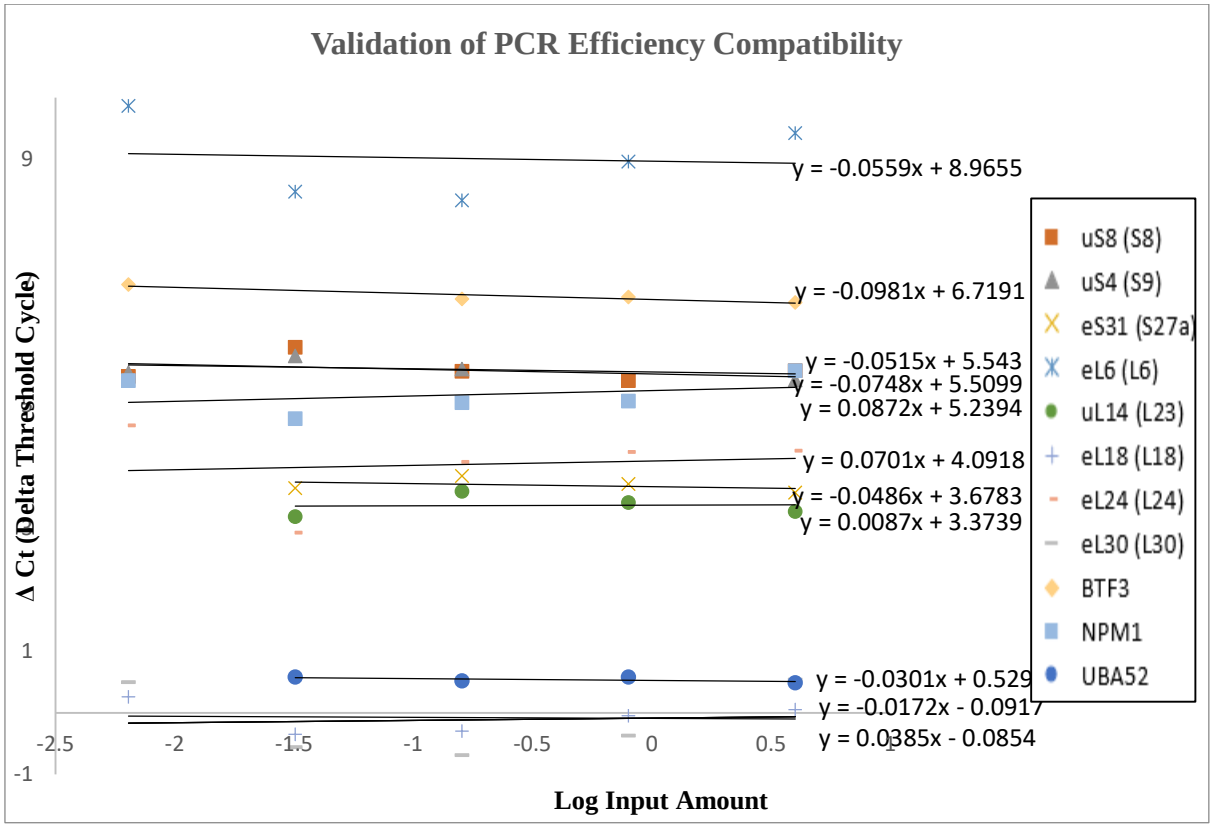

Figure 4.1: Validation plot of ΔC_T vs. log input amount of RNA.

4.3.2 Differential expressions of each target gene in individual NPC cell lines

qPCR assay was performed to determine the differential expression of eleven target genes in six NPC cell lines compared to NP69. ΔC_T values were first obtained by subtracting the average C_T value of *GAPDH* from that of each target gene. Following that, $\Delta\Delta C_T$ was calculated by subtracting the ΔC_T of the normal NP69 cell line from that of each NPC cell line. Standard deviations of $\Delta\Delta C_T$ values were then incorporated to form the upper and lower limit before the final log-form of $2^{-\Delta\Delta C_T}$ (fold difference) calculations (Appendix C). The FD calculation protocol adopted herein is a direct reflection of that published in the highly-cited and reviewed paper by Livak and Schmittgen on equations to analyse quantitative gene expression data using relative quantification (Livak & Schmittgen, 2001). This method incorporates the standard deviation into the final FD calculation for error estimation, thereby leading to a range of values that is distributed asymmetrically due to the conversion of exponential values into a linear comparison.

For data analysis, it is essential to point out that statistical measurement was performed with ΔC_T values and not on the final log-fold difference $2^{-\Delta\Delta C_T}$ values. This is because the application of $2^{-\Delta\Delta C_T}$ values in an unpaired *t*-test would favourably discriminate under-expression data (<1.0) due to relatively consistent values as its range is compressed to the range of 0.00-0.99 whereas up-regulation data ranges from 1.01 to infinity (J. S. Yuan, Reed, Chen, & Stewart, 2006). On the other hand, ΔC_T expression values have an approximate log-normal distribution and therefore, a normal distribution. Hence, ΔC_T data (normalized expression values) can be aptly utilized for statistical significance. Table 4.3 summarizes the fold change values of eleven genes of interest in three biological replicates of each cell line and the corresponding *p*-values for each NPC cell line.

Table 4.3: Normalized mean fold change ($2^{-\Delta\Delta C_T}$) of respective genes in six NPC cell lines relative to normal nasopharyngeal epithelial cell line, NP69, calculated with $\Delta\Delta C_T$ method.

Gene	Cell Line	$2^{-\Delta\Delta C_T}$			Mean FD	SD	*p*-value
		BR1	BR2	BR3			
uS4 (S9)	NP69	1.579	1.025	1.044	**1.216**	0.315	-
	HONE-1	0.26	0.226	0.002	**0.163**	0.140	0.110
	SUNE-1	0.008	0.001	0.151	**0.053**	0.084	0.006
	HK1	0.409	0.038	8.1E-05	**0.149**	0.226	0.097
	TWO1	0.044	0.007	7.9E-05	**0.017**	0.024	0.031
	TWO4	0.253	0.118	0.190	**0.187**	0.068	0.030
	C666-1	0.448	0.202	2.2E-04	**0.217**	0.224	0.104
eS8 (S8)	NP69	1.001	1.01214	1.025	**1.013**	0.012	-
	HONE-1	0.618	0.22036	0.082	**0.307**	0.278	0.068
	SUNE-1	0.072	0.03067	0.081	**0.061**	0.027	0.048
	HK1	0.319	0.18534	0.065	**0.190**	0.127	0.058
	TWO1	0.238	0.45298	0.064	**0.252**	0.195	0.075
	TWO4	0.169	0.28435	0.024	**0.159**	0.130	0.044
	C666-1	0.284	0.09541	0.114	**0.164**	0.104	0.070
eS31	NP69	1.003	1.012	1.025	**1.013**	0.011	-
(S27a)	HONE-1	5.042	1.391	1.054	**2.496**	2.212	0.294
	SUNE-1	0.103	0.168	0.056	**0.109**	0.056	0.021
	HK1	0.648	0.570	0.290	**0.503**	0.188	0.168
	TWO1	0.308	0.525	0.145	**0.326**	0.191	0.069
	TWO4	0.24	0.314	0.089	**0.214**	0.115	0.045
	C666-1	0.131	0.103	0.274	**0.169**	0.092	0.086
eL6 (L6)	NP69	1.032	1.093	1.116	**1.080**	0.043	-
	HONE-1	0.027	0.04	0.414	**0.160**	0.220	0.172
	SUNE-1	2.473	2.459	11.502	**5.478**	5.217	0.274
	HK1	18.24	10.93	1.963	**10.378**	8.153	0.153
	TWO1	4.441	3.315	0.969	**2.908**	1.771	0.114
	TWO4	6.546	10.83	1.815	**6.397**	4.509	0.069
	C666-1	1.968	2.564	2.565	**2.366**	0.344	0.365

Table 4.3 continued

uL14 (L23)	NP69	1.036	1.034	1.299	**1.123**	0.152	-
	HONE-1	0.375	0.081	0.048	**0.168**	0.180	0.072
	SUNE-1	0.237	0.156	0.127	**0.173**	0.057	0.067
	HK1	0.466	0.369	0.082	**0.306**	0.200	0.087
	TWO1	0.265	0.219	0.085	**0.190**	0.094	0.060
	TWO4	0.411	0.426	0.088	**0.308**	0.191	0.095
	C666-1	0.105	0.04	0.097	**0.081**	0.035	0.034
eL18 (L18)	NP69	1.02	1.015	1.026	**1.020**	0.006	-
	HONE-1	3.02	3.762	1.403	**2.728**	1.206	0.102
	SUNE-1	93.702	94.864	73.496	**87.354**	12.015	0.001
	HK1	3.59	5.351	1.096	**3.346**	2.138	0.078
	TWO1	1.358	1.864	1.181	**1.468**	0.354	0.257
	TWO4	2.021	2.525	1.157	**1.901**	0.692	0.141
	C666-1	14.825	17.692	5.01	**12.509**	6.651	0.013
eL24 (L24)	NP69	1.028	1.004	1.143	**1.058**	0.074	-
	HONE-1	1.267	19.012	3.778	**8.019**	9.603	0.262
	SUNE-1	0.827	0.337	0.117	**0.427**	0.363	0.182
	HK1	3.805	1.505	0.112	**1.807**	1.865	0.428
	TWO1	0.654	0.813	0.048	**0.505**	0.404	0.161
	TWO4	0.822	0.858	0.042	**0.574**	0.461	0.182
	C666-1	0.328	0.186	0.062	**0.192**	0.133	0.084
eL30 (L30)	NP69	1.065	1.007	1.146	**1.073**	0.070	-
	HONE-1	3.487	1.765	10.581	**5.278**	4.673	0.157
	SUNE-1	6.261	1.050	1.811	**3.041**	2.815	0.107
	HK1	3.638	2.259	57.282	**21.060**	31.377	0.099
	TWO1	3.221	4.9	20.955	**9.692**	9.790	0.117
	TWO4	1.623	1.918	13.701	**5.747**	6.890	0.220
	C666-1	3.58	1.488	77.642	**27.570**	43.376	0.130

Table 4.3 continued

NPM1	NP69	1.017	1.005	1.042	**1.021**	0.019	-
	HONE-1	0.018	0.034	0.012	**0.021**	0.011	0.001
	SUNE-1	0.48	0.416	0.066	**0.321**	0.223	0.015
	HK1	0.888	0.921	0.009	**0.606**	0.517	0.138
	TWO1	0.259	0.267	0.15	**0.225**	0.065	0.017
	TWO4	0.407	0.395	0.144	**0.315**	0.149	0.031
	C666-1	1.682	1.173	0.214	**1.023**	0.745	0.144
BTF3	NP69	1.012	1.087	1.462	**1.187**	0.241	-
	HONE-1	0.1	0.549	0.49	**0.380**	0.244	0.301
	SUNE-1	0.419	0.064	0.848	**0.444**	0.393	0.293
	HK1	0.157	0.487	0.546	**0.397**	0.210	0.318
	TWO1	0.339	0.428	0.558	**0.442**	0.110	0.162
	TWO4	2.106	8.304	28.411	**12.940**	13.752	0.360
	C666-1	1.592	31.926	3.577	**12.365**	16.969	0.425
UBA52	NP69	1.015	1.018	1.078	**1.037**	0.036	-
	HONE-1	9.665	31.473	3.160	**14.766**	14.830	0.102
	SUNE-1	0.539	0.441	0.251	**0.410**	0.146	0.257
	HK1	0.922	0.996	0.081	**0.666**	0.508	0.229
	TWO1	0.968	0.740	0.113	**0.607**	0.443	0.352
	TWO4	1.337	1.439	0.041	**0.939**	0.779	0.373
	C666-1	0.224	0.806	0.253	**0.428**	0.328	0.209

BR: Biological replicate; FD: Fold difference; SD: Standard deviation. $2^{-\Delta\Delta C_T}$ is the relative expression of fold difference Statistical analysis for *p*-value was derived from ΔC_T (normalized fold difference) with independent, one-tailed, Student's *t*-test with unequal variances (pre-determined, data not shown).

Referring to Table 4.3, the fold difference of each gene in control NP69 (control normal cell line) would always be close to 1.0 (FD ~1.0) due to the normalization step against itself, setting the baseline standard for differential expression determination. Calculated fold difference of more than the baseline 1.0 (FD >1.0) would be considered over-expression while values less than baseline 1.0 (FD <1.0) would be considered under-expression provided the FDs are statistically significant.

A total of four ribosomal protein genes (*uS4 (S9), eS8 (S8), eS31 (S27a)* and *uL14 (L23)*) were found to be consistently under-expressed with a fold change of <0.307, signifying an approximate 70% reduction in expression in NPC cell lines. Out only eleven target genes, only one ribosomal protein genes (*eL18 (L18)*) was up-regulated at least 1.5-fold in all the six NPC cell lines. The rest of the six target proteins revealed inconsistent expression pattern across the cell lines tested (Table 4.3).

The standard deviations for the expression of certain target genes in a biological replicate were observed to be higher than that of the mean FD. The high expression variability demonstrated across different pools of total RNAs with different passage numbers has been shown to be strongly correlated to environmental conditions and genetic perturbations, thus obscuring biological equivalency of samples within a cell line (Kaern, Elston, Blake, & Collins, 2005). Nevertheless, average mean FD from all three biological replicates was calculated in order to capture the biological variation in an entire cell line.

To further examine the differential expression pattern of each gene, the mean fold differences in each NPC cell line are placed side-by-side in a linear y-axis bar graph.

However, it is important to note that such data illustration is not sufficient and may mislead readers due to its linear skewness towards over-expression data (FD >1.0) and the corresponding lack of proportionate representation of down-regulation values (FD <1.0). Therefore, the linear axis is transformed into log_2-y-axis to generate corresponding logarithmic graphs that appropriately emphasize both up- and down-regulations equally.

4.3.3. Differential expressions of genes of interest in collective NPC cell lines

To examine the overall differential transcript expression of each gene in the carcinogenesis of NPC, the means of fold difference (FD) of six NPC cell lines, namely, HONE-1, SUNE-1, HK1, TW01, TW04, and C666-1 were averaged and compared to that of the normal nasopharyngeal epithelium cell line, NP69 (Table 4.4.and Figure 4.2).

Of the eight ribosomal protein genes under study, only *eL18 (L18)* was significantly up-regulated (*p*-value= 0.015). Of the under-regulated RP genes, the reduction of *uS4 (S9), eS8 (S8), eS31 (S27a)* and *uL14 (L23)* were deemed significant. As for the three putative co-acting factors, all were under-expressed though only *NPM1* was significantly down-regulated in NPC cell lines (*p*-value= 0.005) (Table 4.4). Taken together, six of the initial eleven target genes were differentially expressed in NPC cell lines, cumulatively.

Table 4.4: Relative expression of each gene in NPC cell lines compared to NP69.

Gene	Cell Line	Mean FD	SD	*p*- value	Overall Expression
uS4 (S9)	NP69	1.216	0.315	3.59E-04	Under-expression
	NPC	0.131	0.145		
eS8 (S8)	NP69	1.013	0.012	0.044	Under-expression
	NPC	0.189	0.158		
eS31 (S27a)	NP69	1.013	0.011	0.048	Under-expression
	NPC	0.264	0.185		
eL6 (L6)	NP69	1.080	0.043	0.142	Not significant
	NPC	5.505	5.056		
uL14 (L23)	NP69	1.123	0.152	0.040	Under-expression
	NPC	0.204	0.146		
eL18 (L18)	NP69	1.020	0.006	0.015	Over-expression
	NPC	18.218	32.405		
eL24 (L24)	NP69	1.058	0.074	0.179	Not significant
	NPC	0.400	0.340		
eL30 (L30)	NP69	1.073	0.070	0.153	Not significant
	NPC	12.065	21.090		
NPM1	NP69	1.021	0.019	0.005	Under-expression
	NPC	0.293	0.286		
BTF3	NP69	1.187	0.241	0.153	Not significant
	NPC	0.415	0.223		
UBA52	NP69	1.037	0.036	0.481	Not significant
	NPC	0.610	0.458		

FD: Fold difference; SD: Standard deviation. Statistical analysis for *p*-values was performed using independent, single-tailed, Student's *t*-test with unequal variances, with cumulative ΔC_T values of all NPC cell lines (normalized fold difference). Mean fold change >1.0 denotes up-regulation while mean fold change <1.0 denotes down-regulation.

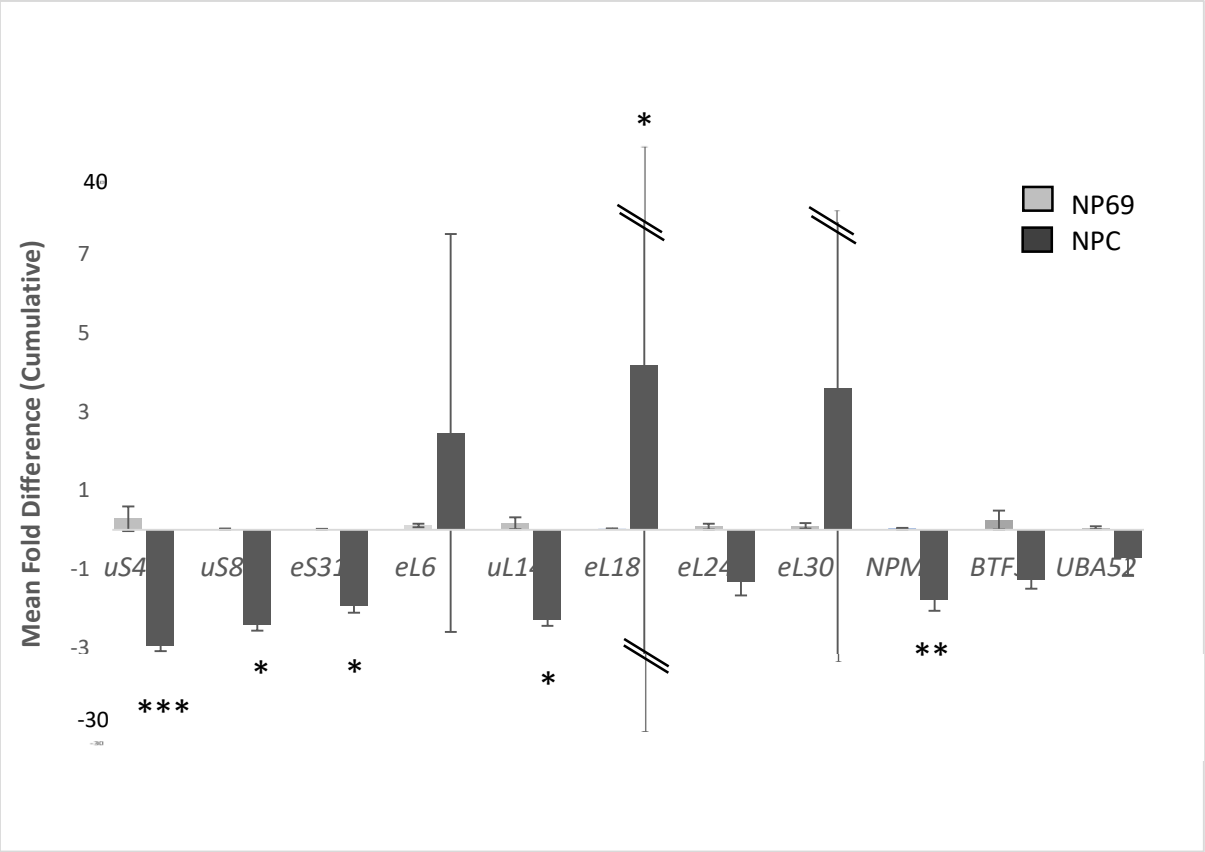

Figure 4.2: Relative fold difference of target genes in collective NPC cell lines. Semi-logarithmic representation of the cumulative mean fold difference (FD) of each target gene in NPC vs NP69 (normal epithelial nasopharyngeal cell line). Corresponding *p*-values are designated with asterisk (*). *: $p < 0.05$; **: $p < 0.01$; ***: $p < 0.001$. Double slant lines indicate a break in gridline sequence of the vertical axis. Error bars represent the standard deviation (SD) of the mean fold difference.

4.3.3.1 *uS4 (S9): uS4 (S9)* was significantly under-expressed in individual SUNE-1, TW01 and TW04 cell lines, as well as NPC cell lines cumulatively

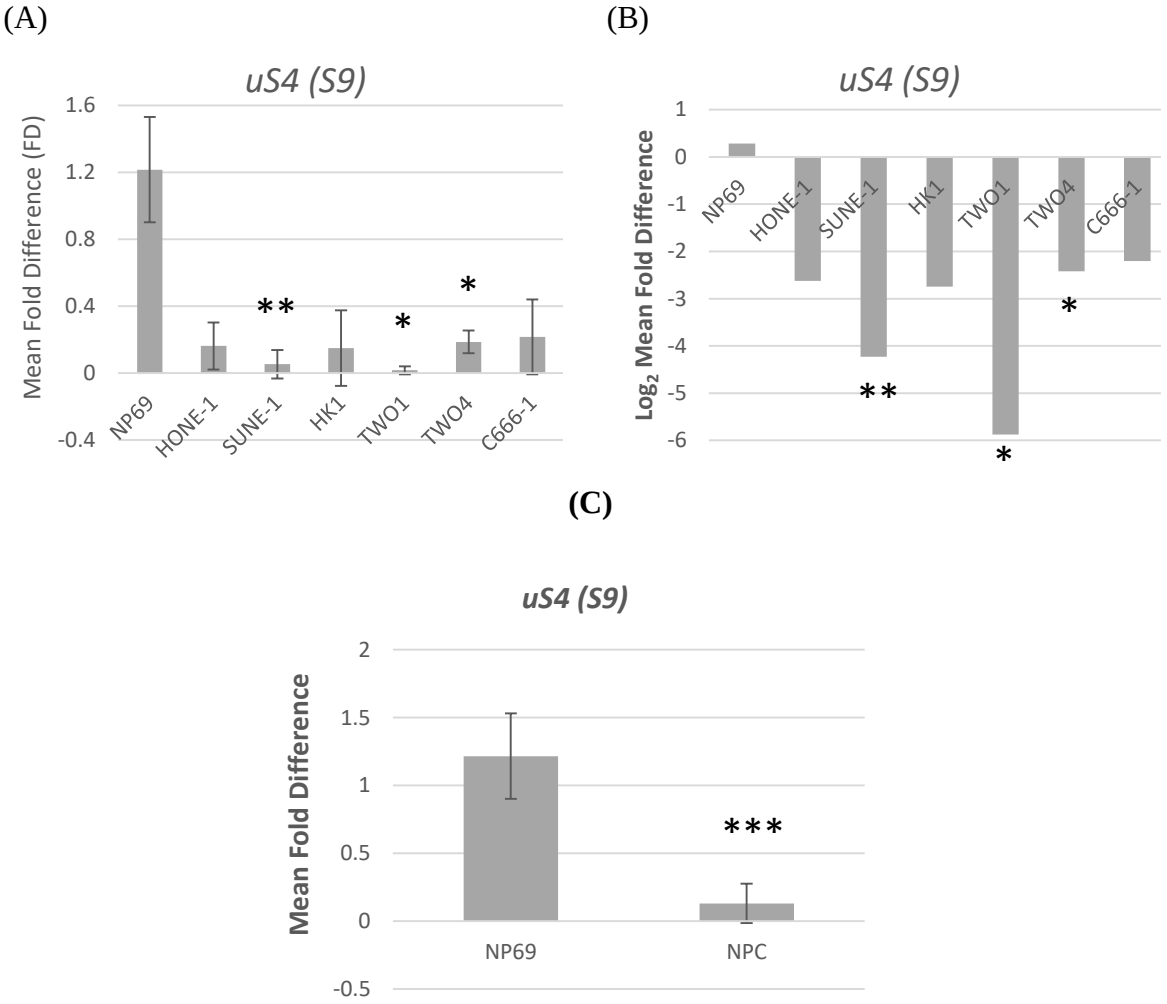

Figure 4.3: Expression of *uS4 (S9)* in six NPC cell lines compared to NP69. (A) Y-axis: mean fold difference (FD) as calculated as $2^{-\Delta\Delta C}{}_{T}$. (B) Y-axis: log-transformed fold difference (FD). (C) cumulative fold difference of *uS4 (S9)* in NPC vs. NP69. Data are presented as mean fold change±SD. Corresponding *p*-values are designated with asterisk (*). *: $p < 0.05$; **: $p < 0.01$; ***: $p < 0.001$.

Ribosomal protein uS4 (S9) was observed to be under-expressed in all NPC cell lines examined compared to NP69. The most drastic drop in expression was recorded in TW01 cell line (FD =0.017±0.024), which was approximately 98% reduction in expression relative

to NP69 (*p*-value =0.031). The most statistically significant reduction of *uS4 (S9)* was observed in SUNE-1 (FD=0.053±0.084; *p*-value=0.006). When the mean fold differences of *uS4 (S9)* in all six NPC cell lines were cumulated, the overall expression pattern showed a significant under-expression in NPC cell lines (mean FD=0.131±0.145; *p*-value 0.0004).

Similar expression pattern was reported in primary cells of SDS, highly invasive breast and pancreatic tumours, as well as in rapidly proliferating anaplastic astrocytoma (Crnogorac-Jurcevic et al., 2001; Zhou, Hess, Liu, Linskey, & Yung, 2005; Bin Amer et al., 2008; Burwick et al., 2011). However, a reversed over-expression trend was observed in colorectal carcinoma and osteosarcoma tissues and cell lines (Frigerio et al., 1995). For the latter, the up-regulation of uS4 (S9) strongly associated with cancer staging and recurrence while its knockdown increased p21 levels, which induced G_1/S cell cycle arrest and apoptosis in a p53-independent manner (Cheng et al., 2017). Surprisingly, despite being identified to be differentially expressed in various cancers and disorders, constitutive and steady level of uS4 (S9) was detected in adenoid cystic carcinoma, oral squamous cell carcinoma, liver cancer, and two subtypes of non-small cell lung cancer (SCLC), lung adenocarcinoma and squamous cell lung cancer, establishing uS4 (S9) as a suitable endogenous housekeeping gene in genetic expression assays (Huang et al., 2003; Kim & Kim, 2003; Brinkmann et al., 2011; Li et al., 2014; Zhan et al., 2014).

Interestingly, the expression of uS4 (S9) seemed to correlate with the differentiation status of the NPC cell lines. As a Type I keratinized well-differentiated NPC cell line, TW01 recorded the greatest reduction of uS4 (S9) expression compared to NP69 (FD=0.017±0.024) (Figure 4.3). After TW01, SUNE-1, HK1 and HONE-1, were ranked second, third and fourth

cell lines, respectively, in which uS4 (S9) was down-regulated- these three cell lines coincidentally are Type IIa non-keratinizing, well- to poorly-differentiated carcinoma. The least reduction was observed in Type IIb non-keratinizing, non-differentiated carcinoma cell lines, TW04 and C666-1. Pearson correlation analysis was conducted, and it validated a strong positive correlation between the relative extent of uS4 (S9) under-expression and the degree of differentiation of the cell lines, suggesting its potential role in cellular differentiation in nasopharyngeal carcinoma (Pearson coefficient, r = +0.780; n= 6).

Meanwhile, further depletion of the presently under-expressed uS4 (S9) in U2OS osteosarcoma cells and U343Mga CI2:6 glioma cells provided evidence for its role in inducing p53-mediated cell cycle arrest and promoting morphological differentiation of glioma cells. This was observed concurrently with an increased expression of glial fibrillary acidic protein (GFAP), a known marker of differentiation, as well as distinct morphological changes. However, uS4 (S9) knockdown in HeLa cells induced p53-dependent inhibition of cell proliferation and apoptosis, thereby ascertaining the diverse pathway and strength of molecular responses following uS4 (S9) depletion in each cancer cell type (Lindström & Nistér, 2010). Apart from that, under-expression of *uS4 (S9)* transcript was also reported in re-plated and non-re-plated (continuous cultures) differentiated neurons compared to undifferentiated cells, in conjunction with retinoic acid-induced neuronal differentiation of human embryonal carcinoma NTERA2 cells (Bévort & Leffers, 2000). Therefore, this interesting association between down-regulated *uS4 (S9)* expression and tumour differentiation in nasopharyngeal carcinoma cells indicate a possible extra-ribosomal function of ribosomal protein uS4 (S9) in cell growth and differentiation modulating pathways as well as a potential histopathology marker for NPC.

4.3.3.2 *eS8 (S8): eS8 (S8)* was significantly down-regulated NPC and specifically in SUNE-1 and TW04 cell lines

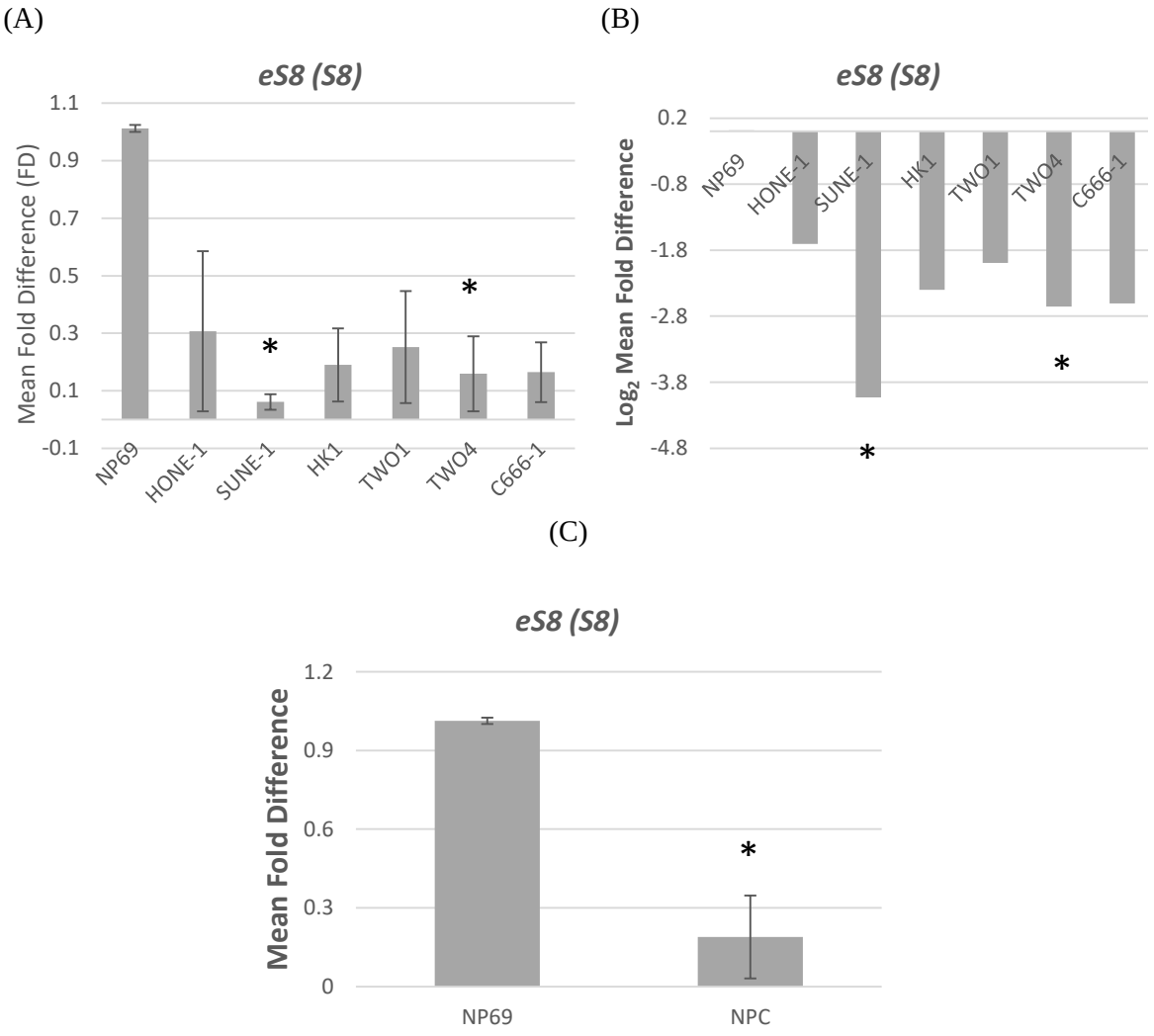

Figure 4.4: Expression of *eS8 (S8)* in six NPC cell lines compared to NP69. (A) Y-axis: mean fold difference (FD) as calculated as $2^{-\Delta\Delta C_T}$. (B) Y-axis: log-transformed fold difference (FD). (C) cumulative fold difference of *eS8 (S8)* in NPC vs. NP69. Data are presented as mean fold change±SD. Corresponding *p*-value is designated with asterisk (*). *: $p< 0.05$.

In all NPC cell lines, *eS8 (S8)* was under-expressed with the lowest dysregulation observed in SUNE-1 (FD=0.061±0.027; *p*-value=0.048), which saw an approximate 93% reduction

compared to NP69. Additionally, *eS8 (S8)* expression in TW01 cell line also recorded a significant down-regulation (FD=0.252±0.195; *p*-value=0.044). Cumulative analysis revealed that *eS8 (S8)* was significantly under-expressed in NPC cell lines relative to NP69 (mean FD=0.189±0.158; *p*-value=0.044) (Figure 4.4).

Though *eS8 (S8)* mRNA was found to be over-expressed in colorectal tumours and polyps in relation to normal colonic mucosa, eS8 (S8) protein was reported to be inversely under-expressed in colorectal carcinoma, revealing the non-conformity of mRNA and protein expression levels due to highly specific and exclusive transcription and translational control to a particular human cancer type (Pogue-Geile et al., 1991; Kasai et al., 2003). Besides colorectal carcinoma, *eS8 (S8)* transcript had been reported to be over-expressed in hepatocellular carcinoma and in association with histological grading of colon tumours (Kondoh et al., 2001). In contrast, the under-expression of *eS8 (S8)* mRNA was also observed in meningiomas brain tumours compared to non-tumoral meningothelial tissues (Pérez-Magán et al., 2010). Despite being differentially expressed in colorectal and brain neoplasms, *eS8 (S8)* has been regarded to be a reliable normalization factor in various molecular expression profiling studies on thyroid cancer (Oler et al., 2008; Camacho et al., 2013).

Relative to other ribosomal protein genes, not much work has been done on elucidating the role of *eS8 (S8)* expression on tumour phenotypes and molecular pathway framework, albeit various reports associating the dysregulation of *eS8 (S8)* expression with tumorigenesis. Herein, we report on the under-expression of *eS8 (S8)* in nasopharyngeal carcinoma cells, though how this observation affects downstream effector pathways remains unclear.

4.1.3.3.3 *eS31 (S27a)*: *uS31 (S27a)* was significantly down-regulated in NPC, and specifically in SUNE-1 and TW04 cell lines

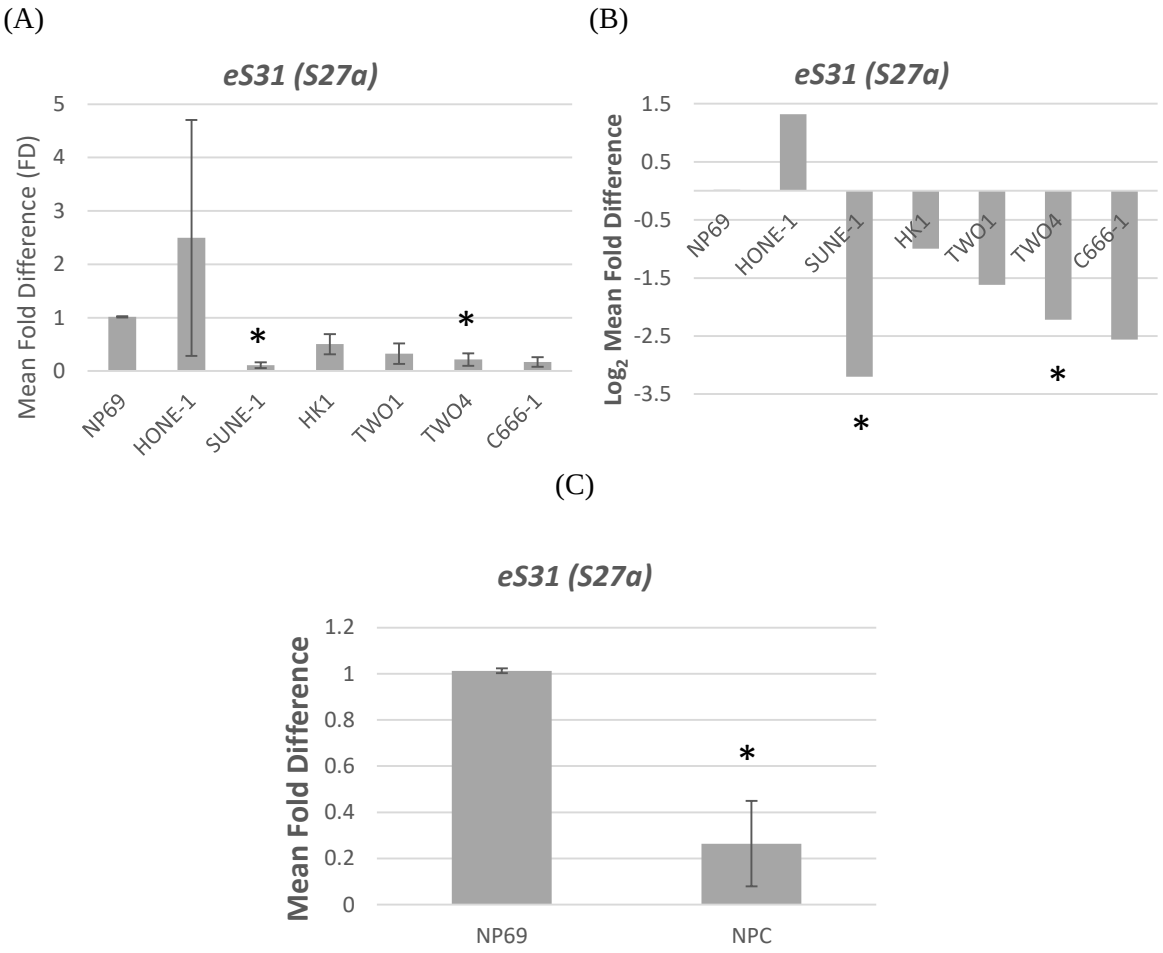

Figure 4.5: Expression of *eS31 (S27a)* in six NPC cell lines compared to NP69. (A) Y-axis: mean fold difference (FD) as calculated as $2^{-\Delta\Delta C_T}$. (B) Y-axis: log-transformed fold difference (FD). (C) cumulative fold difference of *eS31 (S27a)* in NPC vs. NP69. Data are presented as mean fold change±SD. Corresponding *p*-value is designated with asterisk (*). *: $p < 0.05$.

As for *eS31 (S27a)*, it was noted to be under-expressed in all NPC cell lines, except HONE-1 (FD=2.496±2.212; *p*-value 0.294). On the contrary, SUNE-1, once again, recorded the highest reduction of approximately 90% of *eS31 (S27a)* expression (FD=0.109±0.056; *p*-

value=0.021), followed by TW04 cell line (FD=0.214±0.115; *p*-value=0.045). Cumulatively, *eS31 (S27a)* was significantly under-expressed in NPC cell lines (mean FD=0.264±0.185; *p*-value=0.048) (Figure 4.5).

Similarly, the under-expression of *eS31 (S27a)* had also been previously identified in malignant breast cancer tissues and hepatocellular carcinoma when compared to benign fibroadenomas and liver cirrhosis tissues, respectively (Adams et al., 1992; Gunasekaran & Ganeshan, 2014). However, the up-regulation of *eS31 (S27a)* was reported in colorectal renal, and prostate cancer, as well as chronic myeloid leukaemia (CML) and acute leukaemia (AL) (Kanayama et al., 1991; Wong et al., 1993; Wang et al., 2014). The contradictory expression profile of *eS31 (S27a)* across multiple carcinomas reveals the delicate complexity of ribosomal proteins network in promoting the progression of cellular malignancy.

Ribosomal protein eS31 (S27a) has been shown to interact with MDM2 and to inhibit MDM2-mediated p53 degradation (Sun et al., 2011). Following that, the stabilization of p53 level, in turn, elicits an autoregulatory feedback loop on the level of eS31 (S27a) monomers during ribosomal stress (Nosrati et al., 2015). Curiously in nasopharyngeal carcinoma cells, p53 had been reported to be over-expressed, in contrast to the usual case of under-expression under carcinogenic environments (Agaoglu et al., 2004). This could serve as a possible explanation on the down-regulated *eS31 (S27a)* expression in NPC cells observed in this study. However, further work is needed to substantiate such a claim.

4.3.3.4 *eL6 (L6)*: *eL6 (L6)* is not significantly dysregulated in NPC cells

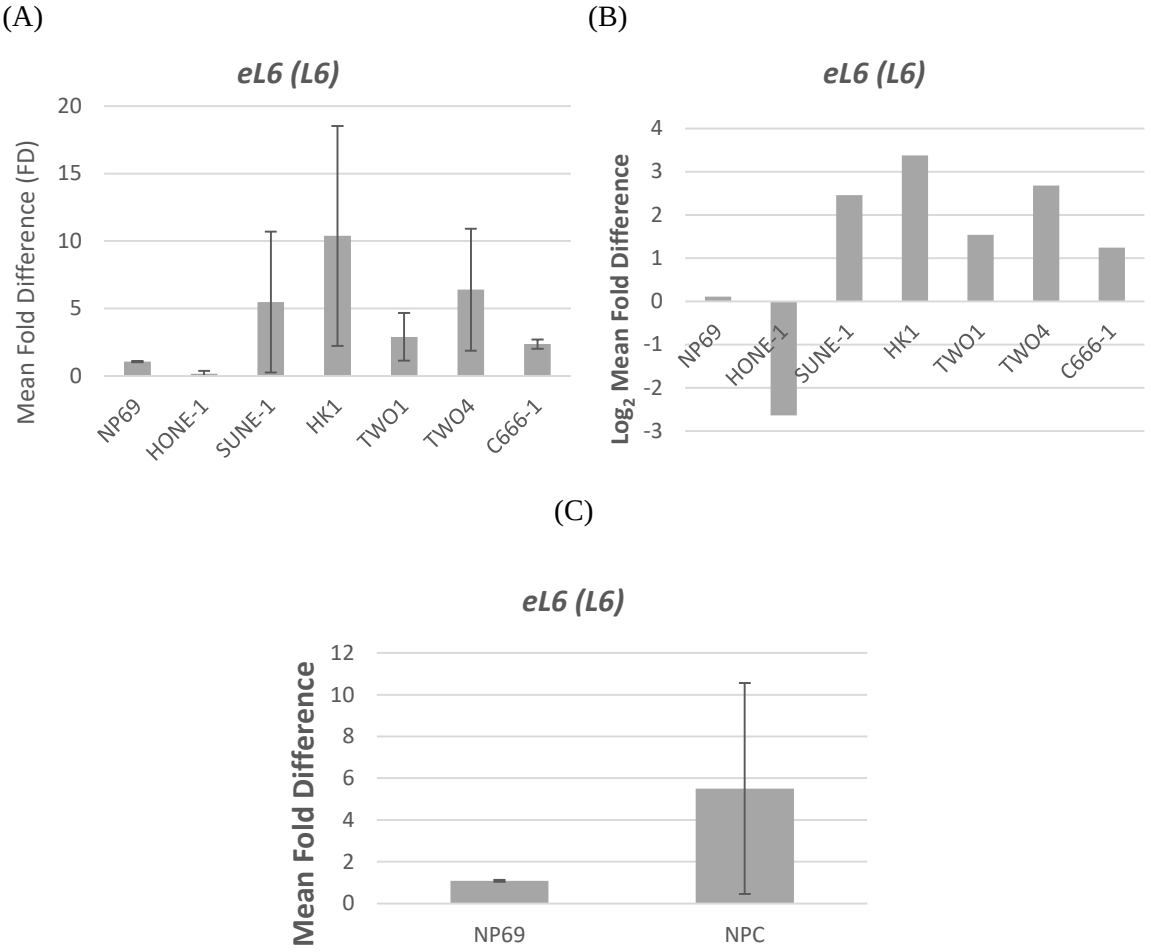

Figure 4.6: Expression of *eL6 (L6)* in six NPC cell lines compared to NP69. (A) Y-axis: mean fold difference (FD) as calculated as $2^{-\Delta\Delta C}{}_{T}$. (B) Y-axis: log-transformed fold difference (FD). (C) cumulative fold difference of *eL6 (L6)* in NPC vs. NP69. Data are presented as mean fold change±SD.

In regard to the differential expression of *eL6 (L6)*, it was found to be not significantly dysregulated in NPC cells. However, a brief overview of the expression pattern of *eL6 (L6)* across the NPC cell lines under study showed that HONE-1 once again turned out to be the 'odd-one-out' from the general pattern observed in other NPC cell lines, similarly observed for the expression of *eS31 (S27a)*. *eL6 (L6)* was up-regulated within a range of 2- to 10-fold

greater than NP69 with the highest induction observed in HK1 cell line, though not significant (FD=10.378±8.153; *p*-value=0.153). Overall, *eL6 (L6)* showed an over-expression in NPC as a whole, though no significant data was obtained with regards to individual and cumulated cell lines (mean FD=5.505±5.056; *p*-value=0.142) (Figure 4.6).

Our findings coincide with many other reports on the up-regulation of *eL6 (L6)*. The over-expression of *eL6 (L6)* in gastric cancer correlates to increased cell proliferation and tumour growth via cyclin E induction while that of multidrug-resistance gastric cells correlates to enhanced resistance against anticancer drugs and drug-induced apoptosis (Du et al., 2005; Gou et al., 2010). On the other hand, under-expression of *eL6 (L6)* was observed in Schwachman-Diamond Syndrome (SDS) bone marrow cells (Rujkijyanont et al., 2009).

As the over-expression of *eL6 (L6)* in nasopharyngeal carcinoma cell lines in comparison to NP69 cells was not statistically significant, this observation posed a possibility that *eL6 (L6)* is not differentially expressed, and thus is not implicated in the tumorigenesis of NPC. However, due to the intricate balance of the molecular environment within a cell, the slightest perturbation within said environment could result in an unfavourable and uncontrolled cascade of cancer-causing molecular events. Therefore, though not statistically significant, our findings revealed an over-expression of *eL6 (L6)* in NPC cell lines.

4.3.3.5 *uL14 (L23)*: *uL14 (L23)* was significantly under-expressed in NPC, specifically in C666-1 cell line

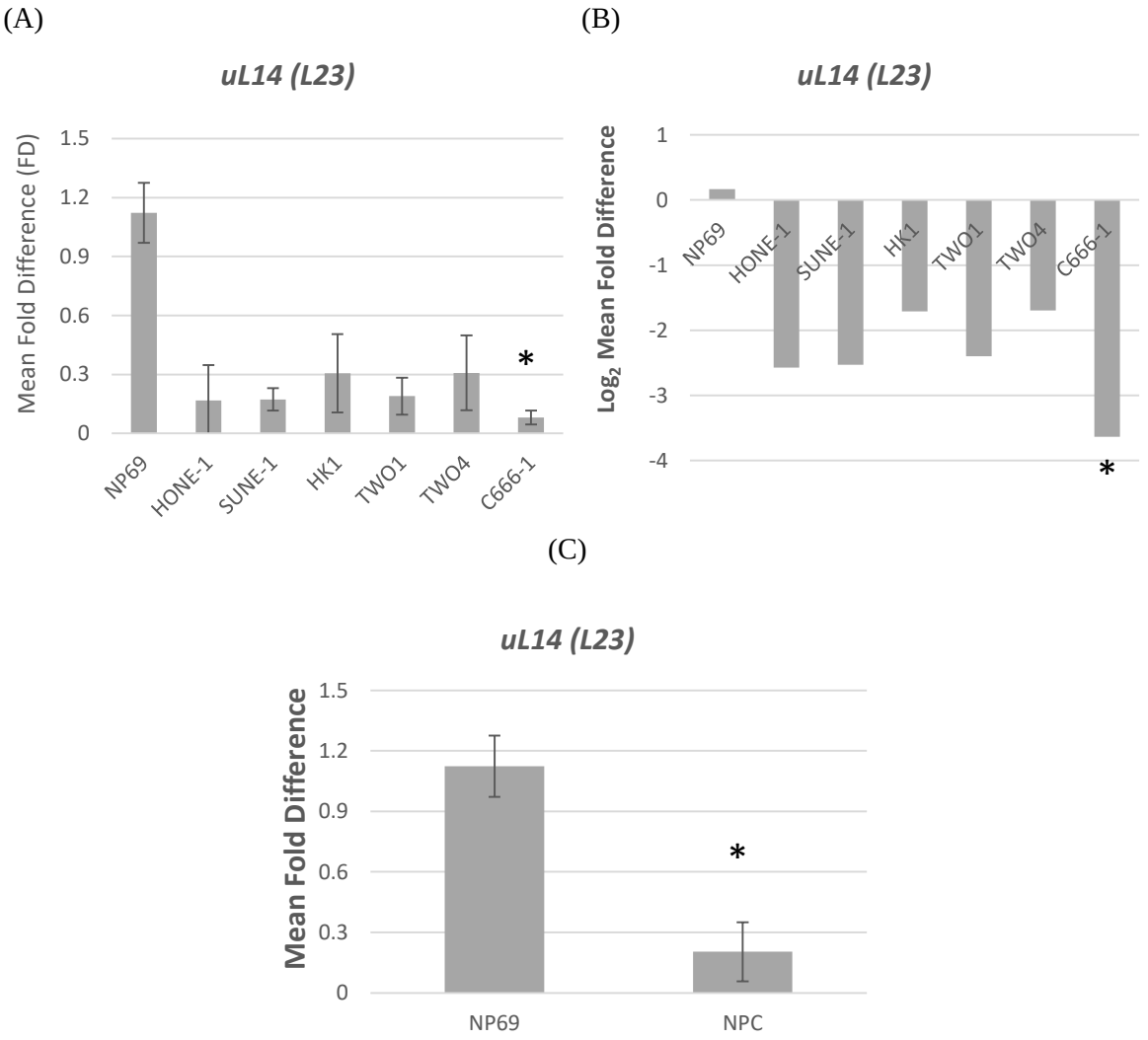

Figure 4.7: Expression of *uL14 (L23)* in six NPC cell lines compared to NP69. (A) Y-axis: mean fold difference (FD) as calculated as $2^{-\Delta\Delta C_T}$. (B) Y-axis: log-transformed fold difference (FD). (C) cumulative fold difference of *uL14 (L23)* in NPC vs. NP69. Data are presented as mean fold change±SD. Corresponding *p*-value is designated with asterisk (*). *: $p< 0.05$.

Compared to NP69, *uL14 (L23)* was found to be more than 50% down-regulated in all NPC cell lines, with the highest reduction of almost 99% observed in the EBV-positive C666-1 cell line (FD=0.081±0.035; *p*-value=0.034). Taken together as NPC vs. NP69, the under-

expression of *uL14 (L23)* was deemed significant (mean FD=0.204±0.146; *p*-value=0.040) (Figure 4.7).

Down-regulation of *uL14 (L23)* was shown in ovarian tumours, Schwachman-Diamond Syndrome (SDS), as well as human papillomavirus (HPV)-E6 D25E expressing cervical cancer cell lines (Grisaru et al., 2007; Rujkijyanont et al., 2009; Jang, Rhee, Jang, & Kim, 2011). In contrast, several studies reported on the over-expression of *uL14 (L23)* in squamous cell carcinoma of the head and neck (SCCHN), multidrug-resistance gastric cancer cells and myelodysplastic syndrome (MDS) (Shi et al., 2004; Russo et al., 2013; Qi et al., 2017).

Herein, we would like to point out an interesting observation in our data. *uL14 (L23)* was found to be down-regulated in a human papillomavirus (HPV)-positive cervical carcinoma cell line, which coincidentally seemed parallel to the overwhelming under-expression of *uL14 (L23)* in the EBV-positive cell line, C666-1, suggesting its association with viral antigens and relevant viral pathways. A plausible link between *uL14 (L23)* and EBV could be explained with the Miz-1- NPM1 regulatory network. EBNA3A, one of the six EBV nuclear antigens, was found to directly bind to Miz-1 and repressed the transcription regulation of target genes by sequestering Miz-1 from its co-activator, NPM1 (Bazot et al., 2014). *uL14 (L23)* was identified to be one such target gene downstream of Miz-1 activation (Wanzel et al., 2008). Taken together, these findings provide a potential EBV-specific scenario in the case of C666-1 whereby the expression of EBV viral antigens eventuated the down-regulation of *uL14 (L23)* by obstructing its transcriptional expression via the Miz-1-NPM1 network. Further investigation needs to be done to justify such claim.

4.3.3.6 *eL18 (L18)*: *eL18 (L18)* was significantly up-regulated in NPC, specifically in SUNE-1 and C666-1 cell lines

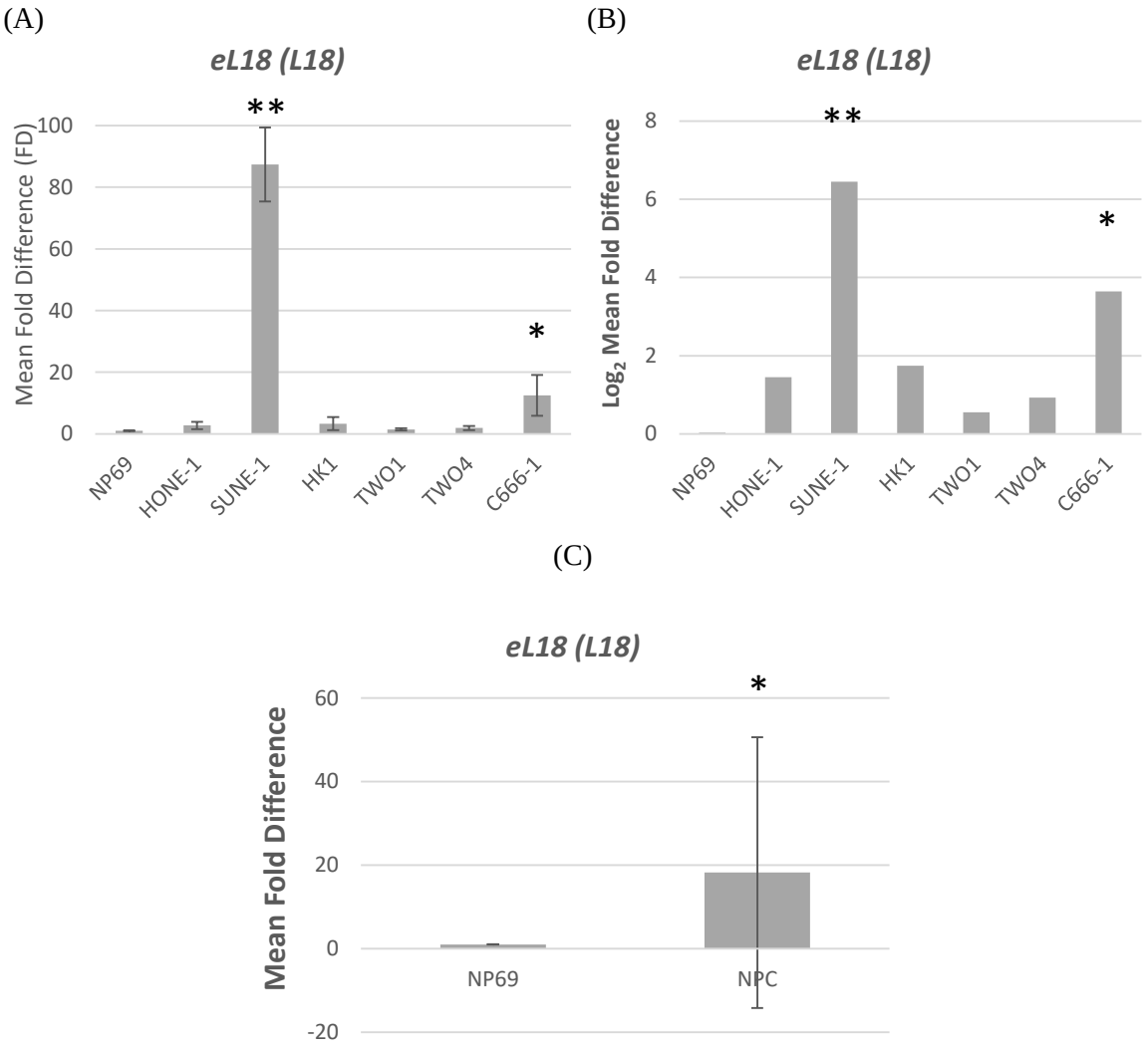

Figure 4.8: Expression of *eL18 (L18)* in six NPC cell lines compared to NP69. (A) Y-axis: mean fold difference (FD) as calculated as $2^{-\Delta\Delta C_T}$. (B) Y-axis: log-transformed fold difference (FD). (C) cumulative fold difference of *eL18 (L18)* in NPC vs. NP69. Data are presented as mean fold change±SD. Corresponding *p*-values are designated with asterisk (*). *: $p< 0.05$; **: $p< 0.01$.

The expression of *eL18 (L18)* was concordantly over-expressed in all six NPC cell lines compared to NP69. Yet again, the expression in SUNE-1 recorded the highest over-expression of 87-fold, with a similar trend observed with that of *eS8 (S8)* and *eS31 (S27a)*

(FD=87.354±12.015; *p*-value=0.001). Another significant reading was exhibited in C666-1 cell line (FD=12.509±6.651; *p*-value=0.013). On the other hand, the expression values of TW01 and TW04 cell lines were considered negligible due to the closeness in values to standard base-line of 1.0. Cumulatively, the over-expression of *eL18 (L18)* in NPC was considered to be significant (mean FD=18.218±32.405; *p*-value=0.015) (Figure 4.8).

By the same token, up-regulation of *eL18 (L18)* mRNA was previously reported in colorectal carcinoma, though not correlated to CLC cancer staging (Kitahara et al., 2001). However, a subsequent study reported on the under-expression of eL18 (L18) protein in CLC when compared to normal colorectal mucosa (Kasai et al., 2003). No differential expression of *eL18 (L18)* was identified in gastric and hepatocellular carcinoma (Barnard et al., 1993).

As shown, studies on the differential expression of *eL18 (L18)* and its implication in tumorigenesis are far too few as *eL18 (L18)* was not found to be dysregulated in multiple cancers. Looking at our result, four out of six NPC cell lines (HONE-1, HK1, TW01 and TW04) somewhat conform to such pattern. Only SUNE-1 and C666-1 NPC cell lines showed significant up-regulation of *eL18 (L18),* which could be an isolated event. However, it remains to be investigated if the expression of *eL18 (L18)* could indeed be negated from NPC progression.

4.3.3.7 *eL24 (L24)*: *eL24 (L24)* was insignificantly dysregulated in NPC

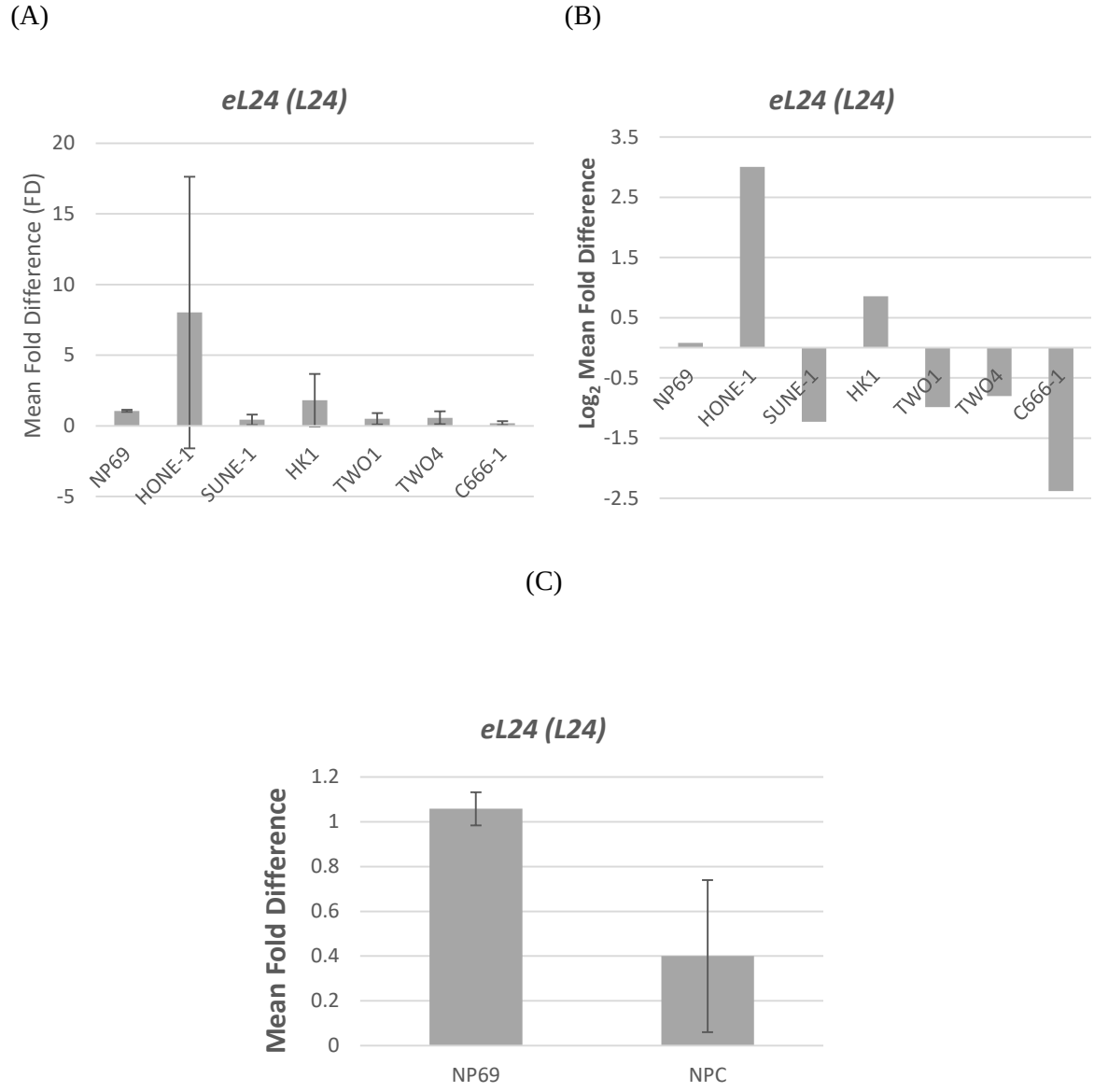

Figure 4.9: Expression of *eL24 (L24)* in six NPC cell lines compared to NP69. (A) Y-axis: mean fold difference (FD) as calculated as $2^{-\Delta\Delta C_T}$. (B) Y-axis: log-transformed fold difference (FD). (C) cumulative fold difference of *eL24 (L24)* in NPC vs. NP69. Data are presented as mean fold change±SD.

As for *eL24 (L24)*, its expression in NPC cell lines revealed a discordant pattern with under-

expression in four of the six cell lines (SUNE-1, TW01, TW04, and C666-1). On the other hand, *eL24 (L24)* was found to be contradictorily over-expressed about 8-fold in HONE-1, the 'odd-one-out' in a few other cases, and HK1, though its fold difference was negligible. The differential expression of *eL24 (L24)* was not significant in individual cell lines as well as cumulated NPC scenario (mean FD=0.400±0.340; *p*-value=0.179) (Figure 4.9)

In contrast to our findings, the up-regulation of *eL24 (L24)* had been identified in breast tumours compared to adjacent non-tumoral mammary tissues as well as in drug-resistant hepatocellular carcinoma cell line (Wilson-Edell et al., 2014). To date, these are the only two existing reviews on the differential expression of *eL24 (L24)* in cancer.

Along the same line, our result revealed an insignificant decrease in *eL24 (L24)* expression in NPC cell lines compared to NP69, suggesting its comparably consistent expression regulation in NPC.

4.3.3.8 *eL30 (L30): eL30 (L30)* was not significantly dysregulated in NPC cells

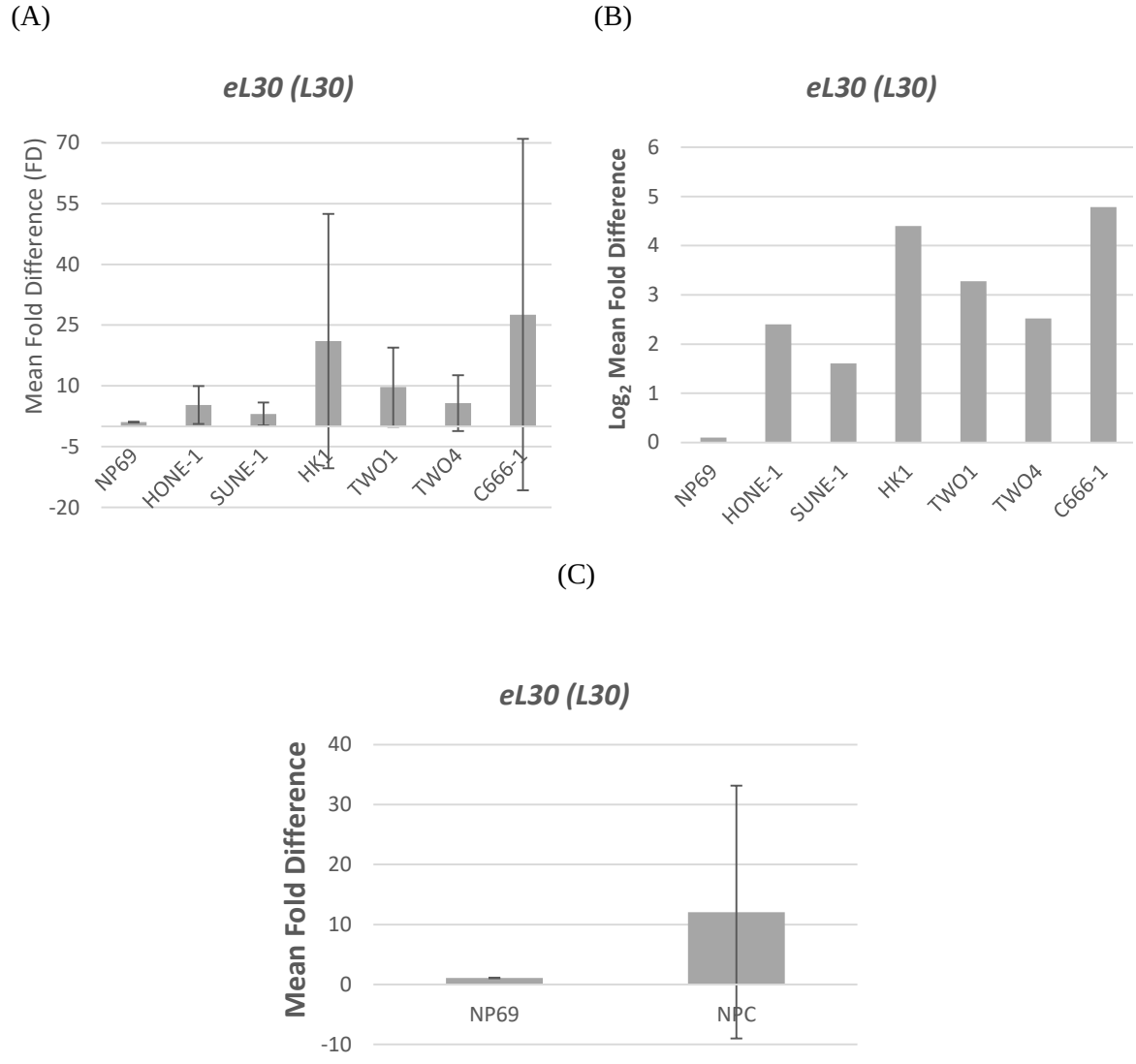

Figure 4.10: Expression of *eL30 (L30)* in six NPC cell lines compared to NP69. (A) Y-axis: mean fold difference (FD) as calculated as $2^{-\Delta\Delta C_T}$. (B) Y-axis: log-transformed fold difference (FD). (C) cumulative fold difference of *eL30 (L30)* in NPC vs. NP69. Data are presented as mean fold change±SD.

The last of the ribosomal protein genes, *eL30 (L30)* was not significantly dysregulated in all NPC cell lines compared to NP69. The expression of *eL30 (L30)* was highest in the EBV-

positive C666-1 cell line (FD=27.570±43.476; *p*-value=0.130). Likewise, overall pattern revealed an up-regulation of *eL30 (L30)* in NPC as a whole, though not significant (mean FD=12.065±21.090; *p*-value=0.153) (Figure 4.10).

A majority of expression analyses of *eL30 (L30)* had validated the reliable usage of *eL30 (L30)* as an endogenous control in head and neck squamous cell carcinoma, breast cancer tissues and oral squamous cell carcinoma based on its unfluctuating expression levels across aforementioned tumours and their corresponding normal counterparts (Squatrito et al., 2004; Martin, 2016; El Hadi et al., 2017; Palve et al., 2018).

Our findings on the up-regulation of *eL30 (L30)* is synonymous to that of a study investigating the 8q chromosomal gain events in medulloblastoma and its association to overall patient survival and prognosis. One of the genes mapped onto chromosome 8q was identified to be *eL30 (L30)* and its over-expression was subsequently detected and correlated to increased tumorigenicity in medulloblastoma tumour samples (De Bortoli et al., 2006). Having mentioned that, even though the expression of *eL30 (L30)* was found to be up-regulated in NPC cell lines relative to NP69, the differential expression was not statically significant, warranting extra precaution in correlating the expression of *eL30 (L30)* in NPC progression.

4.3.3.9 *NPM1*: *NPM1* was significantly under-expressed cumulatively, and specifically in HONE-1, SUNE-1, TW01 and C666-1 cell lines

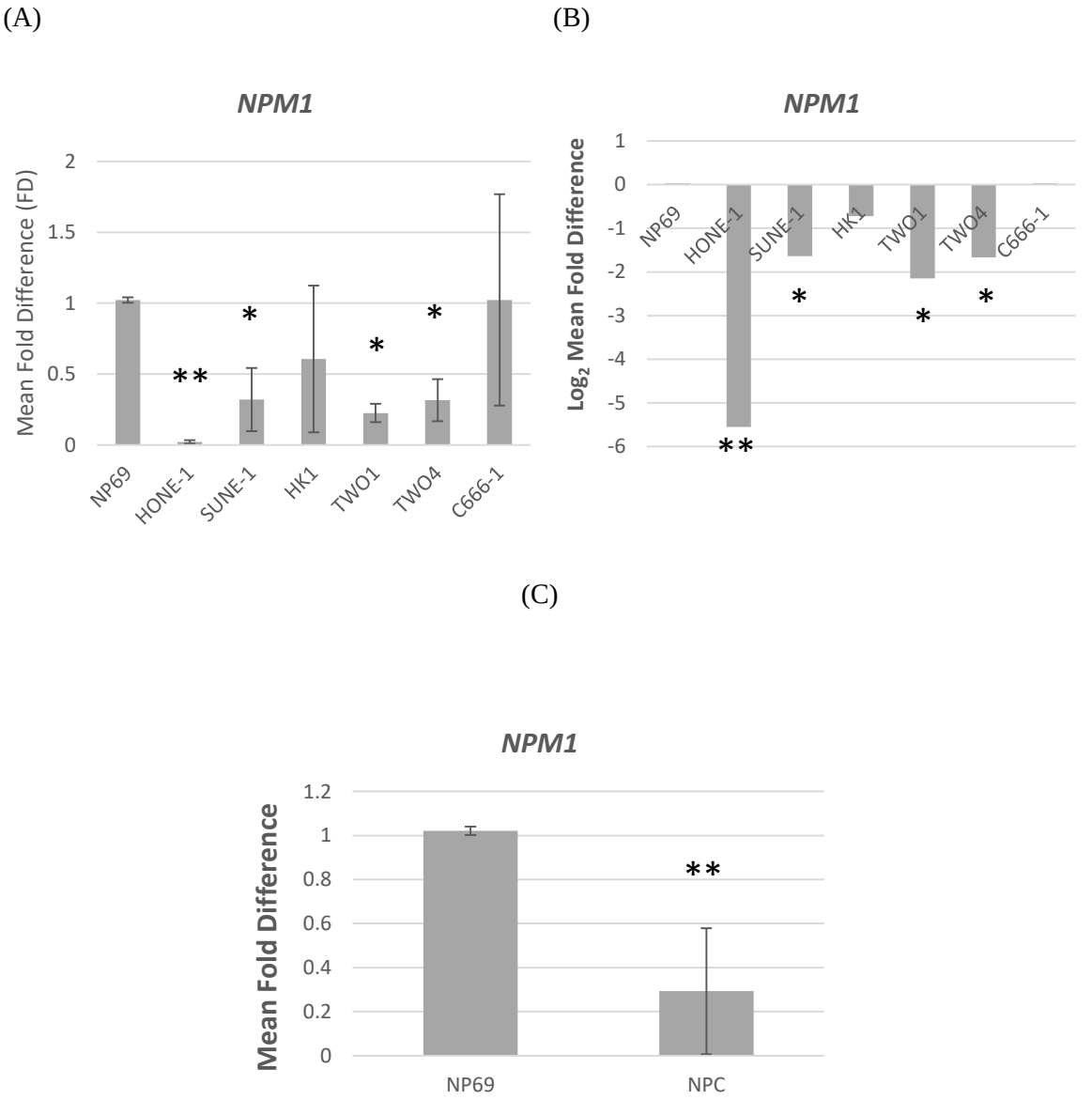

Figure 4.11: Expression of *NPM1* in six NPC cell lines compared to NP69. (A) Y-axis: mean fold difference (FD) as calculated as $2^{-\Delta\Delta C_T}$. (B) Y-axis: log-transformed fold difference (FD). (C) cumulative fold difference of *NPM1* in NPC vs. NP69. Data are presented as mean fold change±SD. Corresponding *p*-values are designated with asterisk (*). *: $p< 0.05$; **: $p< 0.01$.

Nucleophosmin (NPM1/ B23) was found to be consistently under-expressed in all six NPC cell lines, with the lowest reduction of almost 99% observed in HONE-1 (FD=0.021±0.011; *p*-value=0.001), followed by TW01, TW04 and SUNE-1 cell lines, all in which *NPM1* was found to be significantly under-expressed. Expectedly, when the mean fold differences of all cell lines were consolidated, *NPM1* was significantly down-regulated in NPC (mean FD=0.293±0.286; *p*-value=0.005) (Figure 4.11).

As with our findings, a similar expression pattern of *NPM1* was reported in acute myeloid leukaemia (AML) and myelodysplastic syndrome (MDS) due to frequent genetic aberration of *NPM1* such as frameshift mutations, chromosomal translocation and heterozygous deletion along chromosome 5q consequently leading to the under-expression of *NPM1* (Naoe et al., 2006; La Starza et al., 2010; Qiu et al., 2017). Apart from those hematopoietic disorders, the down-regulation of *NPM1* was more drastic in progressive tumour cells compared to regressive tumour cells, suggesting a possible role of *NPM1* in tumour malignancy progression (Takenawa et al., 2013).

To date, there have been no studies on the sequence integrity of *NPM1* in nasopharyngeal carcinoma cells and the delineation of *NPM1* involvement in the development and progression of NPC.

4.3.3.10 *BTF3: BTF3* was not significantly dysregulated in NPC cells

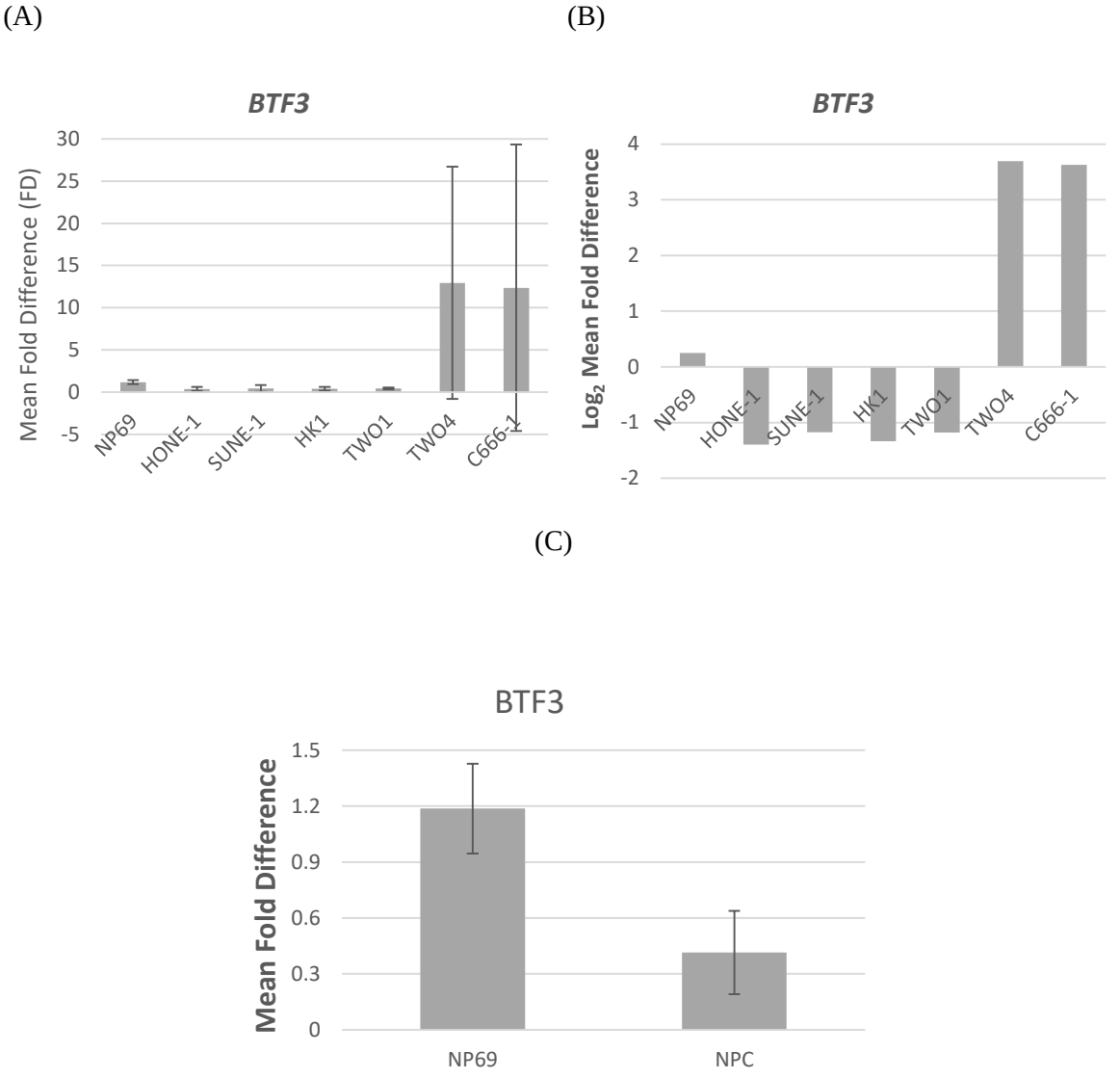

Figure 4.12: Expression of *BTF3* in six NPC cell lines compared to NP69. (A) Y-axis: mean fold difference (FD) as calculated as $2^{-\Delta\Delta C_T}$. (B) Y-axis: log-transformed fold difference (FD). (C) cumulative fold difference of *BTF3* in NPC vs. NP69. Data are presented as mean fold change±SD.

The differential expression of *BTF3* revealed an inconsistent pattern, though it was determined to be lowly-expressed in a majority of the cell lines (HONE-1, SUNE-1, HK1

and TW01) while being induced 12-fold higher in TW04 and C666-1 cell lines compared to NP69. However, none of these differential expressions were deemed significant, regardless of within individual cell lines and cumulatively (mean FD=0.415±0.223; *p*-value=0.153) (Figure 4.12).

Contrary to the under-expression reported in our study, though not statically significant, a general consensus of *BTF3* over-expression was observed across various cancer types. For example, but not limited to, glioblastoma multiforme, colorectal carcinoma, pancreatic ductal adenocarcinoma, prostate cancer and gastric cancer (Odreman et al., 2005; Kusumawidjaja et al., 2007; Liu et al., 2013; Symes et al., 2013; Wang et al., 2013). *BTF3* over-expression had been associated with malignancy progression, cell cycle progression and epithelial-mesenchymal transition (EMT). However, there have been no reports on the under-expression of *BTF3* in carcinogenesis.

4.3.3.11 *UBA52: UBA52* is not significantly dysregulated in NPC cells

(A) (B)

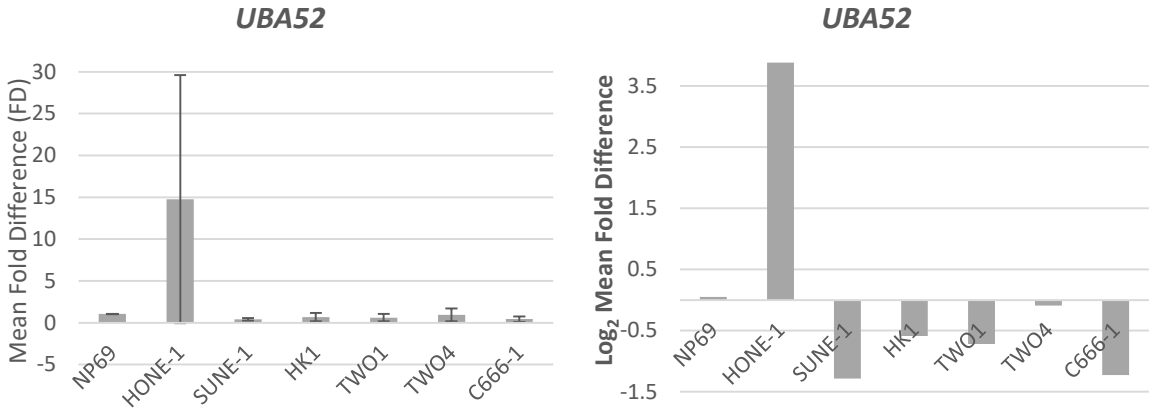

(C)

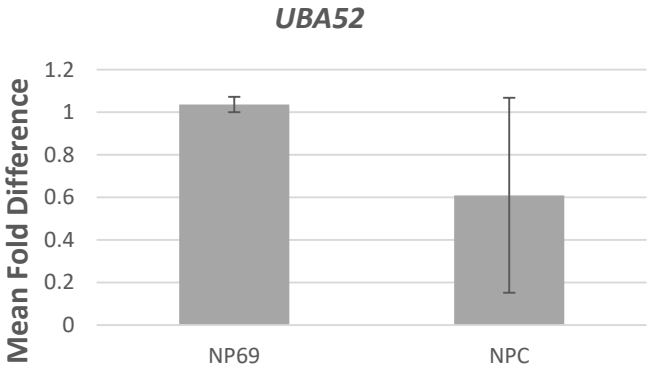

Figure 4.13: Expression of *UBA52* in six NPC cell lines compared to NP69. (A) Y-axis: mean fold difference (FD) as calculated as $2^{-\Delta\Delta C_T}$. (B) Y-axis: log-transformed fold difference (FD). (C) cumulative fold difference of *UBA52* in NPC vs. NP69. Data are presented as mean fold change±SD.

Lastly, *UBA52* showed an expression pattern similar to that of *eS31 (S27a)*, *eL6 (L6)* and *eL24 (L24)*, whereby HONE-1 was observed to be the only differing cell line when compared to the rest. In this case, the dysregulation of *UBA52* was observed in all cell lines, except for

HONE-1, where it was 14-fold induced relative to NP69 (FD=14.766±14.830; *p*-value=0.102). The differential expression of *UBA52* was not considered significant within individual cell lines and when considered as a whole (mean FD=0.610±0.458; *p*-value=0.481) (Figure 4.13).

In comparison with that of other cancers, *UBA*52 was up-regulated in primary renal carcinoma, colorectal carcinoma and in blood of breast cancer patients, but no differential expression was noted in gastric cancer specimens (Kanayama et al., 1991; Barnard et al., 1995; Aarøe et al., 2010). However, there is currently no data supporting the under-expression of *UBA52* in any cancer cases.

4.3.4 Sequence Analyses of Target Genes

In order to detect the presence of genetic aberrations within the individual target genes of interest, sequence analysis was conducted by amplifying full-length cDNAs comprising of complete coding regions (CDS). Multiple sequence alignment for all target genes was performed with ClustalW program and visualized with MultAlin software (Appendix D).

No nucleotide aberrancy was detected for nine of the eleven target genes namely, *eS8 (S8), eS31 (S27a), eL6 (L6), eL18 (L18), eL24 (L24), eL30 (L30), NPM1*, *BTF3* and *UBA52*. Missense mutations were detected in both *ribosomal proteins uS9 (S9)* and *uL14 (L14)*.

4.3.4.1 Missense Mutation Detected in *uS4 (S9)*

The sequence analysis of *uS4 (S9)* revealed a missense mutation (c.244T>A) at position 244 (nt) in the tri-nucleotide sequence (C<u>T</u>T) resulting in a change of nucleotide (C<u>A</u>T)

combination and the replacement of leucine with histidine at codon 63 (p.L63H).

As a broad overview, leucine ($C_6H_{13}NO_2$) is an α-amino acid that comprises of a protonated amine function group ($-NH_3^+$), a deprotonated carboxylic acid group ($-COO^-$) and an isobutyl side chain, rendering it its non-polar, hydrophobic properties. Additionally, with a molar mass of 131.175 $gmol^{-1}$, leucine is regarded as the fourth smallest amino acid out of the twenty known amino acids. On the other hand, histidine ($C_6H_9N_3O_2$) is somewhat structurally identical to leucine in the sense that histidine is similarly composed of a protonated amine group ($-NH_3^+$) and a deprotonated carboxylic acid group ($-COO^-$). However, instead of an isobutyl side chain, histidine contains an imidazole side chain, making it a polar, hydrophilic amino acid with an overall partial positive charge. Due to its bulky imidazole chain, histidine, with a molar mass of 155.157$gmol^{-1}$ is ranked the fourth largest amino acid among the twenty. In comparison, leucine and histidine are of different size, polarity, overall charge and hydrophobicity, making it almost certain that a leucine to histidine replacement within ribosomal protein uS4 (S9) structure would result in distortion of protein conformation, which leads to probable defective protein function.

There are currently no reports on a missense mutation of uS4 (S9) at 244bp, suggesting that our data is specific to nasopharyngeal carcinoma circumstances. Based on a literature search with BioMuta, the leucine to histidine amino acid replacement at codon 63 was not found to coincide with any vital interacting and functional domains or post-translational modification sites previously reported (Dingerdissen et al., 2018). As such, the missense mutation on uS4 (S9) detected herein posed no liability on overall protein function but may negatively affect certain interactions due to the resulting steric alteration but only to a certain extent.

4.3.4.2 Missense Mutation Identified in *eL14 (L23)*

The sequence analysis of *eL14 (L23)* disclosed a missense mutation (c.132T>A) at position 132 (nt) in the tri-nucleotide sequence (TCC) to a (ACC) nucleotide triplet, resulting in a substitution of serine with threonine at codon 41 (p.S41T).

Generally, serine ($C_3H_7NO_3$) is an α-amino acid that is structurally identified by the presence of a protonated amine function group ($-NH_3^+$), a deprotonated carboxylic acid group ($-COO^-$) and a hydroxymethyl group side chain. Taking the individual chargers as a whole, serine, with a molar mass of 105.903 $gmol^{-1}$, is a polar uncharged amino acid. Likewise, threonine ($C_4H_9N_3O_3$), being somewhat structurally identical to serine, possesses a protonated amine group ($-NH_3^+$) and a deprotonated carboxylic acid group ($-COO^-$). Instead of a hydroxymethyl group, threonine contains a hydroxyl group side chain, making it too, a polar uncharged amino acid with a molar mass of 119.120 $gmol^{-1}$. Comparatively, serine and threonine are both polar uncharged amino acids and are only structurally distinctive with an additional $-CH_2$ group within the hydroxyl side chain of threonine as compared to the hydroxymethyl side chain of serine. As such, the serine to threonine substitution would not greatly jeopardize uL14 (L23) protein conformation and functionality.

There are currently no reported mutations at 132nt, which corresponds to codon 41, located within the N-terminal of ribosomal protein uL14 (L23) in any cancer (Dingerdissen et al., 2018), rendering us the first group to report on such discovery in nasopharyngeal carcinoma. Additionally, there are also no previous findings on the functional aspect of uL14 (L23) domains in regulating its various roles.

CHAPTER 5

PROTEIN EXPRESSION OF RIBOSOMAL PROTEINS uS4 (S9), eS8 (S8), eS31 (S27a), uL14 (L23), eL18 (L18) AND NPM1 IN NPC-DERIVED CELL LINES

5.1 Background

Gene expression is a series of highly regulated cellular processes that underlies the fundamental development of a multicellular organism by means of the proper production of functional three-dimensional proteins, which is paramount in dictating a cell's phenotype. Upon the transcription and processing of pre-mRNAs into mature mRNAs, mRNAs are further regulated by various means such as RNA degradation control, RNA transport and localization control, translational control and post-translational control in order to develop into active proteins. As such, the expression of genomic information has been studied at the levels of both transcriptomics and proteomics. Due to the multiple regulation and processing controls post-transcription, the level of mRNA do not necessarily correspond to the protein level and therefore, rendering it an unreliable proxy to predict corresponding protein levels in human cells and tissues (Liu, Beyer, & Aebersold, 2016). Due to the complexities of gene expression regulation in terms of the dynamic cellular scenarios, spatial and temporal discrepancy of mRNAs and availability of 'raw materials' for protein biogenesis, both protein expression levels and that of their coding transcripts are to be ascertained for the comprehensive understanding of cellular processes.

Therefore, in this part of the study, we expounded on the previous transcript expression data by establishing the corresponding protein expression levels of those genes that were

identified to be significantly expressed differentially in NPC cell lines compared to the normal control cell line. Here, we determined the protein expressions of six target proteins, namely ribosomal proteins uS4 (S9), eS8 (S8), eS31 (S27a), uL14 (L23), eL18 (L18) and NPM1 in six NPC cell lines and a normal nasopharyngeal epithelial cell line, NP69.

5.2 Methodology Overview

Protein expression analysis was conducted on ribosomal proteins uS4 (S9), eS8 (S8), eS31 (S27a), uL14 (L23), eL18 (L18) and NPM1, which were previously identified to be significantly expressed differentially in NPC cell lines. Whole cell lysates were extracted from six NPC cell lines (HONE-1, SUNE-1, HK1, TW01, TW04 and C666-1) and NP69. In equal amounts, lysate samples were loaded and separated with SDS-PAGE followed by western blotting (protocol described in Materials and Methods Chapter 3.5). Densitometry was carried out to detect and visualize target proteins. Each target protein was detected in three biological replicates and its expression was normalized to that of beta-actin (*ACTB*) and compared to that of NP69 to obtain fold difference (FD) data.

5.3 Results and Discussion

5.3.1 Western Blot Analysis of uS4 (S9), eS8 (S8), eS31 (S27a), uL14 (L23) and NPM1 in Individual NPC Cell Lines

Protein bands of the normal control, beta-actin and target protein bands of uS4 (S9), eS8 (S8), eS31 (S27a), uL14 (L23), eL18 (L18) and NPM1 are shown in Figures 5.2 to 5.7 and the intensity values are detailed in Table 5.1. Raw value data are included in Appendix E.

Table 5.1: Differential expression of target proteins in NPC cell lines. Normalized protein expressions of uS4 (S9), eS8 (S8), eS31 (S27a), uL14 (L23), eL18 (L18) and NPM1 in NPC cell lines individually and cumulatively. *p*-values were calculated with independent Student's *t*-test and values <0.05 were considered statistically significant.

	NP69 vs Individual NPC Cell Lines				**NP69 vs. Cumulative Cell Lines**		
Target Protein	**Cell Line**	**Mean FD**	**SD**	***p*-value**	**Cumulative**	***p*-value**	**Differential Expression**
uS4 (S9)	NP69	1.000	-	-	1.000	4.183	Over-expression
	HONE-1	2.686	0.842	0.013	2.135±0.526	E-05	
	SUNE-1	2.808	1.641	0.065			
	HK1	1.975	1.342	0.138			
	TW01	1.796	0.317	0.006			
	TW04	2.108	0.344	0.003			
	C666-1	1.439	0.019	1.123E-06			
eS8 (S8)	NP69	1.000	-	-	1.000	3.625	Under-expression
	HONE-1	0.899	0.313	0.303	0.708±0.174	E-05	
	SUNE-1	0.559	0.163	0.005			
	HK1	0.640	0.058	2.196E-04			
	TW01	0.734	0.158	0.022			
	TW04	0.916	0.312	0.332			
	C666-1	0.499	0.084	2.424E-04			
eS31 (S27a)	NP69	1.000	-	-	1.000	4.610	Over-expression
	HONE-1	2.912	0.655	0.004	2.450±0.580	E-07	
	SUNE-1	2.900	1.034	0.017			
	HK1	1.548	0.209	0.005			
	TW01	2.829	0.775	0.007			
	TW04	2.599	0.809	0.013			
	C666-1	1.914	0.675	0.040			

Table 5.1 continued

uL14 (L23)	NP69	1.000	-	-	1.000 1.909±0.533	4.561 E-06	Over-expression
	HONE-1	1.968	0.158	2.221E-04			
	SUNE-1	1.737	0.527	0.036			
	HK1	1.252	0.331	0.129			
	TW01	2.628	0.677	0.007			
	TW04	2.401	0.349	0.001			
	C666-1	1.467	0.367	0.046			
eL18 (L18)	NP69	1.000	-	-	1.000 1.641±0.912	0.121	No significant dysregulation
	HONE-1	1.255	0.781	0.301			
	SUNE-1	2.876	3.654	0.212			
	HK1	1.820	0.768	0.069			
	TW01	1.735	0.200	0.002			
	TW04	2.031	1.642	0.169			
	C666-1	0.126	0.160	3.487E-04			
NPM1	NP69	1.000	-	-	1.000 3.622±1.458	1.064 E-05	Over-expression
	HONE-1	3.983	1.508	0.013			
	SUNE-1	3.246	1.001	0.009			
	HK1	2.349	0.705	0.015			
	TW01	4.050	0.919	0.002			
	TW04	6.074	3.164	0.025			
	C666-1	2.027	0.822	0.048			

FD= Fold difference; SD= Standard deviation

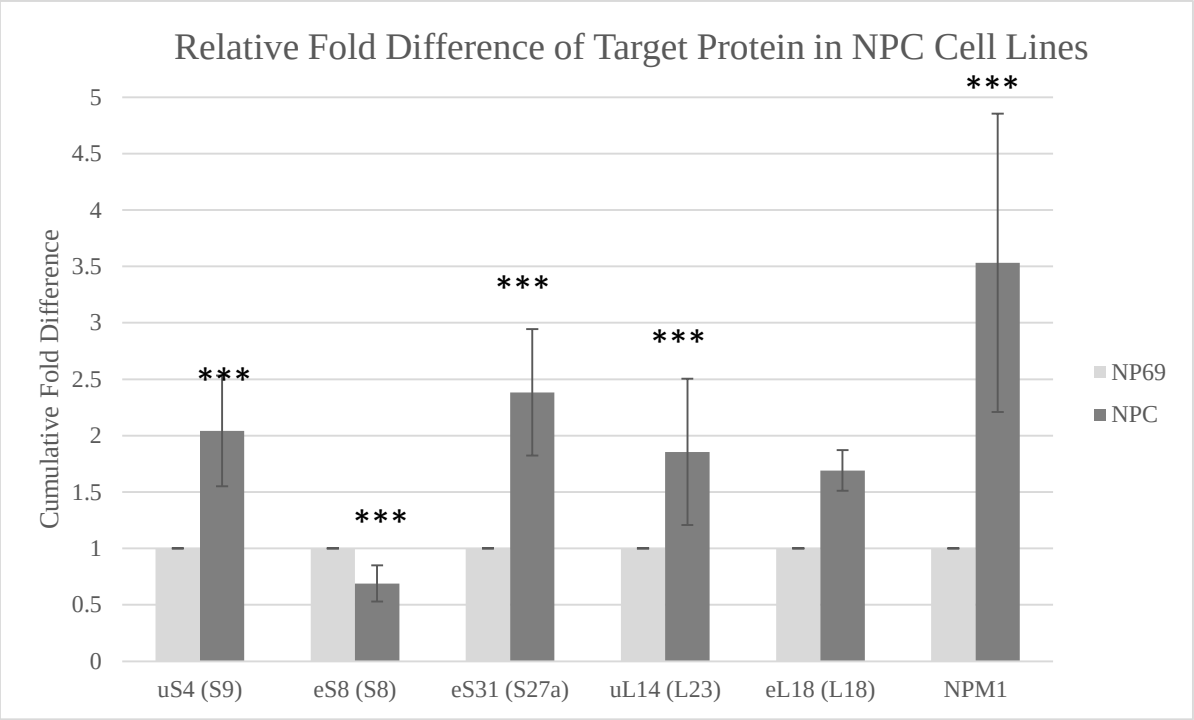

Figure 5.1: Graphical representation of the cumulative mean fold difference of target proteins in NPC cells. Bars are plotted for the cumulative mean fold difference (FD) of six target proteins in NPC vs. NP69. Corresponding *p*-values are designated with asterisk (*).***: $p < 0.001$. Error bars represent the standard error (SE) of the mean fold difference.

Referring to Table 5.1 above, the mean fold difference of each protein in control NP69 cell line would always be 1.0 (FD =1.0) due to the normalization step against itself. Calculated fold difference of more than the base-line 1.0 (FD >1.0) would be considered over-expression while values less than base-line 1.0 (FD <1.0) would be considered under-expression, provided the FDs are statistically significant. At a glance, among the five ribosomal proteins under investigation, four displayed significant dysregulations at their protein levels (Figure 5.1). Of the four, ribosomal protein uS4 (S9), eS31 (S27a), uL14 (L23) were significantly up-regulated in NPC cell lines cumulatively in comparison to NP69, demonstrating a possible oncogenic role in the progression of NPC. On the other hand, ribosomal protein eS8 (S8) was under-expressed in NPC cell lines, thus suggesting a tumour suppressive characteristic of eS8 (S8).

5.3.1.1 Ribosomal Protein uS4 (S9): uS4 (S9) is significantly over-expressed in NPC cell lines

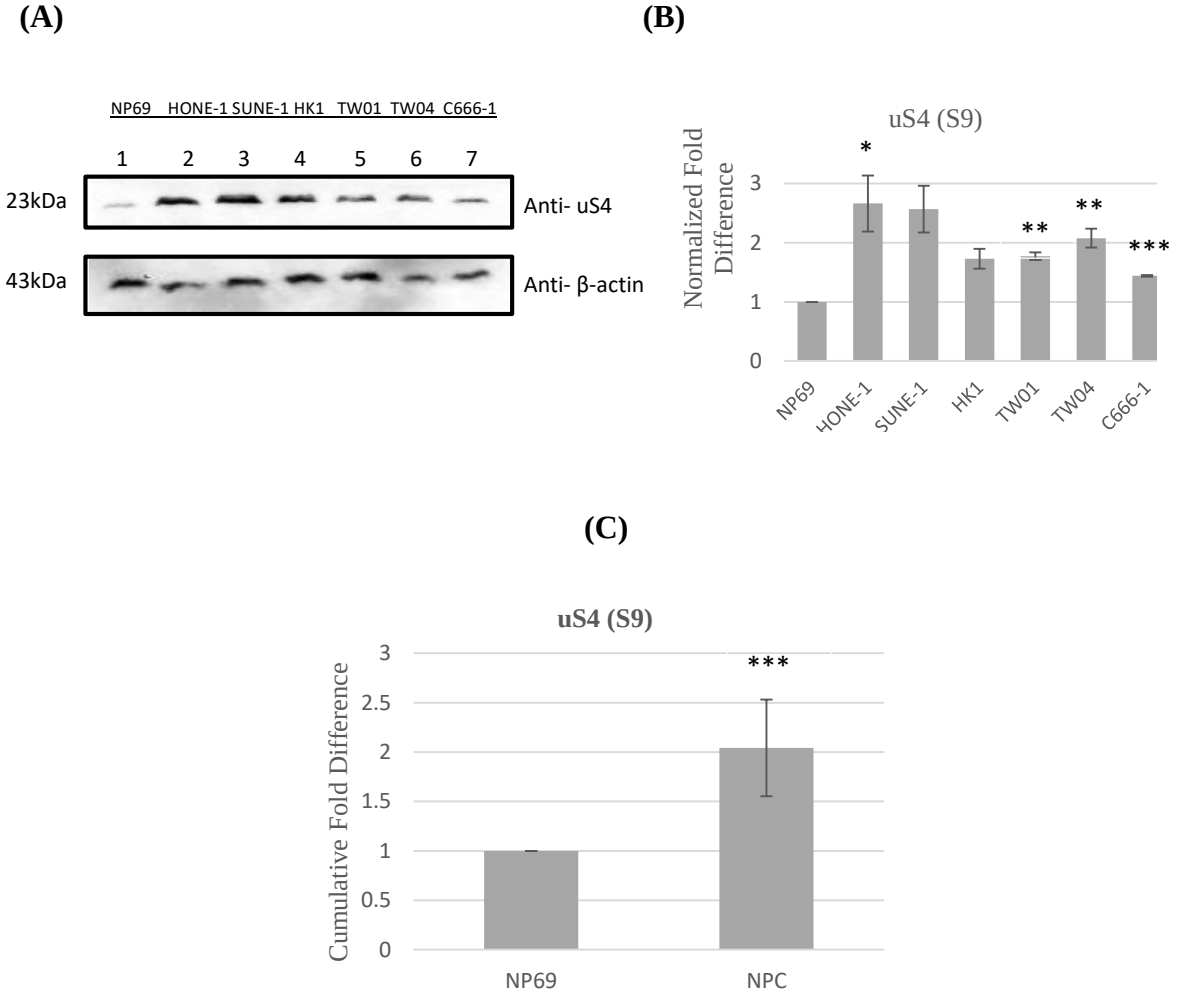

Figure 5.2: Expression of uS4 (S9) protein in six NPC cell lines compared to NP69. (A) Representative western blot of uS4 (S9) in six NPC cell lines and NP69 of biological replicate 1. (B) Graphical representation of uS4 (S9) fold difference (FD) in individual NPC cell lines compared to NP69. (C) Cumulative fold difference of uS4 (S9) in NPC vs. NP69. Corresponding *p*-values are designated with asterisk (*). *: $p< 0.05$; **: $p< 0.01$; ***: $p<0.001$. Error bars represent the standard deviation (SD) of the mean fold difference.

Ribosomal protein uS4 (S9) was found to be consistently over-expressed in all six NPC-derived cell lines, HONE-1, SUNE-1, HK1, TW01, TW04, and C666-1. The highest over-expression of 2.808-fold was recorded in SUNE-1 and followed closely behind with HONE-

1 with 2.686-fold and TW04 with 2.108-fold compared to that of NP69. Taken together, uS4 (S9) was significantly over-expressed with a mean fold difference of 2.135±0.526 (*p*-value=4.182E-05) (Figure 5.2).

In comparison to its corresponding transcript data, in which the uS4 (S9) expression was significantly down-regulated, its up-regulated protein expression presented a rather uncommon expression pattern of uS4 (S9) in the molecular framework of NPC. Our data on the inverse correlation of transcript and protein levels of uS4 (S9) implies the interplay of complicated transcriptional, translational and post-translational regulatory networks in modulating the expression and functionality of uS4 (S9).

In contrast to a common assumption that transcript level is an acceptable indicator for protein expression level, studies on mRNA-protein correspondence have revealed the exceptionally low correlation, at best 40%, between the two factors, invoking suspicion over inferences of a protein's expression and role solely on its mRNA expression level (Koussounadis, Langdon, Um, Harrison, & Smith, 2015). In other words, a majority of mRNA expression levels is inversely correlated to its protein level, therefore imparting the importance of protein analysis in predicting its biological action. This may be the case when multiple post-transcriptional regulations override transcriptional control, for the purpose of biological 'fine-tuning' under specific cellular conditions (Koussounadis et al., 2015).

The genomic context of uS4 (S9) may explain why its mRNA level was down-regulated while its protein level up-regulated in NPC: the relatively short half-life of uS4 (S9) mRNAs due to its self-regulatory mechanism. A study on the role of introns in the regulation of

ribosomal protein genes expression revealed that even though the genetic makeup and function of RPs are highly conserved across species, the evolution of their distinct regulatory machinery is highly dynamic (Plocik & Guthrie, 2012). RP genes are well-represented within the pool of intron-containing genes, and *uS4 (S9)* is a member of such pool due to its multiple variants with non-coding mRNA introns. The introduction of intron deletions in *uS4 (S9)* of *S. cerevisiae* generally showed that introns-containing RPs hampered gene expression via splicing regulation, resulting in the significant under-expression of *uS4 (S9)*. In addition, the over-expression of exogenous uS4 (S9) in *D. melanogaster* altered the alternative splicing mechanism from functional-spliced mRNA to non-functional mRNA isoforms with premature termination codons (PTC+) that were degraded by nonsense-mediated decay (NMD) (Lareau, Brooks, Soergel, Meng, & Brenner, 2007). This shows that increased protein expression of uS4 (S9) negatively regulates its own mRNA production by alternative splicing coupled to NMD, resulting in the reduction of *uS4 (S9)*. Due to its highly conserved sequence and structure, distant uS4 (S9) orthologs in *H. sapiens* were predicted to be auto-regulated in a similar fashion though this, however, is mere surmise and further *in vitro* and *in vivo* interaction assays are required to confirm the binding of ribosomal protein uS4 (S9) to its own mRNA and the auto-regulation of uS4 (S9) in human cells.

uS4 (S9) had been associated with conflicting roles in different cancer types. Firstly, it was down-regulated in invasive breast tumours and was associated with malignant transformation of tumour cells (Bin Amer et al., 2008). In contrast, a study done by Lindstrom and Nistér reported the over-expression of uS4 (S9) in U2OS osteosarcoma cells, glioma and HeLa cervical carcinoma cells. The silencing of uS4 (S9) in U2OS cells promoted tumour regression and induced senescence along with an increased expression of

DNA damage markers, while similar depletion of uS4 (S9) in HeLa cells saw an increase in apoptotic cell death. Moreover, the knockdown of uS4 (S9) disrupted the production of 18S rRNA and activated p53-mediated morphological differentiation in glioma cells. Thus, the inhibition of ribosomal protein uS4 (S9) induced senescence and apoptosis, via p53-mediated pathways, as well as reinitiated morphological differentiation in tumour cells (Lindström & Nistér, 2010). These reports reinforced the implication of uS4 (S9) over-expression in NPC molecular scenario.

5.3.1.2 Ribosomal Protein eS8 (S8): eS8 (S8) is significantly under-expressed in NPC cell lines

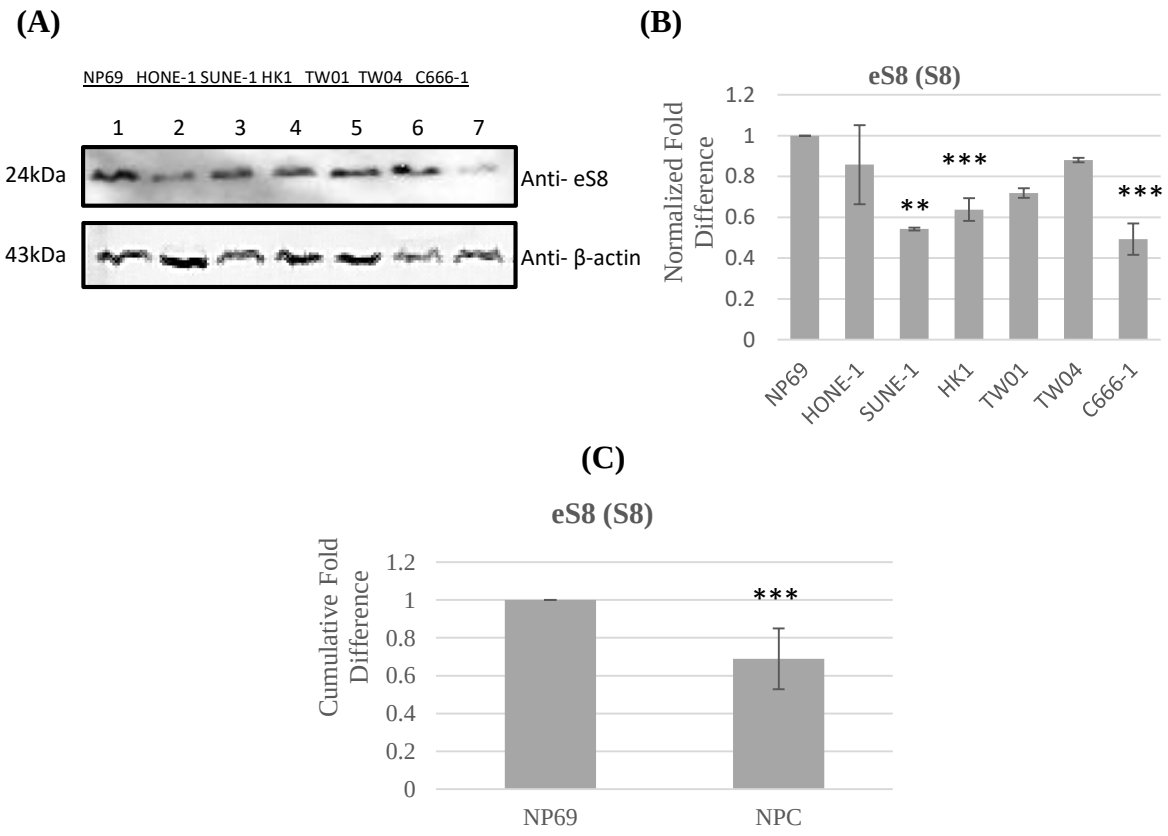

Figure 5.3: Expression of eS8 (S8) in six NPC cell lines compared to NP69. (A) Representative western blot of eS8 (S8) in six NPC cell lines and NP69 of biological replicate 1. (B) Graphical representation of eS8 (S8) fold difference (FD) in individual NPC cell lines compared to NP69. (C) Cumulative fold difference of eS8 (S8) in NPC vs. NP69. Corresponding *p*-values are designated with asterisk (*). **: $p < 0.01$; ***: $p < 0.001$. Error

bars represent the standard deviation (SD) of the mean fold difference.

Ribosomal protein eS8 (S8) was consistently under-expressed in all NPC-derived cell lines relative to NP69. The most drastic down-regulation of eS8 (S8) was displayed in the EBV-positive cell line, C666-1 (FD=0.499±0.084; *p*-value=2.424E-04), followed by that of SUNE-1 (FD=0.559±0.163; *p*-value=0.005) and HK1 (FD=0.640±0.058; *p*-value=2.196E-04), all of which were statistically significant. Cumulatively, eS8 (S8) was significantly under-expressed in NPC cell lines compared to NP69 (mean FD=0.708±0.174; *p*-value=3.625E-05) (Figure 5.3).

The expression trend exhibited by eS8 (S8) protein was agreeable to that of its transcript data, in which *eS8 (S8)* was similarly under-expressed in all NPC cell lines. Although the general patterns of the transcript and protein expression coincided, the expression profile of eS8 (S8) in individual cell lines were disparate, indicating the complex regulation of this protein across different NPC subtypes.

Despite a number of literatures associating the differential expression of *eS8 (S8)* mRNA to carcinogenesis, limited protein expression studies were performed on eS8 (S8). In fact, there have only been two cancer case studies that reported on the significant differential expression of eS8 (S8) protein. Our data is consistent with that performed on colorectal carcinoma, whereby down-regulation of eS8 (S8) was observed in colorectal tumours in relation to normal colon mucosa, while contradicted the over-expression trend of eS8 (S8) in pancreatic ductal adenocarcinoma tissues (PDAC) (Kasai et al., 2003; Chen et al., 2015).

On account of this, there have been only a few reports on the interacting partners of eS8 (S8)

in cancer development. One such study reported that eS8 (S8) interacted and functioned synergistically with CDK11p^{46}, a member of the cyclin-dependent kinase family, to inhibit cap-dependent and internal ribosome entry site (IRES)-mediated mRNA translation initiation (cap-independent) and to increase sensitivity to Fas ligand-induced apoptosis (Hao et al., 2011). *In vitro* ectopic expression of either eS8 (S8) or CDK11p^{46} induced cell apoptosis. Thus, the reduction of eS8 (S8) expression observed in NPC potentially disrupts the concerted cooperation with CDK11p^{46} and dysregulates cellular apoptotic signalling. However, further work is needed to substantiate such a deduction.

5.3.1.3 Ribosomal Protein eS31 (S27a): eS31 (S27a) is significantly over-expressed in NPC cell lines

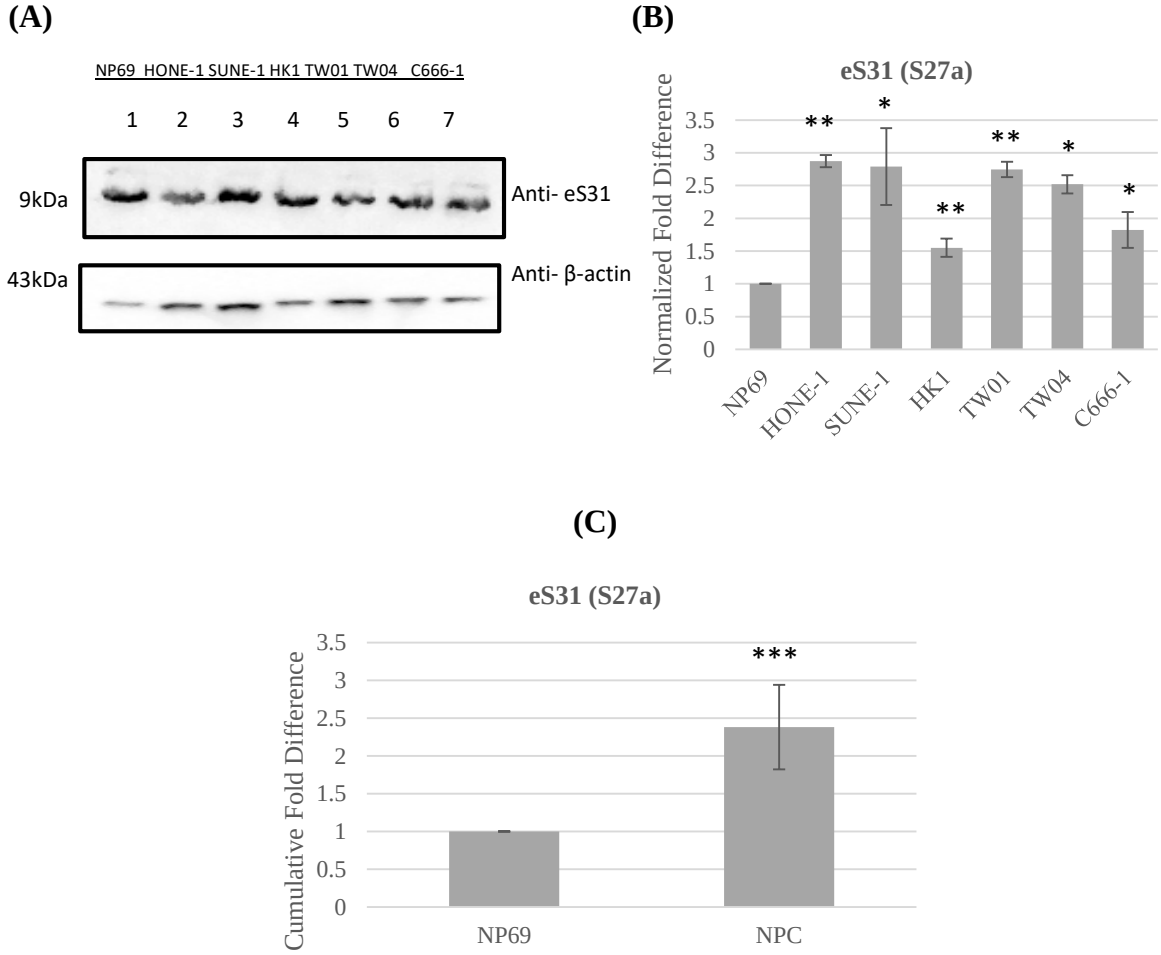

Figure 5.4: Expression of eS31 (S27a) protein in six NPC cell lines compared to NP69. (A) Representative western blot of eS31 (S27a) in six NPC cell lines and NP69 of biological replicate 1. (B) Graphical representation of eS31 (S27a) fold difference (FD) in individual NPC cell lines compared to NP69. (C) Cumulative fold difference of eS31 (S27a) in NPC vs. NP69. Corresponding *p*-values are designated with asterisk (*). *: $p< 0.05$, **: $p< 0.01$. Error bars represent the standard deviation (SD) of the mean fold difference.

Ribosomal protein eS31 (S27a) was consistently and significantly over-expressed in all individual NPC cell lines under study, in comparison to NP69. The highest up-regulation of eS31 (S27a) of close to 3-fold was identified in HONE-1 (FD=2.912±0.655; *p*-value=0.004), comparably followed by SUNE-1 (FD=2.900±1.034; *p*-value=0.017) and TW01 (FD=2.829±0.775; *p*-value=0.007), TW04 (FD=2.599±0.809; *p*-value=0.013), C666-1

(FD=1.914±0.675; *p*-value=0.040) and the least differential expression was noted in HK1 cell line (FD=1.548±0.209; *p*-value=0.005). Taken together, it is evident that eS31 (S27a) was significantly over-expressed in the context of NPC (mean FD=2.450±0.580; *p*-value=4.610E-07) (Figure 5.4).

Cross-referring to its corresponding transcript data, the expression of eS31 (S27a) was congruent only in HONE-1, whereby both transcript and protein were up-regulated. On the other hand, the expression of *eS31 (S27a)* in the other five NPC cell lines were down-regulated, which was in contrast to its protein expression observed in this subset of cell lines, implying a distinct NPC-subtype-dependent regulatory interplay in modulating the expression level of eS31 (S27a).

Similar expression pattern was previously noted in cancers of the colorectal, renal, prostate, as well as in advance-phase chronic myeloid leukaemia (CML) and acute leukaemia (AL) solid tumours. The up-regulation of eS31 (S27a) had been correlated to enhanced cellular proliferation and cell cycle progression, and increased drug-resistance in CML patients, while its suppression reversed such phenotypes (Kanayama et al., 1991; Wong et al., 1993; Wang et al., 2014). As such, eS31 (S27a) possesses the potential as a target molecule in cancer treatment and therapy.

eS31 (S27a) had been demonstrated to be a vital component within the MDM2-p53 network, wherein the interaction of eS31 (S27a) and MDM2 inhibited MDM2-mediated p53 degradation subsequently leading to p53 stabilization, which in turn, negatively regulated eS31 (S27a) levels (Sun et al., 2011). In regard to the up-regulation of p53 levels in NPC,

two hypothetical models could be proposed. Firstly, NPC tumorigenesis tipped the balance between eS31 (S27a) and p53 within the negative autoregulatory loop in favour of the regulation of eS31 (S27a) onto p53 and not the other way around. Secondly, p53 negatively regulates *eS31 (S27a)* in terms of its transcriptional control, resulting in the reduction of *eS31 (S27a)* mRNA level. However, subsequent p53-independent translational and post-translation regulatory mechanisms stabilize eS31 (S27a) protein, thereby feeding into the eS31 (S27a)-MDM2-p53 network. Our data agrees with the latter scenario as evidenced by the reduced *eS31 (S27a)* mRNA level but enhanced eS31 (S27a) protein expression, though it remains unverified.

5.3.1.4 Ribosomal Protein uL14 (L23): uL14 (L23) is significantly over-expressed in NPC cell lines

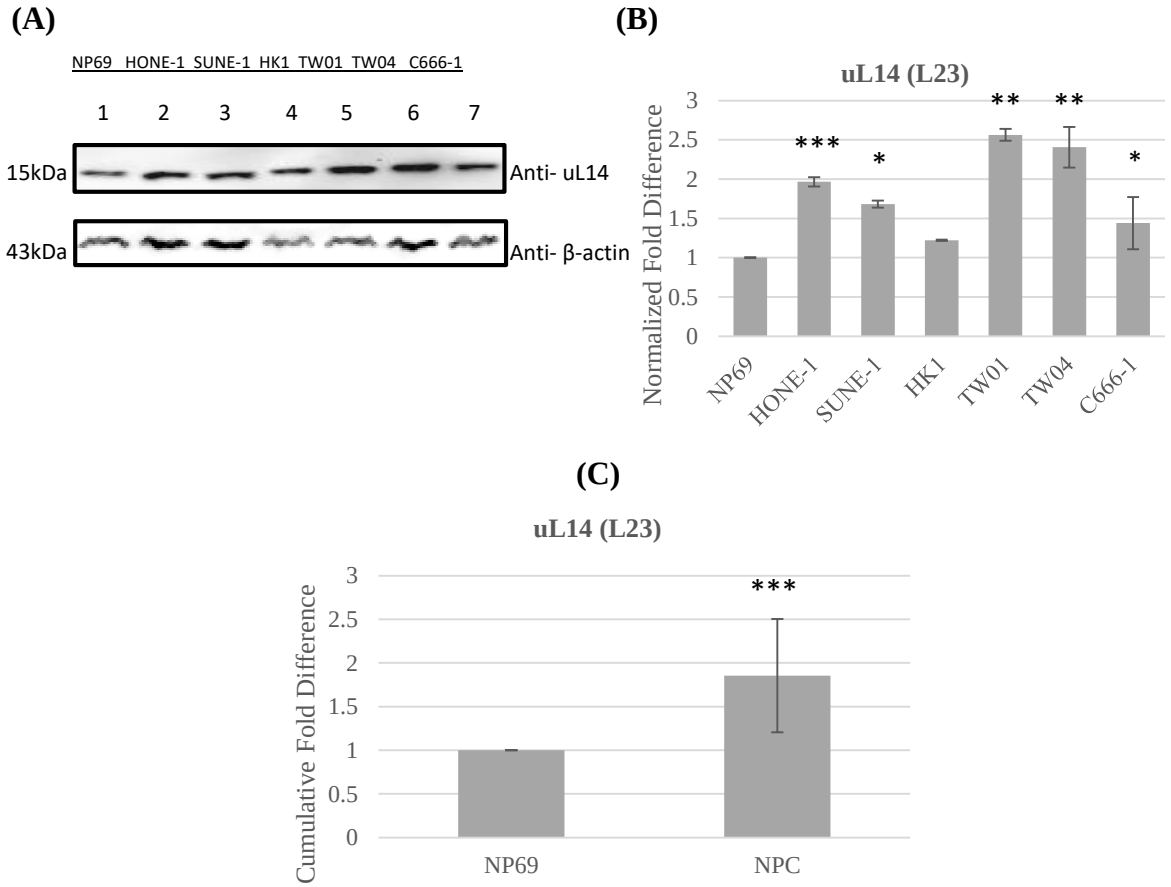

Figure 5.5: Expression of uL14 (L23) protein in six NPC cell lines compared to NP69. (A) Representative western blot of uL14 (L23) in six NPC cell lines and NP69 of biological replicate 1. (B) Graphical representation of uL14 (L23) fold difference (FD) in individual NPC cell lines compared to NP69. (C) Cumulative fold difference of uL14 (L23) in NPC vs. NP69. Corresponding *p*-values are designated with asterisk (*). *: $p< 0.05$, **: $p< 0.01$, ***: $p< 0.001$. Error bars represent the standard deviation (SD) of the mean fold difference.

Ribosomal protein uL14 (L23) was consistently up-regulated in all NPC cell lines. The highest induction of approximately 2.6-fold was observed in the keratinized and differentiated TW01 cell line (FD=2.401±0.349; *p*-value=0.001), and comparably in TW04 (FD=2.401±0.349; *p*-value=0.001), followed by HONE-1 (FD=1.968±0.158; *p*-value=2.220E-04) and SUNE-1 (FD=1.737±0.527; *p*-value=0.036). uL14 (L23) was

similarly over-expressed in HK1 and C666-1 but not statistically significant. Cumulatively, significant uL14 (L23) over-expression was observed in all six NPC cell lines (mean FD=1.909±0.533; *p*-value=4.560E-06) (Figure 5.5).

In comparison to its down-regulated transcript data, uL14 (L23) was inversely over-expressed at its protein level. The mRNA expression *uL14 (L23)* was shown to be the most drastically reduced in C666-1, of about 99% reduction; conversely, uL14 (L23) protein was the least up-regulated in C666-1, displaying a unique expression fingerprinting of uL14 (L23) to the EBV-positive C666-1 cell line.

Similar expression trend was observed in SCCHN, multidrug-resistance gastric cancer cells and MDS (Shi et al., 2004; Russo et al., 2013; Qi et al., 2017). In an SCCHN-focused study, exogenous over-expression of uL14 (L23) in paired non-malignant cells induced carcinogenic transformation (Russo et al., 2013). However, the reverse effect from the ectopic expression of uL14 (L23) was reported in colorectal and gastric cancers, wherein the adenovirus-mediated delivery of exogenous uL14 (L23) into tumour cells enhanced the accumulation of p53 protein and blocked cell proliferation by cell cycle arrest and apoptosis, thereby rendering it a potential cancer therapeutic target (Zhang et al., 2013; Fang et al., 2015). These contradictory reports showcased the highly specific molecular inner workings affiliated to each cancer type.

Based on its established direct interaction with MDM2, the over-expression of uL14 (L23) in NPC could be predicted to associate and sequester MDM2, thereby inhibiting MDM2-mediated p53 ubiquitination and stabilizing p53 levels, leading to the up-regulation of p53

protein previous reported in NPC (Agaoglu et al., 2004; Dai et al., 2004). Apart from MDM2, uL14 (L23) had been predicted to associate with NPM1 within the Miz-1-NPM1 regulatory network (Wanzel et al., 2008; Wiese et al., 2013). Hypothetically, the up-regulated uL14 (L23) expression in NPC would associate with NPM1, an important co-activator of Miz-1, consequently disabling the activation of Miz-1 and Myc-dependent transcription of cell cycle inhibitors, p15 and p21, leading to cell cycle progression and cell proliferation. Again, experimental assays would need to be done to substantiate this.

5.3.1.5 Ribosomal Protein eL18 (L18): eL18 (L18) is over-expressed in NPC cell lines, though not significantly

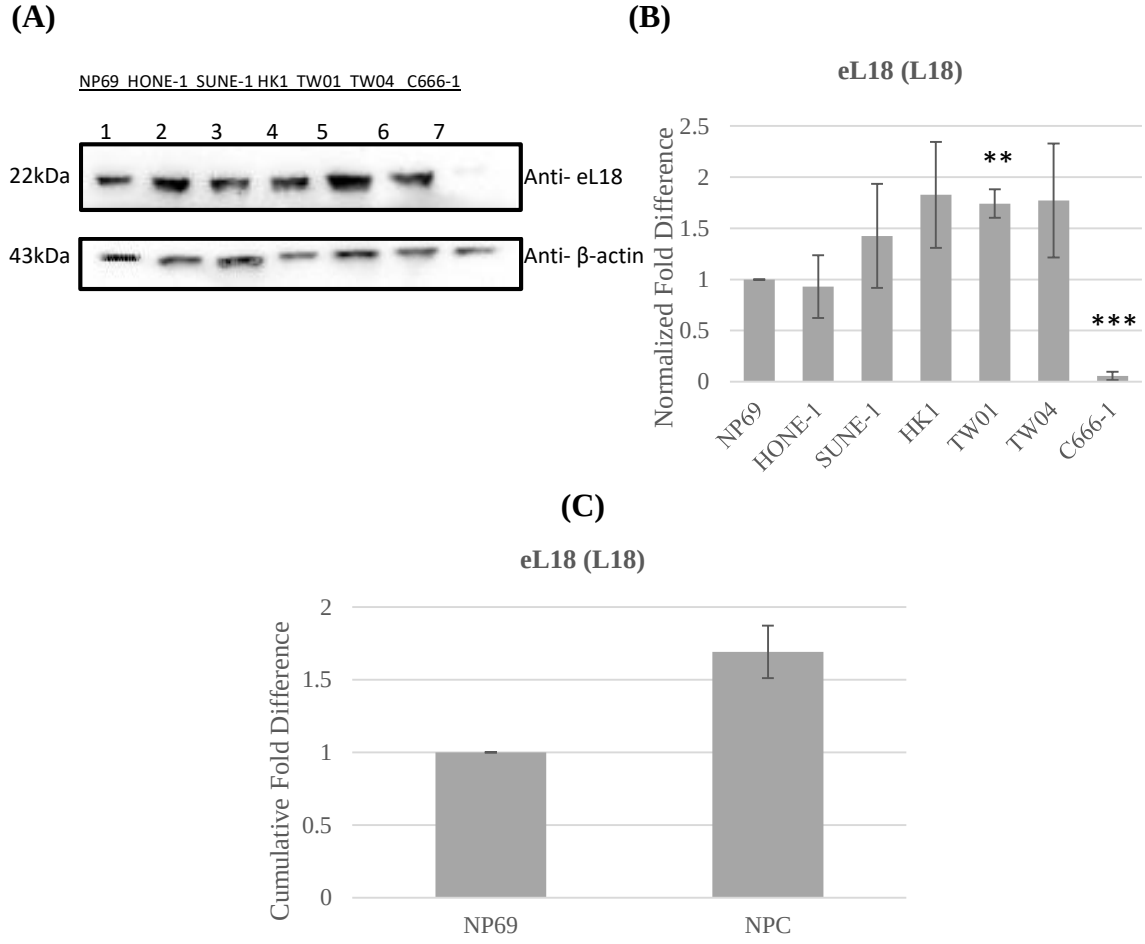

Figure 5.6: Expression of eL18 (L18) protein in six NPC cell lines compared to NP69. (A) Representative western blot of eL18 (L18) in six NPC cell lines and NP69 of biological replicate 2. (B) Graphical representation of eL18 (L18) fold difference (FD) in individual NPC cell lines compared to NP69. (C) Cumulative fold difference of eL18 (L18) in NPC vs. NP69. Corresponding *p*-values are designated with asterisk (*). **: $p < 0.01$; ***: $p < 0.001$. Error bars represent the standard deviation (SD) of the mean fold difference.

Ribosomal protein eL18 (L18) was inconsistently found to be significantly over-expressed in TW01 (FD=1.735±0.200; *p*-value=0.002) and under-expressed in C666-1 (FD=0.126±0.160; *p*-value=3.480E-04). No significant dysregulation was observed in the other cell lines tested (Figure 5.6).

The protein expression of eL18 (L18) in HONE-1 and C666-1 showed inconsistency in comparison to its transcript data, in which *eL18 (L18)* was found to be consistently up-regulated in all NPC cell lines. Interestingly, the under-expression of eL18 (L18) in the only EBV-positive C666-1 cell line was of statistical significance, suggesting a distinct association between eL18 (L18) and EBV factors that are absent in the other NPC cell lines. This finding raises a preliminary implication on the possible EBV-specific role of eL18 (L18) in NPC development.

5.3.1.6 Nucleophosmin NPM1/ B23: NPM1 is significantly over-expressed in NPC cell lines

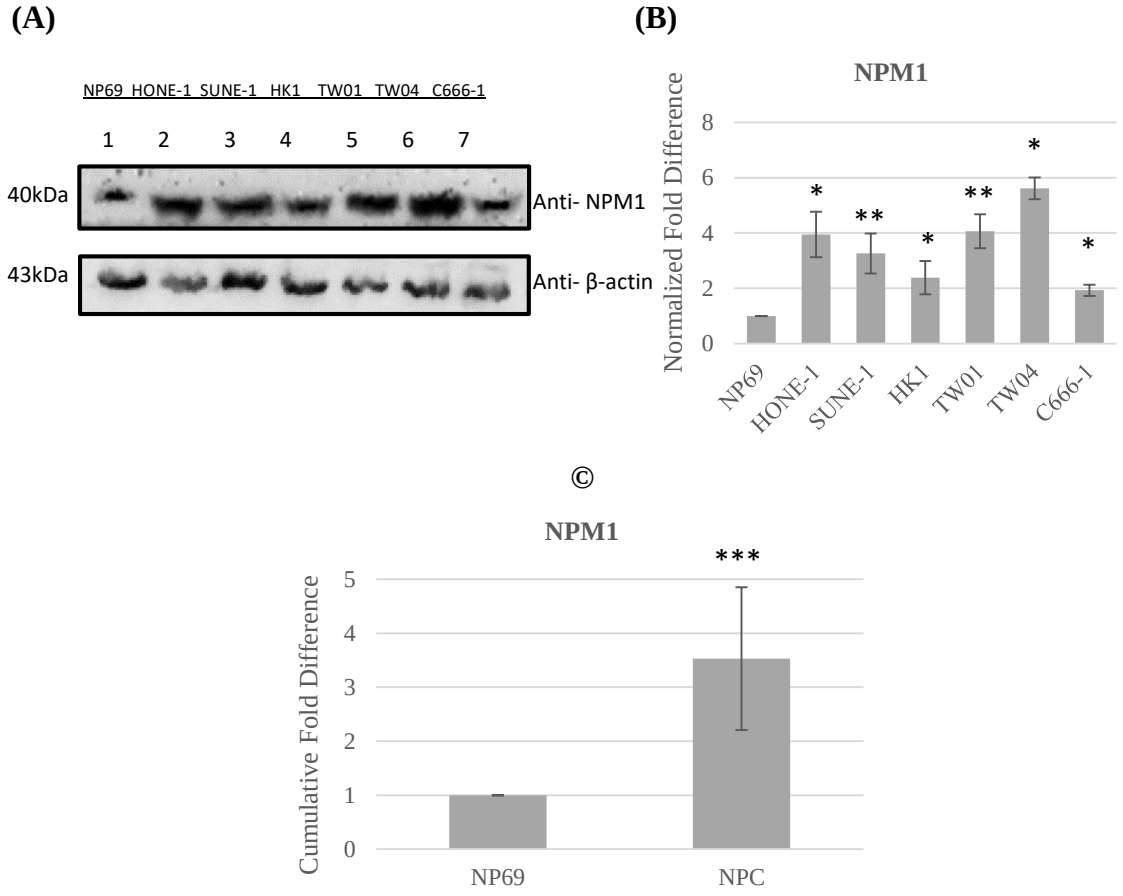

Figure 5.7: Expression of NPM1 protein in six NPC cell lines compared to NP69. (A) Representative western blot of NPM1 in six NPC cell lines and NP69 of biological replicate 1. (B) Graphical representation of NPM1fold difference (FD) in individual NPC cell lines compared to NP69. (C) Cumulative fold difference of NPM1in NPC vs. NP69. Corresponding *p*-values are designated with asterisk (*). *: $p< 0.05$, **: $p< 0.01$. Error bars represent the standard deviation (SD) of the mean fold difference.

Nucleophosmin, also known as NPM1 or B23, was consistently over-expressed across all NPC cell lines under study. The highest over-expression of about 6.1-fold was observed in TW04 (FD=6.074±3.164; *p*-value=0.025). Following that, TW01 (FD=4.050±0.919; *p*-value=0.002) and HONE-1 (FD=3.983±1.508; *p*-value=0.013) displayed comparable expression of NPM1. The expression of NPM1 was also up-regulated in SUNE-1

(FD=3.246±1.001; *p*-value=0.009), HK1 (FD=2.349±0.705; *p*-value=0.015 and the least over-expression was noted in C666-1 (FD=2.027±0.822; *p*-value=0.048). As the enhancement of NPM1 was statistically significant in all NPC cell lines, cumulative analysis demonstrated equally significant up-regulation (mean FD=3.622±1.458; *p*-value=1.064E-05) (Figure 5.7).

Similar to the inverse correlation between transcript and protein expression levels previously described for ribosomal protein uS4 (S9), eS31 (S27a) and uL14 (L23), the corresponding transcript and protein data of NPM1 was not agreeable: *NPM1* was significantly under-expressed in NPC cell lines but its protein levels were significantly up-regulated. Similar converse expression pattern of transcript and protein was observed in acute myelogenous leukaemia (AML) and gastric cancer cells (Bonetti et al., 2008; Leal et al., 2014; Box et al., 2016). This observation points toward a highly specific and highly controlled transcription and translation regulation mechanisms in determining the relative expressions of NPM1 at every level.

Various studies have reported on the similar over-expression trend of NPM1 such as in glioblastoma, hepatocellular carcinoma, ovarian cancer, oral squamous cell carcinoma, prostate cancer, salivary gland adenoid cystic carcinoma and colorectal carcinoma (Coutinho-Camillo et al., 2010; Liu et al., 2012; Londero et al., 2014; Loubeau et al., 2014; Holmberg Olausson et al., 2015; Li et al., 2017). In these cancers, the up-regulation of NPM1 had been implicated with increased resistance to cellular apoptosis, tumour grading, increased proliferation of tumour cells and invasiveness.

NPM1 had been regarded as one of the major regulators of the $p14^{ARF}$-MDM2-p53 network, capable of directly interacting with $p14^{ARF}$, MDM2 and p53. The up-regulation of NPM1 sequestered and retained $p14^{ARF}$ within the nucleoli and inhibited its interaction with MDM2, leading to p53 stabilization (Korgaonkar et al., 2005). NPM1 depletion in leukemic cells showed increased cell cycle arrest and cellular apoptosis due to the accumulation of free $p14^{ARF}$ (Qin et al., 2011). Independent of $p14^{ARF}$, NPM1 was shown to be able to interact directly with MDM2, thereby preventing the proteasomal degradation of p53, further expanding the pool of stabilized p53 (Jin, Itahana, O'Keefe, & Zhang, 2004). Upon further investigation, some studies have also reported NPM1 to be a direct mediator of p53, though this remains inconclusive due to contrasting results by other groups (Colombo, Marine, Danovi, Falini, & Pelicci, 2002; Itahana et al., 2003). Taken together, the multi-faceted ability of NPM1 within the MDM2-p53 network leads to the final outcome of p53 level accumulation, as observed in NPC, demonstrating the likelihood of NPM1's action in NPC (Agaoglu et al., 2004).

CHAPTER 6

IN VITRO AND *IN VIVO* ASSAYS FOR NPM1-ASSOCIATED RIBOSOMAL PROTEINS

6.1 *In Vitro* Pull- down Assay for NPM1-Associated Ribosomal Proteins

6.1.1 Background

Protein-protein interactions (PPIs) are highly specific physical contact between two or more proteins via defined binding domains with specific functional consequences.

Due to their indispensable roles in most biological processes in a cell, such as gene regulation and expression, cell growth and proliferation, cell morphology and motility, intra- and inter-cellular communication and apoptosis, protein expression and function generally modulate the healthy inner keeping of a cell. Aberrancy in this highly controlled mechanism interferes with the interactomics within a cell, resulting in the dysregulation of basic cellular pathways and unfavourable phenotype transformation. As such, it is necessary to delineate the interacting partners of proteins in the effort to logically place the exact role of a protein within the vast cellular molecular framework and to be able to foresee the downstream aftermath of a certain protein expression anomaly as well as to discover potential therapeutic targets for diseases and cancers.

In the previous chapters, we have reported the significant differential transcript expression of five out of eight ribosomal protein genes under study (*uS4 (S9), eS8 (S8), eS31 (S27a), uL14 (L23)* and *eL18 (L18)*), and one of three putative interacting co-factors (*NPM1*).

Following that, out of the five ribosomal proteins, four displayed significant differential expression at its protein level (uS4 (S9), eS8 (S8), eS31 (S27a) and uL14 (L23)), as well as NPM1.

Therefore, in this chapter, we attempted to detect the possible *in vitro* interaction between these differentially expressed ribosomal proteins and NPM1.

6.1.2 Methodology Overview

Pull-down assay was performed with NPM1 and four ribosomal proteins uS4 (S9), eS8 (S8), eS31 (S27a) and uL14 (L23), which were differentially expressed, with opposite trends, at its transcript and protein levels in NPC cell lines. Antibodies specific to each protein were cross-linked to Dynabeads Protein G (Life Technologies, USA) and incubated with cell lysates of TW04 and C666-1 (NPC cell lines) and that of NP69 (normal nasopharyngeal epithelial cell line). After rounds of elution and washings, the beads-protein complex mixtures were denatured and separated with SDS-PAGE and western blot (protocol described in Materials and Methods Chapter 3.5). Cell lysates were immunoprecipitated with antibodies against unspecific IgG control, ribosomal protein or NPM1, and were immunoblotted with ribosomal protein or NPM1 antibodies as indicated. Chemiluminescence immunoassay was carried out to detect and visualize target proteins.

6.1.3 Results and Discussion

6.1.3.1 Endogenous uS4 (S9) Associates with NPM1 *in vitro*

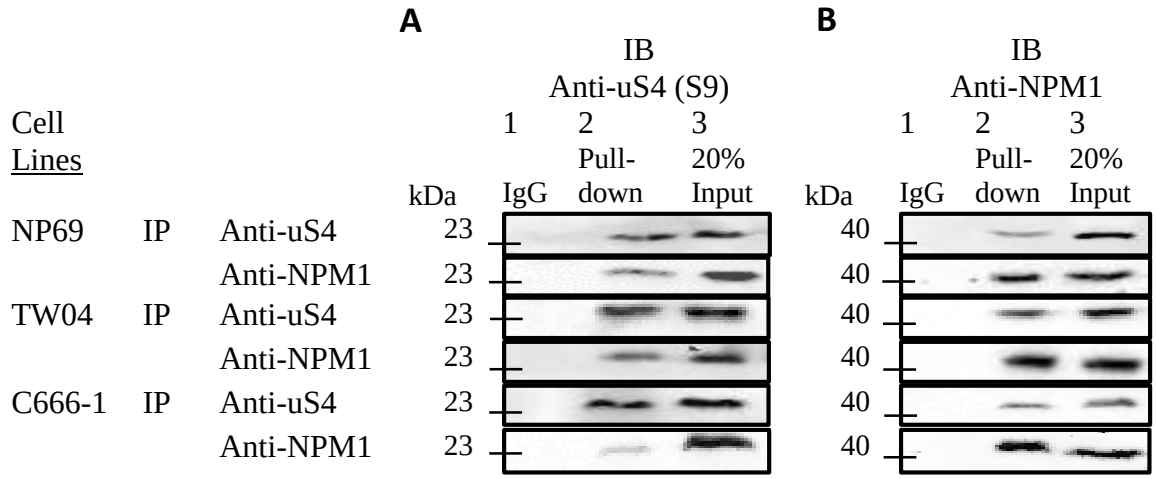

Figure 6.1: Ribosomal protein uS4 (S9) interacted with NPM1 *in vitro*. (A) Co-IP pull-down assay using either uS4 (S9) or NPM1 antibodies to immuno-precipitate (IP) corresponding interacting complex, followed by immunoblotting (IB) with uS4 (S9) antibody. Lane 1 represents the negative control, in which un-conjugated IgG antibodies were used for pull-down to validate the specificity of target proteins against respective antibodies. Replicates in Lane 3 contain 20% of total protein input and that was not subjected to immuno-precipitation to ensure acceptable pull-down efficiency. Ribosomal protein uS4 (S9) were consistently present in pulled-down lysates using anti-NPM1 antibodies in three different cells lines, substantiating its stable association with NPM1. (B) Immuno-precipitation with either uS4 (S9) or NPM1 antibodies and subsequent immuno-blot for NPM1. When pulled-down with NPM1 antibodies, uS4 (S9) was detected in all lysates from NP69, TW04 and C666-1 cell lines, confirming the inverse relationship of NPM1 and uS4 (S9).

Figure 6.1 revealed the *in vitro* interaction of ribosomal protein uS4 (S9) and NPM1 in NP69, TW04 and C666-1 cell lines. To determine if whether endogenous uS4 (S9) associates with and forms a stable protein complex with NPM1, we immunoprecipitated NPM1 with anti-NPM1 antibody and subsequently conducted western blotting with anti-uS4 (S9) antibody. uS4 (S9) protein was clearly detected in NPM1-pulled down lysate and vice versa, confirming a generally strong and stable interaction between the two proteins under investigation. Having said so, a comparatively faint band of uS4 (S9) was observed in lysate

of the EBV-positive cell line, C666-1, when immunoprecipitated with NPM1 relative to that of other cell lines as well as that of the control input band, suggesting a weaker uS4 (S9)-NPM1 interaction under those circumstances (Figure 6.1A, bottom-most panel). To confirm the reciprocal relationship, we repeated the co-IP assay using anti-uS4 (S9) antibody and immunoblotted with anti-NPM1 antibody. As shown in Figure 6.1B, NPM1 was co-precipitated with uS4 (S9). Hence, ribosomal protein uS4 (S9) associated with NPM1 in NP69, TW04 and C666-1 cells, and vice versa, and not with the control IgG antibody.

Our findings coincided with the report by Lindstrom on the discovery of ribosomal protein uS4 (S9) as an NPM1-interacting protein in U2OS osteosarcoma cells, and on the mapping of the binding site of uS4 (S9) to the intact oligomerization domain of NPM1 (Lindström & Zhang, 2008). Even though there seemed to be an overlap in data account between that of ours and Lindstrom, the result reported here should be taken as a research novelty due to the extremely distinct oncogenic environment of the two cancer models: nasopharyngeal carcinoma and osteosarcoma. Studies on cancer-type-specific translational landscape have demonstrated the highly specific functional consequences of proteins to a certain cancer specimen (Vogelstein et al., 2013; Yang et al., 2015). In other words, a gene product may be perturbed differently in different cancers and subsequently function and behave differently. As such, to better distinguish this study from that of Lindstrom, we point out that we systematically analysed the interaction of uS4 (S9) and NPM1 in two NPC cell lines, which were of distinct histopathological sub-types and cellular behaviour, in terms of level of differentiation, invasiveness, prognosis and treatment response, providing a comprehensive representation of the association of uS4 (S9) and NPM1 in nasopharyngeal carcinoma.

At the same time, precaution is due in interpreting the result from this section of our project due to the limitation of the reciprocal co-IP assay. Interaction evidence gathered only suggested the association between uS4 (S9) and NPM1 and not direct interaction due to the possibility of uS4 (S9) and NPM1 co-operating as a complex or as co-factors within the network. Association, in our context, pertains to the stable direct or indirect physical protein-protein aggregation within a complex consisting of the precipitated antigen, target protein partners and/or other intermediary protein or ligands under a specific experimental condition. Direct interaction, on the other hand, refers to experimentally verified interaction between two proteins of interest. In summary, we report on the stable inter-working of ribosomal protein uS4 (S9) and NPM1 in the two major sub-types of NPC cells and normal NP69 cells.

6.1.3.2 No Association was Detected Between eS8 (S8) and NPM1

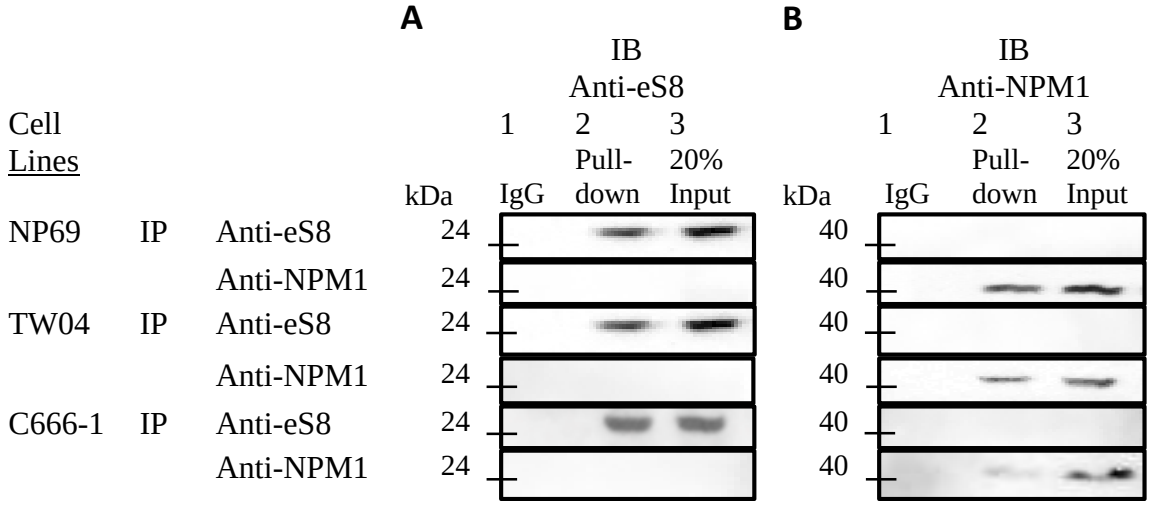

Figure 6.2: Ribosomal protein eS8 (S8) does not interact with NPM1 *in vitro*. Co-IP pull-down assay using either eS8 (S8) or NPM1 antibodies to immuno-precipitate (IP) followed by immunoblotting (IB) with (A) anti-eS8 (S8) antibody and (B) anti-NPM1 antibody.

Figure 6.2 demonstrated the lack of association between ribosomal protein eS8 (S8) and NPM1. Lysate obtained after immuno-precipitation with anti-NPM1 antibodies did not contain detectable eS8 (S8) protein and similar observation was noted when anti-eS8 antibodies were used to pull-down NPM1, thus verifying that ribosomal protein eS8 (S8) does not form a stable interaction with NPM1 and is not part of the NPM1-associated protein complex, and vice versa. This observation came not as a surprise as there is no known interaction of eS8 (S8) and NPM1 reported so far in any disease model. However, this does not eliminate the possibility of inter-dependency of these two proteins due to the biasness of a pull-down assay on stable and strong interacting protein complex and not on transient and distantly-associated proteins.

6.1.3.3 eS31 (S27a) in Complex with NPM1 *in vitro*

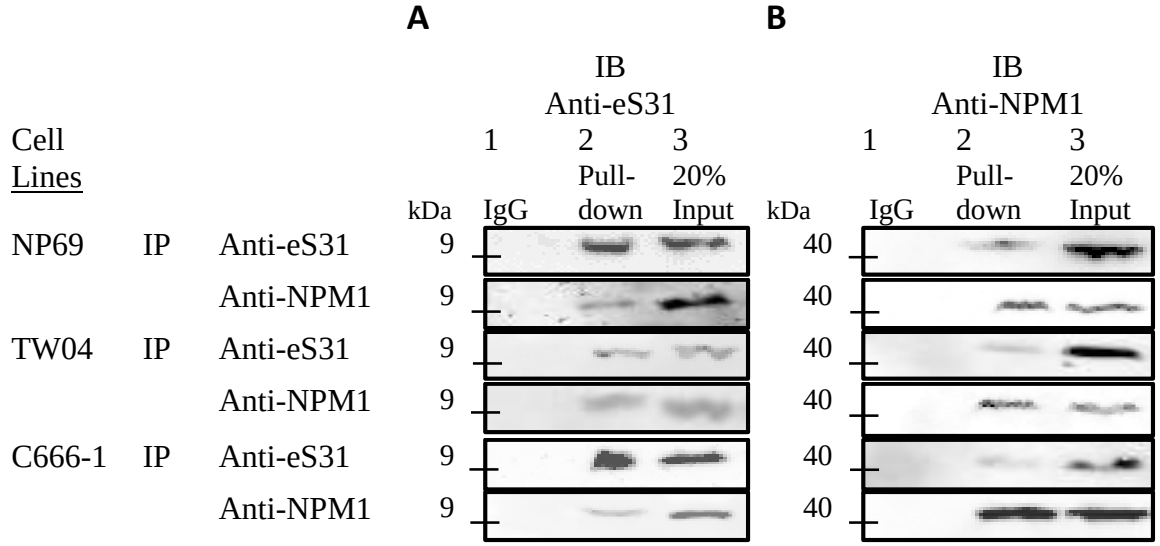

Figure 6.3: Ribosomal protein eS31 (S27a) interacted with NPM1 *in vitro*. (A) NPM1 was detected in eS31 (S27a) pulled-down lysate from all three cell lines. (B) Inversely, eS31 (S27a) protein was present in the anti-NPM1 eluents of three cells lines, thereby validating the two-way association of eS31 (S27a) and NPM1 *in vitro*.

Ribosomal protein eS31 (S27a) was successfully detected in the anti-NPM1 pull-down lysate of TW04 and C666-1 NPC cell lines as well as normal NP69 cells, and the reverse case was also true, demonstrating a stable association between eS31 (S27a) and NPM1. Though interactively strong, the pull-down using anti-eS31 antibodies displayed a relatively lighter NPM1 protein bands (Figure 6.3B; panel 1, 3 and 5) in comparison to the efficiency controls (panel 2, 4 and 6) and input controls as well as the reciprocal pull-down with anti-NPM1 antibodies (Figure 6.3). This observation exposed the weaker eS31 (S27a) hold onto NPM1 or NPM1-associated complex probably due to its comparatively smaller protein size of only 9kDa, in contrast to 40kDa of NPM1.

Our work is in agreement with an extensive large-scale protein-protein interaction mapping using liquid chromatography-mass spectrometry (LC-MS) in HEK293 human embryonic kidney cells (Ewing et al., 2007). The group reported the association of eS31 (S27a) to NPM1 via cyclin-dependent kinase 2 (CDK2) protein as an intermediary factor in a complex. Though, no experimental work was conducted to verify the possibility of a direct interaction between eS31 (S27a) and NPM1.

Other than this, there were no other publications available on this eS31-NPM1 relationship. Therefore, by taking our result and that of Ewing's group, we can deduce certain premises. Firstly, ribosomal protein eS31 (S27a) plays an extra-ribosomal role in the maintenance of genomic stability and centrosome duplication and it assumes its role by associating with CDK2, which in turn phosphorylates NPM1 and promotes its release from the centrosome (Amin, Matsunaga, Uchiyama, & Fukui, 2008). Secondly, considering the fact that antibody against the target protein (eS31) could in fact, precipitate the bait protein (NPM1) and vice

versa, the association between both proteins needed to be steady under the experimental conditions. By putting the results of the two groups together, the eS31-CDK2-NPM1 complex is formed with a strong synergy between the three components and that ribosomal protein eS31 (S27a) and NPM1 binds to distinct sites on CDK2 for eS31 (S27a) to be co-precipitated with NPM1 in a pull-down assay.

6.1.3.4 Endogenous uL14 (L23) Affiliates with NPM1 *in vitro*

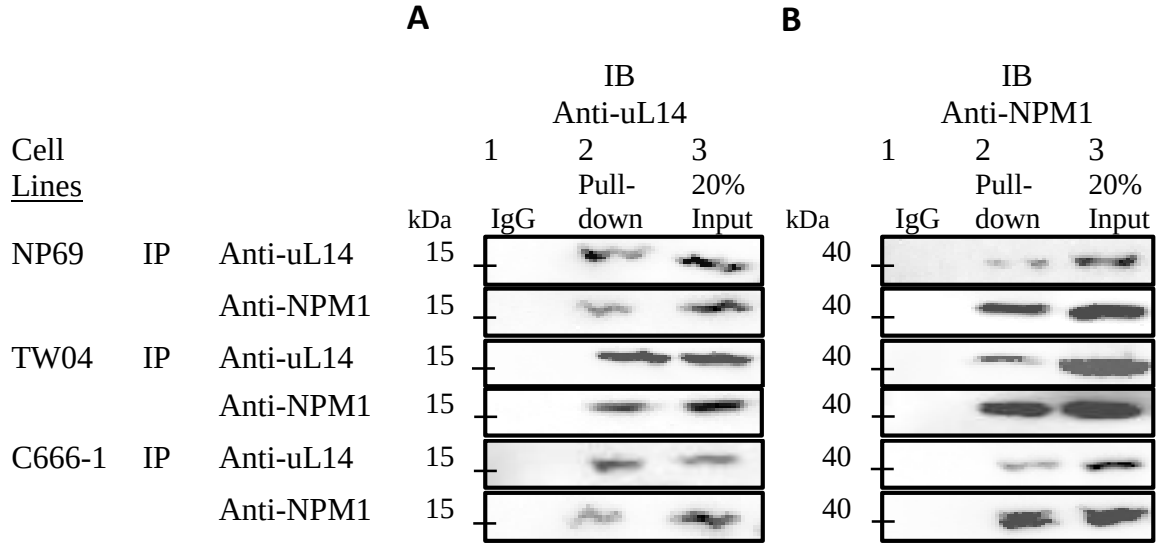

Figure 6.4: Ribosomal protein uL14 (L23) was found to associate with NPM1 *in vitro*. (A) uL14 (L23) ribosomal protein was pull-downed by anti-NPM1 antibodies in all three cell lines, confirming its affiliation with ribosomal protein NPM1 in our experimental conditions. (B) Conversely, anti-uL14 antibodies were able to precipitate ribosomal protein uL14 (L23), thus verifying their association *in vitro*.

Figure 6.4 above revealed the reciprocal association of ribosomal protein uL14 (L23) and NPM1 in TW04 and C666-1 NPC cells as well as normal NP69 cells *in vitro*. In a similar immunodetection trend as that of ribosomal protein uS31 (S27a) and NPM1, the use of anti-uL14 antibody during immuno-precipitation of NPM1 was weaker than that of its reciprocal (Figure 6.4), efficiency controls (Figure 6.4B, panel 2, 4 and 6) and input controls (Figure

6.4B).

Our data is supported by a study done on non-tumorigenic RAT1 cells, ovarian carcinoma cells (HeLa), breast cancer cells (MCF7), osteosarcoma cells (U2OS) and colorectal cancer cells (LS174T) to investigate the Myc-associated zinc-finger protein (Miz-1) pathway. The study reported the functional inhibition of ribosomal protein uL14 (L23) on Miz-1 function, which in turn, was observed to be transactivated by NPM1 (Wanzel et al., 2008). As no direct binding between uL14 (L23) and Miz-1 was observed, the authors inferenced that uL14 (L23) interacted with NPM1 and sequestered it in the nucleolus, thereby preventing the transactivation of Miz-1 catalysed by NPM1 in the nucleus. Our data with nasopharyngeal carcinoma cells supports such claim.

By consolidating the data from our group and that of Wanzel's, it can be deduced that ribosomal protein uL14 (L23) plays a vital role in cell cycle progression and cell growth via the Miz-1-dependent pathway.

6.2 *In Vivo* Protein Interaction Assay for NPM1-Associated Ribosomal Proteins

6.2.1 Background

Previously, we have demonstrated the stable, indirect, *in vitro* interaction between NPM1 and three ribosomal proteins uS4 (S9), eS31 (S27a) and uL14 (L23) with a reciprocal co-immunoprecipitation assay. These ribosomal proteins were detected in the respective NPM1-pulled down eluted lysates and vice versa.

However, co-immunoprecipitation presents a number of drawbacks in terms of its outcome limitation. Firstly, chemical and mechanical stresses of the incubation and washing steps of co-IP allow for the detection of secondary targets (interacting proteins) with only stable and strong protein-protein interactions to the primary target (target antigen) thereby lowering the chances of precipitating transient or low-affinity protein interactors. Secondly, the lysing of cells brings together the pool of cellular proteins that would otherwise not be in the vicinity of each other, resulting in unspecific interactions. Thirdly, the antibody against primary target antigen possesses high epitope specificity, in which could, in some cases, prevents or disrupts protein-protein interactions of protein complexes; and in some cases, failure to precipitate target antigen due to epitope inaccessibility by pre-established protein-protein interactions. Lastly, the outcome analysis of co-immunoprecipitation is limited in the sense that this assay could only demonstrate the potential protein-protein interactions within a pulled-down complex *in vitro* but not the exact nature of interactions between the primary target protein and its corresponding secondary targets. In that respect, we subsequently conducted a mammalian two-hybrid assay to validate the direct association of NPM1 and the targeted ribosomal proteins *in vivo* with mammalian cells that closely mimics actual biological environments.

6.2.2 Methodology Overview

To establish NPM1-RPs assays for the analysis of *in vivo* protein-protein interaction, full-length coding region (CDS) of human ribosomal proteins uS4 (S9), eS31 (S27a) and uL14 (L23) and NPM1, flanked with distinct restriction enzymes sites were designed and cloned in-frame into two Mammalian Two-Hybrid System's expression vectors, pACT and pBIND, containing activation domain and DNA-binding domain, respectively. Specific sets of expression constructs were subsequently transfected into TW04 cells in conjunction with an appropriate internal control vector, pG5*luc*. Reporter assay was conducted 48 hours post-transfection with Dual-Luciferase Reporter Assay System to detect both firefly and *Renilla* luciferases signals. The relative luminescence unit (RLU) for each transfection set was calculated by dividing the value of firefly luciferase activity by that of *Renilla* luciferase. The normalized firefly/*Renilla* activity ratio was then used to determine the induction of firefly activity over that of the background controls (Corporation, 2015).

The comprehensive data for this section, which included all the necessary negative and positive controls, can be found in Appendix F.

6.2.3 Results and Discussion

6.2.3.1 uS4 (S9) Interacts Directly to NPM1 *in vivo*

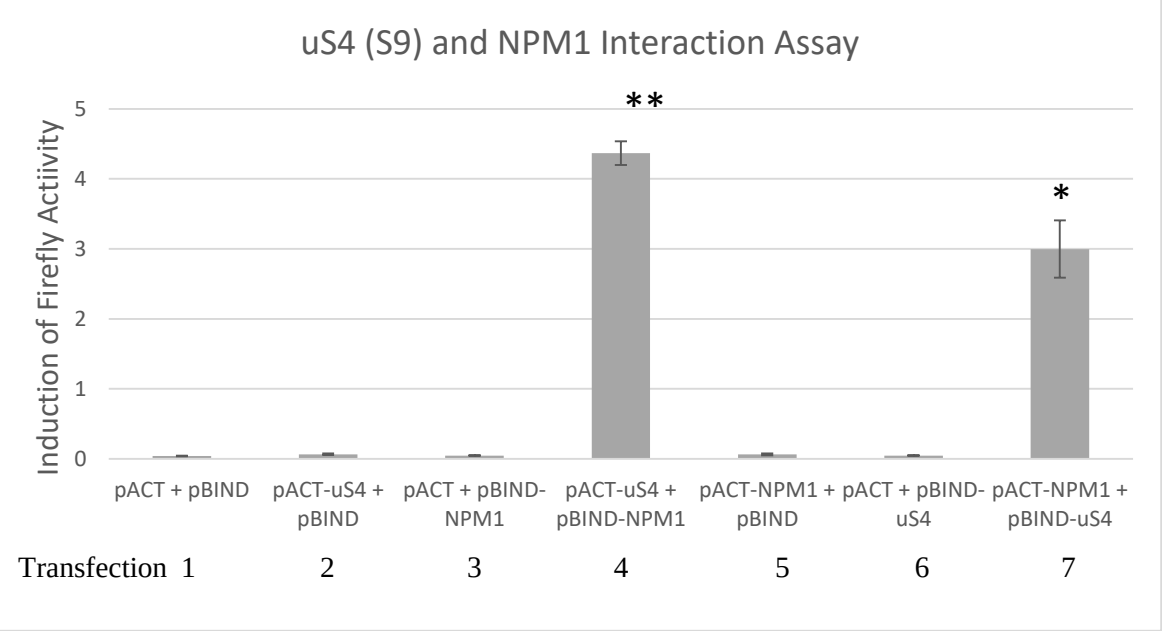

Figure 6.5: Luciferase assay validation of ribosomal protein uS4 (S9) and NPM1 binding in TW04 cells. RLU (relative luminescence unit) of firefly luciferase activity was normalized against that of *Renilla* luciferase for control and two-way experimental sets. Data are presented as mean±SD and statistical analysis was conducted compared to negative controls. Corresponding *p*-values are designated with asterisk (*). *: $p< 0.05$, **: $p< 0.01$. Error bars represent the standard deviation (SD) of the average normalized RFU.

The basal level of firefly luciferase expression of the pG5*luc* vector when co-transfected with pACT and pBIND vectors was ascertained by that of Transfection 1 (Figure 6.5). Transfection 2 aimed to test for the interaction between VP16-uS4 fusion protein and the GAL4 DNA-binding domain as well as the GAL4 binding activity of uS4. Likewise, transfection 3 tested the presence of interaction between GAL4-NPM1 fusion protein and the VP16 activation domain as well as the transcriptional activation activity of NPM1. Transfection 4 examined the potential interaction of VP16-uS4 fusion protein and the GAL4-NPM1 fusion protein, whereby an elevated firefly luciferase activity in contrast to that of the

negative control (transfection 1) indicated successful protein-protein interaction. In order to eliminate the possibility of vector 'directionality' or dependency, transfection 5 to 7 were included. Transfection 5 served similar purpose as transfection 2, while transfection 6 as to transfection 3. Lastly, transfection 7 tested the interaction of VP16-NPM1 fusion protein and GAL4-uS4 fusion protein. In our case, the comparable normalized RFU levels of transfection 1, 2, 3, 5 and 6 showed that there were no undesirable interactions between empty vectors pACT and pBIND, as well as between a fusion protein and its corresponding empty vector.

The co-transfection of pACT-uS4 and pBIND-NPM1 resulted in a 82.841-times higher induction (transfection 4; *p*-value= 0.009) in firefly luciferase activity while its reversed adaptation of pACT-NPM1 and pBIND-uS4 showed 56.812-fold induction (transfection 7; *p*-value= 0.031), revealing a preferential vector directionality to the pACT-uS4 and pBIND-NPM1 combination instead of the reciprocal construct (Appendix F). The elevated firefly transcriptional activity observed demonstrated the *in vivo* interaction of uS4 (S9) and NPM1 in TW04 NPC cells.

Our findings in this section further expounded on our prior *in vitro* findings on the association of ribosomal protein uS4 (S9) and NPM1 in three NPC cell lines. We hereby report on the direct interaction of uS4 (S9) and NPM1 in NPC cells, in parallel with the findings by Lindstrom in osteosarcoma cells (Lindström & Zhang, 2008).

6.2.3.2 No Direct Interaction was Identified Between eS31 (S27a) and NPM1 *in vivo*

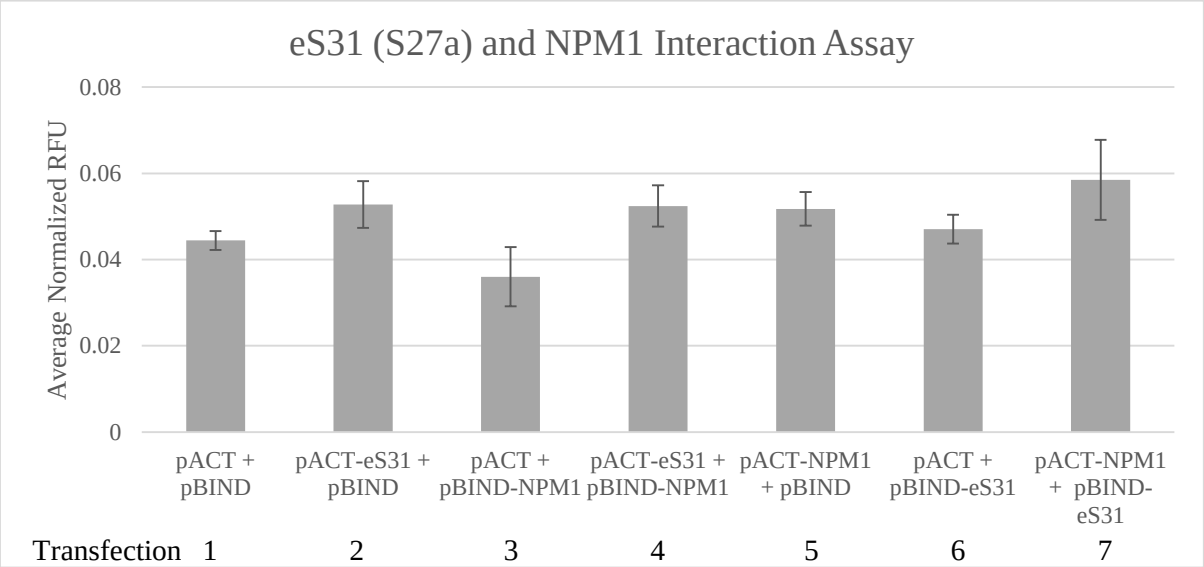

Figure 6.6: Luciferase assay validation of ribosomal protein eS31 (S27a) and NPM1 binding in TW04 cells. Data are presented as mean±SD and statistical analysis was conducted compared to negative controls. Error bars represent the standard deviation (SD) of the average normalized RFU.

The co-transfection of pACT-eS31 and pBIND-NPM1 (transfection 4), as well as its inversed set of pACT-NPM1 and pBIND-eS31 (transfection 7), showed comparable levels of firefly luciferase activity compared to the negative controls (transfection 1, 2, 3, 5 and 6). Transfection 4 and 7 recorded insignificant fold-differences of 1.129 and 1.260 increase, respectively (Appendix F). This confirmed the absence of *in vivo* interaction between ribosomal protein eS31 and NPM1 in TW04 NPC cells as no significant elevation of firefly transcriptional activity was recorded (Figure 6.6).

As previously discussed in Chapter 4.3.3.3, the association of eS31 (S27a) to NPM1 was inferred to be not a direct interaction but instead, via an intermediary protein. Our findings corroborated the biological consequence of eS31 (S27a) in the NPM1-associated pathway does not happen with its direct binding to NPM1 but through co-acting factors.

6.2.3.3 uL14 (L23) Associates Directly to NPM1 *in vivo*

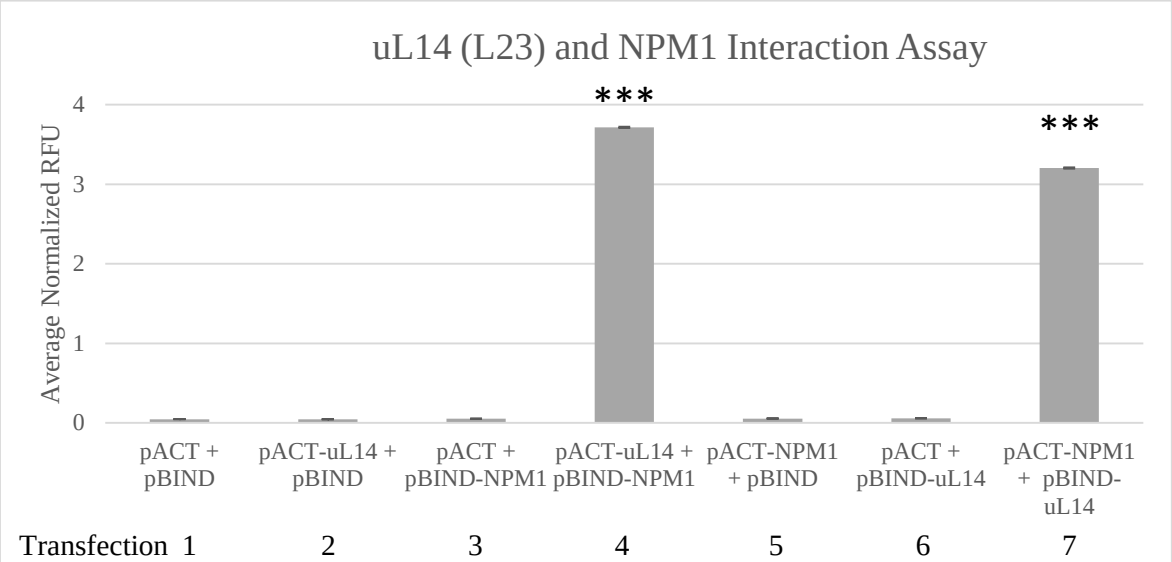

Figure 6.7: Luciferase assay validation of ribosomal protein uL14 (L23) and NPM1 binding in TW04 cells. Data are presented as mean±SD and statistical analysis was conducted compared to negative controls. Corresponding *p*-values are designated with asterisk (*). ***: $p < 0.001$. Error bars represent the standard deviation (SD) of the average normalized RFU.

The result obtained from previous bait protein Co-IP pull-down assay warranted further investigation on the interaction of uL14 (L23) and NPM1 proteins. Figure 6.7 above revealed that the background luciferase activity of control experiments (transfection 1, 2, 3, 5, and 6) was less than when complete recombinant vectors expressing full-length uL14 (L23) and NPM1 were used. The co-transfection of pACT-uL14 and pBIND-NPM1 resulted in a significant 73.758-fold induction in firefly luciferase activity (transfection 4; *p*-value= 1.024E-04) while that of pACT-NPM1 and pBIND-uL14 showed a 63.596-fold increase (transfection 7; *p*-value= 1.805E-04) (Appendix F). The significant elevation in firefly transcriptional activity observed demonstrated the *in vivo* interaction of uL14 (L23) and NPM1 in TW04 NPC cells.

The association of ribosomal protein uL14 (L23) and NPM1 was initially predicted by

Wanzel and his group (2008) during their investigation on the list of regulators of Miz-1, a Myc-associated zinc-finger protein, in various carcinoma cell lines (Wanzel et al., 2008). They reported on the co-operation of uL14 (L23) and NPM1 in negatively modulating Miz-1-dependent cell growth and proliferation pathway by observing that induction of uL14 (L23) in HeLa cells prevented the localization of NPM1 from the nucleolus to the nucleoplasm, which in turned, inhibited the transactivation of Miz-1 in the nucleus. However, the authors asserted that further work was needed to ascertain the nature of the interaction between uL14 (L23) and NPM1 on whether the two proteins bind directly to each other or via mediator proteins in a complex in achieving their concerted effect on Miz-1. Herein, we are able to address that gap and complete the story on the interaction of uL14 (L23) and NPM1. We have shown that wild-type ribosomal protein uL14 (L23) bind directly to NPM1 in NPC cells *in vivo*.

CHAPTER 7

MODE OF INTERACTION BETWEEN RIBOSOMAL PROTEINS AND NPM1 AND HYPOTHETICAL PATHWAY

7.1 Target Site Determination of Ribosomal Protein-NPM1 Interactions

7.1.1 Background

Prior to this, we have successfully demonstrated the strong and stable *in vitro* and *in vivo* interactions of NPM1 with ribosomal protein uS4 (S9) and ribosomal protein uL14 (L23) in normal NP69 and NPC cells. With a pull-down co-IP assay using NP69, TW04 and C666-1 cells, we have detected the presence of NPM1 in uS4 (S9) pulled-down lysate and the reverse was also true. Similarly, NPM1 was also observed in uL14 (L23) pulled-down lysate and was validated by the reciprocal pull down. Subsequently, the *in vivo* interactions were further substantiated with a mammalian two-hybrid system in TW04 cells.

Following these findings, we proceeded to ascertain the interacting domains of the uS4 (S9)-NPM1 and uL14 (L23)- NPM1 interactions *in vivo*. By doing so, we will be able to identify and understand the specific domain-domain interaction between the two ribosomal proteins and NPM1 in mammalian cells and to predict the impact of endogenous and exogenous factors on these interactions. The *in vivo* approach using the reliable Mammalian Two-Hybrid System eliminated possible indirect and unspecific interactions due to domain promiscuity, potentially detected by any *in vitro* pull-down assays.

7.1.2 Methodology Overview

As previously determined in the *in vivo* interaction assay, a stronger vector affiliation for both uS4 (S9)-NPM1 and uL14 (L23)-NPM1 interactions were observed when ribosomal proteins were cloned in-frame to pACT expression vector while NPM1 was fused in-frame to pBIND expression vector (Figure 6.5 and Figure 6.6). To map the binding sites of these interactions, truncated fragments of uS4 (S9), uL14 (L23) and NPM1 were amplified and cloned into the respective expression vectors. The 5' junction between fragment and vector was sequence verified by an external service provider. The constructs were then transfected into NPC TW04 cells and the dual-signal activities of firefly and *Renilla* luciferase were detected 48 hours post-transfection. Data values are included in Appendix G.

7.1.3 Results and Discussion

7.1.3.1 uS4 (S9) Binds to the N- and C-Terminal Domains of NPM1 via its Central Motif

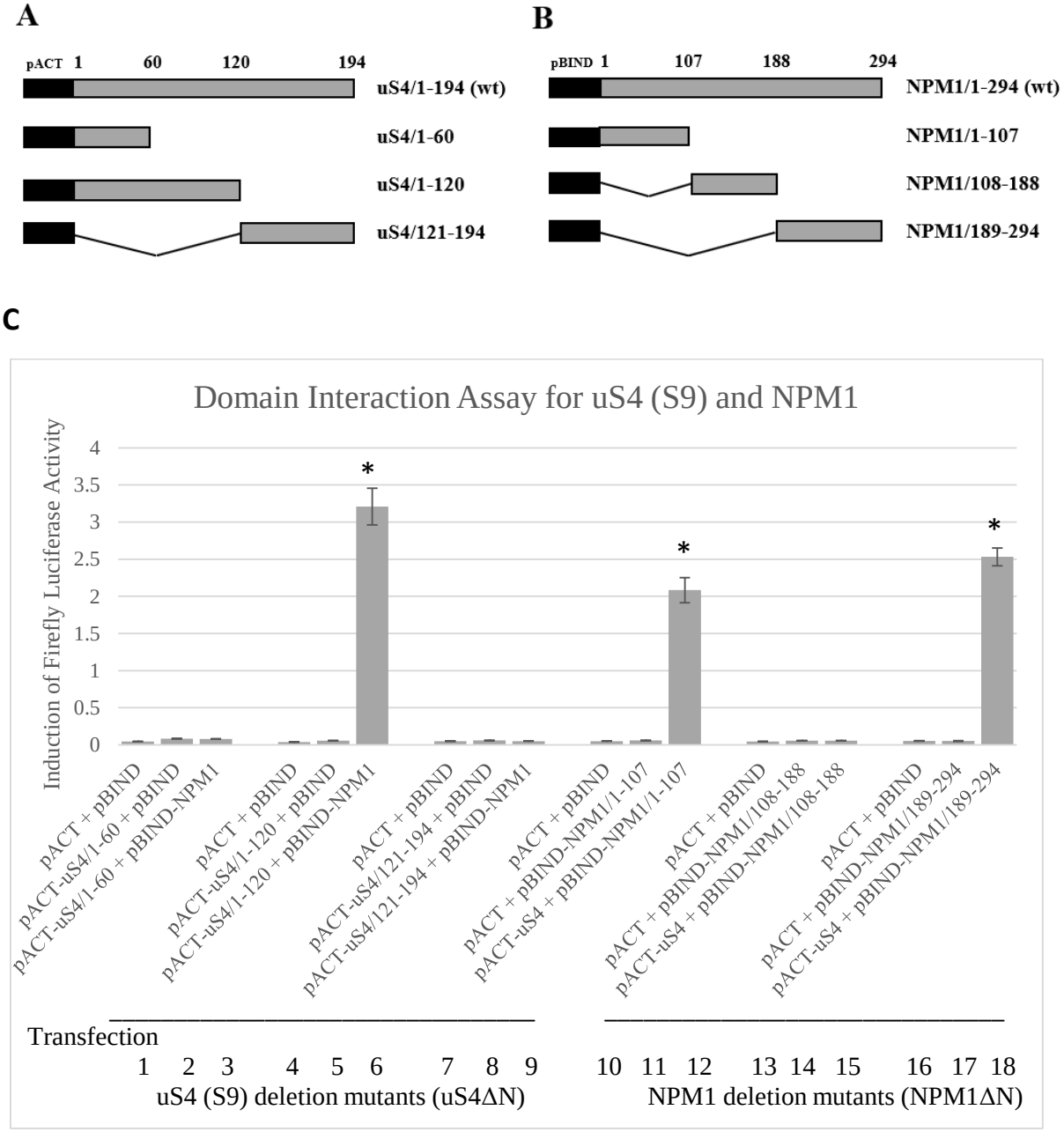

Figure 7.1: The central domain of uS4 (S9) interacted with the N- and C-terminus of NPM1 in TW04 cells. Schematic representation of full-length and truncated mutants of (A) uS4 (S9) and (B) NPM1. Black rectangles represent pACT and pBIND vectors, respectively. Grey fragments indicate fusion protein or its fragments. (C) Interaction between uS4 (S9) and NPM1 involved the central domain of uS4 (S9) as well as the N- and C-terminus of NPM1. Data are presented as mean±SD and statistical analysis was conducted compared to negative controls. Corresponding *p*-values are designated with asterisk (*). *: $p < 0.05$. Error bars represent the standard deviation (SD) of the average normalized RFU.

Referring to Figure 7.1, transfections 1 to 9 were representatives of uS4 (S9) deletion mutants where each of the three experimental sets involved the deletion of the N-terminal, central and C-terminal domains, respectively. No significant elevation of firefly luciferase activity was observed with the co-transfection of pACT-uS4 $(S9)^{1-60}$ and pACT-uS4 $(S9)^{121-194}$ with NPM1, and hence, no *in vivo* interactions were detected between these mutants and full-length NPM1 (transfection 3 and 9). On the other hand, when transiently expressed, pACT-uS4 $(S9)^{1-120}$ and wild-type NPM1 displayed the strongest interaction when compared to other mutants, recording a significant 68.773-fold increase in relative luciferase activity (transfection 6; *p*-value=0.017). In other words, when wild-type NPM1 were co-transfected with either the N- or the C-terminal of uS4 (S9), there was no significant activation of luciferase activity, thereby implying the lack of association of NPM1 with both terminal domains of uS4 (S9). As NPM1 was not shown to be able to interact with the stand-alone N-terminal domain of uS4 (S9), our findings reveal that the central region of uS4 (S9), specifically the 61-120 fragment, is essential for its interaction with NPM1 protein.

The reciprocal assay was conducted to determine the target domain(s) of uS4 (S9) on NPM1. Various functional domains have been previously identified within the length of NPM1, which includes an N-terminal oligomerization domain responsible for its chaperone activity, a C-terminal DNA-binding domain and a central acidic domain for histone binding (Box et al., 2016). To characterize the binding sites of uS4 (S9) on NPM1, we designed a series of NPM1 deletion mutants based on the functional domains of NPM1. *In vivo* translated NPM1 deletion mutants revealed that fragments 1-117 and 189-294 were able to bind to ribosomal protein uS4 (S9) but not the 118-188 fragment. The interactions of pBIND-$NPM1^{1-117}$ and pBIND-$NPM1^{189-294}$ to ribosomal protein uS4 (S9) recorded significant increment in the

relative firefly luciferase signal of 38.601-fold and 48.794-fold, respectively (transfection 12; *p*-value=0.019 and transfection 18; *p*-value=0.011), revealing two distinct binding sites to ribosomal protein uS4 (S9): the N-terminal with an oligomerization domain and the C-terminal, which houses a DNA-binding motif (Box et al., 2016).

A previous study done by Lindstrom and her group reported on the interaction of ribosomal protein uS4 (S9) and NPM1 in osteosarcoma cells and a subsequent report by the same group revealed that the N-domain fragment (aa 1-70) interacted with NPM1 *in vitro* and induced nuclear localization (Lindström & Zhang, 2008; Lindström, 2012). On the same note, our data demonstrated that (1) the 1-60 fragment of uS4 (S9) was unable to form any detectable interaction with NPM1 and (2) the necessary NPM1 binding site was narrowed down to be between 61-120aa on uS4 (S9). Thus, it can be deduced that the region between codon 61-69 of ribosomal protein uS4 (S9) contained the essential target site for its interaction with NPM1 protein. Upon closer inspection, the 61-69 region of uS4 (S9) is comprised of lysine acetylation site at codon 66. Traditionally believed to be exclusively limited to histone proteins responsible for regulating gene transcription, lysine acetylation has been reported in the regulation of molecular chaperones, transcription and cytoskeletal factors as well as effector proteins (Glozak, Sengupta, Zhang, & Seto, 2005). Coincidentally, NPM1 is a member of the acidic histone chaperones family implicated in ribosome biogenesis for its role as a molecular chaperone in shuttling of ribosomal proteins from the cytoplasm to the nucleolus for pre-ribosomal assembly (Lindström, 2011). As such, we have shown that the target site to NPM1 (61-69aa) on ribosomal protein uS4 (S9) coincided with lysine acetylation site (66aa), and this suggests an interesting possibility of the role of uS4 (S9) post-translational modification on its interaction with NPM1, thereby governing the cellular

localization of uS4 (S9).

In addition to that, we have also mapped the binding domain of uS4 (S9) on the N- and C-terminal domains of NPM1 (Figure 7.1). Fragment 1-107 (N-terminal) and 189-294 (C-terminal) of NPM1 were able to interact with wild-type uS4 (S9), demonstrating the presence of a dual-site pattern on NPM1. The N-terminal of NPM1 is also known as its oligomerization domain, where an on-site disruption has been shown to result in nucleoplasmic localization and induction of cell cycle arrest and apoptosis whereas the C-terminal consists of a DNA-binding domain and mutations within this region caused the irregular translocation to the cytoplasm (Hingorani et al., 2000; Falini et al., 2009). In summary, both domains are essential in regulating the localization of NPM1, and thus dictating its molecular function. The spatial and temporal consequences of a dual-binding site to uS4 (S9) on the N- and C-terminal of NPM1 remains to be explored.

7.1.3.2 uL14 (L23) Associates with the N-Terminal Domain of NPM1 via its Central Domain

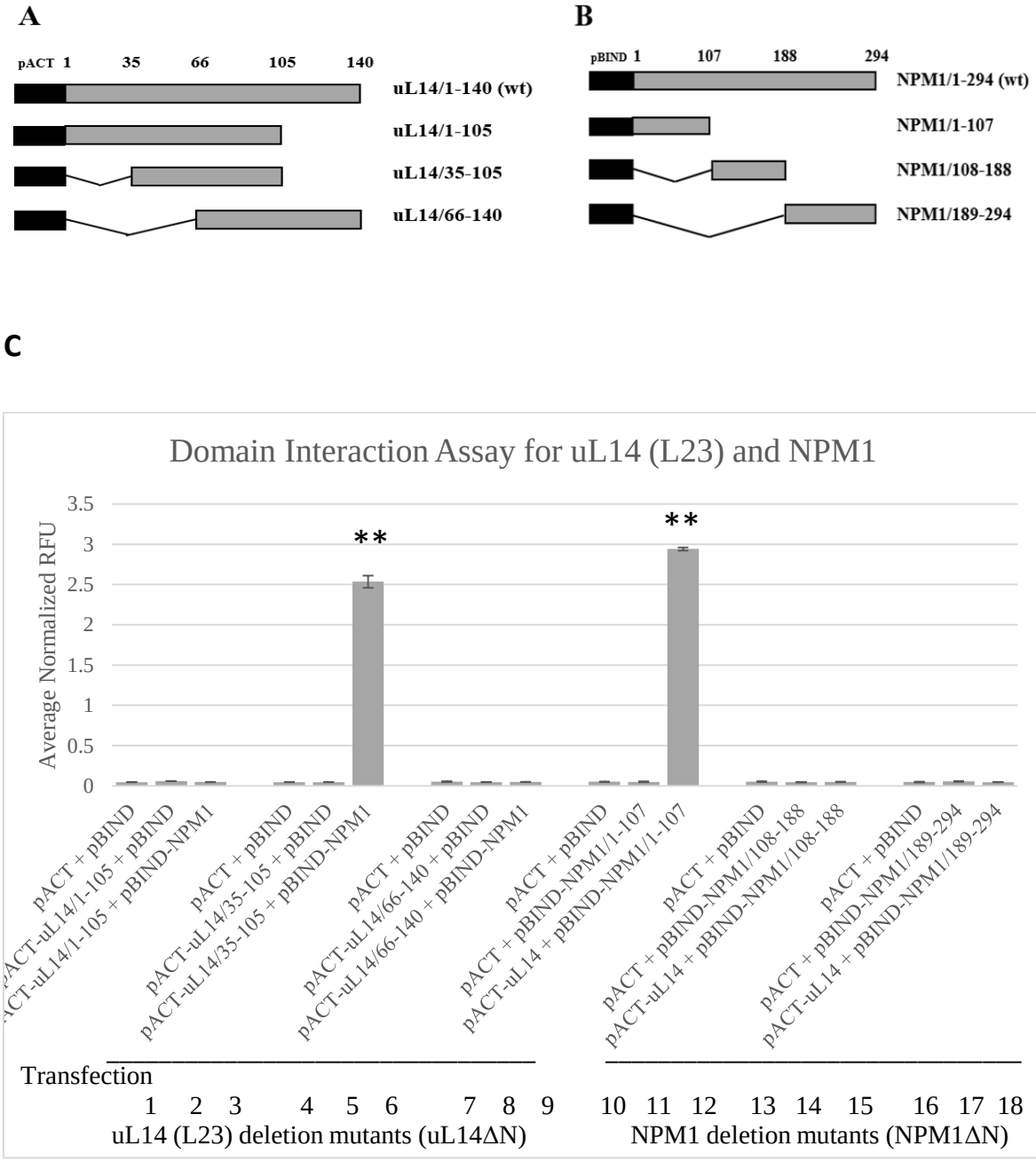

Figure 7.2: The central domain of uL14 (L23) associated with the N-terminal of NPM1 protein in TW04 cells. Schematic representation of full-length and truncated mutants of (A) uL14 (L23) and (B) NPM1. Black rectangles represent pACT and pBIND vectors, respectively. Grey fragments indicant fusion protein or its fragments. (C) Interaction between uL14 (L23) and NPM1 involved the central domain of uL14 (L23) and the N-terminus of NPM1. Data are presented as mean±SD and statistical analysis was conducted compared to negative controls. Corresponding *p*-values are designated with asterisk (*). **: $p < 0.01$. Error bars represent the standard deviation (SD) of the average normalized RFU.

Co-transfection of three uL14 (L23) deletion mutants with wild-type NPM1 revealed that only the 35-105 fragment interacted with NPM1 protein, recording a significant induction of relative firefly luminescence signal of 55.743-fold (transfection 6; *p*-value=0.007). No significant observation was obtained for the interactions between uS4 (S9) and the N- and C-terminals of NPM1. From Figure 7.2, it can be deduced that the essential NPM1 binding site is located between codon 35-66 that is within the central domain of ribosomal protein uL14 (L23).

On the other hand, a statistically significant induction of 58.880-fold was observed when wild-type uL14 (L23) was co-transfected with the pBIND-NPM1$^{1\text{-}117}$ deletion mutant (transfection 12; *p*-value 0.001), but not when the 118-188 and 189-294 NPM1 fragments were *in vivo* translated with uL14 (L23). This showed that the N-terminal of NPM1 is necessary for its interaction with ribosomal protein uL14 (L23).

The central domain of ribosomal protein uL14 (L23) was found to be fully capable of binding to NPM1 at its N-terminal domain. Not only do the central region of uL14 (L23) interacts with NPM1, it has also been reported to preferentially bind to the central acidic domain of MDM2 *in vitro* by reciprocal pull-down assay (Dai et al., 2004). Additionally, the report by Dai also revealed the absence of an additional binding site on the N- and C-terminals of uL14 (L23). Except for this paper, unfortunately, there have been no target site determination study on uL14 (L23) with its known interacting proteins. Even so, we can deduce that the central motif of uL14 (L23) exclusively manages its inter-protein associations and thus, carries the role in modulating its molecular functionality.

7.2 Synergistic Effect of the Interaction between Ribosomal Proteins and NPM1 on MDM2

7.2.1 Background

Previously, we have been successful in determining the binding domains of each interacting partner within the uS4 (S9)-NPM1 interaction as well as the uL14 (L23)-NPM1 interaction using an *in vivo* luciferase assay.

In this part of the thesis, we attempted to delineate the possible synergistic effect of these two afore-mentioned interactions on the activity of MDM2, an established downstream binding partner of NPM1 (described in Literature Review Chapter 2.2.2.1.1). Briefly, mouse double minute 2 homolog (MDM2), an E3 ubiquitin ligase, is a well-known negative regulator of p53 and has been implicated in pathways involved in cell cycle progression and apoptosis. From the review of existing studies conducted in different endemic countries, p53 levels were over-expressed in nasopharyngeal carcinoma biopsy samples in comparison to their corresponding adjacent non-tumoral tissues (Kurniawan & Leong, 2000; Agaoglu et al., 2004; Taweevisit, 2007; Hoe et al., 2009). In addition to that, though missense mutation in the *TP53* gene was detected in approximately half of all human tumours, almost all reports on p53 sequence analyses on NPC revealed the comparatively lack of genetic alterations and mutant p53 protein in NPC tissues and cell lines (Hoe et al., 2009; Hwang et al., 2009; Lin et al., 2014). Having said so, increasing evidence have also demonstrated the possibility of tumour-associated p53 to lose its tumour-suppressive function and gain new roles to induce oncogenesis and malignant transformation (reviewed by Yue et al. (2017)). Therefore, we surmised that the established NPM1-MDM2 interaction would be an interesting starting point in the effort to functionally position ribosomal proteins uS4 (S9) and uL14 (L23)

within the robust NPM1-MDM2-p53 network.

7.2.2 Methodology Overview

By maintaining the use of the mammalian two-hybrid system from the previous assays, we co-transfected TW04 cells, in increasing molar ratio, an additional expression plasmid cloned in-frame with either ribosomal protein uS4 (S9) and uL14 (L23), together with recombinant pACT and pBIND expression vectors. Similar protocol to the interaction assays was used, with added immunoblotting assay subsequent to luciferase signal determination. Data values are included in Appendix H.

7.2.3 Results and Discussion

7.2.3.1 uS4 (S9) is a Negative Regulator of the NPM1-MDM2 Interaction

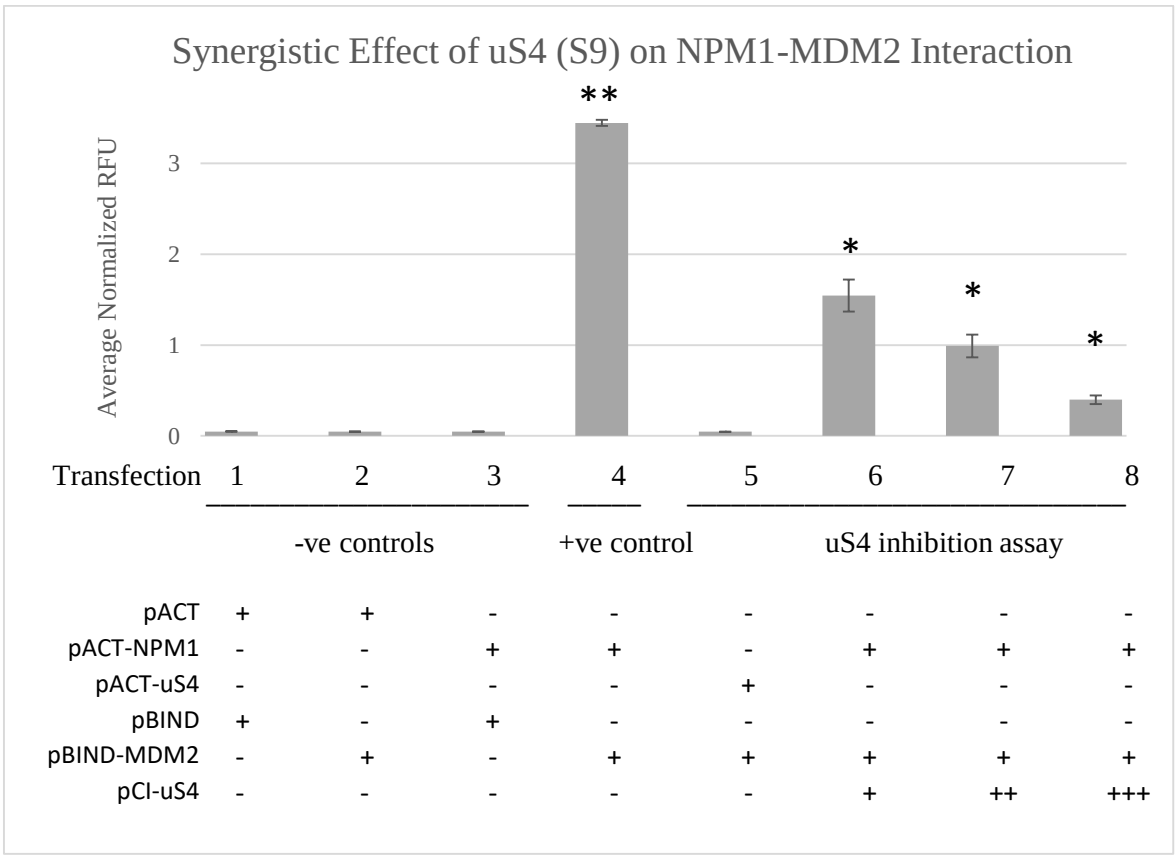

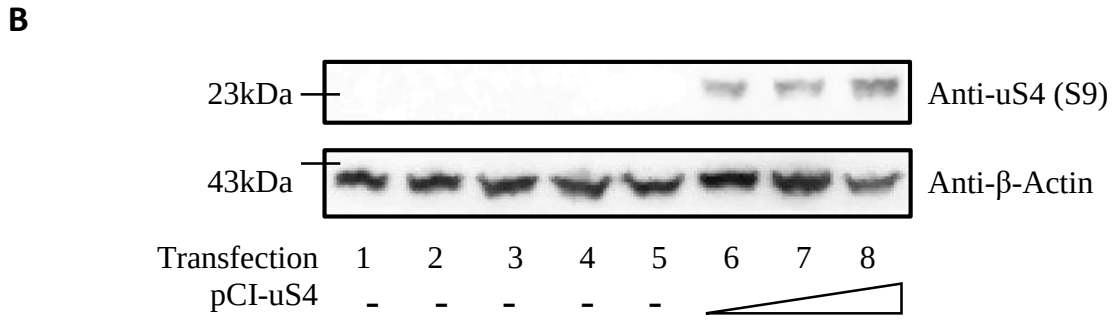

Figure 7.3: The over-expression of uS4 (S9) disrupts NPM1-MDM2 interaction. (A) uS4 (S9) is not a direct binding partner of MDM2 (transfection 5). As the concentration of transfected pCI-uS4 increases, the interaction between NPM1 and MDM2 diminishes (transfection 6 to 8). Data are presented as mean±SD and statistical analysis was conducted compared to negative controls. Corresponding *p*-values are designated with asterisk (*). *: $p < 0.05$; **: $p < 0.01$. Error bars represent the standard deviation (SD) of the average normalized RFU. (B) Immunoblotting of uS4 (S9) with cell lysate extracted from

transformed TW04 cells subsequent to luciferase assay.

We have previously validated that endogenous ribosomal protein uS4 (S9) and NPM1 existed as a complex in NPC cells and subsequently confirmed the direct binding of the central domain of uS4 (S9) to the N- and C-terminals of NPM1 *in vivo*. In this section, we attempted to investigate the functional consequence of the interaction between ribosomal protein uS4 (S9) and NPM1 by analysing its downstream effect on a well-established secondary interaction between NPM1 and MDM2 protein.

Referring to Figure 7.3, transfection 1 to 3 represented the negative controls to ensure that there were no cross-reactivity between empty vectors that would otherwise render the experimental design unspecific. Transfection 4 demonstrated the well-established interaction between NPM1 and MDM2, while that of transfection 5 explored the possibility of an interaction between uS4 (S9) and MDM2. Transfection 6 to 8 included the co-transfection of an additional expression vector fused to uS4 (S9) in an increasing pACT-NPM1: pBIND-MDM2: pCI-US4 ratio from 1:1:1 to 1:1:3 (Figure 7.3A and 7.3B).

According to our findings, although transfection 4 was incorporated as a positive control, we would also like to point out that this is the first report on the interaction of NPM1 and MDM2 in nasopharyngeal carcinoma cells. Such interaction was demonstrated previously reported only in renal cell carcinoma and osteosarcoma (Fukawa et al., 2012; Kurki et al., 2004; Ren et al., 2016).

When uS4 (S9) was *in vivo* translated with MDM2, no enhanced luciferase activity was detected, signifying that ribosomal protein uS4 (S9) did not directly interact with MDM2.

Interestingly, a trend of decreasing firefly luciferase activation was observed as increasing molar ratio of pCI-uS4 was co-transfected (transfection 6 to 8). When only NPM1 and MDM2 proteins were co-transfected, a 73.238-fold activation of firefly luciferase transcription activity (transfection 4; *p*-value=0.002). However, the additional co-transfection of pCI-uS4 resulted in a 55% drop in luciferase signal with an only 32.831-fold (transfection 6; *p*-value=0.026). Further addition of pCI-uS4 resulted in a more drastic drop of 71% in luciferase activity and at its highest molar ratio, a drop of 88% was observed in transfection 7 and 8, respectively. Molecularly, without the interference of ribosomal protein uS4 (S9) in transfection 4, the close interaction of pACT-NPM1 and pBIND-MDM2 brought the VP16 transcription activation domain close enough to the GAL4 DNA-binding domain on pBIND vector to sufficiently induce the basal transcriptional machinery of the firefly luciferase, resulting in a spike in luciferase signal. On the other hand, transfection 6 to 8 demonstrated that the presence of exogenous and endogenous ribosomal protein uS4 (S9) disrupted the NPM1-MDM2 interaction, thereby leading to a sequential reduction in luciferase activity. As such, by disrupting the interaction between NPM1 and MDM2, thereby sequestering NPM1 from MDM2, ribosomal protein uS4 (S9) may positively regulate MDM2, allowing for its succeeding binding to p53 and other known target proteins.

7.2.3.2 uL14 (L23) is a Direct Partner and a Regulator of MDM2

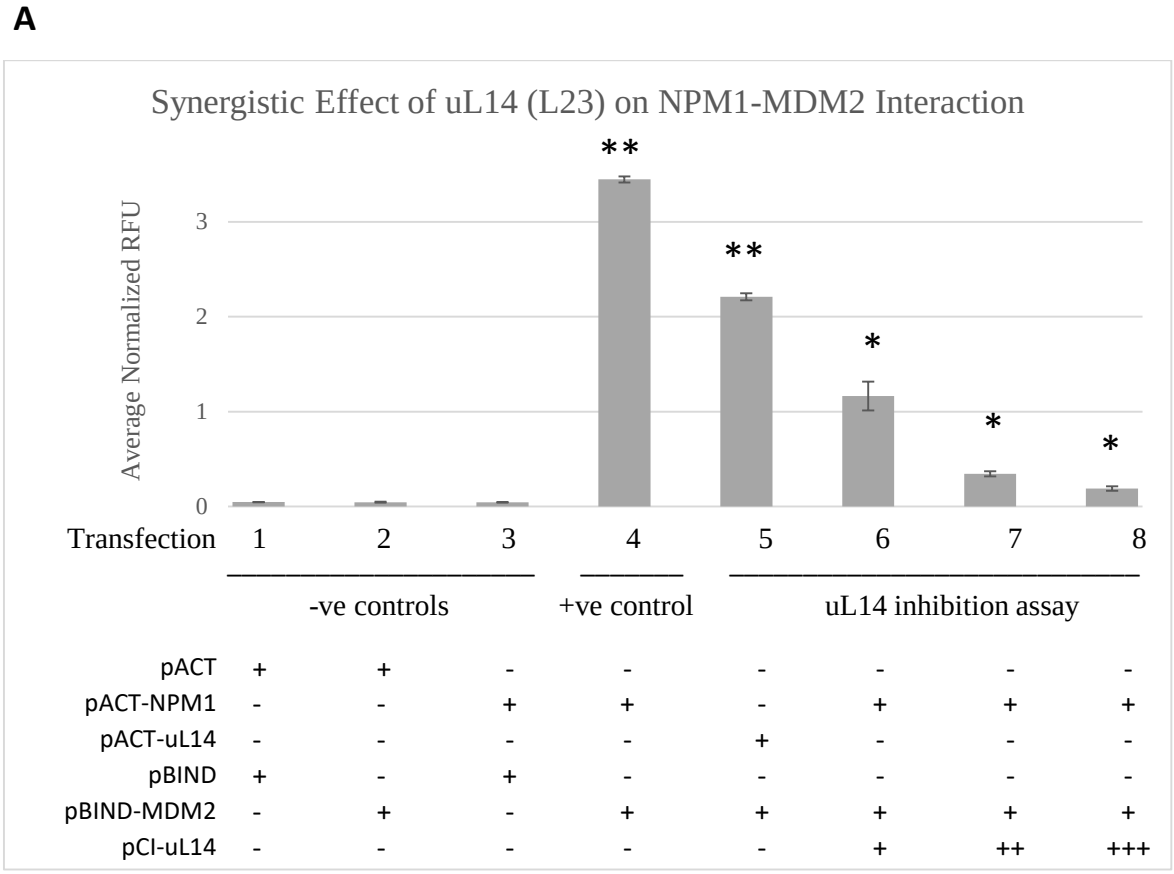

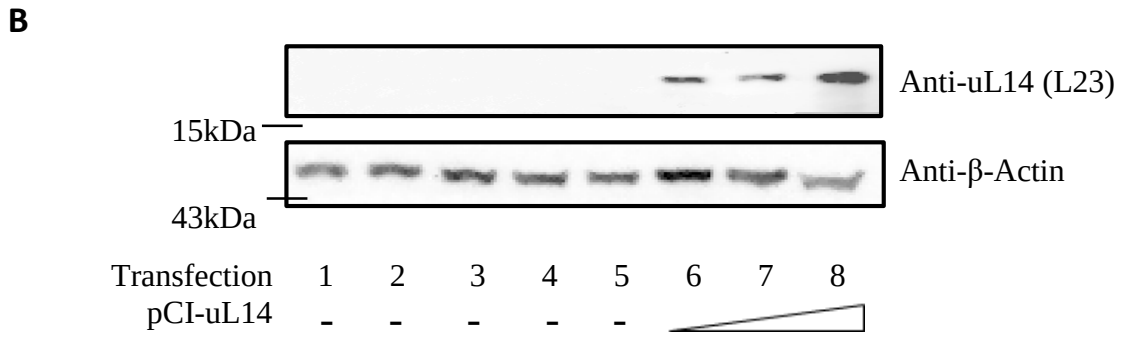

Figure 7.4: The over-expression of uL14 (L23) regulates both NPM1 and MDM2. (A) Ribosomal protein uL14 (L23) is a direct interacting protein of MDM2 (transfection 5). As the concentration of transfected pCI-uL14 increases, the interaction between NPM1 and MDM2 diminishes (transfection 6 to 8). Data are presented as mean±SD and statistical analysis was conducted compared to negative controls. Corresponding *p*-values are designated with asterisk (*). *: $p< 0.05$; **: $p< 0.01$. Error bars represent the standard deviation (SD) of the average normalized RFU. (B) Immunoblotting of uL14 (L23) with TW04 cell lysate subsequent to luciferase assay.

In this section, besides the interaction between NPM1 and MDM2 as verified in transfection 4, we also report on a direct binding of ribosomal protein uL14 (L23) to MDM2, which induced an increase of 46.943-fold (transfection 5; *p*-value=0.004) in firefly luciferase signal (Figure 7.4A). Considering our earlier data on the *in vivo* interaction of uL14 (L23) and NPM1 and taking our observation from this section of the project, this, in turn, disclosed a three-way interaction between uL14 (L23), NPM1 and MDM2.

As we increased the molar ratio of transfected pCI-uL14 vector, there was a steady reduction in luciferase activity across transfection 6 to 8 (Figure 7.4A and 7.4B). For instance, transfection 6 saw a 67% drop in firefly activity, transfection 7 a 90% drop and transfection 8 a drastic 95% drop. The overall reduction as an effect of pCI-uL14 co-transfection was more significant when compared to that of pCI-uS4 (S9) in the previous section (95% vs 88%). This could be attributed to the additional interaction of uL14 (L23), and not uS4 (S9) to MDM2, apart from NPM1. The enhanced level of uL14 (L23) was able to interact with both NPM1 and MDM2, thereby further disrupting the NPM1-MDM2 interaction, leading to a drastic drop in luciferase signal (Figure 7.4A). However, even though our data failed to reveal the preferential binding of uL14 (L23) to either NPM1 or MDM2, it highlighted the highly plastic and dependent uL14 (L23)-NPM1-MDM2 network on the abundance of ribosomal protein uL14 (L23). On the other hand, more work is required to examine the functional relationship between uL14 (L23) and MDM2 in NPC cells.

7.3 Co-localization of Ribosomal Proteins and NPM1 in NPC Cells

7.3.1 Background

Prior to this, our data demonstrated the preferential binding of ribosomal proteins uS4 (S9) and uL14 (L23) to NPM1, thereby sequestering NPM1 from regulating its downstream effector pathways.

In this section, we sought to ascertain the spatial organization of such interactions in order to further understand the functional consequences of the interaction of ribosomal proteins and NPM1 in NPC cells. We have, in previous chapters, shown that both ribosomal proteins uS4 (S9) were significantly elevated in NPC cells compared to normal nasopharyngeal epithelial cells and that both ribosomal proteins were capable of binding directly to NPM1 protein *in vitro* and *in vivo* in a synergistic manner. However, the *in vitro* data obtained were insufficient to determine the co-localization of the respective ribosomal protein and NPM1 as the tested samples were whole cell lysates, comprising of a mixture of cytoplasmic, nucleoplasmic and nucleoli fractions. Despite that, it was sufficient to demonstrate that endogenous ribosomal proteins uS4 (S9) and uL14 (L23) associated with NPM1, either directly or in a complex, to NPM1.

Therefore, herein we tested on the ribosomal protein-NPM1 interaction in separate cellular fractions with reciprocal pull-down assay to determine the co-localization of these proteins in NP69, TW04 and TW04-pCI-RP transfected cells.

7.3.2 Methodology Overview

To establish a transient ribosomal protein uS4 (S9)- and uL14 (L23)-expressing cell line, TW04 cells were transfected with pCI-uS4 (S9), pCI-uL14 (L23) or pCI vector. Transfected cells expressing uS4 (S9) or uL14 (L23) were selected in the presence of G-418 (400 µg/mL) and screened by immunoblotting with anti-uS4 (S9) or anti-uL14 antibody, respectively.

Confluent dishes of NP69, TW04 and TW04-treated cells were trypsinized and resuspended in a hypotonic buffer and homogenized by passing through a 27g needle fitted to a syringe. After the first round of centrifugation, the supernatant was retrieved and kept as the cytoplasmic fraction. Subsequent to that, the pellet was re-suspended in fractionation buffer A and layered with buffer B and centrifuged. After the second round of centrifugation, the supernatant was discarded, and the pellet was re-suspended in buffer B and homogenized with a 25g needle. The homogenized sample was then layered with buffer C and centrifuged. The resulting supernatant was kept as nucleoplasmic fraction and the pellet was washed and re-suspended in Buffer B as the nucleoli fraction. Similar protocol to the previous *in vitro* pull-down assay was then applied.

7.3.3 Results and Discussion

7.3.3.1 Up-regulation of Ribosomal Protein uS4 (S9) Sequestered NPM1 in the Nucleoplasm and Cytoplasm of NPC Cells

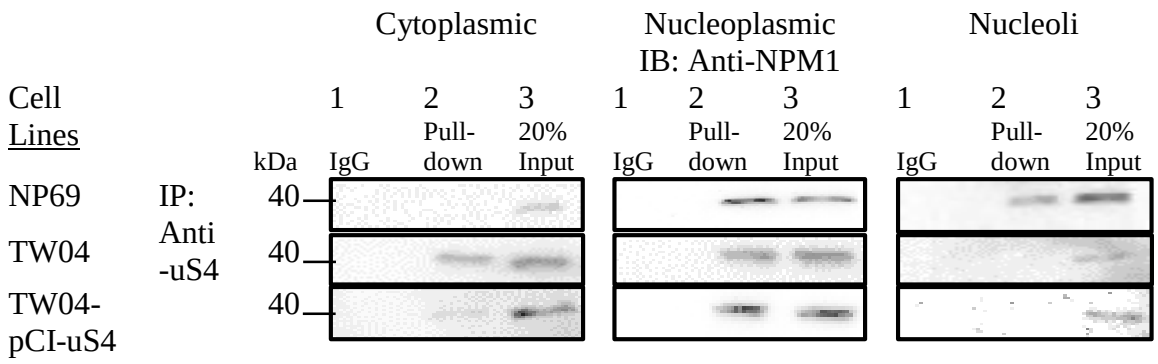

Figure 7.5: Enhanced expression of uS4 (S9) in TW04 cells sequestered NPM1 in the nucleoplasm and cytoplasm of NPC cells. Immunoprecipitation with anti-uS4 antibody was conducted in three sub-cellular fractions of three different cell lines and immunoblotted with anti-NPM1 antibody.

Figure 7.5 demonstrated that for the cytoplasmic fractions of NP69, TW04 and TW04-pCI-uS4, NPM1 protein was found to be relatively abundant in TW04 and TW04-pCI-uS4 transfected cells while being barely detected in that of NP69. This showed an interesting distinct pattern of NPM1 localization in normal nasopharyngeal epithelial cells compared to NPC cells, and that cancer progression could potentially be associated with NPM1 nucleolus export, leading to a reduction in NPM1 localized in the nucleoli. Subsequently, IP with anti-uS4 antibody succeeded in pulling-down NPM1 in the cytoplasmic fraction of TW04 and TW04-pCI-uS4 transfected cells but not in that of NP69 cells.

For the nucleoplasmic fraction, NPM1 was detected in all three cell lines. Upon IP with anti-uS4 (S9) antibody, a distinct NPM1 band was observed in TW04-pCI-uS4 transfected cells while comparatively lighter NPM1 bands were detected in that of TW04 and NP69 cells. On

the other hand, in the nucleoli fraction, the NPM1 band in NP69 was the most apparent. After IP, a distinct NPM1 band was observed NP69 but not in TW04 and TW04 transfected cells.

From our observation, we deduce that in the normal NP69 cells, ribosomal protein uS4 and NPM1 were mainly detected in the nucleoli fractions where both these proteins interacted in a stable manner. Interestingly, the reverse scenario was observed in TW04 and TW04 transfected cells, whereby NPM1 protein was detected in a relatively diminished amount in the nucleolus fractions but was found to be elevated in the cytoplasmic and nucleoplasmic fractions.

For the lack of NPM1 band after immunoprecipitation with anti-uS4 antibodies, it is noteworthy to point out that in this case, however, we are unable to conclude if ribosomal protein uS4 (S9) was indeed incapable of precipitating NPM1 due to the existing low levels of endogenous NPM1 detected in the respective fractions. Even if a stable interaction was formed between uS4 (S9) and NPM1, the amount of NPM1 eluted would be far too little to be detected with immunoblotting.

As such, the induced ectopic expression of ribosomal protein uS4 (S9) increased the amount of NPM1 detected in the nucleoplasmic and cytoplasmic lysates and furthermore, resulted in a higher level of NPM1 immunoprecipitated with anti-uS4 antibody, as evidenced by the lack of NPM1 protein bands in the nucleolus fraction. This revealed that the enhanced expression of uS4 (S9) was capable of co-localizing and sequestering NPM1 within the nucleoplasm and cytoplasm of TW04 cells.

7.3.3.2 Up-regulation of Ribosomal Protein uL14 (L23) Sequestered NPM1 in the Nucleoplasm of NPC Cells

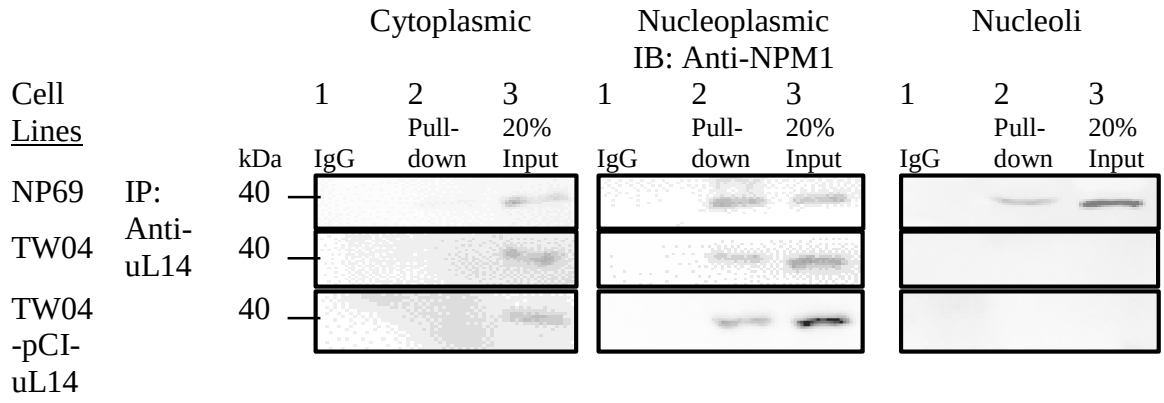

Figure 7.6: Enhanced expression of uL14 (L23) in TW04 cells sequestered NPM1 in the nucleoplasm of NPC cells. Immunoprecipitation with anti-uS4 antibody was conducted in three sub-cellular fractions of three different cell lines and immunoblotted with anti-NPM1 antibody.

Based on Figure 7.6, a similar spatial pattern as reported for uS4 (S9) in the previous section can be observed for the three fractions of NP69. It can be inferred that in NP69 cells, ribosomal protein uL14 (L23) and NPM1 are mainly co-localized within the nucleolus though a small percentage can be found in the cytoplasm and nucleoplasm.

In regard to TW04 and TW04 transfected cells, little to no NPM1 protein was detected in the nucleolus of both cells lines but was faintly detected in the cytoplasmic and predominantly in the nucleolus fraction. Immunoprecipitation with anti-uL14 antibody failed to pull down NPM1 from the cytoplasmic and nucleolus fractions, which could be due to the exceedingly low levels of endogenous NPM1 localized within these subcellular compartments in TW04 and TW04 transfected cells.

The transient transfection of uL14 (L23) in TW04 cells elevated the level of NPM1 pulled down after IP within the nucleoplasm fraction when compared to un-transfected TW04 and NP69 cells. This demonstrated that the ectopic induction of ribosomal protein uL14 (L23) expression sequestered NPM1 within the nucleoplasm of NPC cells.

By consolidating our data on the three-way interaction between uL14 (L23), NPM1 and MDM2 in addition to the localization of the uL14 (L23)-NPM1 complex in TW04 NPC cells, a similar scenario can be observed with the association of ARF tumour suppressor protein with NPM1 and MDM2 in acute T lymphoblastic leukaemia (T-ALL) cells. In the absence of ribosomal stress, NPM1 sequesters ARF protein within the nucleolus, where ARF is predominantly and stably localized (Bertwistle et al., 2004a). The release of ARF from NPM1 to the nucleoplasm, stimulated by ribosomal or oncogenic stress, results in either the proteasomal degradation of ARF or the direct interaction of ARF to MDM2, thereby inhibiting its ubiquitin ligase activity on p53, leading to the stabilization of p53 levels (Rodway, Llanos, Rowe, & Peters, 2004). In summary, the ARF protein is fully capable of interacting with NPM1 and MDM2 under highly specific stimulation. Analogously in our study, ribosomal protein uL14 (L23) interacted in a similar fashion as that of ARF protein in T-ALL. In normal nasopharyngeal epithelial cells, NPM1 sequestered uL14 (L23) within the nucleolus but in TW04 NPC cells, the uL14 (L23)-NPM1 complex was exported to the nucleoplasm, where uL14 (L23) interacted with and regulated both NPM1 and MDM2 in a synergistic manner.

7.4 Hypothetical Network of RP-NPM1-MDM2 Pathways in NP69 and NPC Cells

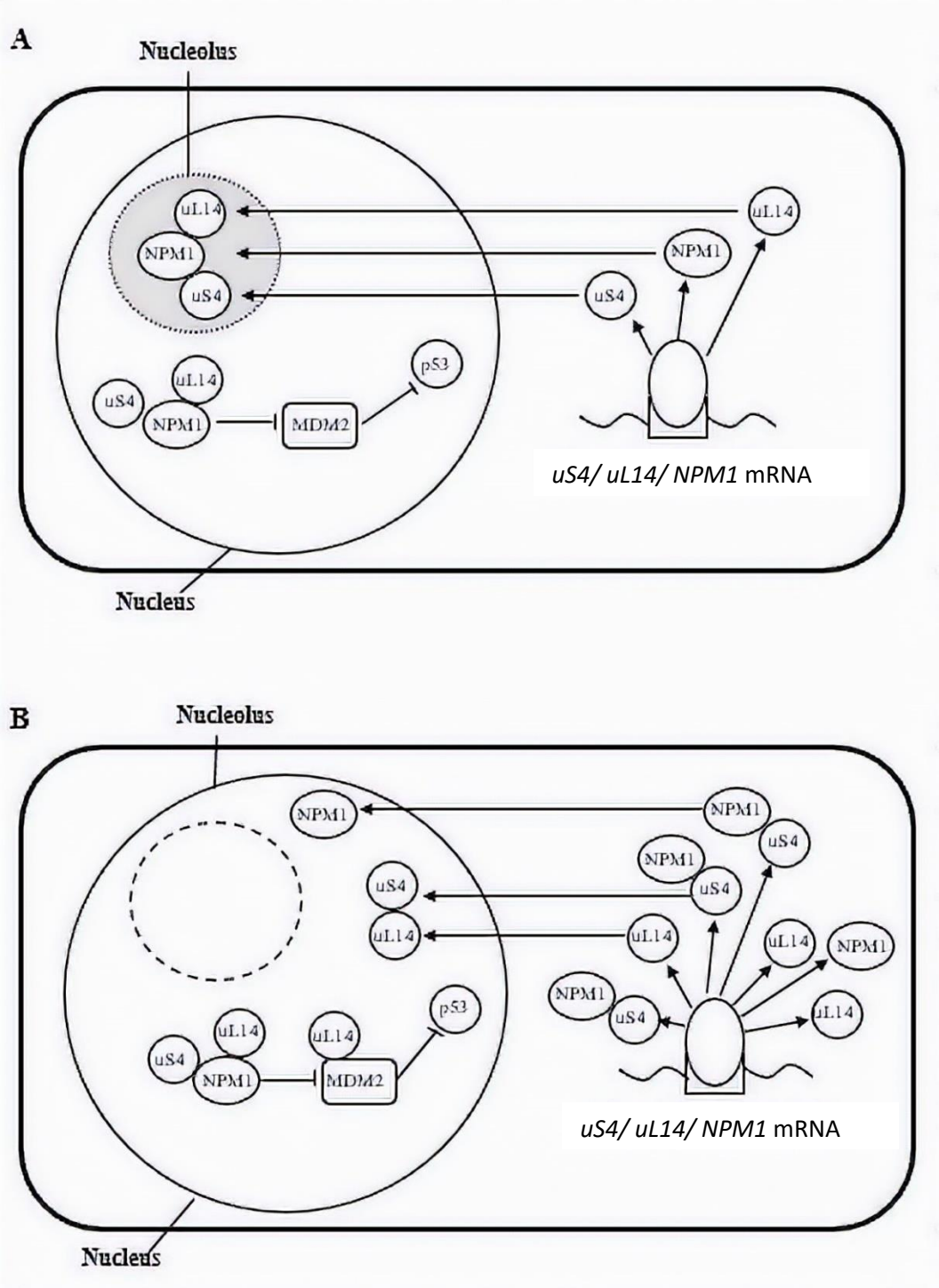

Figure 7.7: A visual representation of the potential RPs-NPM1-MDM2 network. Suggested interaction and localization of ribosomal proteins uS4 (S9) and NPM1 in A) normal nasopharyngeal epithelial cells and B) in nasopharyngeal carcinoma cells.

In normal nasopharyngeal epithelial cells, our model proposed that without nucleolar disruption, the ratio of the synthesis and nucleolar shuttling of RPs and the incorporation into pre-ribosomal subunits are well-balanced. Direct interaction between uS4 (S9) and uL14 (L23) to NPM1 sequestered a large portion of NPM1 in the nucleolus, thereby inhibiting its negative regulation on MDM2. At the same time, a fraction of uS4 (S9) and uL14 (L23) interact with NPM1 in the nucleoplasm. This diagram outlines the delicate control of NPM1 by RPs in normal nasopharyngeal epithelial cells (Figure 7.7A).

On the other hand, under ribosomal stress and nucleolar perturbation, the over-expression of uS4 (S9) and uL14 (L23) translocated NPM1 from the nucleolus and sequestered it in the nucleoplasm. The up-regulation of NPM1 in NPC cells may negatively regulate MDM2 and subsequently, p53 levels. In addition to that, the direct binding of uL14 (L23) may exert similar inhibitory effect on MDM2 by disrupting its E3 ubiquitin ligase activity and therefore, activating and stabilizing p53 levels and its downstream p53-mediated effector pathways in nasopharyngeal carcinoma cells (Figure 7.7B).

CHAPTER 8

GENERAL DISCUSSION

In the effort to reveal novel roles of ribosomal proteins in nasopharyngeal carcinoma, this study on a subset of ribosomal protein genes in NPC cells was conducted. Ribosomal proteins have garnered a renewed wave of interest over the past decade even though these proteins were discovered over 50 years ago, ever since the discovery of extra-ribosomal roles of RPs in vital cellular pathways such as cell growth and proliferation, cell cycle arrest, DNA replication, transcription and translation regulation and many others. Research findings thus far, though limited, bear far-reaching implications and advancements in various aspects within the medical and biotechnology arenas. However, unlike other established protein family groups, ribosomal proteins remain relatively overlooked. In addition to the extensive list of mammalian ribosomal proteins (approximately 80 small and large ribosomal proteins), research on RPs has always been on the slow lane. As such, we believe that RPs possess immense uncharted potential in cancer management due to their ubiquity and their multi-functional capabilities reported so far.

Briefly, the focus of the project began with a very broad catalogue of genes that were predicted to interact via bioinformatics analysis (Choi et al., 2005). By screening for differentially expressed transcripts and subsequently proteins, we were able to continually narrow down our focus to identifying RPs-associated interacting proteins in nasopharyngeal carcinoma cells via *in vitro* and *in vivo* assays (Figure 8.1).

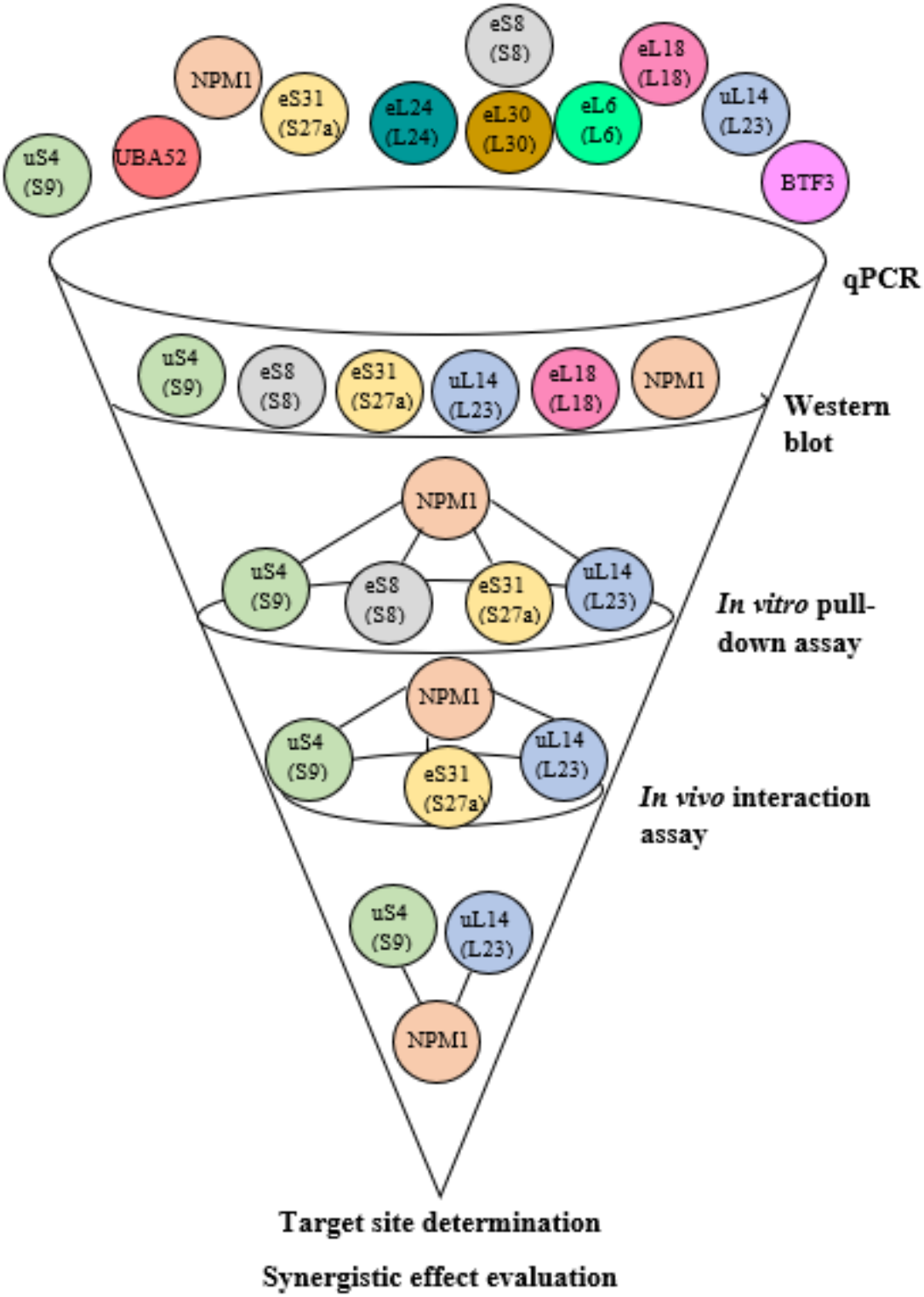

Figure 8.1: Schematic diagram of the overall research workflow.

From a list of eight RP genes and three putative co-acting factors that was generated via bioinformatics analysis and extensive literature search, three RP genes (*uS4 (S9), eS8 (S8)* and *uL14 (L23)*) were significantly down-regulated, while two RP genes (*eL18 (L18)* and *eL30 (L30)*) and a potential target partner, *NPM1*, were significantly up-regulated. The remaining five GOIs (*eL6 (L6), eL24 (L24), eL30 (L30), BTF3* and *UBA52)* were not differentially expressed in NPC cell lines, which may be the result of a substantial amount of variation in expression levels across the array of cells lines tested or the transcriptionally unperturbed circumstances of these genes. The findings from the RT-qPCR assessment and the roles of dysregulated RPs and the predicted protein partner were subsequently validated through western blot analysis. From the list of six differentially expressed genes, five displayed dysregulations at their protein levels, and were identified to be uS4 (S9), eS8 (S8), eS31 (S27a), uL14 (L23) and NPM1, thereby eliminating eL18 (L18) from the updated cluster of proteins of interest.

Sequence analysis of the GOIs revealed missense mutations in *ribosomal protein uS4 (S9)* and *uL14 (L23),* resulting in leucine to histidine and a serine to threonine replacement, respectively. Upon further investigation, the respective locations of the detected mutations did not coincide with any vital post-translational modification sites or any reported interacting domains. Additionally, without a shift in reading frame, the missense mutations detected raised no pertinent hazard to the overall protein structure and function. However, further bioinformatics and mutagenesis works are needed to verify such claims because even though a mutation is not found within a crucial domain, it could potentially disrupt three-dimensional protein-protein interaction when stretches of amino acids are folded and arranged in a way that brings together unsuspecting residues that are essential in maintaining

a protein's spatial conformations. Nevertheless, this is the first of such reports on the discovery of missense mutations on ribosomal protein *uS4 (S9)* and *uL14 (L23*), while detecting no sequence aberrations on ribosomal protein *eS8 (S8), eS31 (S27a), eL6 (L6), eL18 (L18), eL24 (L24), eL30 (L30), NPM1, BTF3* and *UBA52* in NPC cells.

A cursory literature search revealed the heterogeneity of RP expression and conflicting evidence on RP's roles across the multitude of cancer types. As outlined in Table 2.7 (Section 2.3.2.5), a ribosomal protein may be found up-regulated in one cancer, but downregulated in another, demonstrating an unanticipated plasticity and a highly specific pattern of RP expression implicated in normal and malignant human cell types. In addition to that, transcript and protein levels of these proteins, in some cases, may not be congruous. This highlights the complicated interplay of various transcriptional, translational and post-translational controls responsible in regulating the expression of a gene.

In regard to our data, many of the RPs in our list have been well established to regulate oncogenic phenotypes in different cancer types, but not in NPC. While we reported the under-expression of eS8 (S8) at both its mRNA and protein levels, we also reveal the up-regulation of uS4 (S9), eS31 (S27a), uL14 (L23) and NPM1 proteins though a downregulation was recorded at its transcript level, suggesting a hyper-activated translational and post-translational regulatory network that override transcriptional control in NPC cells. Apart from that, such scenario can be attributed to technical implications of issues surrounding qPCR data analysis and/or western blot image qualities. In regards to the former, fold difference variations within the triplicate experimental assays as well as within the array of cell lines tested could present certain skewness in the final data output; and for

the latter, the variation in clarity and pixel saturation of inter-assay densitometry blots could potentially reduce the accuracy of quantified data. Clearly, we have shown that uS4 (S9), eS8 (S8), eS31 (S27a), uL14 (L23) and NPM1 are active players in the tumorigenesis of NPC and to have displayed distinctive transcript and protein expression patterns specific to NPC as well as the histopathological subtypes of NPC. As such, characteristics of uS4 (S9), eS8 (S8), eS31 (S27a), uL14 (L23) and NPM1 can be feasibly exploited to develop a distinctive screen for the diagnosis and histopathological classification of NPC with the repertoire of genes as potential biomarkers with clinical applications.

Protein-protein interaction between these differentially expressed proteins was investigated with *in vitro* and *in vivo* analyses. NP69 was included to represent the normal nasopharyngeal epithelial cells, TW04 for type IIb NPC, which formed 95% of NPC cases in endemic areas, and C666-1 for EBV-harbouring NPC cells. Ribosomal protein uS4 (S9), eS31 (S27a) and uL14 (L23) were found to be associated with NPM1 in the whole cell lysates of NP69, TW04 and C666-1 cells. In all three cell lines tested, NPM1 protein was successfully pulled-down together with uS4 (S9), eS31 (S27a) and uL14 (L23) complexes and vice versa, verifying that there was no cell line-specific association. As such, the association between the three target RPs and NPM1 were promoted neither by the carcinogenic microenvironment within nasopharyngeal cells nor by the infection of EBV. As no association was observed between eS8 (S8) and NPM1 despite the significant under-expression of eS8 (S8) in NPC cells, eS8 (S8) may not regulate NPM1-associated pathways in NPC cells and that association to NPM1 is specific to a subset of RPs, and not all.

Nevertheless, this succeeding research emphasis on uS4 (S9) and uL14 (L23) does not

necessarily undermine the involvement and contribution of other RPs in NPC. Despite not being able to co-precipitate with NPM1, it is possible that eS8 (S8) or other RPs with different allosteric conformations may bind to NPM1 *en masse* or in a sequential orchestration based on the temporal and spatial circumstances within a cell. For instance, ribosomal protein eS19 (S19) was found to be able to interact with MDM2 in Namalwa cells, which is an EBV-positive Burkitt's lymphoma cell line, but not when it was ectopically expressed with MDM2 in HEK-293 cells, demonstrating the specificity of protein-protein interactions to cellular microenvironment conditions (Wei et al., 2013; Zhou, Hao, Liao, Zhang, et al., 2013).

In vivo interaction assay in TW04 cells further validated the *in vitro* association between uS4 (S9) and uL14 (L23). This system provided additional advantages over the traditional yeast two-hybrid system or any *in vitro* reciprocal assays with its utilization of a user-preferred host cell that is a close representation to that of a *in vivo* microenvironment. Its lack of false-positives due to the domain construction framework and the accompanying recommended controls, as well as the rapid and convenient detection and quantitation process render this system superior. An elevation in firefly luciferase transcription activity will be observed when there is a positive and direct interaction between two co-transfected recombinant proteins. TW04 cells were used in this part of the study due to the higher prevalence and thus, biological relevance of Type IIb.

No direct interaction was detected between eS31 (S27a) and NPM1 even though eS31 (S27a) was found to be associated with NPM1 *in vitro*. As the *in vivo* mammalian two-hybrid system tested for the presence of direct interaction, no elevation in firefly activity was observed

when eS31 (S27a) and NPM1 fusion proteins were co-translated in TW04 cells. Our data demonstrated that ribosomal protein eS31 (S27a) may be involved in NPM1-associated pathways, not by direct association with NPM1 but in a complex with intermediary proteins that modulate the functional interaction of eS31 (S27a) and NPM1. We hereby propose a hypothetical possibility of the association of eS31 (S27a) to NPM1 without any form of direct interaction. eS31 (S27a) was previously reported to interact with the central acidic domain of MDM2 and repress MDM2-mediated p53 ubiquitination (Sun et al., 2011). On the other hand, the binding domain for NPM1 was mapped onto the N-terminal of MDM2, in which its p53 interaction domain was also located (Kurki et al., 2004). By combining the findings from these papers, we propose that ribosomal protein eS31 (S27a) associates with NPM1 via MDM2 as an intermediary factor. By targeting separate domains on MDM2, eS31 (S27a) and NPM1 may synergistically exist as a complex with MDM2, and not as molecular competitors. This hypothesis is in line with our data. As we have found that eS31 (S27a) associates with NPM1 in a complex, and not directly, the up-regulated expression of eS31 (S27a) reported earlier could potentially work in synergy with NPM1 to sequester MDM2 from binding and ubiquitinating p53 in NPC cells.

When wild-type uS4 (S9) and uL14 (L23) fusion proteins were co-transfected with NPM1, significant increment in firefly luciferase signals were recorded over the negative controls, with preferred vector directionality when ribosomal proteins and NPM1 were cloned in-frame into pACT and pBIND expression vectors, respectively. The direct binding of uL14 (L23) to NPM1 showed relatively higher normalized firefly activity compared to that of uS4 (S9) to NPM1, thus revealing a more dynamic and stronger reciprocal relationship between uL14 (L23) and NPM1, which could be attributed to better structural compatibilities of both

interacting proteins. For instance, even though ribosomal protein uL5 (L11) and uL18 (L5) were both shown to interact with MDM2, a preferential binding to uL5 (L11) over uL18 (L5) was reported due to its more favourable domain compatibility to the zinc finger domain of MDM2, which resulted in a MDM2 conformational change that allowed for even tighter binding to uL5 (L11) (Lohrum, Ludwig, Kubbutat, Hanlon, & Vousden, 2003; Zhang et al., 2003; Zheng et al., 2015).

Upon further investigation, the central region of ribosomal protein uS4 (S9) was found to bind directly to the N- and C-terminal domains of NPM1. Closely similar studies were conducted by Lindstrom and her team, which reported the *in vitro* interaction of the N-terminal domain of uS4 (S9) and NPM1 and promoted nuclear localization in osteosarcoma cells (Lindström & Zhang, 2008; Lindström, 2012). At first glance, it would have seemed that the results from our study and that of Lindstrom's were contradictory. However, as previously detailed in Section 7.1.3.1, Lindstrom reported that the N-terminal fragment of uS4 (S9) (1-70aa) was able to interact with NPM1 *in vitro*. In our study, the N-terminal fragment of uS4 (S9) was designed to span codon 1-60 and was unable to bind to NPM1 *in vivo*, thereby pinning down the essential binding site to NPM1 to be between codon 61-69. It is noteworthy to point out that Lindstrom reported that two uS4 (S9) fragments (1-70aa and 70-140aa) were able to bind to NPM1 in an *in vitro* binding assay using purified GST-fused NPM1 and uS4-FLAG mutants (Lindström, 2012). In contrast to that, our *in vivo* interaction assay revealed a reversed pattern, in which we found two binding sites on NPM1 instead of uS4 (S9). However, the focus of that group was to delineate the binding site of NPM1 on uS4 (S9) and hence, no experimental tests were conducted to examine the corresponding binding site of uS4 (S9) on NPM1.

In regard to our data, it is interesting to note the ability of uS4 (S9) to perform dual interactions to two mutually exclusive ends of the NPM1 protein. The N-terminal of NPM1 regulates oligomerization and protein chaperone activity while the C-terminal contains a DNA-binding domain and a nucleolar localization signal (Hingorani et al., 2000). The central motif of ribosomal protein uS4 (S9) recognizes specific regions within these NPM1 domains and upon binding, mediates the oligomerization and nucleolus localization of NPM1 (Lindström, 2011). Protein partner binding to the C-terminal domain of NPM1, on the other hand, potentially disrupts the nucleolar localization signal, leading to the accumulation of NPM1 in the nucleoplasm and cytoplasm. Our data revealed a stronger affinity of uS4 (S9) to the C-terminal of NPM1 than the N-terminal domain and sequestered endogenous NPM1 in the nucleoplasm and cytoplasm of NPC cells.

By comparing TW04 and TW04-pCI-uS4 transfected cells, we were able to ensure that any molecular changes observed during the co-localization assessment of uS4 (S9) and NPM1 are not due to the countless genetic perturbations within NPC cells in relation to normal nasopharyngeal epithelial cells (TW04 vs. NP69), but solely on the ectopic expression of uS4 (S9). In such a scenario, the over-expression of uS4 (S9) in NPC cells appears to preferentially bind to the C-terminal domain of NPM1 and increases its nucleoplasm retention. Our observation is in line with the general consensus that the nucleolus is a bio-sensor for cellular stresses caused by either external or internal stress-inducing agents, and as a result of that, induces nucleoplasmic translocation of nucleolar protein such as NPM1 (Kurki et al., 2004; Yang et al., 2016). The reason behind the nucleolus being labelled as a stress-sensor is that in actively proliferating tumour cells under carcinogenic stress, ribosomal biogenesis within the nucleolus is hyperactivated to keep up with the increasing

demands of enhanced protein synthesis. In the event of a failure in the innate surveillance mechanism that governs disruptive ribosome production, tumour suppressor genes such as p53 are activated and nucleolar disruption is induced, which in turn promotes nucleolar translocation (Nicolas et al., 2016). As such, in normal nasopharyngeal epithelial cells, we observed the co-localization of uS4 (S9) and NPM1 in the nucleus of NP69 cells, which implies a healthy and well-balanced ratio of ribosomal protein production in the cytoplasm that gets continuously shuttled into the nucleus for pre-ribosomal subunit processing. In contrast, the dysregulated expression level of ribosomal protein uS4 (S9) in TW04 cells, as a result of abnormal ribosomal biogenesis, binds preferentially to the C-terminal of NPM1 and prevents its nucleolus localization. In addition to that, the loss of nucleolar retention could also be a possible explanation for the accumulation of co-localization of uS4 (S9) in the nucleoplasm and cytoplasm of TW04 cells.

We also investigated the disposition of uS4 (S9) and NPM1 interaction in the regulation of a downstream effector protein. NPM1 is a well-established protein partner of MDM2 and acts as a p53 co-activator by binding MDM2 (Kurki et al., 2004). As uS4 (S9) was observed to positively regulate MDM2 by sequestering NPM1, it can be logically deduced that the over-expression of uS4 (S9) directly interact and sequester NPM1 within the nucleoplasm and cytoplasm subcellular compartments of NPC cells, thereby transactivating MDM2. These observations provide evidence that ribosomal protein uS4 (S9) regulates the cell fate by sequestering NPM1 to the nucleoplasm and preventing the inhibition of MDM2.

Ribosomal protein uL14 (L23) was also found to directly bind to the N-terminal of NPM1 via its central domain. Besides being able to interact with NPM1, the central domain of uL14

(L23) was reported to be able to interact with the central acidic domain of MDM2 *in vitro* (Dai & Lu, 2004; Jin et al., 2004). In contrast to the dual uS4 (S9) binding sites detected on NPM1, uL14 (L23) could only bind directly to the oligomerization N-terminal domain, and as such, promoted NPM1 translocation to the nucleolus. In normal nasopharyngeal epithelial cells, uL14 (L23) and NPM1 interacted stably within the nucleus. Nucleolar disruption due to carcinogenic transformation in TW04 cells completely diminished the pool of NPM1 in the nucleolus and translocated uL14 (L23) and NPM1 into the nucleoplasm and not the cytoplasm. Over-expression of uL14 (L23) increased the accumulated pool of NPM1 in the nucleoplasm thereby sequestering NPM1 in the nucleoplasm of NPC cells.

In addition to that, our data revealed a dual-regulatory ability of ribosomal protein uL14 (L23) on MDM2. The direct interaction of uL14 (L23) and MDM2 demonstrated the former's role as a negative regulator of MDM2 as its interaction with MDM2 would result in the inhibition of MDM2-mediated p53 ubiquitination. On the other hand, as a positive regulator, uL14 (L23) was shown to be fully capable of disrupting the interaction of NPM1 and MDM2 *in vivo* by sequestering either NPM1 or MDM2, in which in the event of the former would result in the transactivation of MDM2, while the latter, coupled with our data on the direct binding of uL14 (L23) to MDM2, would inhibit the ubiquitination of p53. In U2OS cells, the overexpression of uL14 (L23) inhibited MDM2-mediated p53 ubiquitination via direct binding and if similar circumstance remains true for NPC cells, in which uL14 (L23) was over-expressed, it is hypothetically possible that uL14 (L23) binds with higher affinity to MDM2 instead of NPM1 under carcinogenic stress (Jin et al., 2004). In addition to uL14 (L23), MDM2 binds to uL5 (L11) as a consequence of two established nucleolar sensing pathways. Firstly, nucleolus disruption releases uL5 (L11) into the

nucleoplasm where it binds to MDM2 and activates the level of p53 (Bhat, Itahana, Jin, & Zhang, 2004). Secondly, nucleolar aberration induces the translation rate of RP-enriched 5'-terminal oligopyrimidine tract (5'-TOP) mRNAs, which alternatively increases the concentration of free, unassembled uL5 (L11) in the cytoplasm available to interact with MDM2 (Fumagalli et al., 2009). The data from our investigation agrees with that of the first, and not the second regulatory RP-MDM2-p53 model as the over-expression of uL14 (L23) in NPC cells resulted in the nucleoplasm retention of NPM1 and not within the nucleoli or the cytoplasm compartments, the latter being a principal site of NPM1 localization in the event of ribosomal biogenesis perturbation for the second model. Additional work is needed to dwell into the intricate balance among the three-way relationship of uL14 (L23), NPM1 and MDM2 in NPC cells.

By comparing the molecular landscapes of normal nasopharyngeal epithelial cells and NPC cells, the over-expression of uS4 (S9) and uL14 (L23) promoted NPM1 translocation from the nucleolus into the nucleoplasm, where the direct binding of uS4 (S9) and uL14 (L23) to NPM1 transactivated MDM2 and promoted MDM2-mediated p53 ubiquitination. Besides that, the over-expression of NPM1 was also detected in NPC cells, which could potentially allow NPM1 to 'escape' the regulatory control of RPs, resulting in the activation of p53 levels as detected in NPC tumours (Agaoglu et al., 2004). Additionally, the direct binding of uL14 (L23) to MDM2 observed in NPC cells may exert a similar inhibitory effect as NPM1 on MDM2 as shown in osteosarcoma cells, which furthers stabilize p53 (Dai et al., 2004; Wanzel et al., 2008).

As such, our study effectively adds ribosomal proteins on to the expanding list of key players

responsible for the regulation of NPC-specific, p53-dependent mechanisms, which consists of well-established effector proteins such as Akt, NFκB, MDM2 and many others (Figure 8.2). We have demonstrated the extra-ribosomal function of ribosomal proteins uS4 (S9) and uL14 (L23) in cell cycle progression and apoptosis by analysing their respective modes of interaction to NPM1. At the same time, we have also revealed the delicate regulatory control of the over-expression of uS4 (S9) and uL14 (L23) on the interaction and localization of NPM1 in NPC cells. However, questions such as 'what are other functional targets of ribosomal proteins?', 'what are the functional implications of dual-binding sites of uS4 (S9) to NPM1?', 'what are the regulatory consequences of the three-way uL14 (L23)-NPM1-MDM2 network in NPC cells?' as well as 'what are the co-acting partners of other dysregulated ribosomal proteins in NPC cells?' remain to be answered.

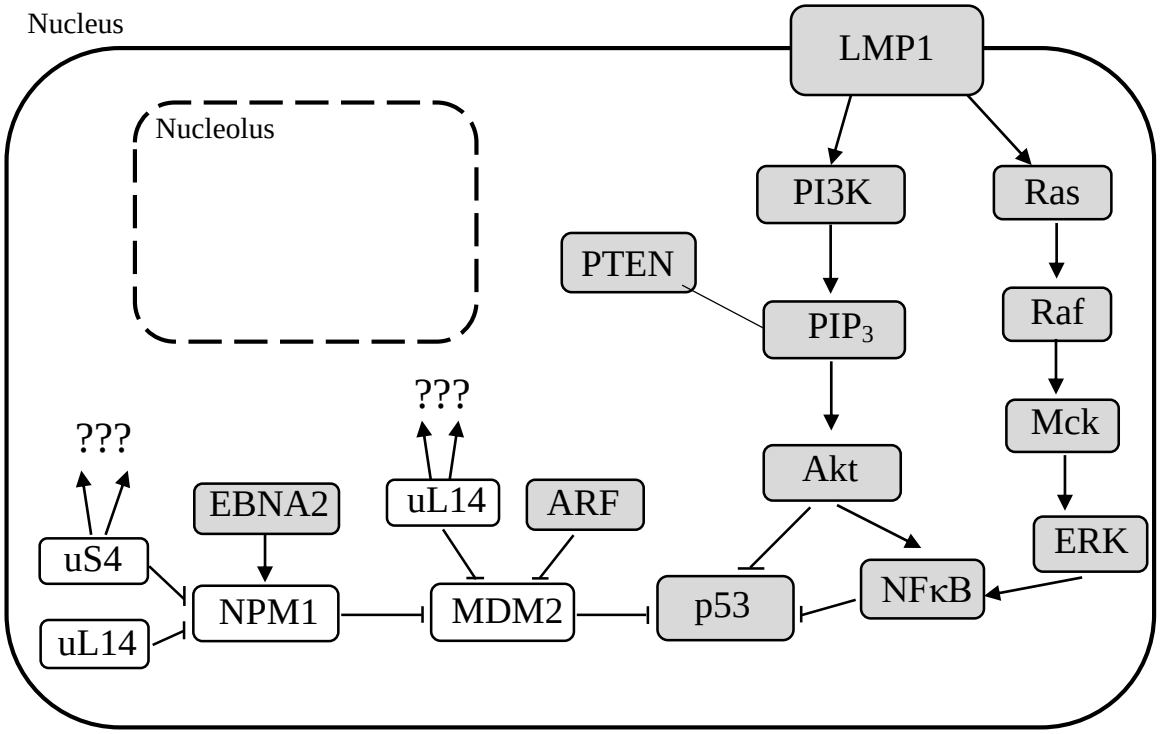

Figure 8.2: A visual illustration of major p53-associated molecular pathways in nasopharyngeal carcinoma cells. Shaded boxes represent established NPC-related pathways. The pointed tip and flat-tipped arrows signify activation and inhibition, respectively (adapted

from Li et al. (2010), Liu et al. (2012), and Tulalamba & Janvilisri (2012)).

Our findings are limited to a certain extent due to the usage of NPC cell lines in place of paired primary tumours samples. Even so, cell lines do provide a number of advantages in terms of cost-effectiveness, convenience in method of procurement and transfer, ease in cell culture propagation and maintenance, unlimited supply of material and non-obligatory ethical review associated with animal or human tissues. Most importantly, cells within a population are direct clones of each other, thereby giving rise to a homologous population of cells, which is the basis for consistent sample variation and reproducible results. On the other hand, since cell lines are genetically modified to replicate and expand infinitely, their innate landscape, phenotypes and stimuli responsiveness may be altered in the process. Moreover, prolonged continued passaging of cells can further discriminate passaged cells from parental cells as clonal selection that happens during each round of serial passage gradually reduces genotypic and phenotypic variation, therefore resulting in a shift from heterogeneity to homogeneity in cultures. When this happens, the cell lines fail to sufficiently represent primary cells (which are highly heterogenic) and flawed interpretations could arise. In addition to that, cell line work is highly prone to cross-contamination and mycoplasma contamination.

At the same time, we are aware of certain pitfalls involved when evaluating ribosomal protein mutants as they are structurally complex protein consisting of an extended RNA binding domain (Draper & Reynaldo, 1999). Sequence manipulation in terms of sequential deletions in generating truncated mutants that only expresses a specific fragment of the wild-type protein might result in a distinct behaviour that would likely impact its structural folding and localization and thus, its biomolecular interaction with downstream target proteins.

Taken together, this project has identified the dysregulation of expression levels of ribosomal protein genes and a subset of their putative co-acting factors. The structural and functional implication of the interaction of ribosomal protein uS4 (S9) and uL14 (L23) to NPM1 in NPC cells have been successfully validated. Though it is necessary to highlight here that while this study emphasizes on the interaction between ribosomal proteins and NPM1, the roles of RPs go beyond that of single target protein, as evidenced by the several implicated pathways involving the dysregulation of RPs. Hence, additional identification and validation of other target genes of RPs are necessary for a better understanding of the comprehensive characterization of ribosomal proteins in nasopharyngeal carcinoma. Research on ribosomal proteins in nasopharyngeal carcinoma has only begun to gain momentum, and it is expected that the roles of ribosomal protein uS4 (S9) and uL14 (L23) as oncogenes and their potential as biomarkers for cancer management will be established in the coming years.

CHAPTER 9

CONCLUSION AND FURTHER WORK

9.1 Conclusion

This project has demonstrated the transcriptional and translational dysregulation in expression levels of a subset of ribosomal protein genes in nasopharyngeal carcinoma-derived cell lines in comparison to a normal nasopharyngeal epithelial cell line that might have possible involvement in the tumorigenicity of NPC. *In vitro* and *in vivo* protein-protein interaction assays revealed a novel target protein, NPM1, of two differentially expressed ribosomal proteins uS4 (S9) and uL14 (L23) in NPC cells. uS4 (S9) interacted with the N- and C-terminal domains on NPM1 via its central motif while the central domain of uL14 (L23) directly bind to the N-terminal domain of NPM1. Empirical evidence on the over-expression of both uS4 (S9) and uL14 (L23) have revealed its association to the translocation of NPM1 from the nucleolus under ribosomal stress. In the nucleoplasm, the binding of uS4 (S9) and uL14 (L23) to NPM1 was able to disrupt the NPM1-MDM2 interaction, with MDM2 being a major p53-negative regulator. On the other hand, the over-expression of NPM1 protein may tip the scale in favour of circumventing the RPs-NPM1 control to bind to MDM2 and inhibit MDM2-mediated p53 ubiquitination, thereby increasing the endogenous level of p53 in NPC cells. These findings paint a clearer picture of the expression and functional implications of ribosomal proteins in the tumorigenicity of nasopharyngeal carcinoma.

9.2 Further Study

Subsequent work using gene knockdown studies could further improve our current understanding on the functional consequences of the interaction between ribosomal proteins, uS4 (S9) and uL14 (L23), and NPM1, as well as other co-acting partners. By either transiently or stably knocking-down uS4 (S9) and uL14 (L23) in nasopharyngeal carcinoma cells, the expression levels of NPM1 and other predicted protein partners can be determined, thereby revealing the regulatory capacity of ribosomal proteins. Besides that, *in vitro* functional assays can be carried out on RP-deficient NPC cells in order to investigate the implication of ribosomal proteins in various cellular pathways, such as cell viability, proliferation, invasion, cell cycle progression, and apoptosis in nasopharyngeal carcinoma.

REFERENCES

Aarøe, J., Lindahl, T., Dumeaux, V., Saebø, S., Tobin, D., Hagen, N., . . . Børresen-Dale, A. L. (2010). Gene expression profiling of peripheral blood cells for early detection of breast cancer. *Breast Cancer Research, 12*(1), R7.

Adams, S. M., Sharp, M. G., Walker, R. A., Brammar, W. J., & Varley, J. M. (1992). Differential expression of translation-associated genes in benign and malignant human breast tumours. *British Journal of Cancer, 65*(1), 65-71.

Agaoglu, F. Y., Dizdar, Y., Dogan, O., Alatli, C., Ayan, I., Savci, N., . . . Altun, M. (2004). P53 overexpression in nasopharyngeal carcinoma. *In Vivo, 18*(5), 555-560.

Ali, M. Y. (1965). Histology of the human nasopharyngeal mucosa. *Journal of Anatomy, 99*(Pt 3), 657-672.

Amin, M. A., Matsunaga, S., Uchiyama, S., & Fukui, K. (2008). Nucleophosmin is required for chromosome congression, proper mitotic spindle formation, and kinetochore-microtubule attachment in HeLa cells. *FEBS Letters, 582*(27), 3839-3844.

Amin, M. B., Greene, F. L., Edge, S. B., Compton, C. C., Gershenwald, J. E., Brookland, R. K., . . . Winchester, D. P. (2017). Nasopharynx. In *AJCC Cancer Staging Manual* (8th ed., pp. 103-111). New York, NY: Springer.

Anderson, S. J., Lauritsen, J. P., Hartman, M. G., Foushee, A. M., Lefebvre, J. M., Shinton, S. A., . . . Wiest, D. L. (2007). Ablation of ribosomal protein L22 selectively impairs alphabeta T cell development by activation of a p53-dependent checkpoint. *Immunity, 26*(6), 759-772.

Armstrong, R. W., Imrey, P. B., Lye, M. S., Armstrong, M. J., Yu, M. C., & Sani, S. (1998). Nasopharyngeal carcinoma in Malaysian Chinese: salted fish and other dietary exposures. *International Journal of Cancer, 77*(2), 228-235.

Armstrong, R. W., Kannan Kutty, M., Dharmalingam, S. K., & Ponnudurai, J. R. (1979). Incidence of nasopharyngeal carcinoma in Malaysia, 1968--1977. *British Journal of Cancer, 40*(4), 557-567.

Artero-Castro, A., Kondoh, H., Fernández-Marcos, P. J., Serrano, M., Ramón y Cajal, S., & Lleonart, M. E. (2009). Rplp1 bypasses replicative senescence and contributes to transformation. *Experimental Cell Research, 315*(8), 1372-1383.

Arthurs, C., Murtaza, B. N., Thomson, C., Dickens, K., Henrique, R., Patel, H. R. H., . . . Ahmed, A. (2017). Expression of ribosomal proteins in normal and cancerous human prostate tissue. *PLoS One, 12*(10), e0186047.

Ayan, I., Kaytan, E., & Ayan, N. (2003). Childhood nasopharyngeal carcinoma: from biology to treatment. *The Lancet Oncology, 4*(1), 13-21.

Baba, Y., Tsukuda, M., Mochimatsu, I., Furukawa, S., Kagata, H., Satake, K., . . . Nagashima, Y. (2001). Reduced expression of p16 and p27 proteins in nasopharyngeal carcinoma. *Cancer Detection and Prevention, 25*(5), 414-419.

Bai, D., Zhang, J., Xiao, W., & Zheng, X. (2014). Regulation of the HDM2-p53 pathway by ribosomal protein L6 in response to ribosomal stress. *Nucleic Acids Research, 42*(3), 1799-1811.

Baker, R. T., & Board, P. G. (1991). The human ubiquitin-52 amino acid fusion protein gene shares several structural features with mammalian ribosomal protein genes. *Nucleic Acids Research, 19*(5), 1035-1040.

Ban, N., Beckmann, R., Cate, J. H., Dinman, J. D., Dragon, F., Ellis, S. R., . . . Yusupov, M. (2014). A new system for naming ribosomal proteins. *Current Opinion in Structural Biology, 24*, 165-169.

Barnard, G. F., Mori, M., Staniunas, R. J., Begum, N. A., Bao, S., Puder, M., . . . Chen, L. B. (1995). Ubiquitin fusion proteins are overexpressed in colon cancer but not in gastric cancer. *Biochimica et Biophysica Acta, 1272*(3), 147-153.

Barnard, G. F., Staniunas, R. J., Mori, M., Puder, M., Jessup, M. J., Steele, G. D., & Chen, L. B. (1993). Gastric and hepatocellular carcinomas do not overexpress the same ribosomal protein messenger RNAs as colonic carcinoma. *Cancer Researcg, 53*(17), 4048-4052.

Bazot, Q., Deschamps, T., Tafforeau, L., Siouda, M., Leblanc, P., Harth-Hertle, M. L., . . . Manet, E. (2014). Epstein-Barr virus nuclear antigen 3A protein regulates CDKN2B transcription via interaction with MIZ-1. *Nucleic Acids Research, 42*(15), 9700-9716.

Bee, A., Brewer, D., Beesley, C., Dodson, A., Forootan, S., Dickinson, T., . . . Foster, C. S. (2011). siRNA knockdown of ribosomal protein gene RPL19 abrogates the aggressive phenotype of human prostate cancer. *PLoS One, 6*(7), e22672.

Bee, A., Ke, Y., Forootan, S., Lin, K., Beesley, C., Forrest, S. E., & Foster, C. S. (2006). Ribosomal protein l19 is a prognostic marker for human prostate cancer. *Clinical Cancer Research, 12*(7 Pt 1), 2061-2065.

Ben Ayoub Hizem Wided, B. H., Hsairi Hamadi, Ben Abdallah, & Mansour. (2015). Nasopharyngeal Carcinoma Incidence in North Tunisia: Negative Trends in Adults but not Adolescents, 1994-2006. *Asian Pacific Journal of Cancer Prevention, 16*(7), 2653-2657.

Ben-Shem, A., Garreau de Loubresse, N., Melnikov, S., Jenner, L., Yusupova, G., & Yusupov, M. (2011). The structure of the eukaryotic ribosome at 3.0 Å resolution. *Science, 334*(6062), 1524-1529. doi:10.1126/science.1212642

Benelli, D., Marzi, S., Mancone, C., Alonzi, T., la Teana, A., & Londei, P. (2009). Function and ribosomal localization of aIF6, a translational regulator shared by archaea and eukarya. *Nucleic Acids Research, 37*(1), 256-267. doi:10.1093/nar/gkn959

Bertucci, F., Salas, S., Eysteries, S., Nasser, V., Finetti, P., Ginestier, C., . . . Houlgatte, R. (2004). Gene expression profiling of colon cancer by DNA microarrays and correlation with histoclinical parameters. *Oncogene, 23*(7), 1377-1391.

Bertwistle, D., Sugimoto, M., & Sherr, C. J. (2004a). Physical and functional interactions of the Arf tumor suppressor protein with nucleophosmin/B23. *Molecular and Cell Biology, 24*(3), 985-996.

Bertwistle, D., Sugimoto, M., & Sherr, C. J. (2004b). Physical and functional interactions of the Arf tumor suppressor protein with nucleophosmin/B23. *Molecular and Cell Biology, 24*(3), 985-996.

Bhat, K. P., Itahana, K., Jin, A., & Zhang, Y. (2004). Essential role of ribosomal protein L11 in mediating growth inhibition-induced p53 activation. *EMBO Journal, 23*(12), 2402-2412.

Bibas, M., & Antinori, A. (2009). EBV and HIV-Related Lymphoma. *Mediterranean Journal of Hematology and Infectious Diseases, 1*(2), e2009032.

Bin Amer, S. M., Maqbool, Z., Nirmal, M. S., Qattan, A. T., Hussain, S. S., Jeprel, H. A., . . . Al-Tweigeri, T. A. (2008). Gene expression profiling in women with breast cancer in a Saudi population. *Saudi Medical Journal, 29*(4), 507-513.

Biosystems, A. (2008). Guide to Performing Relative Quantitation of Gene Expression Using Real-Time Quantitative PCR.

Bonetti, P., Davoli, T., Sironi, C., Amati, B., Pelicci, P. G., & Colombo, E. (2008). Nucleophosmin and its AML-associated mutant regulate c-Myc turnover through Fbw7 gamma. *Journal of Cell Biology, 182*(1), 19-26.

Boulon, S., Westman, B. J., Hutten, S., Boisvert, F. M., & Lamond, A. I. (2010). The nucleolus under stress. *Molecular Cell, 40*(2), 216-227.

Box, J. K., Paquet, N., Adams, M. N., Boucher, D., Bolderson, E., O'Byrne, K. J., & Richard, D. J. (2016). Nucleophosmin: from structure and function to disease development. *BMC Molecular Biology, 17*(1), 19.

Bray, F., Ferlay, J., Soerjomataram, I., Siegel, R. L., Torre, L. A., & Jemal, A. (2018). Global cancer statistics 2018: GLOBOCAN estimates of incidence and mortality worldwide for 36 cancers in 185 countries. *CA Cancer Journal for Clinicians, 68*(6), 394-424.

Brinkmann, O., Kastratovic, D. A., Dimitrijevic, M. V., Konstantinovic, V. S., Jelovac, D. B., Antic, J., . . . Wong, D. T. (2011). Oral squamous cell carcinoma detection by salivary biomarkers in a Serbian population. *Oral Oncology, 47*(1), 51-55.

Bursać, S., Brdovčak, M. C., Pfannkuchen, M., Orsolić, I., Golomb, L., Zhu, Y., . . . Volarevic, S. (2012). Mutual protection of ribosomal proteins L5 and L11 from degradation is essential for p53 activation upon ribosomal biogenesis stress. *Proceedings of the National Academy of Sciences USA, 109*(50), 20467-20472.

Burt, R. D., Vaughan, T. L., & McKnight, B. (1992). Descriptive epidemiology and survival analysis of nasopharyngeal carcinoma in the United States. *International Journal of Cancer, 52*(4), 549-556.

Burwick, N., Shimamura, A., & Liu, J. M. (2011). Non-Diamond Blackfan anemia disorders of ribosome function: Shwachman Diamond syndrome and 5q- syndrome. *Seminar Hematology, 48*(2), 136-143.

Bévort, M., & Leffers, H. (2000). Down regulation of ribosomal protein mRNAs during neuronal differentiation of human NTERA2 cells. *Differentiation, 66*(2-3), 81-92.

Calmon, M. F., Mota, M. T., Babeto, É., Candido, N. M., Girol, A. P., Mendiburu, C. F., . . . Rahal, P. (2013). Overexpression of ANXA1 in penile carcinomas positive for high-risk HPVs. *PLoS One, 8*(1), e53260.

Camacho, C. P., Lindsey, S. C., Melo, M. C., Yang, J. H., Germano-Neto, F., Valente, F. e. O., . . . Maciel, R. M. (2013). Measurement of calcitonin and calcitonin gene-related peptide mRNA refines the management of patients with medullary thyroid cancer and may replace calcitonin-stimulation tests. *Thyroid, 23*(3), 308-316.

Cao, B., Fang, Z., Liao, P., Zhou, X., Xiong, J., Zeng, S., & Lu, H. (2017). Cancer-mutated ribosome protein L22 (RPL22/eL22) suppresses cancer cell survival by blocking p53-MDM2 circuit. *Oncotarget, 8*(53), 90651-90661.

Cao, Q., Zhang, J., & Zhang, T. (2018). AIMP2-DX2 Promotes the Proliferation, Migration, and Invasion of Nasopharyngeal Carcinoma Cells. *Biomedical Research International, 2018*, 9253036.

Castro, M. E., Leal, J. F., Lleonart, M. E., Ramon, Y. C. S., & Carnero, A. (2008). Loss-of-function genetic screening identifies a cluster of ribosomal proteins regulating p53 function. *Carcinogenesis, 29*(7), 1343-1350.

Chan, A. S., To, K. F., Lo, K. W., Ding, M., Li, X., Johnson, P., & Huang, D. P. (2002). Frequent chromosome 9p losses in histologically normal nasopharyngeal epithelia from southern Chinese. *International Journal of Cancer, 102*(3), 300-303.

Chan, A. S., To, K. F., Lo, K. W., Mak, K. F., Pak, W., Chiu, B., . . . Huang, D. P. (2000). High frequency of chromosome 3p deletion in histologically normal nasopharyngeal epithelia from southern Chinese. *Cancer Research, 60*(19), 5365-5370.

Chan, A. T., Leung, S. F., Ngan, R. K., Teo, P. M., Lau, W. H., Kwan, W. H., . . . Zee, B. C. (2005). Overall survival after concurrent cisplatin-radiotherapy compared with radiotherapy alone in locoregionally advanced nasopharyngeal carcinoma. *Journal of the National Cancer Institute, 97*(7), 536-539.

Chan, B. F., McCarron P. (2005). *Nasopharyngeal carcinoma.* Paper presented at the WHO calssification of tumours:Pathology and genetics of head and neck tumours., Lyon.

Chan JKC, B. F., McCarron P. (2005). *Nasopharyngeal carcinoma.* Paper presented at the WHO calssification of tumours:Pathology and genetics of head and neck tumours., Lyon.

Chan, K. C. A., Woo, J. K. S., King, A., Zee, B. C. Y., Lam, W. K. J., Chan, S. L., . . . Lo, Y. M. D. (2017). Analysis of Plasma Epstein-Barr Virus DNA to Screen for Nasopharyngeal Cancer. *New England Journal of Medicine, 377*(6), 513-522.

Chan, S. H., Day, N. E., Kunaratnam, N., Chia, K. B., & Simons, M. J. (1983). HLA and nasopharyngeal carcinoma in Chinese--a further study. *International Journal of Cancer, 32*(2), 171-176.

Chang, E. T., & Adami, H. O. (2006). The enigmatic epidemiology of nasopharyngeal carcinoma. *Cancer Epidemiology Biomarkers and Prevention, 15*(10), 1765-1777.

Chao, J. A., & Williamson, J. R. (2004). Joint X-ray and NMR refinement of the yeast L30e-mRNA complex. *Structure, 12*(7), 1165-1176.

Chen, D., Zhang, Z., Li, M., Wang, W., Li, Y., Rayburn, E. R., . . . Zhang, R. (2007). Ribosomal protein S7 as a novel modulator of p53-MDM2 interaction: binding to

MDM2, stabilization of p53 protein, and activation of p53 function. *Oncogene, 26*(35), 5029-5037.

Chen, J., Guo, K., & Kastan, M. B. (2012). Interactions of nucleolin and ribosomal protein L26 (RPL26) in translational control of human p53 mRNA. *Journal of Biological Chemistry, 287*(20), 16467-16476.

Chen, J., Wei, Y., Feng, Q., Ren, L., He, G., Chang, W., . . . Qin, X. (2016). Ribosomal protein S15A promotes malignant transformation and predicts poor outcome in colorectal cancer through misregulation of p53 signaling pathway. *Internation Journal of Oncology, 48*(4), 1628-1638.

Chen, R., Dawson, D. W., Pan, S., Ottenhof, N. A., de Wilde, R. F., Wolfgang, C. L., . . . Brentnall, T. A. (2015). Proteins associated with pancreatic cancer survival in patients with resectable pancreatic ductal adenocarcinoma. *Lab Invest, 95*(1), 43-55.

Cheng, D. D., Zhu, B., Li, S. J., Yuan, T., Yang, Q. C., & Fan, C. Y. (2017). Down-regulation of RPS9 Inhibits Osteosarcoma Cell Growth through Inactivation of MAPK Signaling Pathway. *Journal of Cancer, 8*(14), 2720-2728.

Cheng, Y., Ho, R. L., Chan, K. C., Kan, R., Tung, E., Lung, H. L., . . . Lung, M. L. (2015). Anti-angiogenic pathway associations of the 3p21.3 mapped BLU gene in nasopharyngeal carcinoma. *Oncogene, 34*(32), 4219-4228.

Chester, K. A., Robson, L., Begent, R. H., Talbot, I. C., Pringle, J. H., Primrose, L., . . . Malcolm, A. D. (1989). Identification of a human ribosomal protein mRNA with increased expression in colorectal tumours. *Biochimica et Biophysica Acta, 1009*(3), 297-300.

Cheung, S. T., Huang, D. P., Hui, A. B., Lo, K. W., Ko, C. W., Tsang, Y. S., . . . Lee, J. C. (1999). Nasopharyngeal carcinoma cell line (C666-1) consistently harbouring Epstein-Barr virus. *International Journal of Cancer, 83*(1), 121-126.

Choesmel, V., Fribourg, S., Aguissa-Touré, A. H., Pinaud, N., Legrand, P., Gazda, H. T., & Gleizes, P. E. (2008). Mutation of ribosomal protein RPS24 in Diamond-Blackfan anemia results in a ribosome biogenesis disorder. *Human Molecular Genetics, 17*(9), 1253-1263.

Choi, J. K., Yu, U., Yoo, O. J., & Kim, S. (2005). Differential coexpression analysis using microarray data and its application to human cancer. *Bioinformatics, 21*(24), 4348-4355.

Chow, L. S., Lo, K. W., Kwong, J., To, K. F., Tsang, K. S., Lam, C. W., . . . Huang, D. P. (2004). RASSF1A is a target tumor suppressor from 3p21.3 in nasopharyngeal carcinoma. *International Journal of Cancer, 109*(6), 839-847.

Coghill, A. E., Wang, C. P., Verkuijilen, S. A. W. M., Yu, K. J., Hsu, W. L., Middeldorp, J. M., & Hildesheim, A. (2018). Evaluation of nasal and nasopharyngeal swab collection for the detection of Epstein-Barr virus in nasopharyngeal carcinoma. *J Medical Virology, 90*(1), 191-195.

Cogliano, V. J., Grosse,Y., Baan, R.A., Straif, K., Secretan M.B., El Ghissassi, F. (2005). Summary of IARC monographs on formaldehyde, 2-butoxyethanol, and 1-tert-butoxy-2-propanol. In W. G. f. V. 88. (Ed.), (Vol. 113, pp. 1205-1208).

Cole, S. E., LaRiviere, F. J., Merrikh, C. N., & Moore, M. J. (2009). A convergence of rRNA and mRNA quality control pathways revealed by mechanistic analysis of nonfunctional rRNA decay. *Molecular Cell, 34*(4), 440-450.

Colombo, E., Marine, J. C., Danovi, D., Falini, B., & Pelicci, P. G. (2002). Nucleophosmin regulates the stability and transcriptional activity of p53. *Nature Cell Biol, 4*(7), 529-533.

Corpet, F. (1988). Multiple sequence alignment with hierarchical clustering. *Nucleic Acids Research, 16*(22), 10881-10890.

Corporation, P. (2015). Dual-Luciferase Reporter Assay System Technical Manual.

Coutinho-Camillo, C. M., Lourenço, S. V., Nishimoto, I. N., Kowalski, L. P., & Soares, F. A. (2010). Nucleophosmin, p53, and Ki-67 expression patterns on an oral squamous cell carcinoma tissue microarray. *Human Pathology, 41*(8), 1079-1086.

Crnogorac-Jurcevic, T., Efthimiou, E., Capelli, P., Blaveri, E., Baron, A., Terris, B., . . . Lemoine, N. R. (2001). Gene expression profiles of pancreatic cancer and stromal desmoplasia. *Oncogene, 20*(50), 7437-7446.

Crook, T., Nicholls, J. M., Brooks, L., O'Nions, J., & Allday, M. J. (2000). High level expression of deltaN-p63: a mechanism for the inactivation of p53 in undifferentiated nasopharyngeal carcinoma (NPC)? *Oncogene, 19*(30), 3439-3444.

Cui, D., Li, L., Lou, H., Sun, H., Ngai, S. M., Shao, G., & Tang, J. (2014). The ribosomal protein S26 regulates p53 activity in response to DNA damage. *Oncogene, 33*(17), 2225-2235.

Daftuar, L., Zhu, Y., Jacq, X., & Prives, C. (2013). Ribosomal proteins RPL37, RPS15 and RPS20 regulate the Mdm2-p53-MdmX network. *PLoS One, 8*(7), e68667.

Dai, M. S., Arnold, H., Sun, X. X., Sears, R., & Lu, H. (2007). Inhibition of c-Myc activity by ribosomal protein L11. *EMBO Journal, 26*(14), 3332-3345.

Dai, M. S., & Lu, H. (2004). Inhibition of MDM2-mediated p53 ubiquitination and degradation by ribosomal protein L5. *Journal of Biological Chemistry, 279*(43), 44475-44482.

Dai, M. S., Sun, X. X., & Lu, H. (2010). Ribosomal protein L11 associates with c-Myc at 5 S rRNA and tRNA genes and regulates their expression. *Journal of Biological Chemistry, 285*(17), 12587-12594.

Dai, M. S., Zeng, S. X., Jin, Y., Sun, X. X., David, L., & Lu, H. (2004). Ribosomal protein L23 activates p53 by inhibiting MDM2 function in response to ribosomal perturbation but not to translation inhibition. *Molecular Cell Biology, 24*(17), 7654-7668.

Dai, W., Zheng, H., Cheung, A. K., & Lung, M. L. (2016). Genetic and epigenetic landscape of nasopharyngeal carcinoma. *Chinese Clinical Oncology, 5*(2), 16.

Davies, B., & Fried, M. (1993). The structure of the human intron-containing S8 ribosomal protein gene and determination of its chromosomal location at 1p32-p34.1. *Genomics, 15*(1), 68-75.

Dawson, C. W., Port, R. J., & Young, L. S. (2012). The role of the EBV-encoded latent membrane proteins LMP1 and LMP2 in the pathogenesis of nasopharyngeal carcinoma (NPC). *Seminar in Cancer Biology, 22*(2), 144-153.

De Bortoli, M., Castellino, R. C., Lu, X. Y., Deyo, J., Sturla, L. M., Adesina, A. M., . . . Kim, J. Y. (2006). Medulloblastoma outcome is adversely associated with overexpression of EEF1D, RPL30, and RPS20 on the long arm of chromosome 8. *BMC Cancer, 6*, 223.

Devi, B. C., Pisani, P., Tang, T. S., & Parkin, D. M. (2004). High incidence of nasopharyngeal carcinoma in native people of Sarawak, Borneo Island. *Cancer Epidemiology Biomarkers and Prevention, 13*(3), 482-486.

Dingerdissen, H. M., Torcivia-Rodriguez, J., Hu, Y., Chang, T. C., Mazumder, R., & Kahsay, R. (2018). BioMuta and BioXpress: mutation and expression knowledgebases for cancer biomarker discovery. *Nucleic Acids Researcg, 46*(D1), D1128-D1136.

Donati, G., Montanaro, L., & Derenzini, M. (2012). Ribosome biogenesis and control of cell proliferation: p53 is not alone. *Cancer Research, 72*(7), 1602-1607.

Donati, G., Peddigari, S., Mercer, C. A., & Thomas, G. (2013). 5S ribosomal RNA is an essential component of a nascent ribosomal precursor complex that regulates the Hdm2-p53 checkpoint. *Cell Reports, 4*(1), 87-98.

Donner, M. W., Bosma, J. F., & Robertson, D. L. (1985). Anatomy and physiology of the pharynx. *Gastrointestinal Radiology, 10*(3), 196-212.

Draper, D. E., & Reynaldo, L. P. (1999). RNA binding strategies of ribosomal proteins. *Nucleic Acids Research, 27*(2), 381-388.

Du, J., Shi, Y., Pan, Y., Jin, X., Liu, C., Liu, N., . . . Fan, D. (2005). Regulation of multidrug resistance by ribosomal protein l6 in gastric cancer cells. *Cancer Biology and Therapy, 4*(2), 242-247.

Dungworth, D. L. (1993). The Respiratory System. In *Pathology of Domestic Animals.* (pp. 539-699). New York: Academic Press.

Durand, F. (1837). Cancer de pharynx- Ossification dans la substance musculaire du coeur. *Bulletin de l'Association des anotomistes, 12*, 73-80.

Ebert, B. L. (2009). Deletion 5q in myelodysplastic syndrome: a paradigm for the study of hemizygous deletions in cancer. *Leukemia, 23*(7), 1252-1256.

Ebert, B. L., Pretz, J., Bosco, J., Chang, C. Y., Tamayo, P., Galili, N., . . . Golub, T. R. (2008). Identification of RPS14 as a 5q- syndrome gene by RNA interference screen. *Nature, 451*(7176), 335-339. doi:10.1038/nature06494

Effert, P., McCoy, R., Abdel-Hamid, M., Flynn, K., Zhang, Q., Busson, P., . . . Raab-Traub, N. (1992). Alterations of the p53 gene in nasopharyngeal carcinoma. *Journal of Virology, 66*(6), 3768-3775.

Ekenel, M., Keskin, S., Basaran, M., Ozdemir, C., Meral, R., Altun, M., . . . Bavbek, S. E. (2011). Induction chemotherapy with docetaxel and cisplatin is highly effective for locally advanced nasopharyngeal carcinoma. *Oral Oncology, 47*(7), 660-664.

El Hadi, H., Abdellaoui-Maane, I., Kottwitz, D., El Amrani, M., Bouchoutrouch, N., Qmichou, Z., . . . Moumen, A. (2017). Development and evaluation of a novel RT-qPCR based test for the quantification of HER2 gene expression in breast cancer. *Gene, 605*, 114-122.

Elenbaas, B., Dobbelstein, M., Roth, J., Shenk, T., & Levine, A. J. (1996). The MDM2 oncoprotein binds specifically to RNA through its RING finger domain. *Molecular Medicine, 2*(4), 439-451.

Ewing, J. (1929). Lymphoepithelioma. *American Journal of Pathology, 5*(2), 99-108.107.

Ewing, R. M., Chu, P., Elisma, F., Li, H., Taylor, P., Climie, S., . . . Figeys, D. (2007). Large-scale mapping of human protein-protein interactions by mass spectrometry. *Molecular System Biology, 3*, 89.

Falini, B., Bolli, N., Liso, A., Martelli, M. P., Mannucci, R., Pileri, S., & Nicoletti, I. (2009). Altered nucleophosmin transport in acute myeloid leukaemia with mutated NPM1: molecular basis and clinical implications. *Leukemia, 23*(10), 1731-1743.

Fan, H., Li, J., Jia, Y., Wu, J., Yuan, L., Li, M., . . . Xu, B. (2017). Silencing of Ribosomal Protein L34 (RPL34) Inhibits the Proliferation and Invasion of Esophageal Cancer Cells. *Oncology Research, 25*(7), 1061-1068.

Fang, H., Kang, J., Du, R., Zhao, X., Zhang, X., Ren, D., . . . Wen, J. (2015). Growth inhibitory effect of adenovirus-mediated tissue-targeted expression of ribosomal protein L23 on human colorectal carcinoma cells. *Oncology Reports, 34*(2), 763-770.

Farrow, D. C., Vaughan, T. L., Berwick, M., Lynch, C. F., Swanson, G. M., & Lyon, J. L. (1998). Diet and nasopharyngeal cancer in a low-risk population. *International Journal of Cancer, 78*(6), 675-679.

Ferreira-Cerca, S., Poll, G., Gleizes, P. E., Tschochner, H., & Milkereit, P. (2005). Roles of eukaryotic ribosomal proteins in maturation and transport of pre-18S rRNA and ribosome function. *Molecular Cell, 20*(2), 263-275.

Filip, A. M., Klug, J., Cayli, S., Fröhlich, S., Henke, T., Lacher, P., . . . Meinhardt, A. (2009). Ribosomal protein S19 interacts with macrophage migration inhibitory factor and attenuates its pro-inflammatory function. *Journal of Biological Chemistry, 284*(12), 7977-7985.

Frebourg, T., Malkin, D., & Friend, S. (1991). Cancer risks from germ line tumor suppressor gene mutations. *Princess Takamatsu Symposium, 22*, 61-70.

Frigerio, J. M., Dagorn, J. C., & Iovanna, J. L. (1995). Cloning, sequencing and expression of the L5, L21, L27a, L28, S5, S9, S10 and S29 human ribosomal protein mRNAs. *Biochimica et Biophysica Acta, 1262*(1), 64-68.

Fukawa, T., Ono, M., Matsuo, T., Uehara, H., Miki, T., Nakamura, Y., . . . Katagiri, T. (2012). DDX31 regulates the p53-HDM2 pathway and rRNA gene transcription through its

interaction with NPM1 in renal cell carcinomas. *Cancer Research*, *72*(22), 5867-5877.

Fumagalli, S., Di Cara, A., Neb-Gulati, A., Natt, F., Schwemberger, S., Hall, J., . . . Thomas, G. (2009). Absence of nucleolar disruption after impairment of 40S ribosome biogenesis reveals an rpL11-translation-dependent mechanism of p53 induction. *Nature Cell Biology*, *11*(4), 501-508.

Gallicchio, L., Matanoski, G., Tao, X. G., Chen, L., Lam, T. K., Boyd, K., . . . Alberg, A. J. (2006). Adulthood consumption of preserved and nonpreserved vegetables and the risk of nasopharyngeal carcinoma: a systematic review. *International Journal of Cancer*, *119*(5), 1125-1135.

Gao, M., Li, X., Dong, W., Jin, R., Ma, H., Yang, P., . . . Song, L. (2013). Ribosomal protein S7 regulates arsenite-induced GADD45α expression by attenuating MDM2-mediated GADD45α ubiquitination and degradation. *Nucleic Acids Research*, *41*(10), 5210-5222.

Gao, N., & Frank, J. (2006). A library of RNA bridges. *Nature Chemical Biology*, *2*, 231-232.

Gartmann, M., Blau, M., Armache, J. P., Mielke, T., Topf, M., & Beckmann, R. (2010). Mechanism of eIF6-mediated inhibition of ribosomal subunit joining. *Journal of Biological Chemistry*, *285*(20), 14848-14851.

Gazda, H. T., Kho, A. T., Sanoudou, D., Zaucha, J. M., Kohane, I. S., Sieff, C. A., & Beggs, A. H. (2006). Defective ribosomal protein gene expression alters transcription, translation, apoptosis, and oncogenic pathways in Diamond-Blackfan anemia. *Stem Cells*, *24*(9), 2034-2044.

Geng, W., Qin, F., Ren, J. X., Xu, X. H., & Wang, A. Y. (2018). Effects of ribosomal protein L41 (RPL41) on the proliferation and apoptosis of human retinoblastoma Y79 cells and its mechanisms. *Recent Advances in Ophthalmology*, *38*(3), 214-217.

Glaser, R., Zhang, H. Y., Yao, K. T., Zhu, H. C., Wang, F. X., Li, G. Y., . . . Li, Y. P. (1989). Two epithelial tumor cell lines (HNE-1 and HONE-1) latently infected with Epstein-Barr virus that were derived from nasopharyngeal carcinomas. *Proceedings of the National Academy of Sciences USA, 86*(23), 9524-9528.

Glozak, M. A., Sengupta, N., Zhang, X., & Seto, E. (2005). Acetylation and deacetylation of non-histone proteins. *Gene, 363*, 15-23.

Goldsmith, D. B., West, T. M., & Morton, R. (2002). HLA associations with nasopharyngeal carcinoma in Southern Chinese: a meta-analysis. *Clinical Otolaryngol and Allied Sciences, 27*(1), 61-67.

Goodfellow, S. J., & Zomerdijk, J. C. (2013). Basic mechanisms in RNA polymerase I transcription of the ribosomal RNA genes. *Subcellular Biochemistry, 61*, 211-236.

Gou, Y., Shi, Y., Zhang, Y., Nie, Y., Wang, J., Song, J., . . . Fan, D. (2010). Ribosomal protein L6 promotes growth and cell cycle progression through upregulating cyclin E in gastric cancer cells. *Biochemica et Biophysica Research Communication, 393*(4), 788-793.

Grammatica, L., Achille, G., Piepoli, S., & Paradiso, A. (1999). Early, late symptoms and histological type of nasopharyngeal carcinoma. *Oncology Reports, 6*(6), 1395-1398.

Green, C. D., Thompson, P. D., Johnston, P. G., & El-Tanani, M. K. (2007). Interaction between transcription factor, basal transcription factor 3, and the NH2-terminal domain of human estrogen receptor alpha. *Molecular Cancer Research, 5*(11), 1191-1200.

Grein, S., & Pyerin, W. (1999). BTF3 is a potential new substrate of protein kinase CK2. *Molecular and Cellular Biochemistry, 191*(1-2), 121-128.

Grisaru, D., Hauspy, J., Prasad, M., Albert, M., Murphy, K. J., Covens, A., . . . Rosen, B. (2007). Microarray expression identification of differentially expressed genes in serous epithelial ovarian cancer compared with bulk normal ovarian tissue and ovarian surface scrapings. *Oncology Reports, 18*(6), 1347-1356.

Grou, C. P., Pinto, M. P., Mendes, A. V., Domingues, P., & Azevedo, J. E. (2015). The de novo synthesis of ubiquitin: identification of deubiquitinases acting on ubiquitin precursors. *Science Reports, 5*, 12836.

Gu, J., Kawai, H., Nie, L., Kitao, H., Wiederschain, D., Jochemsen, A. G., . . . Yuan, Z. M. (2002). Mutual dependence of MDM2 and MDMX in their functional inactivation of p53. *Journal of Biological Chemistry, 277*(22), 19251-19254.

Gunasekaran, V. P., & Ganeshan, M. (2014). Inverse correlation of ribosomal protein S27A and multifunctional protein YB-1 in hepatocellular carcinoma. *Clinical Biochemistry, 47*(13-14), 1262-1264.

Guo, P., Wang, Y., Dai, C., Tao, C., Wu, F., Xie, X., . . . Chen, G. (2018). Ribosomal protein S15a promotes tumor angiogenesis via enhancing Wnt/β-catenin-induced FGF18 expression in hepatocellular carcinoma. *Oncogene, 37*(9), 1220-1236.

Guo, X., Shi, Y., Gou, Y., Li, J., Han, S., Zhang, Y., . . . Fan, D. (2011). Human ribosomal protein S13 promotes gastric cancer growth through down-regulating p27(Kip1). *Journal of Cellular and Molecular Medicine, 15*(2), 296-306.

Guo, Y. L., Kong, Q. S., Liu, H. S., & Tan, W. B. (2014). Drug resistance effects of ribosomal protein L24 overexpression in hepatocellular carcinoma HepG2 cells. *Asian Pacific Journal of Cancer Prevention, 15*(22), 9853-9857.

Hagner, P. R., Mazan-Mamczarz, K., Dai, B., Balzer, E. M., Corl, S., Martin, S. S., . . . Gartenhaus, R. B. (2011). Ribosomal protein S6 is highly expressed in non-Hodgkin lymphoma and associates with mRNA containing a 5' terminal oligopyrimidine tract. *Oncogene, 30*(13), 1531-1541.

Halic, M., Becker, T., Frank, J., Spahn, C. M., & Beckmann, R. (2005). Localization and dynamic behavior of ribosomal protein L30e. *Nature Structural and Molecular Biology, 12*(5), 467-468.

Hamdi Cherif, M., Serraino, D., Mahnane, A., Laouamri, S., Zaidi, Z., Boukharouba, H., . . . Bidoli, E. (2014). Time trends of cancer incidence in Setif, Algeria, 1986-2010: an observational study. *BMC Cancer, 14*, 637.

Hao, Y., Kong, X., Ruan, Y., Gan, H., Chen, H., Zhang, C., . . . Gu, J. (2011). CDK11p46 and RPS8 associate with each other and suppress translation in a synergistic manner. *Biochemica et Biophysica Research Communication, 407*(1), 169-174.

Hara, E., Smith, R., Parry, D., Tahara, H., Stone, S., & Peters, G. (1996). Regulation of p16CDKN2 expression and its implications for cell immortalization and senescence. *Molecular Cell Biology, 16*(3), 859-867.

Hardell, L., Johansson, B. , Axelson, O. . (1982). Epidemiological study of nasal and nasopharyngeal cancer and their relation to phenoxy acid or chlorophenol exposure. *American Journal of Industrial Medicine., 3*(3), 247-257.

Harms, J., Schluenzen, F., Zarivach, R., Bashan, A., Gat, S., Agmon, I., . . . Yonath, A. (2001). High resolution structure of the large ribosomal subunit from a mesophilic eubacterium. *Cell, 107*(5), 679-688.

Harms, K. L., & Chen, X. (2006). The functional domains in p53 family proteins exhibit both common and distinct properties. *Cell Death and Differentiation, 13*(6), 890-897.

Hartman, H., Favaretto, P., & Smith, T. F. (2006). The archaeal origins of the eukaryotic translational system. *Archaea, 2*(1), 1-9.

He, X., Li, Y., Dai, M. S., & Sun, X. X. (2016). Ribosomal protein L4 is a novel regulator of the MDM2-p53 loop. *Oncotarget, 7*(13), 16217-16226.

He, Y. C., Shen, Y., Cao, Y., Tang, F. Q., Tian, D. F., Huang, C. F., . . . Cao, D. (2016). Overexpression of AKR1B10 in nasopharyngeal carcinoma as a potential biomarker. *Cancer Biomarker, 16*(1), 127-135.

Henderson, B. E., Louie, E., SooHoo Jing, J., Buell, P., & Gardner, M. B. (1976). Risk factors associated with nasopharyngeal carcinoma. *New England Journal of Medicine, 295*(20), 1101-1106.

Hepeng, J. (2008). A controversial bid to thwart the 'Cantonese cancer'. *Science, 321*(5893), 1154-1155.

Hildesheim, A., Anderson, L. M., Chen, C. J., Cheng, Y. J., Brinton, L. A., Daly, A. K., . . . Chhabra, S. K. (1997). CYP2E1 genetic polymorphisms and risk of nasopharyngeal carcinoma in Taiwan. *Journal of the National Cancer Institute, 89*(16), 1207-1212.

Hildesheim, A., Chen, C. J., Caporaso, N. E., Cheng, Y. J., Hoover, R. N., Hsu, M. M., . . . Yang, C. S. (1995). Cytochrome P4502E1 genetic polymorphisms and risk of nasopharyngeal carcinoma: results from a case-control study conducted in Taiwan. *Cancer Epidemiology Biomarkers and Prevention, 4*(6), 607-610.

Hildesheim, A., Dosemeci, M., Chan, C. C., Chen, C. J., Cheng, Y. J., Hsu, M. M., . . . Yang, C. S. (2001). Occupational exposure to wood, formaldehyde, and solvents and risk of nasopharyngeal carcinoma. *Cancer Epidemiology Biomarkers and Prevention, 10*(11), 1145-1153.

Hingorani, K., Szebeni, A., & Olson, M. O. (2000). Mapping the functional domains of nucleolar protein B23. *Journal of Biological Chemistry, 275*(32), 24451-24457.

Hjalgrim, H., Friborg, J., Melbye, M. (2007). The epidemiology of EBV and its association with malignant disease. In *Human Herpesvirus: Biology, Therapy and Immunoprophylaxis.*: Cambridge University Press.

Hoe, S. L., Lee, E. S., Khoo, A. S., & Peh, S. C. (2009). p53 and nasopharyngeal carcinoma: a Malaysian study. *Pathology, 41*(6), 561-565.

Holmberg Olausson, K., Elsir, T., Moazemi Goudarzi, K., Nistér, M., & Lindström, M. S. (2015). NPM1 histone chaperone is upregulated in glioblastoma to promote cell survival and maintain nucleolar shape. *Science Reports, 5*, 16495.

Hong, S. W., Kim, S. M., Jin, D. H., Kim, Y. S., & Hur, D. Y. (2017). RPS27a enhances EBV-encoded LMP1-mediated proliferation and invasion by stabilizing of LMP1. *Biochemica et Biophysica Research Communication, 491*(2), 303-309.

Hoppe, R. T., Williams, J., Warnke, R., Goffinet, D. R., & Bagshaw, M. A. (1978). Carcinoma of the nasopharynx--the significance of histology. *International Journal of Radiation Oncology Biology Physics, 4*(3-4), 199-205.

Horn, H. F., & Vousden, K. H. (2008). Cooperation between the ribosomal proteins L5 and L11 in the p53 pathway. *Oncogene, 27*(44), 5774-5784.

Houseley, J., LaCava, J., & Tollervey, D. (2006). RNA-quality control by the exosome. *Nature Reviews Molecular Cell Biology, 7*(7), 529-539.

Hsu, Y. A., Lin, H. J., Sheu, J. J., Shieh, F. K., Chen, S. Y., Lai, C. H., . . . Chen, B. H. (2011). A novel interaction between interferon-inducible protein p56 and ribosomal protein L15 in gastric cancer cells. *DNA Cell Biology, 30*(9), 671-679.

Hu, L., Lin, Z., Wu, Y., Dong, J., Zhao, B., Cheng, Y., . . . Zeng, M. (2016). Comprehensive profiling of EBV gene expression in nasopharyngeal carcinoma through paired-end transcriptome sequencing. *Frontiers in Medicine, 10*(1), 61-75.

Hu, L. F., Eiriksdottir, G., Lebedeva, T., Kholodniouk, I., Alimov, A., Chen, F., . . . Ernberg, I. (1996). Loss of heterozygosity on chromosome arm 3p in nasopharyngeal carcinoma. *Genes Chromosomes Cancer, 17*(2), 118-126.

Huang, C. J., Chien, C. C., Yang, S. H., Chang, C. C., Sun, H. L., Cheng, Y. C., . . . Lin, C. M. (2008). Faecal ribosomal protein L19 is a genetic prognostic factor for survival in colorectal cancer. *Journal of Cellular and Molecular Medicine, 12*(5B), 1936-1943.

Huang, D., Chen, W., He, R., Yu, F., Zhang, Z., & Qiu, W. (2003). Different cDNA microarray patterns of gene expression reflecting changes during metastatic progression in adenoid cystic carcinoma. *World Journal of Surgical Oncology, 1*(1), 28.

Huang, D. P., Ho, J. H., Poon, Y. F., Chew, E. C., Saw, D., Lui, M., . . . Lau, W. H. (1980). Establishment of a cell line (NPC/HK1) from a differentiated squamous carcinoma of the nasopharynx. *International Journal of Cancer, 26*(2), 127-132.

Huang, D. P., Ho, J. H., Saw, D., & Teoh, T. B. (1978). Carcinoma of the nasal and paranasal regions in rats fed Cantonese salted marine fish. *IARC Science Publication* (20), 315-328.

Huang, X. P., Zhao, C. X., Li, Q. J., Cai, Y., Liu, F. X., Hu, H., . . . Wang, M. R. (2006). Alteration of RPL14 in squamous cell carcinomas and preneoplastic lesions of the esophagus. *Gene, 366*(1), 161-168.

Huberts, D. H., & van der Klei, I. J. (2010). Moonlighting proteins: an intriguing mode of multitasking. *Biochimica et Biophysica Acta, 1803*(4), 520-525.

Hui, A. B., Lo, K. W., Leung, S. F., Teo, P., Fung, M. K., To, K. F., . . . Huang, D. P. (1999). Detection of recurrent chromosomal gains and losses in primary nasopharyngeal carcinoma by comparative genomic hybridisation. *International Journal of Cancer, 82*(4), 498-503.

Hwang, Y. C., Lu, T. Y., Huang, D. Y., Kuo, Y. S., Kao, C. F., Yeh, N. H., . . . Lin, C. T. (2009). NOLC1, an enhancer of nasopharyngeal carcinoma progression, is essential for TP53 to regulate MDM2 expression. *American Journal of Pathology, 175*(1), 342-354.

Iadevaia, V., Caldarola, S., Biondini, L., Gismondi, A., Karlsson, S., Dianzani, I., & Loreni, F. (2010). PIM1 kinase is destabilized by ribosomal stress causing inhibition of cell cycle progression. *Oncogene, 29*(40), 5490-5499.

IARC. (1993). Some naturally occurring substances: food items and constituents,heterocyclic aromatic amines and mycotoxins. In *IARC monographs on the evaluation of carcinogenic risks to humans.* (Vol. 56). Lyon: IARC Press.

Idol, R. A., Robledo, S., Du, H. Y., Crimmins, D. L., Wilson, D. B., Ladenson, J. H., . . . Mason, P. J. (2007). Cells depleted for RPS19, a protein associated with Diamond Blackfan Anemia, show defects in 18S ribosomal RNA synthesis and small ribosomal subunit production. *Blood Cells Molecules and Diseases, 39*(1), 35-43.

Iizumi, Y., Oishi, M., Taniguchi, T., Goi, W., Sowa, Y., & Sakai, T. (2013). The flavonoid apigenin downregulates CDK1 by directly targeting ribosomal protein S9. *PLoS One, 8*(8), e73219.

Inuzuka, H., Tseng, A., Gao, D., Zhai, B., Zhang, Q., Shaik, S., . . . Wei, W. (2010). Phosphorylation by casein kinase I promotes the turnover of the Mdm2 oncoprotein via the SCF(beta-TRCP) ubiquitin ligase. *Cancer Cell, 18*(2), 147-159.

Itahana, K., Bhat, K. P., Jin, A., Itahana, Y., Hawke, D., Kobayashi, R., & Zhang, Y. (2003). Tumor suppressor ARF degrades B23, a nucleolar protein involved in ribosome biogenesis and cell proliferation. *Molecular Cell, 12*(5), 1151-1164.

Jackson, M. W., & Berberich, S. J. (2000). MdmX protects p53 from Mdm2-mediated degradation. *Molecular Cell Biology, 20*(3), 1001-1007.

Jang, C. Y., Kim, H. D., & Kim, J. (2012). Ribosomal protein S3 interacts with TRADD to induce apoptosis through caspase dependent JNK activation. *Biochemica et Biophysica Research Communication, 421*(3), 474-478.

Jang, M., Rhee, J. E., Jang, D. H., & Kim, S. S. (2011). Gene Expression Profiles are Altered in Human Papillomavirus-16 E6 D25E-Expressing Cell Lines. *Journal of Virology, 8*.

Jansen, J. G., Tsaalbi-Shtylik, A., & de Wind, N. (2015). Roles of mutagenic translesion synthesis in mammalian genome stability, health and disease. *DNA Repair (Amsterdam), 29*, 56-64.

Jeyakumar, A., Brickman, T. M., & Doerr, T. (2006). Review of nasopharyngeal carcinoma. *Ear Nose Throat Journal, 85*(3), 168-170, 172-163, 184.

Jin, A., Itahana, K., O'Keefe, K., & Zhang, Y. (2004). Inhibition of HDM2 and activation of p53 by ribosomal protein L23. *Molecular Cell Biology, 24*(17), 7669-7680.

Jing, J., Louie, E., Henderson, B. E., & Terasaki, P. (1977). Histocompatibility leukocyte antigen patterns in nasopharyngeal carcinoma cases from California. *National Cancer Institute Monographs, 47*, 153-156.

Jones, D. T., Lechertier, T., Reynolds, L. E., Mitter, R., Robinson, S. D., Kirn-Safran, C. B., & Hodivala-Dilke, K. M. (2013). Endogenous ribosomal protein L29 (RPL29): a newly identified regulator of angiogenesis in mice. *Disease Models and Mechanisms, 6*(1), 115-124.

Jäkel, S., & Görlich, D. (1998). Importin beta, transportin, RanBP5 and RanBP7 mediate nuclear import of ribosomal proteins in mammalian cells. *EMBO Journal, 17*(15), 4491-4502.

Kaern, M., Elston, T. C., Blake, W. J., & Collins, J. J. (2005). Stochasticity in gene expression: from theories to phenotypes. *Nature Review on Genetics, 6*(6), 451-464.

Kam, M. K., Leung, S. F., Zee, B., Chau, R. M., Suen, J. J., Mo, F., . . . Chan, A. T. (2007). Prospective randomized study of intensity-modulated radiotherapy on salivary gland function in early-stage nasopharyngeal carcinoma patients. *Journal of Clinical Oncology, 25*(31), 4873-4879.

Kamb, A., Shattuck-Eidens, D., Eeles, R., Liu, Q., Gruis, N. A., Ding, W., . . . Weaver-Feldhaus, J. (1994). Analysis of the p16 gene (CDKN2) as a candidate for the chromosome 9p melanoma susceptibility locus. *Nature Genetics, 8*(1), 23-26.

Kanayama, H., Tanaka, K., Aki, M., Kagawa, S., Miyaji, H., Satoh, M., . . . Ichihara, A. (1991). Changes in expressions of proteasome and ubiquitin genes in human renal cancer cells. *Cancer Research, 51*(24), 6677-6685.

Karhemo, P. R., Rivinoja, A., Lundin, J., Hyvönen, M., Chernenko, A., Lammi, J., . . . Laakkonen, P. (2011). An extensive tumor array analysis supports tumor suppressive role for nucleophosmin in breast cancer. *American Journal of Pathology, 179*(2), 1004-1014.

Kasai, H., Nadano, D., Hidaka, E., Higuchi, K., Kawakubo, M., Sato, T. A., & Nakayama, J. (2003). Differential expression of ribosomal proteins in human normal and neoplastic colorectum. *Journal of Histochemistry and Cytochemistry, 51*(5), 567-574.

Khanna, N., Reddy, V. G., Tuteja, N., & Singh, N. (2000). Differential gene expression in apoptosis: identification of ribosomal protein S29 as an apoptotic inducer. *Biochemica et Biophysica Research Communication, 277*(2), 476-486.

Khanna, N., Sen, S., Sharma, H., & Singh, N. (2003). S29 ribosomal protein induces apoptosis in H520 cells and sensitizes them to chemotherapy. *Biochemica et Biophysica Research Communication, 304*(1), 26-35.

Khatter, H., Myasnikov, A. G., Natchiar, S. K., & Klaholz, B. P. (2015). Structure of the human 80S ribosome. *Nature, 520*(7549), 640-645.

Kibbe, W. A. (2007). OligoCalc: an online oligonucleotide properties calculator. *Nucleic Acids Research, 35*(Web Server issue), W43-46.

Kim, J. H., You, K. R., Kim, I. H., Cho, B. H., Kim, C. Y., & Kim, D. G. (2004). Over-expression of the ribosomal protein L36a gene is associated with cellular proliferation in hepatocellular carcinoma. *Hepatology, 39*(1), 129-138.

Kim, S., & Kim, T. (2003). Selection of optimal internal controls for gene expression profiling of liver disease. *Biotechniques, 35*(3), 456-458, 460.

Kim, S. H., Jang, Y. H., Chau, G. C., Pyo, S., & Um, S. H. (2013). Prognostic significance and function of phosphorylated ribosomal protein S6 in esophageal squamous cell carcinoma. *Modern Pathology, 26*(3), 327-335.

Kirschner, L. S., & Stratakis, C. A. (2000). Structure of the human ubiquitin fusion gene Uba80 (RPS27a) and one of its pseudogenes. *Biochemica et Biophysica Research Communication, 270*(3), 1106-1110.

Kitahara, O., Furukawa, Y., Tanaka, T., Kihara, C., Ono, K., Yanagawa, R., . . . Tsunoda, T. (2001). Alterations of gene expression during colorectal carcinogenesis revealed by cDNA microarrays after laser-capture microdissection of tumor tissues and normal epithelia. *Cancer Research, 61*(9), 3544-3549.

Klinge, S., Voigts-Hoffmann, F., Leibundgut, M., Arpagaus, S., & Ban, N. (2011). Crystal structure of the eukaryotic 60S ribosomal subunit in complex with initiation factor 6. *Science, 334*(6058), 941-948.

Kobayashi, M., Oshima, S., Maeyashiki, C., Nibe, Y., Otsubo, K., Matsuzawa, Y., . . . Watanabe, M. (2016). The ubiquitin hybrid gene UBA52 regulates ubiquitination of ribosome and sustains embryonic development. *Science Reports, 6*, 36780.

Kobayashi, T., Sasaki, Y., Oshima, Y., Yamamoto, H., Mita, H., Suzuki, H., . . . Shinomura, Y. (2006). Activation of the ribosomal protein L13 gene in human gastrointestinal cancer. *International Journal of Molecular Medicine, 18*(1), 161-170.

Koike, A., Nishikawa, H., Wu, W., Okada, Y., Venkitaraman, A. R., & Ohta, T. (2010). Recruitment of phosphorylated NPM1 to sites of DNA damage through RNF8-dependent ubiquitin conjugates. *Cancer Research, 70*(17), 6746-6756.

Kondoh, N., Schweinfest, C. W., Henderson, K. W., & Papas, T. S. (1992). Differential expression of S19 ribosomal protein, laminin-binding protein, and human lymphocyte antigen class I messenger RNAs associated with colon carcinoma progression and differentiation. *Cancer Research, 52*(4), 791-796.

Kondoh, N., Shuda, M., Tanaka, K., Wakatsuki, T., Hada, A., & Yamamoto, M. (2001). Enhanced expression of S8, L12, L23a, L27 and L30 ribosomal protein mRNAs in human hepatocellular carcinoma. *Anticancer Research, 21*(4A), 2429-2433.

Kong Q-L, H. L.-J., Cao J-Y, Huang Y-J, Xu L-H, Liang Y, et al. (2010). Epstein-Barr Virus-Encoded LMP2A Induces an Epithelial–Mesenchymal Transition and Increases the Number of Side Population Stem-like Cancer Cells in Nasopharyngeal Carcinoma. . *PLoS Pathogens, 6*(6).

Kongruttanachok, N., Sukdikul, S., Setavarin, S., Kerekhjanarong, V., Supiyaphun, P., Voravud, N., . . . Mutirangura, A. (2001). Cytochrome P450 2E1 polymorphism and nasopharyngeal carcinoma development in Thailand: a correlative study. *BMC Cancer, 1*, 4.

Korgaonkar, C., Hagen, J., Tompkins, V., Frazier, A. A., Allamargot, C., Quelle, F. W., & Quelle, D. E. (2005). Nucleophosmin (B23) targets ARF to nucleoli and inhibits its function. *Molecular Cell Biology, 25*(4), 1258-1271.

Koussounadis, A., Langdon, S. P., Um, I. H., Harrison, D. J., & Smith, V. A. (2015). Relationship between differentially expressed mRNA and mRNA-protein correlations in a xenograft model system. *Science Reports, 5*, 10775.

Kurki, S., Peltonen, K., Latonen, L., Kiviharju, T. M., Ojala, P. M., Meek, D., & Laiho, M. (2004). Nucleolar protein NPM interacts with HDM2 and protects tumor suppressor protein p53 from HDM2-mediated degradation. *Cancer Cell, 5*(5), 465-475.

Kurniawan, A. N., & Leong, A. S.-Y. (2000). p53 protein overexpression in nasopharyngeal carcinoma in Indonesian patients. *Medical Journal of Indonesia, 9*(3), 209-216.

Kusumawidjaja, G., Kayed, H., Giese, N., Bauer, A., Erkan, M., Giese, T., . . . Kleeff, J. (2007). Basic transcription factor 3 (BTF3) regulates transcription of tumor-associated genes in pancreatic cancer cells. *Cancer Biology Therapy, 6*(3), 367-376.

Kwong, J., Lo, K. W., To, K. F., Teo, P. M., Johnson, P. J., & Huang, D. P. (2002). Promoter hypermethylation of multiple genes in nasopharyngeal carcinoma. *Clinical Cancer Research, 8*(1), 131-137.

Küppers, R. (2009). The biology of Hodgkin's lymphoma. *Nature Review Cancer, 9*(1), 15-27.

La Starza, R., Matteucci, C., Gorello, P., Brandimarte, L., Pierini, V., Crescenzi, B., . . . Mecucci, C. (2010). NPM1 deletion is associated with gross chromosomal rearrangements in leukemia. *PLoS One, 5*(9), e12855.

LaCava, J., Houseley, J., Saveanu, C., Petfalski, E., Thompson, E., Jacquier, A., & Tollervey, D. (2005). RNA degradation by the exosome is promoted by a nuclear polyadenylation complex. *Cell, 121*(5), 713-724.

Lafontaine, D. L., & Tollervey, D. (2001). The function and synthesis of ribosomes. *Nature Review on Molecular Cell Biology, 2*(7), 514-520.

Larburu, N., Montellese, C., O'Donohue, M. F., Kutay, U., Gleizes, P. E., & Plisson-Chastang, C. (2016). Structure of a human pre-40S particle points to a role for RACK1 in the final steps of 18S rRNA processing. *Nucleic Acids Research, 44*(17), 8465-8478.

Lareau, L. F., Brooks, A. N., Soergel, D. A., Meng, Q., & Brenner, S. E. (2007). The coupling of alternative splicing and nonsense-mediated mRNA decay. *Advances in Experimental Medicine and Biology, 623*, 190-211.

Leal, M. F., Mazzotti, T. K., Calcagno, D. Q., Cirilo, P. D., Martinez, M. C., Demachki, S., . . . Smith, M. C. (2014). Deregulated expression of Nucleophosmin 1 in gastric cancer and its clinicopathological implications. *BMC Gastroenterol, 14*, 9.

Lecompte, O., Ripp, R., Thierry, J. C., Moras, D., & Poch, O. (2002). Comparative analysis of ribosomal proteins in complete genomes: an example of reductive evolution at the domain scale. *Nucleic Acids Research, 30*(24), 5382-5390.

Lee, A. W., Foo, W., Mang, O., Sze, W. M., Chappell, R., Lau, W. H., & Ko, W. M. (2003). Changing epidemiology of nasopharyngeal carcinoma in Hong Kong over a 20-year period (1980-99): an encouraging reduction in both incidence and mortality. *International Journal of Cancer, 103*(5), 680-685.

Lee, J. T., & Ko, C. Y. (2005). Has survival improved for nasopharyngeal carcinoma in the United States? *Otolaryngol Head Neck Surg, 132*(2), 303-308.

Lee, S. B., Kwon, I. S., Park, J., Lee, K. H., Ahn, Y., Lee, C., . . . Ahn, J. Y. (2010). Ribosomal protein S3, a new substrate of Akt, serves as a signal mediator between neuronal apoptosis and DNA repair. *Journal of Biological Chemistry, 285*(38), 29457-29468.

Lee, S. Y., Park, J. H., Kim, S., Park, E. J., Yun, Y., & Kwon, J. (2005). A proteomics approach for the identification of nucleophosmin and heterogeneous nuclear ribonucleoprotein C1/C2 as chromatin-binding proteins in response to DNA double-strand breaks. *Biochemistry Journal, 388*(Pt 1), 7-15.

Lee, Y., & Nazar, R. N. (2003). Terminal structure mediates 5 S rRNA stability and integration during ribosome biogenesis. *Journal of Biological Chemistry, 278*(9), 6635-6641.

Leong, J. L., Loh, K. S., Putti, T. C., Goh, B. C., & Tan, L. K. (2004). Epidermal growth factor receptor in undifferentiated carcinoma of the nasopharynx. *Laryngoscope, 114*(1), 153-157.

Lerman, M. I., & Minna, J. D. (2000). The 630-kb lung cancer homozygous deletion region on human chromosome 3p21.3: identification and evaluation of the resident candidate tumor suppressor genes. The International Lung Cancer Chromosome 3p21.3 Tumor Suppressor Gene Consortium. *Cancer Research, 60*(21), 6116-6133.

Lessard, F., Brakier-Gingras, L., & Ferbeyre, G. (2019). Ribosomal Proteins Control Tumor Suppressor Pathways in Response to Nucleolar Stress. *Bioessays, 41*(3), e1800183.

Li, B., Vilardell, J., & Warner, J. R. (1996). An RNA structure involved in feedback regulation of splicing and of translation is critical for biological fitness. *Proceedings of the National Academy of Sciences USA, 93*(4), 1596-1600.

Li, C., Chen, D., Luo, M., Ge, M., & Zhu, J. (2014). Knockdown of ribosomal protein L39 by RNA interference inhibits the growth of human pancreatic cancer cells in vitro and in vivo. *Biotechnology Journal, 9*(5), 652-663.

Li, C., Ge, M., Yin, Y., Luo, M., & Chen, D. (2012). Silencing expression of ribosomal protein L26 and L29 by RNA interfering inhibits proliferation of human pancreatic cancer PANC-1 cells. *Molecular and Cellular Biochemistry, 370*(1-2), 127-139.

Li, C. C., Yu, M. C., & Henderson, B. E. (1985). Some epidemiologic observations of nasopharyngeal carcinoma in Guangdong, People's Republic of China. *National Cancer Institute Monograms, 69*, 49-52.

Li, L., Guo, L., Tao, Y., Zhou, S., Wang, Z., Luo, W., . . . Cao, Y. (2007). Latent membrane protein 1 of Epstein-Barr virus regulates p53 phosphorylation through MAP kinases. *Cancer Letters, 255*(2), 219-231.

Li, L., Tao, Q., Jin, H., van Hasselt, A., Poon, F. F., Wang, X., . . . Cao, Y. (2010). The tumor suppressor UCHL1 forms a complex with p53/MDM2/ARF to promote p53

signaling and is frequently silenced in nasopharyngeal carcinoma. *Clinical Cancer Research, 16*(11), 2949-2958.

Li, L., Zhou, S., Chen, X., Guo, L., Li, Z., Hu, D., . . . Cao, Y. (2008). The activation of p53 mediated by Epstein-Barr virus latent membrane protein 1 in SV40 large T-antigen transformed cells. *FEBS Letters, 582*(5), 755-762.

Li, M., Luo, J., Brooks, C. L., & Gu, W. (2002). Acetylation of p53 inhibits its ubiquitination by Mdm2. *Journal of Biological Chemistry*, *277*(52), 50607-50611.

Li, S., Zhang, X., Zhou, Z., Huang, Z., & Liu, L. (2017). Downregulation of nucleophosmin expression inhibited proliferation and induced apoptosis in salivary gland adenoid cystic carcinoma. *Journal of Oral Pathology and Medicine, 46*(3), 175-181.

Li, W. Y., Ng, Y. F., Zhang, H., Guo, Z. D., Guo, D. J., Kwan, Y. W., . . . Chan, S. W. (2014). Emodin elicits cytotoxicity in human lung adenocarcinoma A549 cells through inducing apoptosis. *Inflammopharmacology, 22*(2), 127-134.

Li, X., Wang, E., Zhao, Y. D., Ren, J. Q., Jin, P., Yao, K. T., & Marincola, F. M. (2006). Chromosomal imbalances in nasopharyngeal carcinoma: a meta-analysis of comparative genomic hybridization results. *Journal of Translational Medicine, 4*, 4.

Li, Y. Y., Chung, G. T., Lui, V. W., To, K. F., Ma, B. B., Chow, C., . . . Lo, K. W. (2017). Exome and genome sequencing of nasopharynx cancer identifies NF-κB pathway activating mutations. *Nature Communication, 8*, 14121.

Li, Z., & Hann, S. R. (2009). The Myc-nucleophosmin-ARF network: a complex web unveiled. *Cell Cycle, 8*(17), 2703-2707.

Lian, Y. F., Yuan, J., Cui, Q., Feng, Q. S., Xu, M., Bei, J. X., . . . Feng, L. (2016). Upregulation of KLHDC4 Predicts a Poor Prognosis in Human Nasopharyngeal Carcinoma. *PLoS One, 11*(3), e0152820.

Liao, J. M., Zhou, X., Gatignol, A., & Lu, H. (2014). Ribosomal proteins L5 and L11 co-operatively inactivate c-Myc via RNA-induced silencing complex. *Oncogene, 33*(41), 4916-4923.

Liao, Q., Guo, X., Li, X., Xiong, W., Yang, J., Chen, P., . . . Li, G. (2013). Prohibitin is an important biomarker for nasopharyngeal carcinoma progression and prognosis. *Eur Journal of Cancer Prevention, 22*(1), 68-76.

Licitra, L., Bernier, J., Cvitkovic, E., Grandi, C., Spinazzé, S., Bruzzi, P., . . . Molinari, R. (2003). Cancer of the nasopharynx. *Critical Review on Oncology and Hematology, 45*(2), 199-213.

Lim, M. J., & Wang, X. W. (2006). Nucleophosmin and human cancer. *Cancer Detection and Prevention, 30*(6), 481-490.

Lin, C. T., Chan, W. Y., Chen, W., Huang, H. M., Wu, H. C., Hsu, M. M., . . . Wang, C. C. (1993). Characterization of seven newly established nasopharyngeal carcinoma cell lines. *Laboratory Investigation, 68*(6), 716-727.

Lin, D. C., Meng, X., Hazawa, M., Nagata, Y., Varela, A. M., Xu, L., . . . Koeffler, H. P. (2014). The genomic landscape of nasopharyngeal carcinoma. *Nature Genetics, 46*(8), 866-871.

Lin, J. C., Jan, J. S., Hsu, C. Y., Liang, W. M., Jiang, R. S., & Wang, W. Y. (2003). Phase III study of concurrent chemoradiotherapy versus radiotherapy alone for advanced nasopharyngeal carcinoma: positive effect on overall and progression-free survival. *Journal of Clinical Oncology, 21*(4), 631-637.

Lindsey A. Torre, Freddie Bray, Rebecca L. Siegel , Jacques Ferlay , Joannie Lortet-Tieulent, & Ahmedin Jemal. (2015). Global cancer statistics, 2012. *CA: Cancer Journal for Clinicians, 65*(2), 87-108.

Lindström, M. S. (2009). Emerging functions of ribosomal proteins in gene-specific transcription and translation. *Biochemica et Biophysica Research Communication, 379*(2), 167-170.

Lindström, M. S. (2011). NPM1/B23: A Multifunctional Chaperone in Ribosome Biogenesis and Chromatin Remodeling. *Biochemistry Research International, 2011*, 195209.

Lindström, M. S. (2012). Elucidation of motifs in ribosomal protein S9 that mediate its nucleolar localization and binding to NPM1/nucleophosmin. *PLoS One, 7*(12), e52476.

Lindström, M. S., & Nistér, M. (2010). Silencing of ribosomal protein S9 elicits a multitude of cellular responses inhibiting the growth of cancer cells subsequent to p53 activation. *PLoS One, 5*(3), e9578.

Lindström, M. S., & Zhang, Y. (2008). Ribosomal protein S9 is a novel B23/NPM-binding protein required for normal cell proliferation. *Journal of Biological Chemistry, 283*(23), 15568-15576.

Liu, C. D., Chen, Y. L., Min, Y. L., Zhao, B., Cheng, C. P., Kang, M. S., . . . Peng, C. W. (2012). The nuclear chaperone nucleophosmin escorts an Epstein-Barr Virus nuclear antigen to establish transcriptional cascades for latent infection in human B cells. *PLoS Pathology, 8*(12), e1003084.

Liu, H., Liang, S., Yang, X., Ji, Z., Zhao, W., Ye, X., & Rui, J. (2015). RNAi-mediated RPL34 knockdown suppresses the growth of human gastric cancer cells. *Oncology Reports, 34*(5), 2267-2272.

Liu, Q., Zhou, J. P., Li, B., Huang, Z. C., Dong, H. Y., Li, G. Y., . . . Nie, S. L. (2013). Basic transcription factor 3 is involved in gastric cancer development and progression. *World Journal of Gastroenterology, 19*(28), 4495-4503.

Liu, X., Liu, D., Qian, D., Dai, J., An, Y., Jiang, S., . . . Liu, D. X. (2012). Nucleophosmin (NPM1/B23) interacts with activating transcription factor 5 (ATF5) protein and promotes proteasome- and caspase-dependent ATF5 degradation in hepatocellular carcinoma cells. *Journal of Biological Chemistry, 287*(23), 19599-19609.

Liu, Y., Beyer, A., & Aebersold, R. (2016). On the Dependency of Cellular Protein Levels on mRNA Abundance. *Cell, 165*(3), 535-550.

Liu, Y., Zhang, F., Zhang, X. F., Qi, L. S., Yang, L., Guo, H., & Zhang, N. (2012). Expression of nucleophosmin/NPM1 correlates with migration and invasiveness of colon cancer cells. *Journal of Biomedical Sciences, 19*, 53.

Livak, K. J., & Schmittgen, T. D. (2001). Analysis of relative gene expression data using real-time quantitative PCR and the 2(-Delta Delta C(T)) Method. *Methods, 25*(4), 402-408.

Llanos, S., & Serrano, M. (2010). Depletion of ribosomal protein L37 occurs in response to DNA damage and activates p53 through the L11/MDM2 pathway. *Cell Cycle, 9*(19), 4005-4012.

Lo, K. W., Kwong, J., Hui, A. B., Chan, S. Y., To, K. F., Chan, A. S., . . . Huang, D. P. (2001). High frequency of promoter hypermethylation of RASSF1A in nasopharyngeal carcinoma. *Cancer Research, 61*(10), 3877-3881.

Lo, K. W., Teo, P. M., Hui, A. B., To, K. F., Tsang, Y. S., Chan, S. Y., . . . Huang, D. P. (2000). High resolution allelotype of microdissected primary nasopharyngeal carcinoma. *Cancer Research, 60*(13), 3348-3353.

Lohrum, M. A., Ludwig, R. L., Kubbutat, M. H., Hanlon, M., & Vousden, K. H. (2003). Regulation of HDM2 activity by the ribosomal protein L11. *Cancer Cell, 3*(6), 577-587.

Londero, A. P., Orsaria, M., Tell, G., Marzinotto, S., Capodicasa, V., Poletto, M., . . . Mariuzzi, L. (2014). Expression and prognostic significance of APE1/Ref-1 and NPM1 proteins in high-grade ovarian serous cancer. *American Journal of Clinical Pathology, 141*(3), 404-414.

Loubeau, G., Boudra, R., Maquaire, S., Lours-Calet, C., Beaudoin, C., Verrelle, P., & Morel, L. (2014). NPM1 silencing reduces tumour growth and MAPK signalling in prostate cancer cells. *PLoS One, 9*(5), e96293.

Lu, C. C., Chen, J. C., Jin, Y. T., Yang, H. B., Chan, S. H., & Tsai, S. T. (2003). Genetic susceptibility to nasopharyngeal carcinoma within the HLA-A locus in Taiwanese. *International Journal of Cancer, 103*(6), 745-751.

Lu, C. C., Chen, J. C., Tsai, S. T., Jin, Y. T., Tsai, J. C., Chan, S. H., & Su, I. J. (2005). Nasopharyngeal carcinoma-susceptibility locus is localized to a 132 kb segment containing HLA-A using high-resolution microsatellite mapping. *International Journal of Cancer, 115*(5), 742-746.

Lung, H. L., Cheng, Y., Kumaran, M. K., Liu, E. T., Murakami, Y., Chan, C. Y., . . . Lung, M. L. (2004). Fine mapping of the 11q22-23 tumor suppressive region and involvement of TSLC1 in nasopharyngeal carcinoma. *International Journal of Cancer, 112*(4), 628-635.

Lung, M. L., Cheung, A. K., Ko, J. M., Lung, H. L., Cheng, Y., & Dai, W. (2014). The interplay of host genetic factors and Epstein-Barr virus in the development of nasopharyngeal carcinoma. *Chinese Journal of Cancer, 33*(11), 556-568.

Luo, L. Y., Herrera, I., Soosaipillai, A., & Diamandis, E. P. (2002). Identification of heat shock protein 90 and other proteins as tumour antigens by serological screening of an ovarian carcinoma expression library. *British Journal of Cancer, 87*(3), 339-343.

Luo, S., Zhao, J., Fowdur, M., Wang, K., Jiang, T., & He, M. (2016). Highly expressed ribosomal protein L34 indicates poor prognosis in osteosarcoma and its knockdown suppresses osteosarcoma proliferation probably through translational control. *Science Reports, 6*, 37690.

Ma, B. B., & Chan, A. T. (2005). Recent perspectives in the role of chemotherapy in the management of advanced nasopharyngeal carcinoma. *Cancer, 103*(1), 22-31.

Ma, X. R., Sim, E. U., Ling, T. Y., Tiong, T. S., Subramaniam, S. K., & Khoo, A. S. (2012). Expression trend of selected ribosomal protein genes in nasopharyngeal carcinoma. *Malays Journal of Medical Science, 19*(4), 23-30.

Maggi, L. B., Kuchenruether, M., Dadey, D. Y., Schwope, R. M., Grisendi, S., Townsend, R. R., . . . Weber, J. D. (2008). Nucleophosmin serves as a rate-limiting nuclear export chaperone for the Mammalian ribosome. *Molecular Cell Biology, 28*(23), 7050-7065.

Mainou, B. A., Everly, D. N., & Raab-Traub, N. (2005). Epstein-Barr virus latent membrane protein 1 CTAR1 mediates rodent and human fibroblast transformation through activation of PI3K. *Oncogene, 24*(46), 6917-6924.

Mao, M. J., Xue, N., Wang, X. P., Chi, P. D., Liu, Y. J., Huang, Q., . . . Liu, W. L. (2018). Chemokine CCL27 is a novel plasma biomarker for identification the nasopharyngeal carcinoma patients from the Epstein-Barr virus capsid antigen-specific IgA seropositive population. *BMC Cancer, 18*(1), 9.

Marechal, V., Elenbaas, B., Piette, J., Nicolas, J. C., & Levine, A. J. (1994). The ribosomal L5 protein is associated with mdm-2 and mdm-2-p53 complexes. *Molecular Cell Biology, 14*(11), 7414-7420.

Marks, J. E., Phillips, J. L., & Menck, H. R. (1998). The National Cancer Data Base report on the relationship of race and national origin to the histology of nasopharyngeal carcinoma. *Cancer, 83*(3), 582-588.

Martin, J. L. (2016). Validation of Reference Genes for Oral Cancer Detection Panels in a Prospective Blinded Cohort. *PLoS One, 11*(7), e0158462.

Matallanas, D., Romano, D., Yee, K., Meissl, K., Kucerova, L., Piazzolla, D., . . . O'neill, E. (2007). RASSF1A elicits apoptosis through an MST2 pathway directing proapoptotic transcription by the p73 tumor suppressor protein. *Molecular Cell, 27*(6), 962-975.

Matragkou, C. N., Papachristou, E. T., Tezias, S. S., Tsiftsoglou, A. S., Choli-Papadopoulou, T., & Vizirianakis, I. S. (2008). The potential role of ribosomal protein S5 on cell cycle arrest and initiation of murine erythroleukemia cell differentiation. *Journal of Cellular Biochemistry, 104*(4), 1477-1490.

Maya, R., Balass, M., Kim, S. T., Shkedy, D., Leal, J. F., Shifman, O., . . . Oren, M. (2001). ATM-dependent phosphorylation of Mdm2 on serine 395: role in p53 activation by DNA damage. *Genes and Development, 15*(9), 1067-1077.

McDonald, J. M., Pelloski, C. E., Ledoux, A., Sun, M., Raso, G., Komaki, R., . . . Aldape, K. (2008). Elevated phospho-S6 expression is associated with metastasis in adenocarcinoma of the lung. *Clinical Cancer Research, 14*(23), 7832-7837.

Meng, X., Tackmann, N. R., Liu, S., Yang, J., Dong, J., Wu, C., . . . Zhang, Y. (2016). RPL23 Links Oncogenic RAS Signaling to p53-Mediated Tumor Suppression. *Cancer Research, 76*(17), 5030-5039.

Michaux, L. (1845). Carcinome de base du crane, in. Godtfredsen E: Ophthalmologic and neurologic symptoms at malignant nasopharyngeal tumours; clinical study

comprising 454 cases: with special reference to histopathology and possibility of earlier recognition. *Acta Psychiatrica Scandinavica, 34*, 1-323.

Miliani de Marval, P. L., & Zhang, Y. (2011). The RP-Mdm2-p53 pathway and tumorigenesis. *Oncotarget, 2*(3), 234-238.

Mitrea, D. M., Grace, C. R., Buljan, M., Yun, M. K., Pytel, N. J., Satumba, J., . . . Kriwacki, R. W. (2014). Structural polymorphism in the N-terminal oligomerization domain of NPM1. *Proceedings of the National Academy of Sciences USA, 111*(12), 4466-4471.

Mizushima, S. N., M. (1970). Assembly mapping of 30S ribosomal proteins from E. coli. *Nature, 226*(5252), 1214.

Moniz, H., Gastou, M., Leblanc, T., Hurtaud, C., Crétien, A., Lécluse, Y., . . . Pédiatrique-SHIP, D. G. o. S. d. H. e. d. I. (2012). Primary hematopoietic cells from DBA patients with mutations in RPL11 and RPS19 genes exhibit distinct erythroid phenotype in vitro. *Cell Death and Diseases, 3*, e356.

Moore, S. B., Pearson, G. R., Neel, H. B., & Weiland, L. H. (1983). HLA and nasopharyngeal carcinoma in North American Caucasoids. *Tissue Antigens, 22*(1), 72-75.

Muir, C. S., Shanmugaratnam, K. (1967). *Cancer of the nasopharynx.* Paper presented at the Union for International Cancer Control, Munksgaard, Copenhagen.

Mukhopadhyay, R., Ray, P. S., Arif, A., Brady, A. K., Kinter, M., & Fox, P. L. (2008). DAPK-ZIPK-L13a axis constitutes a negative-feedback module regulating inflammatory gene expression. *Molecular Cell, 32*(3), 371-382.

Myung, J., Kim, K. B., & Crews, C. M. (2001). The ubiquitin-proteasome pathway and proteasome inhibitors. *Medical Research Review, 21*(4), 245-273.

Mäkitie, A. A., MacMillan, C., Ho, J., Shi, W., Lee, A., O'Sullivan, B., . . . Kamel-Reid, S. (2003). Loss of p16 expression has prognostic significance in human nasopharyngeal carcinoma. *Clinical Cancer Research, 9*(6), 2177-2184.

Nag, S., Qin, J., Srivenugopal, K. S., Wang, M., & Zhang, R. (2013). The MDM2-p53 pathway revisited. *Journal of Biomedical Research, 27*(4), 254-271.

Nagao-Kitamoto, H., Setoguchi, T., Kitamoto, S., Nakamura, S., Tsuru, A., Nagata, M., . . . Komiya, S. (2015). Ribosomal protein S3 regulates GLI2-mediated osteosarcoma invasion. *Cancer Letters, 356*(2 Pt B), 855-861.

Nakanishi, Y., Wakisaka, N., Kondo, S., Endo, K., Sugimoto, H., Hatano, M., . . . Yoshizaki, T. (2017). Progression of understanding for the role of Epstein-Barr virus and management of nasopharyngeal carcinoma. *Cancer Metastasis Review, 36*(3), 435-447.

Nakao, A., Yoshihama, M., & Kenmochi, N. (2004). RPG: the Ribosomal Protein Gene database. *Nucleic Acids Research, 32*(Database issue), D168-170.

Nakhoul, H., Ke, J., Zhou, X., Liao, W., Zeng, S. X., & Lu, H. (2014). Ribosomopathies: mechanisms of disease. *Clinical Medicine Insights: Blood Disorders, 7*, 7-16.

Nam, J. M., McLaughlin, J. K., & Blot, W. J. (1992). Cigarette smoking, alcohol, and nasopharyngeal carcinoma: a case-control study among U.S. whites. *Journal of the National Cancer Institute, 84*(8), 619-622.

Naoe, T., Suzuki, T., Kiyoi, H., & Urano, T. (2006). Nucleophosmin: a versatile molecule associated with hematological malignancies. *Cancer Science, 97*(10), 963-969.

Narla, A., Hurst, S. N., & Ebert, B. L. (2011). Ribosome defects in disorders of erythropoiesis. *International Journal of Hematology, 93*(2), 144-149.

National Cancer Registry, M. o. H., Malaysia. (2017). *Summary of Malaysian National Cancer Registry Report 2007-2011*. Retrieved from Putrajaya, Malaysia:

Ng, T. P. (1986). A case-referent study of cancer of the nasal cavity and sinuses in Hong Kong. *International Journal of Epidemiology, 15*(2), 171-175.

Nicolas, E., Parisot, P., Pinto-Monteiro, C., de Walque, R., De Vleeschouwer, C., & Lafontaine, D. L. (2016). Involvement of human ribosomal proteins in nucleolar structure and p53-dependent nucleolar stress. *Nature Communication, 7*, 11390.

Nigro, E., Imperlini, E., Scudiero, O., Monaco, M. L., Polito, R., Mazzarella, G., . . . Daniele, A. (2015). Differentially expressed and activated proteins associated with non small cell lung cancer tissues. *Respiratory Research, 16*, 74.

Nissan, T. A., Bassler, J., Petfalski, E., Tollervey, D., & Hurt, E. (2002). 60S pre-ribosome formation viewed from assembly in the nucleolus until export to the cytoplasm. *EMBO Journal, 21*(20), 5539-5547.

Nosrati, N., Kapoor, N. R., & Kumar, V. (2015). DNA damage stress induces the expression of ribosomal protein S27a gene in a p53-dependent manner. *Gene, 559*(1), 44-51.

O'Donohue, M. F., Choesmel, V., Faubladier, M., Fichant, G., & Gleizes, P. E. (2010). Functional dichotomy of ribosomal proteins during the synthesis of mammalian 40S ribosomal subunits. *Journal of Cell Biology, 190*(5), 853-866.

Odreman, F., Vindigni, M., Gonzales, M. L., Niccolini, B., Candiano, G., Zanotti, B., . . . Vindigni, A. (2005). Proteomic studies on low- and high-grade human brain astrocytomas. *Journal of Proteome Research, 4*(3), 698-708.

Ofir-Rosenfeld, Y., Boggs, K., Michael, D., Kastan, M. B., & Oren, M. (2008). Mdm2 regulates p53 mRNA translation through inhibitory interactions with ribosomal protein L26. *Molecular Cell, 32*(2), 180-189.

Oler, G., Camacho, C. P., Hojaij, F. C., Michaluart, P., Riggins, G. J., & Cerutti, J. M. (2008). Gene expression profiling of papillary thyroid carcinoma identifies transcripts correlated with BRAF mutational status and lymph node metastasis. *Clinical Cancer Research, 14*(15), 4735-4742.

Pacific., W. R. O. f. t. W. (1982). *Report of the symposium on nasopharyngeal carcinoma.* Paper presented at the Symposium on Nasopharyngeal Carcinoma., Manila, Philippines.

Pagano, J. S., Blaser, M., Buendia, M. A., Damania, B., Khalili, K., Raab-Traub, N., & Roizman, B. (2004). Infectious agents and cancer: criteria for a causal relation. *Seminars in Cancer Biology, 14*(6), 453-471.

Palade, G. E. (1955). A small particulate component of the cytoplasm. *Journal of Biophysics Biochemistry and Cytology, 1*(1), 59-68.

Palve, V., Pareek, M., Krishnan, N. M., Siddappa, G., Suresh, A., Kuriakose, M. A., & Panda, B. (2018). A minimal set of internal control genes for gene expression studies in head and neck squamous cell carcinoma. *PeerJournal, 6*, e5207.

Pan, Z. G., Kashuba, V. I., Liu, X. Q., Shao, J. Y., Zhang, R. H., Jiang, J. H., . . . Zeng, Y. X. (2005). High frequency somatic mutations in RASSF1A in nasopharyngeal carcinoma. *Cancer Biology and Therapy, 4*(10), 1116-1122.

Peng, H., Tang, L. L., Liu, X., Chen, L., Li, W. F., Mao, Y. P., . . . Ma, J. (2018). Anti-epidermal growth factor receptor therapy concurrently with induction chemotherapy in locoregionally advanced nasopharyngeal carcinoma. *Cancer Science, 109*(5), 1609-1616.

Pestova, T. V., Kolupaeva, V. G., Lomakin, I. B., Pilipenko, E. V., Shatsky, I. N., Agol, V. I., & Hellen, C. U. (2001). Molecular mechanisms of translation initiation in

eukaryotes. *Proceedings of the National Academy of Sciences USA, 98*(13), 7029-7036.

Picksley, S. M., & Lane, D. P. (1993). The p53-mdm2 autoregulatory feedback loop: a paradigm for the regulation of growth control by p53? *Bioessays, 15*(10), 689-690.

Pimtanothai, N., Kangwanshiratada, O., & Charoenwongse, P. (2003). Serological analysis of human leukocyte antigens-A and -B antigens in Thai patients with nasopharyngeal carcinoma. *Journal of the Medical Association of Thailand, 86 Suppl 2*, S237-241.

Plafker, S. M., & Macara, I. G. (2002). Ribosomal protein L12 uses a distinct nuclear import pathway mediated by importin 11. *Molecular Cell Biology, 22*(4), 1266-1275.

Platonova, O., Akey, I. V., Head, J. F., & Akey, C. W. (2011). Crystal structure and function of human nucleoplasmin (npm2): a histone chaperone in oocytes and embryos. *Biochemistry, 50*(37), 8078-8089.

Plocik, A. M., & Guthrie, C. (2012). Diverse forms of RPS9 splicing are part of an evolving autoregulatory circuit. *PLoS Genetics, 8*(3), e1002620.

Poddar, D., Basu, A., Baldwin, W. M., Kondratov, R. V., Barik, S., & Mazumder, B. (2013). An extraribosomal function of ribosomal protein L13a in macrophages resolves inflammation. *Journal of Immunology, 190*(7), 3600-3612.

Pogue-Geile, K., Geiser, J. R., Shu, M., Miller, C., Wool, I. G., Meisler, A. I., & Pipas, J. M. (1991). Ribosomal protein genes are overexpressed in colorectal cancer: isolation of a cDNA clone encoding the human S3 ribosomal protein. *Molecular Cell Biology, 11*(8), 3842-3849.

Pérez-Magán, E., Rodríguez de Lope, A., Ribalta, T., Ruano, Y., Campos-Martín, Y., Pérez-Bautista, G., . . . Meléndez, B. (2010). Differential expression profiling analyses identifies downregulation of 1p, 6q, and 14q genes and overexpression of 6p histone

cluster 1 genes as markers of recurrence in meningiomas. *Neuro-Oncology, 12*(12), 1278-1290.

Qi, Y., Li, X., Chang, C., Xu, F., He, Q., Zhao, Y., & Wu, L. (2017). Ribosomal protein L23 negatively regulates cellular apoptosis via the RPL23/Miz-1/c-Myc circuit in higher-risk myelodysplastic syndrome. *Science Reports, 7*(1), 2323.

Qin, F. X., Shao, H. Y., Chen, X. C., Tan, S., Zhang, H. J., Miao, Z. Y., . . . Zhang, L. (2011). Knockdown of NPM1 by RNA interference inhibits cells proliferation and induces apoptosis in leukemic cell line. *International Journal of Medical Science, 8*(4), 287-294.

Qiu, G. H., Tan, L. K., Loh, K. S., Lim, C. Y., Srivastava, G., Tsai, S. T., . . . Tao, Q. (2004). The candidate tumor suppressor gene BLU, located at the commonly deleted region 3p21.3, is an E2F-regulated, stress-responsive gene and inactivated by both epigenetic and genetic mechanisms in nasopharyngeal carcinoma. *Oncogene, 23*(27), 4793-4806.

Qiu, S. W., Wan, Y. L., Wang, M., & Wang, J. X. (2017). Effects of NPM1 gene expression on acute myeloid leukemia cell lines and its mechanism. *Zhonghua Xue Ye Xue Za Zhi, 38*(11), 940-944.

Rabl, J., Leibundgut, M., Ataide, S. F., Haag, A., & Ban, N. (2011). Crystal structure of the eukaryotic 40S ribosomal subunit in complex with initiation factor 1. *Science, 331*(6018), 730-736.

Rao, S., Cai, K. Q., Stadanlick, J. E., Greenberg-Kushnir, N., Solanki-Patel, N., Lee, S. Y., . . . Wiest, D. L. (2016). Ribosomal Protein Rpl22 Controls the Dissemination of T-cell Lymphoma. *Cancer Research, 76*(11), 3387-3396.

Rao, S., Lee, S. Y., Gutierrez, A., Perrigoue, J., Thapa, R. J., Tu, Z., . . . Wiest, D. L. (2012). Inactivation of ribosomal protein L22 promotes transformation by induction of the stemness factor, Lin28B. *Blood, 120*(18), 3764-3773.

Reddy, S. P., Raslan, W. F., Gooneratne, S., Kathuria, S., & Marks, J. E. (1995). Prognostic significance of keratinization in nasopharyngeal carcinoma. *American Journal of Otolaryngology, 16*(2), 103-108.

Redman, K. L., & Rechsteiner, M. (1989). Identification of the long ubiquitin extension as ribosomal protein S27a. *Nature, 338*(6214), 438-440.

Regaud, C. (1921). Lympho-épitheliome de l'hypopharynx traité par laroentgenthérapie. *Bulletin de la Societe de Franc Otorhinolaryngol., 34*, 209-214.

Ren, Z., Aerts, J. L., Vandenplas, H., Wang, J. A., Gorbenko, O., Chen, J. P., . . . De Grève, J. (2016). Phosphorylated STAT5 regulates p53 expression via BRCA1/BARD1-NPM1 and MDM2. *Cell Death and Diseases, 7*(12), e2560.

Rickinson, A. B., & Kieff, E. (2001). Epstein-Barr virus. In *Field's virology* (4th edition ed., pp. 2575–2627). Philadelphia, Pa, USA: Lippincott Williams & Wilkins.

Roberts, R. B. (1958). "Introduction". In *Microsomal Particles and Protein Synthesis* (pp. viii). New York: Pergamon Press, Inc.

Rodway, H., Llanos, S., Rowe, J., & Peters, G. (2004). Stability of nucleolar versus non-nucleolar forms of human p14(ARF). *Oncogene, 23*(37), 6186-6192.

Rowe, M., Fitzsimmons, L., & Bell, A. I. (2014). Epstein-Barr virus and Burkitt lymphoma. *Chinese Journal of Cancer, 33*(12), 609-619.

Ruggero, D., & Pandolfi, P. P. (2003). Does the ribosome translate cancer? *Nature Review on Cancer, 3*(3), 179-192.

Rujkijyanont, P., Adams, S. L., Beyene, J., & Dror, Y. (2009). Bone marrow cells from patients with Shwachman-Diamond syndrome abnormally express genes involved in ribosome biogenesis and RNA processing. *British Journal of Haematology, 145*(6), 806-815.

Russo, A., Esposito, D., Catillo, M., Pietropaolo, C., Crescenzi, E., & Russo, G. (2013). Human rpL3 induces G_1/S arrest or apoptosis by modulating p21 (waf1/cip1) levels in a p53-independent manner. *Cell Cycle, 12*(1), 76-87.

Russo, A., & Russo, G. (2017). Ribosomal Proteins Control or Bypass p53 during Nucleolar Stress. *International Journal of Molecular Science, 18*(1).

Russo, A., Saide, A., Cagliani, R., Cantile, M., Botti, G., & Russo, G. (2016). rpL3 promotes the apoptosis of p53 mutated lung cancer cells by down-regulating CBS and NFκB upon 5-FU treatment. *Science Reports, 6*, 38369.

Russo, N., Wang, X., Liu, M., Banerjee, R., Goto, M., Scanlon, C., . . . D'Silva, N. J. (2013). A novel approach to biomarker discovery in head and neck cancer using an autoantibody signature. *Oncogene, 32*(42), 5026-5037.

Salek-Ardakani, S., Arrand, J. R., & Mackett, M. (2002). Epstein-Barr virus encoded interleukin-10 inhibits HLA-class I, ICAM-1, and B7 expression on human monocytes: implications for immune evasion by EBV. *Virology, 304*(2), 342-351.

Salvador, J. M., Brown-Clay, J. D., & Fornace, A. J. (2013). Gadd45 in stress signaling, cell cycle control, and apoptosis. *Advances in Experimental Medical Biology, 793*, 1-19.

Shanmugaratnam, K., Chan, S. H., de-Thé, G., Goh, J. E., Khor, T. H., Simons, M. J., & Tye, C. Y. (1979). Histopathology of nasopharyngeal carcinoma: correlations with epidemiology, survival rates and other biological characteristics. *Cancer, 44*(3), 1029-1044.

Shanmugaratnam, K., Sobin, L. H. (1978). *Nasopharyngeal carcinoma.* Paper presented at the International histological classification of tumors., Geneva.

Shanmugaratnam, K., Sobin, L. H., Barnes, L. (1991). *World Health Organization histological classification of tumours. Histological typing of tumours of he upper respiratory tract and ear.*, Berlin Heidelberg.

Shav-Tal, Y., Blechman, J., Darzacq, X., Montagna, C., Dye, B. T., Patton, J. G., . . . Zipori, D. (2005). Dynamic sorting of nuclear components into distinct nucleolar caps during transcriptional inhibition. *Molecular Biology of the Cell, 16*(5), 2395-2413.

Shen, B., Arese, M., Gualandris, A., & Rifkin, D. B. (1998). Intracellular association of FGF-2 with the ribosomal protein L6/TAXREB107. *Biochemica et Biophysica Research Communication, 252*(2), 524-528.

Shi, D., Shi, H., Sun, D., Chen, J., Zhang, X., Wang, X., . . . Feng, L. (2017). Nucleocapsid Interacts with NPM1 and Protects it from Proteolytic Cleavage, Enhancing Cell Survival, and is Involved in PEDV Growth. *Science Reports, 7*, 39700.

Shi, S., Cao, X., Gu, M., You, B., Shan, Y., & You, Y. (2015). Upregulated Expression of SOX4 Is Associated with Tumor Growth and Metastasis in Nasopharyngeal Carcinoma. *Disease Markers, 2015*, 658141.

Shi, Y., Zhai, H., Wang, X., Han, Z., Liu, C., Lan, M., . . . Fan, D. (2004). Ribosomal proteins S13 and L23 promote multidrug resistance in gastric cancer cells by suppressing drug-induced apoptosis. *Experimental Cell Research, 296*(2), 337-346.

Shivakumar, L., Minna, J., Sakamaki, T., Pestell, R., & White, M. A. (2002). The RASSF1A tumor suppressor blocks cell cycle progression and inhibits cyclin D1 accumulation. *Molecular Cell Biology, 22*(12), 4309-4318.

Sim, E. U., Chan, S. L., Ng, K. L., Lee, C. W., & Narayanan, K. (2016). Human Ribosomal Proteins RPeL27, RPeL43, and RPeL41 Are Upregulated in Nasopharyngeal Carcinoma Cell Lines. *Disease Markers, 2016*, 5179594.

Sim, E. U., Ng, K. L., Lee, C. W., & Narayanan, K. (2017). The u*S8* , *uS4* , *eS31* , and *uL14* Ribosomal Protein Genes Are Dysregulated in Nasopharyngeal Carcinoma Cell Lines. *Biomedical Research International*, 4876954.

Sim, E. U. H., Toh, A. K. L., & Tiong, T. S. (2008). Short Communication: Preliminary Findings of Down-regulated Genes in Nasopharyngeal Carcinoma. *Asia Pacific Journal of Molecular Biology and Biotechnology, 16*(3), 79-84.

Simons, M. J., Wee, G. B., Day, N. E., Morris, P. J., Shanmugaratnam, K., & De-Thé., G. B. (1974). Immunogenetic aspects of nasopharyngeal carcinoma: I. Differences in HL-A antigen profiles between patients and control groups. . *International Journal of Cancer., 13*(1), 122-134.

Sloan, K. E., Bohnsack, M. T., & Watkins, N. J. (2013). The 5S RNP couples p53 homeostasis to ribosome biogenesis and nucleolar stress. *Cell Reports, 5*(1), 237-247.

Smolock, E. M., Korshunov, V. A., Glazko, G., Qiu, X., Gerloff, J., & Berk, B. C. (2012). Ribosomal protein L17, RpL17, is an inhibitor of vascular smooth muscle growth and carotid intima formation. *Circulation, 126*(20), 2418-2427.

Society., A. C. (2017). *Cancer Facts & Figures 2017.* Retrieved from Atlanta, USA.:

Song, M. J., Jung, C. K., Park, C. H., Hur, W., Choi, J. E., Bae, S. H., . . . Yoon, S. K. (2011). RPL36 as a prognostic marker in hepatocellular carcinoma. *Pathology International, 61*(11), 638-644.

Spruck, C. H., Tsai, Y. C., Huang, D. P., Yang, A. S., Rideout, W. M., Gonzalez-Zulueta, M., . . . Jones, P. A. (1992). Absence of p53 gene mutations in primary nasopharyngeal carcinomas. *Cancer Research, 52*(17), 4787-4790.

Squatrito, M., Mancino, M., Donzelli, M., Areces, L. B., & Draetta, G. F. (2004). EBP1 is a nucleolar growth-regulating protein that is part of pre-ribosomal ribonucleoprotein complexes. *Oncogene, 23*(25), 4454-4465.

Sriamporn, S., Vatanasapt, V., Pisani, P., Yongchaiyudha, S., & Rungpitarangsri, V. (1992). Environmental risk factors for nasopharyngeal carcinoma: a case-control study in northeastern Thailand. *Cancer Epidemiology Biomarkers Prevention, 1*(5), 345-348.

Stad, R., Ramos, Y. F., Little, N., Grivell, S., Attema, J., van Der Eb, A. J., & Jochemsen, A. G. (2000). Hdmx stabilizes Mdm2 and p53. *Journal of Biological Chemistry, 275*(36), 28039-28044.

Stelow, E. B., & Wenig, B. M. (2017). Update From The 4th Edition of the World Health Organization Classification of Head and Neck Tumours: Nasopharynx. *Head Neck Pathology, 11*(1), 16-22.

Stelter, P., Huber, F. M., Kunze, R., Flemming, D., Hoelz, A., & Hurt, E. (2015). Coordinated Ribosomal L4 Protein Assembly into the Pre-Ribosome Is Regulated by Its Eukaryote-Specific Extension. *Molecular Cell, 58*(5), 854-862.

Stowe, R. P., Pierson, D.L., Barrett, A.D. (2001). Elevated stress hormone levels relate to Epstein-Barr virus reactivation in astronauts. *Psychosomatic Medicine, 11*, 215-225.

Strunk, B. S., Loucks, C. R., Su, M., Vashisth, H., Cheng, S., Schilling, J., . . . Skiniotis, G. (2011). Ribosome assembly factors prevent premature translation initiation by 40S assembly intermediates. *Science, 333*(6048), 1449-1453.

Su, X. L., Hou, Y. L., Yan, X. H., Ding, X., Hou, W. R., Sun, B., & Zhang, S. N. (2012). Expression, purification, and evaluation for anticancer activity of ribosomal protein L31 gene (RPL31) from the giant panda (Ailuropoda melanoleuca). *Molecular Biology Reports, 39*(9), 8945-8954.

Sun, B., Hou, Y. L., Hou, W. R., Zhang, S. N., Ding, X., & Su, X. L. (2012). cDNA cloning, overexpression, purification and pharmacologic evaluation for anticancer activity of ribosomal protein L23A gene (RPL23A) from the Giant Panda. *International Journal of Molecular Science, 13*(2), 2133-2147.

Sun, X. X., DeVine, T., Challagundla, K. B., & Dai, M. S. (2011). Interplay between ribosomal protein S27a and MDM2 protein in p53 activation in response to ribosomal stress. *Journal of Biological Chemistry, 286*(26), 22730-22741.

Sun, X. X., Wang, Y. G., Xirodimas, D. P., & Dai, M. S. (2010). Perturbation of 60 S ribosomal biogenesis results in ribosomal protein L5- and L11-dependent p53 activation. *Journal of Biological Chemistry, 285*(33), 25812-25821.

Sun, Y., Hegamyer, G., & Colburn, N. H. (1993). Nasopharyngeal carcinoma shows no detectable retinoblastoma susceptibility gene alterations. *Oncogene, 8*(3), 791-795.

Symes, A. J., Eilertsen, M., Millar, M., Nariculam, J., Freeman, A., Notara, M., . . . Ahmed, A. (2013). Quantitative analysis of BTF3, HINT1, NDRG1 and ODC1 protein over-expression in human prostate cancer tissue. *PLoS One, 8*(12), e84295.

Takagi, M., Absalon, M. J., McLure, K. G., & Kastan, M. B. (2005). Regulation of p53 translation and induction after DNA damage by ribosomal protein L26 and nucleolin. *Cell, 123*(1), 49-63.

Takenawa, T., Kuramitsu, Y., Wang, Y., Okada, F., Tokuda, K., Kitagawa, T., . . . Nakamura, K. (2013). Proteomic analysis showed down-regulation of nucleophosmin in

progressive tumor cells compared to regressive tumor cells. *Anticancer Research, 33*(1), 153-160.

Tang, C. E., Tan, T., Li, C., Chen, Z. C., Ruan, L., Wang, H. H., . . . Xiao, Z. Q. (2010). Identification of Galectin-1 as a novel biomarker in nasopharyngeal carcinoma by proteomic analysis. *Oncology Reports, 24*(2), 495-500.

Taweevisit, M. (2007). Overexpression of p53 and neoplastic cell proliferation in undifferentiated nasopharyngeal carcinoma. *Southeast Asian Journal of Tropical Medicine and Public Health, 38*(1), 136-140.

Teng, T., Thomas, G., & Mercer, C. A. (2013). Growth control and ribosomopathies. *Current Opinion in Genetics and Development, 23*(1), 63-71.

Teng, Z. P., Ooka, T., Huang, D. P., & Zeng, Y. (1996). Detection of Epstein-Barr Virus DNA in well and poorly differentiated nasopharyngeal carcinoma cell lines. *Virus Genes, 13*(1), 53-60.

Thomas, F., & Kutay, U. (2003). Biogenesis and nuclear export of ribosomal subunits in higher eukaryotes depend on the CRM1 export pathway. *Journal of Cell Science, 116*(Pt 12), 2409-2419.

Thompson, J. D., Higgins, D. G., & Gibson, T. J. (1994). CLUSTAL W: improving the sensitivity of progressive multiple sequence alignment through sequence weighting, position-specific gap penalties and weight matrix choice. *Nucleic Acids Research, 22*(22), 4673-4680.

Thomson, E., Ferreira-Cerca, S., & Hurt, E. (2013). Eukaryotic ribosome biogenesis at a glance. *Journal of Cell Science, 126*(Pt 21), 4815-4821.

Toussirot, E., & Roudier, J. (2008). Epstein-Barr virus in autoimmune diseases. *Best Practice & Research. Clinical Rheumatology, 22*(5), 883-896.

Traub, P., & Nomura, M. (1968a). Structure and function of E. coli ribosomes. V. Reconstitution of functionally active 30S ribosomal particles from RNA and proteins. *Proceedings of the National Academy of Science USA, 59*(3), 777-784.

Traub, P., & Nomura, M. (1968b). Structure and function of Escherichia coli ribosomes. I. Partial fractionation of the functionally active ribosomal proteins and reconstitution of artificial subribosomal particles. *Journal of Molecular Biology, 34*(3), 575-593.

Trotter , W. (1911). On certain Clinically Obscure Tumours of the Nasopharynx. *British Medical Journal, 2*, 1057.

Tsao, S. W., Tramoutanis, G., Dawson, C. W., Lo, A. K., & Huang, D. P. (2002). The significance of LMP1 expression in nasopharyngeal carcinoma. *Seminars on Cancer Biology, 12*(6), 473-487.

Tsao, S. W., Wang, X., Liu, Y., Cheung, Y. C., Feng, H., Zheng, Z., . . . Huang, D. P. (2002). Establishment of two immortalized nasopharyngeal epithelial cell lines using SV40 large T and HPV16E6/E7 viral oncogenes. *Biochimica et Biophysica Acta, 1590*(1-3), 150-158.

Tschochner, H., & Hurt, E. (2003). Pre-ribosomes on the road from the nucleolus to the cytoplasm. *Trends in Cell Biology, 13*(5), 255-263.

Tsofack, S. P., Meunier, L., Sanchez, L., Madore, J., Provencher, D., Mes-Masson, A. M., & Lebel, M. (2013). Low expression of the X-linked ribosomal protein S4 in human serous epithelial ovarian cancer is associated with a poor prognosis. *BMC Cancer, 13*, 303.

Tulalamba, W., & Janvilisri, T. (2012). Nasopharyngeal carcinoma signaling pathway: an update on molecular biomarkers. *Internaitonal Journal of Cell Biology, 2012*, 594681.

Ueda, T., Kohama, Y., Kuge, A., Kido, E., & Sakurai, H. (2017). GADD45 family proteins suppress JNK signaling by targeting MKK7. *Archives of Biochemistry and Biophysics*, *635*, 1-7.

van Beek, J., zur Hausen, A., Klein Kranenbarg, E., van de Velde, C. J., Middeldorp, J. M., van den Brule, A. J., . . . Bloemena, E. (2004). EBV-positive gastric adenocarcinomas: a distinct clinicopathologic entity with a low frequency of lymph node involvement. *Journal of Clinical Oncology*, *22*(4), 664-670.

Vascotto, C., Fantini, D., Romanello, M., Cesaratto, L., Deganuto, M., Leonardi, A., . . . Tell, G. (2009). APE1/Ref-1 interacts with NPM1 within nucleoli and plays a role in the rRNA quality control process. *Molecular Cell Biology*, *29*(7), 1834-1854.

Vincent, M., Oved, K., Morag, A., Pasmanik-Chor, M., Oron-Karni, V., Shomron, N., & Gurwitz, D. (2012). Genome-wide transcriptomic variations of human lymphoblastoid cell lines: insights from pairwise gene-expression correlations. *Pharmacogenomics*, *13*(16), 1893-1904.

Vogelstein, B., Lane, D., & Levine, A. J. (2000). Surfing the p53 network. *Nature*, *408*(6810), 307-310.

Vogelstein, B., Papadopoulos, N., Velculescu, V. E., Zhou, S., Diaz, L. A., & Kinzler, K. W. (2013). Cancer genome landscapes. *Science*, *339*(6127), 1546-1558.

Volarevic, S., Stewart, M. J., Ledermann, B., Zilberman, F., Terracciano, L., Montini, E., . . . Thomas, G. (2000). Proliferation, but not growth, blocked by conditional deletion of 40S ribosomal protein S6. *Science*, *288*(5473), 2045-2047.

Waller, J. P., & Harris, J. I. (1961). Studies on the composition of the protein from Escherichia coli ribosomes. *Proceedings of the National Academy of Science USA*, *47*, 18-23.

Wang, A., Xu, S., Zhang, X., He, J., Yan, D., Yang, Z., & Xiao, S. (2011). Ribosomal protein RPL41 induces rapid degradation of ATF4, a transcription factor critical for tumour cell survival in stress. *Journal of Pathology*, *225*(2), 285-292.

Wang, C. J., Frånbergh-Karlson, H., Wang, D. W., Arbman, G., Zhang, H., & Sun, X. F. (2013). Clinicopathological significance of BTF3 expression in colorectal cancer. *Tumour Biology*, *34*(4), 2141-2146.

Wang, H., Xie, B., Kong, Y., Tao, Y., Yang, G., Gao, M., . . . Wu, X. (2016). Overexpression of RPS27a contributes to enhanced chemoresistance of CML cells to imatinib by the transactivated STAT3. *Oncotarget, 7*(14), 18638-18650.

Wang, H., Yu, J., Zhang, L., Xiong, Y., Chen, S., Xing, H., . . . Wang, J. (2014). RPS27a promotes proliferation, regulates cell cycle progression and inhibits apoptosis of leukemia cells. *Biochemica et Biophysica Research Communication, 446*(4), 1204-1210.

Wang, H., Zhao, L. N., Li, K. Z., Ling, R., Li, X. J., & Wang, L. (2006). Overexpression of ribosomal protein L15 is associated with cell proliferation in gastric cancer. *BMC Cancer*, *6*, 91.

Wang, M., Hu, Y., & Stearns, M. E. (2009). RPS2: a novel therapeutic target in prostate cancer. *Journal of Experimental and Clinical Cancer Research*, *28*, 6.

Wang, Q., Yang, C., Zhou, J., Wang, X., Wu, M., & Liu, Z. (2001). Cloning and characterization of full-length human ribosomal protein L15 cDNA which was overexpressed in esophageal cancer. *Gene, 263*(1-2), 205-209.

Wang, S., Huang, J., He, J., Wang, A., Xu, S., Huang, S. F., & Xiao, S. (2010). RPL41, a small ribosomal peptide deregulated in tumors, is essential for mitosis and centrosome integrity. *Neoplasia, 12*(3), 284-293.

Wang, S., Lu, L. C., Fang, W. Y., & Yao, K. T. (2007). Differentially expressed transcription factor-related genes in nasopharyngeal carcinoma and nasopharyngeal tissues. *Nan Fang Yi Ke Da Xue Xue Bao, 27*(2), 146-149.

Wang, W., Nag, S., Zhang, X., Wang, M. H., Wang, H., Zhou, J., & Zhang, R. (2015). Ribosomal proteins and human diseases: pathogenesis, molecular mechanisms, and therapeutic implications. *Medical Research Review, 35*(2), 225-285.

Wang, Z., Hou, J., Lu, L., Qi, Z., Sun, J., Gao, W., . . . Yang, G. (2013). Small ribosomal protein subunit S7 suppresses ovarian tumorigenesis through regulation of the PI3K/AKT and MAPK pathways. *PLoS One, 8*(11), e79117.

Wanzel, M., Russ, A. C., Kleine-Kohlbrecher, D., Colombo, E., Pelicci, P. G., & Eilers, M. (2008). A ribosomal protein L23-nucleophosmin circuit coordinates Mizl function with cell growth. *Nature Cell Biology, 10*(9), 1051-1061.

Warner, J. R., & McIntosh, K. B. (2009). How common are extraribosomal functions of ribosomal proteins? *Molecular Cell, 34*(1), 3-11.

Warner, J. R., Vilardell, J., & Sohn, J. H. (2001). Economics of ribosome biosynthesis. *Cold Spring Harbour Symposia on Quantitative Biology, 66*, 567-574.

Weber, J. D., Taylor, L. J., Roussel, M. F., Sherr, C. J., & Bar-Sagi, D. (1999). Nucleolar Arf sequesters Mdm2 and activates p53. *Nature Cell Biology, 1*(1), 20-26.

Wee, J. T., Ha, T. C., Loong, S. L., & Qian, C. N. (2010). Is nasopharyngeal cancer really a "Cantonese cancer"? *Chinese Journal of Cancer, 29*(5), 517-526.

Wei, J., Kishton, R. J., Angel, M., Conn, C. S., Dalla-Venezia, N., Marcel, V., . . . Yewdell, J. W. (2019). Ribosomal Proteins Regulate MHC Class I Peptide Generation for Immunosurveillance. *Molecular Cell*.

Wei, S., Chen, X., McGraw, K., Zhang, L., Komrokji, R., Clark, J., . . . List, A. (2013). Lenalidomide promotes p53 degradation by inhibiting MDM2 auto-ubiquitination in myelodysplastic syndrome with chromosome 5q deletion. *Oncogene, 32*(9), 1110-1120.

Wenig, B. M. (2015). *Atlas of Head and Neck Pathology* . (Third edition. ed.). Toronto: Elsevier Health Sciences.

West, S., Hildesheim, A., & Dosemeci, M. (1993). Non-viral risk factors for nasopharyngeal carcinoma in the Philippines: results from a case-control study. *International Journal of Cancer, 55*(5), 722-727.

Wiese, K. E., Walz, S., von Eyss, B., Wolf, E., Athineos, D., Sansom, O., & Eilers, M. (2013). The role of MIZ-1 in MYC-dependent tumorigenesis. *Cold Spring Harb Perspectives in Medicine, 3*(12), a014290.

Wilson-Edell, K. A., Kehasse, A., Scott, G. K., Yau, C., Rothschild, D. E., Schilling, B., . . . Benz, C. C. (2014). RPL24: a potential therapeutic target whose depletion or acetylation inhibits polysome assembly and cancer cell growth. *Oncotarget, 5*(13), 5165-5176.

Wittmann, H. G., Stöfflet, G., Hindennach, I., Kurland, C. G., Birge, E. A., Randall-Hazelbauer, L., . . . Bickle, T. A. (1971). Correlation of 30S ribosomal proteins of Escherichia coli isolated in different laboratories. *Molecular Genetics and Genemics, 111*(4), 327-333.

Wittmann-Liebold, B., Kopke, A. K. E., Arndt, E., Kromer, W., Hatakeyama, T., & Wittmann, H. G. (1990). Sequence comparison and evolution of ribosomal proteins and their genes. In W. E. Hill, A, R. A. Garrett, P. B. Moore, D. Schlessigner, & J.

R. Warner (Eds.), *The Ribosome Structure, Function and Evolution* (pp. 598-616). Washington DC, USA: American Society for Microbiology.

Wong, J. M., Mafune, K., Yow, H., Rivers, E. N., Ravikumar, T. S., Steele, G. D., & Chen, L. B. (1993). Ubiquitin-ribosomal protein S27a gene overexpressed in human colorectal carcinoma is an early growth response gene. *Cancer Research, 53*(8), 1916-1920.

Wool, I. G. (1979). The structure and function of eukaryotic ribosomes. *Annual Review of Biochemistry, 48*, 719-754.

Wool, I. G., Chan, Y. L., & Glück, A. (1995). Structure and evolution of mammalian ribosomal proteins. *Biochemistry and Cell Biology, 73*(11-12), 933-947.

Wortel, I. M. N., van der Meer, L. T., Kilberg, M. S., & van Leeuwen, F. N. (2017). Surviving Stress: Modulation of ATF4-Mediated Stress Responses in Normal and Malignant Cells. *Trends Endocrinology and Metabolism, 28*(11), 794-806.

Wu, L., Li, X., Xu, F., Chang, C., He, Q., Zhang, Z., & Zhang, Y. (2012). Over-expression of RPL23 in myelodysplastic syndromes is associated with apoptosis resistance of CD34+ cells and predicts poor prognosis and distinct response to CHG chemotherapy or decitabine. *Annals of Hematology, 91*(10), 1547-1554.

Wu, L., Zheng, K., Yan, C., Pan, X., Liu, Y., Liu, J., . . . Shen, Y. (2019). Genome-wide study of salivary microRNAs as potential noninvasive biomarkers for detection of nasopharyngeal carcinoma. *BMC Cancer, 19*(1), 843.

Wu, M. H., & Yung, B. Y. (2002). UV stimulation of nucleophosmin/B23 expression is an immediate-early gene response induced by damaged DNA. *Journal of Biological Chemistry, 277*(50), 48234-48240.

Wu, Q., Gou, Y., Wang, Q., Jin, H., Cui, L., Zhang, Y., . . . Fan, D. (2011). Downregulation of RPL6 by siRNA inhibits proliferation and cell cycle progression of human gastric cancer cell lines. *PLoS One, 6*(10), e26401.

Xie, X., Guo, P., Yu, H., Wang, Y., & Chen, G. (2018). Ribosomal proteins: insight into molecular roles and functions in hepatocellular carcinoma. *Oncogene, 37*(3), 277-285.

Xiong, X., Zhao, Y., He, H., & Sun, Y. (2011). Ribosomal protein S27-like and S27 interplay with p53-MDM2 axis as a target, a substrate and a regulator. *Oncogene, 30*(15), 1798-1811.

Xu, M., Wang, Y., Chen, L., Pan, B., Chen, F., Fang, Y., . . . Chen, G. (2014). Down-regulation of ribosomal protein S15A mRNA with a short hairpin RNA inhibits human hepatic cancer cell growth in vitro. *Gene, 536*(1), 84-89.

Xu, M., Yao, Y., Chen, H., Zhang, S., Cao, S. M., Zhang, Z., . . . Liu, J. (2019). Genome sequencing analysis identifies Epstein-Barr virus subtypes associated with high risk of nasopharyngeal carcinoma. *Nature Genetics, 51*(7), 1131-1136.

Yadaiah, M., Sudhamalla, B., Rao, P. N., Roy, K. R., Ramakrishna, D., Hussain Syed, G., . . . Bhuyan, A. K. (2013). Arrested cell proliferation through cysteine protease activity of eukaryotic ribosomal protein S4. *FASEB Journal, 27*(2), 803-810.

Yadavilli, S., Mayo, L. D., Higgins, M., Lain, S., Hegde, V., & Deutsch, W. A. (2009). Ribosomal protein S3: A multi-functional protein that interacts with both p53 and MDM2 through its KH domain. *DNA Repair (Amsterdam), 8*(10), 1215-1224.

Yang, A., Kaghad, M., Wang, Y., Gillett, E., Fleming, M. D., Dötsch, V., . . . McKeon, F. (1998). p63, a p53 homolog at 3q27-29, encodes multiple products with

transactivating, death-inducing, and dominant-negative activities. *Molecular Cell, 2*(3), 305-316.

Yang, C., Zang, W., Ji, Y., Li, T., Yang, Y., & Zheng, X. (2019). Ribosomal protein L6 (RPL6) is recruited to DNA damage sites in a poly(ADP-ribose) polymerase-dependent manner and regulates the DNA damage response. *Journal of Biological Chemistry, 294*(8), 2827-2838.

Yang, F., Petsalaki, E., Rolland, T., Hill, D. E., Vidal, M., & Roth, F. P. (2015). Protein domain-level landscape of cancer-type-specific somatic mutations. *PLoS Computational Biology, 11*(3), e1004147.

Yang, K., Wang, M., Zhao, Y., Sun, X., Yang, Y., Li, X., . . . Yi, J. (2016). A redox mechanism underlying nucleolar stress sensing by nucleophosmin. *Nature Communication, 7*, 13599.

Yang, M., Sun, H., Wang, H., Zhang, S., Yu, X., & Zhang, L. (2013). Down-regulation of ribosomal protein L22 in non-small cell lung cancer. *Medical Oncology, 30*(3), 646.

Yang, X. Y., Ren, C. P., Wang, L., Li, H., Jiang, C. J., Zhang, H. B., . . . Yao, K. T. (2005). Identification of differentially expressed genes in metastatic and non-metastatic nasopharyngeal carcinoma cells by suppression subtractive hybridization. *Cell Oncology, 27*(4), 215-223.

Yang, Z. Y., Jiang, H., Qu, Y., Wei, M., Yan, M., Zhu, Z. G., . . . Gu, Q. L. (2013). Metallopanstimulin-1 regulates invasion and migration of gastric cancer cells partially through integrin β4. *Carcinogenesis, 34*(12), 2851-2860.

Yang, Z. Y., Qu, Y., Zhang, Q., Wei, M., Liu, C. X., Chen, X. H., . . . Gu, Q. L. (2012). Knockdown of metallopanstimulin-1 inhibits NF-κB signaling at different levels: the

role of apoptosis induction of gastric cancer cells. *International Journal of Cancer, 130*(12), 2761-2770.

Ye, J., Coulouris, G., Zaretskaya, I., Cutcutache, I., Rozen, S., & Madden, T. L. (2012). Primer-BLAST: a tool to design target-specific primers for polymerase chain reaction. *BMC Bioinformatics, 13*, 134.

Yoshizaki, T., Ito, M., Murono, S., Wakisaka, N., Kondo, S., & Endo, K. (2012). Current understanding and management of nasopharyngeal carcinoma. *Auris Nasus Larynx, 39*(2), 137-144.

Young, L. S., Yap, L. F., & Murray, P. G. (2016). Epstein-Barr virus: more than 50 years old and still providing surprises. *Nature Review on Cancer, 16*(12), 789-802.

Yu, G., Hsu, W. L., Coghill, A. E., Yu, K. J., Wang, C. P., Lou, P. J., . . . Goldstein, A. M. (2019). Whole-Exome Sequencing of Nasopharyngeal Carcinoma Families Reveals Novel Variants Potentially Involved in Nasopharyngeal Carcinoma. *Science Reports, 9*(1), 9916.

Yu, K. J., Hsu, W. L., Pfeiffer, R. M., Chiang, C. J., Wang, C. P., Lou, P. J., . . . Hildesheim, A. (2011). Prognostic utility of anti-EBV antibody testing for defining NPC risk among individuals from high-risk NPC families. *Clinical Cancer Research, 17*(7), 1906-1914.

Yu, M. C., Garabrant, D. H., Huang, T. B., & Henderson, B. E. (1990). Occupational and other non-dietary risk factors for nasopharyngeal carcinoma in Guangzhou, China. *International Journal of Cancer, 45*(6), 1033-1039.

Yu, M. C., Ho, J. H., Lai, S. H., & Henderson, B. E. (1986). Cantonese-style salted fish as a cause of nasopharyngeal carcinoma: report of a case-control study in Hong Kong. *Cancer Research, 46*(2), 956-961.

Yu, M. C., Huang, T. B., & Henderson, B. E. (1989). Diet and nasopharyngeal carcinoma: a case-control study in Guangzhou, China. *International Journal of Cancer, 43*(6), 1077-1082.

Yuan, J. M., Wang, X. L., Xiang, Y. B., Gao, Y. T., Ross, R. K., & Yu, M. C. (2000). Preserved foods in relation to risk of nasopharyngeal carcinoma in Shanghai, China. *International Journal of Cancer, 85*(3), 358-363.

Yuan, J. S., Reed, A., Chen, F., & Stewart, C. N. (2006). Statistical analysis of real-time PCR data. *BMC Bioinformatics, 7*, 85.

Yue, X., Zhao, Y., Xu, Y., Zheng, M., Feng, Z., & Hu, W. (2017). Mutant p53 in Cancer: Accumulation, Gain-of-Function, and Therapy. *Journal of Molecular Biology, 429*(11), 1595-1606.

Yusupov, M. M., Yusupova, G. Z., Baucom, A., Lieberman, K., Earnest, T. N., Cate, J. H., & Noller, H. F. (2001). Crystal structure of the ribosome at 5.5 A resolution. *Science, 292*(5518), 883-896.

Yusupova, G., & Yusupov, M. (2014). High-resolution structure of the eukaryotic 80S ribosome. *Annual Review of Biochemistry, 83*, 467-486.

Zhan, C., Zhang, Y., Ma, J., Wang, L., Jiang, W., Shi, Y., & Wang, Q. (2014). Identification of reference genes for qRT-PCR in human lung squamous-cell carcinoma by RNA-Seq. *Acta Biochimica et Biophysica Sinica (Shanghai), 46*(4), 330-337.

Zhang, C., Qie, Y., Yang, T., Wang, L., Du, E., Liu, Y., . . . Zhang, Z. (2018). Kinase PIM1 promotes prostate cancer cell growth via c-Myc-RPS7-driven ribosomal stress. *Carcinogenesis*.

Zhang, C., Zhang, T., Song, E., Himaya, S. W., Chen, X., & Zheng, L. (2014). Ribosomal protein S15A augments human osteosarcoma cell proliferation in vitro. *Cancer Biotherapy and Radiopharmaceuticals, 29*(10), 451-456.

Zhang, D. Z., Chen, B. H., Zhang, L. F., Cheng, M. K., Fang, X. J., & Wu, X. J. (2017). Basic Transcription Factor 3 Is Required for Proliferation and Epithelial-Mesenchymal Transition via Regulation of FOXM1 and JAK2/STAT3 Signaling in Gastric Cancer. *Oncology Research, 25*(9), 1453-1462.

Zhang, M., Zhang, J., Yan, W., & Chen, X. (2016). p73 expression is regulated by ribosomal protein RPL26 through mRNA translation and protein stability. *Oncotarget, 7*(48), 78255-78268.

Zhang, Q. X., H., Chai, S. C., Hoang, Q. Q., & Lu, H. (2011). Hydrophilic residues are crucial for ribosomal protein L11 (RPL11) interaction with zinc finger domain of MDM2 and p53 protein activation. *The Journal of Biological Chemistry, 286*(4), 38264-38274.

Zhang, S. W. C., W.Q., & Kong, L. Z. (2007). An annual report cancer incidence in 35 cancer registries in China. *Bulletin of Chinese Cancer, 16*(7), 494-506.

Zhang, W., Tong, D., Liu, F., Li, D., Li, J., Cheng, X., & Wang, Z. (2016). RPS7 inhibits colorectal cancer growth via decreasing HIF-1α-mediated glycolysis. *Oncotarget, 7*(5), 5800-5814.

Zhang, X., Wang, W., Wang, H., Wang, M. H., Xu, W., & Zhang, R. (2013). Identification of ribosomal protein S25 (RPS25)-MDM2-p53 regulatory feedback loop. *Oncogene, 32*(22), 2782-2791.

Zhang, Y., Shi, Y., Li, X., Du, W., Luo, G., Gou, Y., . . . Fan, D. (2010). Inhibition of the p53-MDM2 interaction by adenovirus delivery of ribosomal protein L23 stabilizes

p53 and induces cell cycle arrest and apoptosis in gastric cancer. *Journal of Gene Medicine, 12*(2), 147-156.

Zhang, Y., Wang, J., Yuan, Y., Zhang, W., Guan, W., Wu, Z., . . . He, F. (2010). Negative regulation of HDM2 to attenuate p53 degradation by ribosomal protein L26. *Nucleic Acids Research, 38*(19), 6544-6554.

Zhang, Y., Wolf, G. W., Bhat, K., Jin, A., Allio, T., Burkhart, W. A., & Xiong, Y. (2003). Ribosomal protein L11 negatively regulates oncoprotein MDM2 and mediates a p53-dependent ribosomal-stress checkpoint pathway. *Molecular Cell Biology, 23*(23), 8902-8912.

Zhang, Y. F., Zhang, B. C., Zhang, A. R., Wu, T. T., Liu, J., Yu, L. F., . . . Rao, Z. G. (2013). Co-transduction of ribosomal protein L23 enhances the therapeutic efficacy of adenoviral-mediated p53 gene transfer in human gastric cancer. *Oncology Reports, 30*(4), 1989-1995.

Zhang, Z. C., Fu, S., Wang, F., Wang, H. Y., Zeng, Y. X., & Shao, J. Y. (2014). Oncogene mutational profile in nasopharyngeal carcinoma. *Onco Targets Therapy, 7*, 457-467.

Zhao, X., Shen, L., Feng, Y., Yu, H., Wu, X., Chang, J., . . . Wang, J. (2015). Decreased expression of RPS15A suppresses proliferation of lung cancer cells. *Tumour Biology, 36*(9), 6733-6740.

Zhen, Y., Zhang, Y., & Yu, Y. (2017). A Cell-Line-Specific Atlas of PARP-Mediated Protein Asp/Glu-ADP-Ribosylation in Breast Cancer. *Cell Report, 21*(8), 2326-2337.

Zheng, J., Lang, Y., Zhang, Q., Cui, D., Sun, H., Jiang, L., . . . Tang, J. (2015). Structure of human MDM2 complexed with RPL11 reveals the molecular basis of p53 activation. *Genes and Development, 29*(14), 1524-1534.

Zheng, S. E., Yao, Y., Dong, Y., Lin, F., Zhao, H., Shen, Z., . . . Tang, L. N. (2009). Down-regulation of ribosomal protein L7A in human osteosarcoma. *Journal of Cancer Research and Clinical Oncology, 135*(8), 1025-1031.

Zheng, X., Luo, Y., Christensson, B., & Drettner, B. (1994). Induction of nasal and nasopharyngeal tumours in Sprague-Dawley rats fed with Chinese salted fish. *Acta Otolaryngolica, 114*(1), 98-104.

Zhou, F., Roy, B., & von Arnim, A. G. (2010). Translation reinitiation and development are compromised in similar ways by mutations in translation initiation factor eIF3h and the ribosomal protein RPL24. *BMC Plant Biology, 10*, 193.

Zhou, Q., Hou, Z., Zuo, S., Zhou, X., Feng, Y., Sun, Y., & Yuan, X. (2019). LUCAT1 promotes colorectal cancer tumorigenesis by targeting the ribosomal protein L40-MDM2-p53 pathway through binding with UBA52. *Cancer Science*, *110*(4), 1194-1207.

Zhou, X., Cui, J., Macias, V., Kajdacsy-Balla, A. A., Ye, H., Wang, J., & Rao, P. N. (2007). The progress on genetic analysis of nasopharyngeal carcinoma. *Computational Functional Genomics*, *2007*(3), 57513.

Zhou, X., Hao, Q., Liao, J., Zhang, Q., & Lu, H. (2013). Ribosomal protein S14 unties the MDM2-p53 loop upon ribosomal stress. *Oncogene, 32*(3), 388-396.

Zhou, X., Hao, Q., Liao, J. M., Liao, P., & Lu, H. (2013). Ribosomal protein S14 negatively regulates c-Myc activity. *Journal of Biological Chemistry, 288*(30), 21793-21801.

Zhou, Y., Liao, Q., Li, X., Wang, H., Wei, F., Chen, J., . . . Li, G. (2016). HYOU1, Regulated by LPLUNC1, Is Up-Regulated in Nasopharyngeal Carcinoma and Associated with Poor Prognosis. *Journal of Cancer, 7*(4), 367-376.

Zhou, Y. H., Hess, K. R., Liu, L., Linskey, M. E., & Yung, W. K. (2005). Modeling prognosis for patients with malignant astrocytic gliomas: quantifying the expression of multiple genetic markers and clinical variables. *Neuro Oncology, 7*(4), 485-494.

Zhu, K., Levine, R. S., Brann, E. A., Gnepp, D. R., & Baum, M. K. (1997). Cigarette smoking and nasopharyngeal cancer: an analysis of the relationship according to age at starting smoking and age at diagnosis. *Journal of Epidemiology, 7*(2), 107-111.

Zhu, L., Luo, K., Gu, X. H., Hou, N., Huang, C. P., Lou, Q., . . . Zhang, K. (2015). CXCR7 expression in nasopharyngeal carcinoma tissues correlates with disease severity. *International Journal of Clinical Experimental Medicine, 8*(11), 21257-21261.

Ziv, O., Zeisel, A., Mirlas-Neisberg, N., Swain, U., Nevo, R., Ben-Chetrit, N., . . . Livneh, Z. (2014). Identification of novel DNA-damage tolerance genes reveals regulation of translesion DNA synthesis by nucleophosmin. *Nature Communication, 5*, 5437.

Zou, X. N., Lu, S. H., & Liu, B. (1994). Volatile N-nitrosamines and their precursors in Chinese salted fish--a possible etological factor for NPC in china. *International Journal of Cancer, 59*(2), 155-158.

APPENDICES

Appendix A. qPCR Primers Amplification Efficiency Validation.

Gene	Input		C_T Values				Gradient, m	Efficiency (%)	Amplification
	Input	**Log Input**	**$C_{T,1}$**	**$C_{T,2}$**	**Average C_T**	**SD**			
GAPDH	4.000	0.602	11.59	11.59	11.59	0.00	-3.236	103.715	1.037
	0.800	-0.097	13.84	13.73	13.79	0.078			
	0.160	-0.795	16.15	16.46	16.31	0.219			
	0.032	-1.495	18.87	18.63	18.75	0.170			
	0.007	-2.194	20.09	20.75	20.42	0.467			
Beta Actin	4.000	0.602	7.27	7.66	7.465	0.276	-3.169	106.803	1.068
	0.800	-0.097	8.97	9.33	9.15	0.255			
	0.160	-0.795	11.31	11.61	11.46	0.212			
	0.032	-1.495	14.08	14.04	14.06	0.028			
	0.007	-2.194	15.67	16.50	16.08	0.587			
uS4 (S9)	4.000	0.602	16.59	17.00	16.8	0.290	-3.445	95.108	0.951
	0.800	-0.097	19.14	18.39	18.77	0.530			
	0.160	-0.795	21.52	22.27	21.9	0.530			
	0.032	-1.495	24.3	24.79	24.55	0.346			
	0.008	-2.194	25.75	26.15	25.95	0.283			
eS8 (S8)	4.000	0.602	17.01	17.29	17.15	0.198	-3.436	95.450	0.955
	0.800	-0.097	19.34	19.03	19.19	0.219			
	0.160	-0.795	22.27	21.44	21.86	0.587			
	0.032	-1.495	24.81	24.92	24.87	0.078			
	0.007	-2.194	26.41	26.22	26.32	0.134			
eS31 (S27a)	4.000	0.602	14.84	15.49	15.17	0.460	-3.612	89.171	0.892
	0.800	-0.097	17.47	17.55	17.51	0.057			
	0.160	-0.795	20.09	20.23	20.16	0.099			
	0.032	-1.495	22.21	22.58	22.4	0.262			
	0.007	-2.194	24.93	25.76	25.35	0.587			

eL6 (L6)	4.000	0.602	21.89	20.14	21.01	1.237	-3.292	101.264	1.013
	0.800	-0.097	23.01	22.49	22.75	0.368			
	0.160	-0.795	24.75	24.52	24.64	0.163			
	0.032	-1.495	27.99	26.45	27.22	1.089			
	0.007	-2.194	31.01	29.56	30.28	1.025			
uL14	4.000	0.602	14.59	15.13	14.86	0.382	-3.375	97.832	0.978
(L23)	0.800	-0.097	16.87	17.55	17.21	0.481			
	0.160	-0.795	19.66	20.15	19.91	0.346			
	0.032	-1.495	21.59	22.28	21.94	0.488			
	0.007	-2.194	24.46	24.52	24.29	0.042			
eL18	4.000	0.602	11.68	11.6	11.64	0.057	-3.253	102.959	1.030
(L18)	0.800	-0.097	13.75	13.72	13.74	0.021			
	0.160	-0.795	16.14	15.88	16.01	0.184			
	0.032	-1.495	18.55	18.25	18.40	0.212			
	0.007	-2.194	20.71	20.64	20.68	0.049			
eL24	4.000	0.602	16.33	15.37	15.85	0.679	-3.166	106.953	1.069
(L24)	0.800	-0.097	18.23	17.82	18.03	0.290			
	0.160	-0.795	20.51	20.26	20.39	0.177			
	0.032	-1.495	20.92	22.43	21.68	1.068			
	0.007	-2.194	25.11	25.07	25.09	0.028			
eL30	4.000	0.602	12.14	12.12	12.13	0.014	-3.196	105.538	1.055
(L30)	0.800	-0.097	13.47	13.36	13.42	0.078			
	0.160	-0.795	15.64	15.59	15.62	0.035			
	0.032	-1.495	18.02	18.36	18.19	0.240			
	0.007	-2.194	20.95	20.88	20.92	0.049			
NPM1	4.000	0.602	17.01	17.29	17.15	0.198	-3.152	107.615	1.076
	0.800	-0.097	19.00	18.72	18.86	0.198			
	0.160	-0.795	21.43	21.27	21.35	0.113			
	0.032	-1.495	23.46	23.6	23.53	0.099			
	0.007	-2.194	25.66	25.98	25.82	0.226			
BTF3	4.000	0.602	18.15	18.36	18.26	0.148	-3.398	96.920	0.969
	0.800	-0.097	20.24	20.85	20.55	0.431			

	0.160	-0.795	23.14	23.61	23.38	0.332			
	0.032	-1.495	25.50	26.61	26.06	0.785			
	0.007	-2.194	27.37	27.38	27.38	0.007			
UBA52	4.000	0.602	12.01	12.15	12.08	0.099	-3.379	97.672	0.977
	0.800	-0.097	14.37	14.36	14.37	0.007			
	0.160	-0.795	16.66	17.00	16.83	0.240			
	0.032	-1.495	19.08	19.58	19.33	0.353			
	0.007	-2.194	21.31	21.50	21.41	0.134			

Appendix B. Validation of Target and Control PCR Efficiency Compatibility.

1. Compatibility of GAPDH as Reference Gene.

Gene	Log Input	Average $C_{T,\ Target}$	Average $C_{T,\ GAPDH}$	ΔC_T *	Slope	Absolute slope
uS4 (S9)	0.602	16.80	11.59	5.21	-0.075	0.075
	-0.097	18.77	13.79	4.98		
	-0.795	21.90	16.31	5.59		
	-1.495	24.55	18.75	5.80		
	-2.194	25.95	20.42	5.53		
eS8 (S8)	0.602	17.15	11.59	5.56	-0.052	0.052
	-0.097	19.19	13.79	5.40		
	-0.795	21.86	16.31	5.55		
	-1.495	24.87	18.75	6.12		
	-2.194	26.32	20.42	5.80		
eS31	0.602	15.17	11.59	3.58	0.047	0.047
(S27a)	-0.097	17.51	13.79	3.72		
	-0.795	20.16	16.31	3.85		
	-1.495	22.40	18.75	3.65		
	-2.194	25.35	20.42	4.93		
eL6 (L6)	0.602	21.015	11.59	9.43	-0.056	0.056
	-0.097	22.75	13.79	8.96		
	-0.795	24.64	16.31	8.33		
	-1.495	27.22	18.75	8.47		
	-2.194	30.29	20.42	9.87		
uL14	0.602	14.86	11.59	3.27	0.009	0.009
(L23)	-0.097	17.21	13.79	3.42		
	-0.795	19.91	16.31	3.60		
	-1.495	21.94	18.75	3.19		
	-2.194	24.29	20.42	3.87		
eL18	0.602	11.64	11.59	0.05	-0.017	0.017
(L18)	-0.097	13.74	13.79	-0.05		

	-0.795	16.01	16.31	-0.30		
	-1.495	18.40	18.75	-0.35		
	-2.194	20.68	20.42	0.26		
eL24	0.602	15.85	11.59	4.26	0.070	0.070
(L24)	-0.097	18.03	13.79	4.24		
	-0.795	20.39	16.31	4.08		
	-1.495	21.68	18.75	2.93		
	-2.194	25.09	20.42	4.67		
eL30	0.602	12.13	11.59	0.54	0.039	0.039
(L30)	-0.097	13.42	13.79	-0.37		
	-0.795	15.62	16.31	-0.69		
	-1.495	18.19	18.75	-0.56		
	-2.194	20.92	20.42	0.50		
NPM1	0.602	17.15	11.59	5.56	0.087	0.087
	-0.097	18.86	13.79	5.07		
	-0.795	21.35	16.31	5.04		
	-1.495	23.53	18.75	4.78		
	-2.194	25.82	20.42	5.40		
BTF3	0.602	18.26	11.59	6.67	-0.098	0.098
	-0.097	20.55	13.79	6.76		
	-0.795	23.38	16.31	7.07		
	-1.495	26.06	18.75	7.31		
	-2.194	27.38	20.42	6.96		
UBA52	0.602	12.08	11.59	0.49	-0.030	0.030
	-0.097	14.37	13.79	0.58		
	-0.795	16.83	16.31	0.52		
	-1.495	19.33	18.75	0.58		
	-2.194	21.41	20.42	0.99		

*Excluded extreme outliers are denoted in grey.

2. Compatibility of Beta-actin (ACTB) as Reference Gene.

Gene	Log Input	Average $C_{T,\ Target}$	Average $C_{T,\ ACTB}$	ΔC_T *	Absolute slope	Absolute slope after removal of outlier #
uS4 (S9)	0.602	16.80	7.47	9.34	0.276	**0.205**
	-0.097	18.77	9.15	9.62		
	-0.795	21.90	11.46	10.44		
	-1.495	24.55	14.06	10.49		
	-2.194	25.95	16.09	9.87		
eS8 (S8)	0.602	17.15	7.47	9.69	0.268	**0.188**
	-0.097	19.19	9.15	10.04		
	-0.795	21.86	11.46	10.40		
	-1.495	24.87	14.06	10.81		
	-2.194	26.32	16.09	10.24		
eS31	0.602	15.17	7.47	7.71	0.443	**0.321**
(S27a)	-0.097	17.51	9.15	8.36		
	-0.795	20.16	11.46	8.70		
	-1.495	22.40	14.06	8.34		
	-2.194	25.35	16.09	9.27		
eL6 (L6)	0.602	21.02	7.47	13.55	0.123	**0.123**
	-0.097	22.75	9.15	13.60		
	-0.795	24.64	11.46	13.18		
	-1.495	27.22	14.06	13.16		
	-2.194	30.29	16.09	14.20		
uL14	0.602	14.86	7.47	7.40	0.206	0.019
(L23)	-0.097	17.21	9.15	8.06		
	-0.795	19.91	11.46	8.45		
	-1.495	21.94	14.06	7.88		
	-2.194	24.29	16.09	8.21		
eL18	0.602	11.64	7.47	4.18	0.084	N/A
(L18)	-0.097	13.74	9.15	4.59		
	-0.795	16.01	11.46	4.55		
	-1.495	18.4	14.06	4.34		
	-2.194	20.68	16.085	4.60		

eL24	0.602	15.85	7.47	8.39	0.003	N/A
(L24)	-0.097	18.03	9.15	8.88		
	-0.795	20.39	11.46	8.93		
	-1.495	21.68	14.06	7.62		
	-2.194	25.09	16.085	9.01		
eL30	0.602	12.13	7.47	4.67	0.029	N/A
(L30)	-0.097	13.42	9.15	4.27		
	-0.795	15.62	11.46	4.16		
	-1.495	18.19	14.06	4.13		
	-2.194	20.92	16.085	4.84		
NPM1	0.602	17.15	7.47	9.69	0.020	N/A
	-0.097	18.86	9.15	9.71		
	-0.795	21.35	11.46	9.89		
	-1.495	23.53	14.06	9.47		
	-2.194	25.82	16.085	9.74		
BTF3	0.602	18.26	7.47	10.80	0.229	0.034
	-0.097	20.55	9.15	11.40		
	-0.795	23.38	11.46	11.92		
	-1.495	26.06	14.06	12.00		
	-2.194	27.38	16.085	11.30		
UBA52	0.602	12.08	7.47	4.615	0.210	0.031
	-0.097	14.37	9.15	5.22		
	-0.795	16.83	11.46	5.37		
	-1.495	19.33	14.06	5.27		
	-2.194	21.41	16.085	5.33		

* Excluded extreme outliers are denoted in grey.

Incompatible slopes (>1.0), even after exclusion of outliers, are in bold.

Appendix C. Raw qPCR C_T Data and $2^{-\Delta\Delta C_T}$ Calculation.

uS4 (S9)			GAPDH		ΔC_T		$\Delta\Delta C_T$		$2^{-\Delta\Delta C_T}$ (upper)		$2^{-\Delta\Delta C_T}$ (lower)		FD
	Average C_T	SD	Average $C_{T,\ GAPDH}$	SD	ΔC_T	SD	$\Delta\Delta C_T$	SD	$\Delta\Delta C_T$ + SD	$2^{-\Delta\Delta C_T}$	$\Delta\Delta C_T$ - SD	$2^{-\Delta\Delta C_T}$	
Biological Replicate 1													
NP69	21.44	1.485	18.56	0.050	2.89	1.486	0.00	1.486	1.486	0.357	-1.486	2.801	1.579
HONE-1	20.85	0.580	15.91	0.000	4.94	0.580	2.06	0.580	2.635	0.161	1.475	0.360	0.260
SUNE-1	25.57	0.615	14.47	2.022	11.1	2.114	8.21	2.114	10.324	0.001	6.096	0.015	0.008
HK1	17.87	0.078	13.66	0.304	4.21	0.314	1.33	0.314	1.639	0.321	1.011	0.450	0.409
TWO1	22.49	0.601	14.95	0.184	7.54	0.629	4.65	0.629	5.279	0.026	4.022	0.062	0.044
TWO4	18.80	0.354	13.88	0.205	4.92	0.409	2.04	0.409	2.449	0.183	1.631	0.323	0.253
C666-1	16.03	2.517	10.30	0.841	5.74	2.654	2.85	2.654	5.504	0.022	0.196	0.873	0.448
Biological Replicate 2													
NP69	19.67	0.304	18.39	0.106	1.28	0.322	0.00	0.322	0.322	0.800	-0.320	1.250	1.025
HONE-1	19.08	0.057	15.63	0.276	3.46	0.282	2.18	0.282	2.457	0.182	1.893	0.269	0.226
SUNE-1	24.73	0.445	12.16	0.820	12.57	0.933	11.3	0.933	12.220	2.00E-04	10.350	8.00E-04	0.001
HK1	19.03	0.325	12.96	0.361	6.08	0.486	4.80	0.486	5.281	0.026	4.309	0.050	0.038
TWO1	25.19	3.217	16.33	1.167	8.86	3.422	7.58	1.196	8.776	0.002	6.384	0.012	0.007
TWO4	18.72	0.856	14.25	0.049	4.47	0.857	3.19	0.561	3.751	0.074	2.629	0.162	0.118
C666-1	13.37	0.707	9.54	0.481	3.83	0.855	2.55	0.855	3.405	0.094	1.695	0.309	0.202
Biological Replicate 3													
NP69	28.77	0.346	24.88	0.247	3.89	0.426	0.00	0.426	0.426	0.744	-0.426	1.343	1.044
HONE-1	28.62	0.304	15.61	0.035	13.01	0.306	9.12	0.306	9.426	0.001	8.814	0.002	0.002
SUNE-1	23.37	1.358	16.19	0.092	7.19	1.361	3.30	1.361	4.656	0.040	1.934	0.262	0.151
HK1	32.17	0.042	14.67	0.240	17.50	0.244	13.61	0.244	13.854	6.85E-05	13.366	9.47E-05	8.11E-05

TWO1	34.70	1.485	16.50	0.346	18.21	1.525	14.32	1.525	15.840	1.71E-05	12.790	1.41E-04	7.91E-05
TWO4	24.22	1.273	17.43	0.099	6.79	1.277	2.90	1.277	4.177	0.055	1.623	0.325	0.190
C666-1	32.39	0.856	16.08	0.014	16.31	0.856	12.42	0.856	13.271	1.01E-04	11.559	3.31E-04	2.16E-04

eS8 (S8)			GAPDH		ΔC_T		$\Delta\Delta C_T$		$2^{-\Delta\Delta C_T}$ (upper)		$2^{-\Delta\Delta C_T}$ (lower)		FD
	Average C_T	SD	Average $C_{T,\ GAPDH}$	SD	ΔC_T	SD	$\Delta\Delta C_T$	SD	$\Delta\Delta C_T$ + SD	$2^{-\Delta\Delta C_T}$	$\Delta\Delta C_T$ - SD	$2^{-\Delta\Delta C_T}$	
Biological Replicate 1													
NP69	18.32	0.049	18.56	0.049	-0.24	0.070	0.00	0.070	0.070	0.953	-0.070	1.050	1.001
HONE-1	12.73	0.608	11.47	1.556	1.26	1.670	1.5	1.670	3.170	0.111	-0.170	1.125	0.618
SUNE-1	17.60	0.552	13.94	0.219	3.67	0.594	3.91	0.594	4.499	0.044	3.311	0.101	0.072
HK1	15.38	0.240	13.93	0.290	1.46	0.377	1.7	0.377	2.072	0.238	1.318	0.401	0.319
TWO1	16.83	0.304	14.95	0.184	1.88	0.355	2.12	0.355	2.470	0.180	1.760	0.295	0.238
TWO4	16.24	0.255	13.88	0.205	2.37	0.327	2.61	0.327	2.932	0.131	2.278	0.206	0.169
C666-1	12.13	0.042	10.39	0.714	1.75	0.715	1.99	0.715	2.700	0.154	1.270	0.415	0.284
Biological Replicate 2													
NP69	18.12	18.4	18.26	0.198	-0.13	0.225	0.00	0.225	0.225	0.856	-0.225	1.168	1.012
HONE-1	11.76	0.537	9.55	0.410	2.21	0.676	2.34	0.676	3.011	0.124	1.659	0.317	0.220
SUNE-1	19.29	1.683	13.54	0.389	5.76	1.727	5.88	1.727	7.607	0.005	4.153	0.056	0.031
HK1	15.67	0.127	13.26	0.537	2.41	0.552	2.54	0.552	3.087	0.118	1.983	0.253	0.185
TWO1	16.26	0.127	15.23	0.141	1.03	0.190	1.16	0.190	1.345	0.394	0.965	0.512	0.453
TWO4	15.96	0.269	14.25	0.049	1.72	0.273	1.84	0.273	2.113	0.231	1.567	0.338	0.284
C666-1	13.28	1.308	9.45	0.354	3.83	1.355	3.95	1.355	5.305	0.025	2.595	0.166	0.095
Biological Replicate 3													
NP69	19.36	0.205	22.88	0.247	-3.52	0.321	0.00	0.321	0.321	0.800	-0.320	1.250	1.025
HONE-1	15.94	0.658	15.69	0.233	0.25	0.698	3.77	0.698	4.468	0.045	3.072	0.119	0.082
SUNE-1	18.59	0.148	18.47	0.021	0.12	0.150	3.64	0.150	3.790	0.072	3.490	0.089	0.081

HK1	15.13	0.247	14.67	0.240	0.46	0.345	3.98	0.345	4.320	0.050	3.630	0.081	0.065
TWO1	16.98	0.057	16.50	0.346	0.49	0.351	4.01	0.351	4.356	0.049	3.654	0.079	0.064
TWO4	19.62	0.990	17.43	0.099	2.19	0.995	5.71	0.995	6.705	0.010	4.715	0.038	0.024
C666-1	15.70	0.021	16.08	0.014	-0.38	0.025	3.14	0.026	3.160	0.112	3.110	0.116	0.114

eL31 (S27a)			GAPDH		ΔC_T		$\Delta\Delta C_T$		$2^{-\Delta\Delta C_T}$ (upper)		$2^{-\Delta\Delta C_T}$ (lower)		FD
	Average C_T	SD	Average $C_{T,\ GAPDH}$	SD	ΔC_T	SD	$\Delta\Delta C_T$	SD	$\Delta\Delta C_T$ + SD	$2^{-\Delta\Delta C_T}$	$\Delta\Delta C_T$ - SD	$2^{-\Delta\Delta C_T}$	
Biological Replicate 1													
NP69	19.01	0.106	18.56	0.049	0.45	0.117	0.00	0.117	0.117	0.922	-0.120	1.085	1.003
HONE-1	10.35	0.643	11.47	1.556	-1.13	1.683	-1.60	1.613	0.037	0.974	-3.190	9.110	5.042
SUNE-1	17.72	0.318	13.94	0.219	3.78	0.386	3.33	0.386	3.716	0.076	2.944	0.130	0.103
HK1	14.72	0.276	13.54	0.467	1.18	0.542	0.73	0.542	1.267	0.416	0.183	0.881	0.648
TWO1	17.12	0.233	14.95	0.184	2.16	0.297	1.72	0.228	1.943	0.260	1.487	0.357	0.308
TWO4	16.48	0.262	13.88	0.205	2.60	0.332	2.15	0.510	2.660	0.158	1.640	0.321	0.240
C666-1	13.97	0.559	10.39	0.714	3.58	0.907	3.13	0.766	3.896	0.067	2.364	0.194	0.131
Biological Replicate 2													
NP69	19.58	0.198	18.77	0.106	0.81	0.225	0.00	0.225	0.225	0.856	-0.225	1.168	1.012
HONE-1	9.98	0.318	9.55	0.410	0.43	0.519	-0.39	0.519	0.134	0.911	-0.904	1.871	1.391
SUNE-1	16.98	0.049	13.54	0.389	3.44	0.392	2.63	0.392	3.022	0.123	2.238	0.212	0.168
HK1	14.86	0.481	13.07	0.523	1.79	0.711	0.98	0.711	1.691	0.310	0.269	0.830	0.570
TWO1	17.03	0.375	15.23	0.141	1.80	0.401	0.99	0.401	1.386	0.383	0.584	0.667	0.525
TWO4	16.87	0.643	14.25	0.049	2.62	0.645	1.81	0.645	2.455	0.182	1.165	0.446	0.314
C666-1	13.98	1.131	9.45	0.354	4.53	1.185	3.72	1.185	4.905	0.033	2.535	0.173	0.103
Biological Replicate 3													
NP69	20.88	0.205	22.88	0.247	-2.00	0.321	0.00	0.321	0.321	0.800	-0.320	1.250	1.025
HONE-1	16.24	0.141	18.31	0.106	-2.07	0.177	-0.10	0.177	0.112	0.925	-0.240	1.182	1.054

SUNE-1	18.77	0.658	16.47	0.021	2.30	0.658	4.30	0.658	4.958	0.032	3.642	0.080	0.056
HK1	15.50	1.146	14.67	0.240	-0.17	0.361	1.83	0.361	2.191	0.219	1.469	0.361	0.290
TWO1	17.01	1.266	16.50	0.346	1.51	1.170	2.83	0.361	3.191	0.110	2.469	0.181	0.145
TWO4	18.93	0.120	17.43	0.099	1.50	0.156	3.50	0.156	3.651	0.080	3.339	0.099	0.089
C666-1	14.60	0.134	14.72	0.014	-0.13	0.135	1.88	0.135	2.010	0.248	1.740	0.299	0.274

eL6 (L6)			GAPDH		ΔC_T		$\Delta\Delta C_T$		$2^{-\Delta\Delta C_T}$ (upper)		$2^{-\Delta\Delta C_T}$ (lower)		FD
	Average C_T	SD	Average $C_{T,\ GAPDH}$	SD	ΔC_T	SD	$\Delta\Delta C_T$	SD	$\Delta\Delta C_T$ + SD	$2^{-\Delta\Delta C_T}$	$\Delta\Delta C_T$ - SD	$2^{-\Delta\Delta C_T}$	
Biological Replicate 1													
NP69	30.69	0.361	18.53	0.092	12.16	0.372	0.00	0.364	0.364	0.777	-0.366	1.287	1.032
HONE-1	35.69	0.537	18.11	0.643	17.59	0.838	5.43	0.838	6.263	0.013	4.587	0.042	0.027
SUNE-1	24.84	0.141	13.94	0.219	10.91	0.261	-1.30	0.387	-0.874	1.825	-1.644	3.121	2.473
HK1	21.93	0.007	13.93	0.290	8.00	0.290	-4.22	0.290	-3.873	14.62	-4.455	21.86	18.240
TWO1	24.01	0.552	16.67	0.233	7.35	0.599	-2.04	0.599	-1.434	2.697	-2.633	6.185	4.441
TWO4	25.69	0.304	18.99	0.106	6.70	0.322	-2.70	0.322	-2.355	5.109	-3.034	7.984	6.546
C666-1	22.21	1.598	10.30	0.841	11.92	1.806	-0.25	1.578	1.333	0.397	-1.825	3.538	1.968
Biological Replicate 2													
NP69	31.24	0.608	18.42	0.148	12.83	0.626	0.00	0.617	0.617	0.652	-0.617	1.534	1.093
HONE-1	36.49	1.195	18.89	1.757	17.60	2.116	4.78	0.617	5.392	0.024	4.158	0.056	0.040
SUNE-1	25.10	0.262	13.54	0.389	11.56	0.469	-1.27	0.311	-0.954	1.937	-1.576	2.982	2.459
HK1	23.02	0.962	13.26	0.537	9.76	1.102	-3.07	1.102	-1.963	3.945	-4.167	17.960	10.935
TWO1	24.41	0.014	16.20	0.106	8.22	0.107	-1.73	0.107	-1.618	3.069	-1.832	3.560	3.315
TWO4	25.28	0.057	18.78	0.064	6.51	0.085	-3.44	0.085	-3.350	10.245	-3.520	11.475	10.835
C666-1	21.07	0.403	9.54	0.481	11.53	0.627	-1.34	0.412	-0.888	1.850	-1.712	3.277	2.564
Biological Replicate 3													
NP69	30.18	0.643	22.88	0.247	7.30	0.689	0.00	0.689	0.689	0.628	-0.697	1.613	1.116

HONE-1	24.30	0.269	15.69	0.233	8.62	0.356	1.32	0.356	1.671	0.314	0.959	0.514	0.414
SUNE-1	25.89	0.049	22.11	0.092	3.78	0.104	-3.50	0.104	-3.428	10.670	-3.624	12.333	11.502
HK1	22.05	0.021	14.67	0.240	7.38	0.241	0.08	0.241	0.316	0.803	-0.166	1.122	1.963
TWO1	24.10	0.071	16.33	1.167	7.78	1.169	0.48	1.169	1.644	0.327	-0.694	1.618	0.969
TWO4	24.55	0.134	18.08	0.262	6.47	0.294	-0.88	0.294	-0.536	1.456	-1.124	2.185	1.815
C666-1	22.03	0.106	16.08	0.014	5.95	0.107	-1.47	0.107	-1.248	2.375	-1.462	2.755	2.565

uL14 (L23)			GAPDH		ΔC_T		$\Delta\Delta C_T$		$2^{-\Delta\Delta C_T}$ (upper)		$2^{-\Delta\Delta C_T}$ (lower)		FD
	Average C_T	SD	Average $C_{T,\ GAPDH}$	SD	ΔC_T	SD	$\Delta\Delta C_T$	SD	$\Delta\Delta C_T$ + SD	$2^{-\Delta\Delta C_T}$	$\Delta\Delta C_T$ - SD	$2^{-\Delta\Delta C_T}$	
Biological Replicate 1													
NP69	17.81	0.375	18.53	0.092	-0.72	0.386	0.00	0.386	0.386	0.765	-0.386	1.307	1.036
HONE-1	10.66	0.813	9.93	0.212	0.73	0.840	1.45	0.307	1.745	0.298	1.145	0.452	0.375
SUNE-1	15.31	0.014	13.94	0.219	1.38	0.220	2.10	0.220	2.315	0.201	1.875	0.273	0.237
HK1	13.74	0.233	13.33	0.163	0.41	0.284	1.13	0.284	1.414	0.375	0.846	0.556	0.466
TWO1	16.17	0.184	14.95	0.184	1.22	0.260	1.94	0.260	2.287	0.218	1.685	0.312	0.265
TWO4	14.46	0.064	13.88	0.205	0.58	0.215	1.30	0.215	1.515	0.357	1.085	0.471	0.411
C666-1	13.34	0.976	10.30	0.841	3.05	1.289	3.77	1.289	5.054	0.036	2.477	0.186	0.105
Biological Replicate 2													
NP69	17.15	0.346	18.42	0.148	-1.27	0.377	0.00	0.377	0.377	0.775	-0.377	1.299	1.034
HONE-1	13.41	0.255	10.91	0.452	2.50	0.519	3.77	0.640	4.410	0.047	3.130	0.114	0.081
SUNE-1	15.03	0.297	13.54	0.389	1.50	0.489	2.77	0.489	3.254	0.105	2.276	0.207	0.156
HK1	13.69	0.127	13.29	0.827	0.40	0.836	1.67	0.836	2.506	0.176	0.834	0.561	0.369
TWO1	16.17	0.184	15.23	0.141	0.94	0.232	2.21	0.232	2.442	0.184	1.978	0.254	0.219
TWO4	14.30	0.523	14.25	0.049	0.06	0.526	1.33	0.526	1.851	0.277	0.799	0.575	0.426
C666-1	13.17	0.735	9.54	0.481	3.63	0.879	4.90	0.879	5.779	0.018	4.021	0.062	0.040
Biological Replicate 3													

NP69	18.68	1.061	22.88	0.247	-4.20	1.089	0.00	1.089	1.089	0.47	-1.089	2.127	1.299
HONE-1	15.90	0.127	15.69	0.233	0.22	0.266	4.41	0.266	4.676	0.039	4.144	0.057	0.048
SUNE-1	17.29	0.304	18.47	0.021	-1.18	0.305	3.02	0.305	3.320	0.178	2.716	0.153	0.127
HK1	14.22	0.58	14.67	0.240	-0.45	0.628	3.75	0.628	4.373	0.048	3.117	0.115	0.082
TWO1	16.01	0.58	16.50	0.346	-0.48	0.675	3.71	0.676	4.386	0.048	3.035	0.122	0.085
TWO4	16.78	0.304	17.43	0.099	-0.66	0.320	3.54	0.320	3.860	0.069	3.227	0.107	0.088
C666-1	15.66	1.697	16.08	0.014	-0.42	1.697	3.78	1.131	4.906	0.033	2.644	0.160	0.097

eL18 (L18)			GAPDH		ΔC_T		$\Delta\Delta C_T$		$2^{-\Delta\Delta C_T}$ (upper)		$2^{-\Delta\Delta C_T}$ (lower)		FD
	Average C_T	SD	Average $C_{T,\ GAPDH}$	SD	ΔC_T	SD	$\Delta\Delta C_T$	SD	$\Delta\Delta C_T$ + SD	$2^{-\Delta\Delta C_T}$	$\Delta\Delta C_T$ - SD	$2^{-\Delta\Delta C_T}$	
Biological Replicate 1													
NP69	22.18	0.276	18.53	0.092	3.65	0.291	0.00	0.291	0.291	0.818	-0.291	1.223	1.027
HONE-1	18.09	0.608	15.91	0.000	2.18	0.608	-1.47	0.608	-0.862	1.817	-2.078	4.223	3.027
SUNE-1	9.955	0.12	12.16	1.527	-2.21	1.532	-5.86	1.532	-4.323	20.014	-7.387	167.390	93.702
HK1	15.15	0.120	13.33	0.163	1.82	0.202	-1.83	0.202	-1.628	3.097	-2.032	4.097	3.590
TWO1	18.17	0.028	14.95	0.184	3.22	0.186	-0.43	0.186	-0.244	1.184	-0.616	1.533	1.358
TWO4	16.53	0.021	13.88	0.205	2.65	0.206	-1.98	0.206	-0.794	1.734	-1.206	2.307	2.021
C666-1	10.35	0.431	10.30	0.841	0.05	0.946	-3.60	0.946	-2.654	6.296	-4.546	23.350	14.825
Biological Replicate 2													
NP69	22.35	0.205	18.42	0.148	3.93	0.253	0.00	0.253	0.253	0.839	-0.253	1.192	1.015
HONE-1	17.67	0.028	15.63	0.276	2.05	0.277	-1.89	0.277	-1.608	3.048	-2.162	4.476	3.762
SUNE-1	10.02	0.064	12.31	1.032	-2.37	1.034	-6.23	1.034	-5.191	36.528	-7.259	153.280	94.864
HK1	15.03	0.120	13.29	0.827	1.74	0.836	-2.19	0.836	-1.354	2.556	-3.026	8.145	5.351
TWO1	18.27	0.057	15.23	0.141	3.04	0.152	-0.89	0.152	-0.738	1.667	-1.042	2.069	1.864
TWO4	16.84	0.028	14.25	0.049	2.68	0.057	-1.34	0.057	-1.278	2.425	-1.392	2.624	2.525
C666-1	9.405	0.064	9.54	0.481	-0.14	0.485	-4.07	0.485	-3.586	11.969	-4.550	23.430	17.692

Biological Replicate 3													
NP69	24.95	0.212	22.88	0.247	2.08	0.326	0.00	0.326	0.326	0.798	-0.326	1.253	1.026
HONE-1	20.52	1.442	18.31	0.106	2.22	1.446	0.14	1.446	1.586	0.333	-1.306	2.473	1.403
SUNE-1	19.94	0.184	24.050	0.092	-4.11	0.206	-6.19	0.206	-5.979	63.095	-6.391	83.897	73.496
HK1	17.10	1.223	14.67	0.240	2.43	1.247	0.35	1.247	1.5967	0.331	-0.897	1.862	1.096
TWO1	18.53	0.078	16.69	0.092	1.84	0.120	-0.24	0.120	-0.115	1.083	-0.355	1.279	1.181
TWO4	19.97	0.078	18.08	0.262	1.89	0.273	-0.19	0.273	0.088	0.941	-0.458	1.374	1.157
C666-1	15.94	0.071	16.19	0.092	-0.25	0.116	-2.32	0.116	-2.204	4.608	-2.436	5.411	5.010

eL24 (L24)			GAPDH		ΔC_T		$\Delta\Delta C_T$		$2^{-\Delta\Delta C_T}$ (upper)		$2^{-\Delta\Delta C_T}$ (lower)		FD
	Average C_T	SD	Average $C_{T,\ GAPDH}$	SD	ΔC_T	SD	$\Delta\Delta C_T$	SD	$\Delta\Delta C_T$ + SD	$2^{-\Delta\Delta C_T}$	$\Delta\Delta C_T$ - SD	$2^{-\Delta\Delta C_T}$	
Biological Replicate 1													
NP69	20.76	0.339	18.56	0.049	2.21	0.343	0.00	0.343	0.343	0.788	-0.343	1.268	1.028
HONE-1	19.16	0.361	16.61	1.478	2.55	1.521	0.35	1.521	1.866	0.274	-1.176	2.260	1.267
SUNE-1	16.44	0.170	13.94	0.219	2.51	0.277	0.36	0.277	0.577	0.670	0.023	0.984	0.827
HK1	13.90	0.106	13.54	0.467	0.36	0.479	-1.85	0.477	-1.371	2.587	-2.329	5.023	3.805
TWO1	17.86	0.474	14.95	0.184	2.91	0.508	0.77	0.508	1.208	0.433	0.192	0.876	0.654
TWO4	16.38	0.071	13.88	0.205	2.51	0.217	0.39	0.217	0.517	0.699	0.083	0.944	0.822
C666-1	14.43	0.438	10.39	0.714	4.05	0.838	1.84	0.838	2.678	0.156	1.002	0.499	0.328
Biological Replicate 2													
NP69	20.28	0.057	18.39	0.106	1.82	0.129	0.00	0.128	0.120	0.920	-0.12	1.087	1.004
HONE-1	17.50	0.863	19.34	1.103	-1.84	1.407	-3.67	1.406	-2.255	4.772	-5.055	33.25	19.012
SUNE-1	16.98	0.141	13.54	0.389	3.45	0.414	1.63	0.414	2.044	0.243	1.216	0.430	0.337
HK1	14.39	0.071	13.07	0.523	1.32	0.528	-0.58	0.528	0.033	0.977	-1.023	2.032	1.505
TWO1	17.36	0.106	15.23	0.141	2.13	0.177	0.31	0.177	0.487	0.714	0.133	0.912	0.813
TWO4	16.29	0.092	14.25	0.049	2.04	0.104	0.23	0.104	0.329	0.796	0.121	0.920	0.858

C666-1	13.74	0.049	9.45	0.354	4.29	0.357	2.47	0.357	2.827	0.141	2.113	0.231	0.186
Biological Replicate 3													
NP69	20.52	0.721	22.88	0.247	-2.36	0.763	0.00	0.763	0.763	0.589	-0.763	1.696	1.143
HONE-1	14.05	0.198	18.31	0.106	-4.26	0.225	-1.99	0.225	-1.675	3.194	-2.125	4.361	3.778
SUNE-1	19.43	0.820	18.47	0.021	0.97	0.821	3.32	0.821	4.141	0.057	2.580	0.177	0.117
HK1	15.57	0.467	14.67	0.240	0.90	0.525	3.26	0.525	3.780	0.073	2.739	0.151	0.112
TWO1	18.83	0.870	16.50	0.346	2.33	0.936	4.69	0.936	5.621	0.020	3.749	0.074	0.048
TWO4	19.67	0.000	17.43	0.099	2.24	0.099	4.66	0.099	4.694	0.039	4.496	0.044	0.042
C666-1	18.35	1.414	16.08	0.014	2.27	1.414	4.63	1.414	6.039	0.015	3.211	0.108	0.062

eL30 (L30)			GAPDH		ΔC_T		$\Delta\Delta C_T$		$2^{-\Delta\Delta C_T}$ (upper)		$2^{-\Delta\Delta C_T}$ (lower)		FD
	Average C_T	SD	Average $C_{T,\ GAPDH}$	SD	ΔC_T	SD	$\Delta\Delta C_T$	SD	$\Delta\Delta C_T$ + SD	$2^{-\Delta\Delta C_T}$	$\Delta\Delta C_T$ - SD	$2^{-\Delta\Delta C_T}$	
Biological Replicate 1													
NP69	21.63	0.509	18.53	0.092	3.11	0.517	0.00	0.517	0.517	0.699	-0.517	1.431	1.065
HONE-1	17.25	0.304	15.91	0.000	1.34	0.304	-1.78	0.304	-1.466	2.762	-2.074	4.211	3.487
SUNE-1	19.45	0.588	18.88	0.092	0.58	0.587	-2.54	0.587	-1.943	3.845	-3.117	8.676	6.261
HK1	14.59	0.163	13.33	0.163	1.26	0.230	-1.85	0.230	-1.615	3.063	-2.075	4.213	3.638
TWO1	16.38	0.042	14.95	0.184	1.43	0.189	-1.67	0.189	-1.486	2.802	-1.864	3.639	3.221
TWO4	16.30	0.113	13.88	0.205	2.43	0.234	-0.68	0.234	-0.446	1.362	-0.914	1.885	1.623
C666-1	12.49	1.605	10.30	0.841	2.19	1.812	-0.92	1.812	0.897	0.537	-2.727	6.622	3.580
Biological Replicate 2													
NP69	20.47	0.078	18.42	0.148	2.05	0.168	0.00	0.168	0.168	0.899	-0.168	1.123	1.007
HONE-1	16.89	0.156	15.63	0.276	1.27	0.317	-0.79	0.317	-0.468	1.384	-1.102	2.146	1.765
SUNE-1	16.81	0.219	14.47	1.032	2.34	1.055	0.285	1.055	1.340	0.395	-0.770	1.706	1.050
HK1	14.43	0.382	13.29	0.827	1.15	0.911	-0.91	0.911	0.006	0.996	-1.816	3.521	2.259
TWO1	16.37	0.000	16.33	1.167	0.05	1.167	-1.87	1.167	-0.698	1.623	-3.032	8.178	4.900

TWO4	16.51	0.502	14.25	0.049	2.26	0.504	0.21	0.505	0.715	0.609	-0.294	1.226	1.918
C666-1	11.31	0.820	9.54	0.481	1.77	0.951	-0.28	0.951	0.671	0.628	-1.231	2.347	1.488
Biological Replicate 3													
NP69	29.76	0.728	22.88	0.247	6.88	0.769	0.00	0.769	0.769	0.587	-0.769	1.704	1.146
HONE-1	19.09	0.092	15.61	0.035	3.48	0.098	-3.48	0.099	-3.302	9.859	-3.498	11.3	10.581
SUNE-1	24.56	1.188	18.47	0.021	6.10	1.188	-0.79	0.460	-0.325	1.253	-1.245	2.370	1.811
HK1	15.93	0.771	14.67	0.240	1.26	0.807	-5.63	0.807	-4.818	28.209	-6.432	86.36	57.282
TWO1	19.57	1.344	16.50	0.346	3.08	1.387	-3.81	1.388	-2.418	5.343	-5.192	36.57	20.955
TWO4	20.58	0.354	17.43	0.099	3.15	0.367	-3.73	0.367	-3.363	10.290	-4.097	17.11	13.701
C666-1	17.35	1.492	16.08	0.014	1.27	1.492	-5.62	1.492	-4.123	17.420	-7.107	137.9	77.642

NPM1			GAPDH		ΔC_T		$\Delta\Delta C_T$		$2^{-\Delta\Delta C_T}$ (upper)		$2^{-\Delta\Delta C_T}$ (lower)		FD
	Average C_T	SD	Average $C_{T,\ GAPDH}$	SD	ΔC_T	SD	$\Delta\Delta C_T$	SD	$\Delta\Delta C_T$ + SD	$2^{-\Delta\Delta C_T}$	$\Delta\Delta C_T$ - SD	$2^{-\Delta\Delta C_T}$	
Biological Replicate 1													
NP69	20.71	0.255	18.53	0.092	2.19	0.271	0.00	0.271	0.271	0.829	-0.271	1.206	1.017
HONE-1	26.42	0.771	18.11	0.643	8.31	1.004	6.13	1.004	7.129	0.007	5.121	0.029	0.018
SUNE-1	17.29	0.516	13.94	0.219	3.35	0.561	1.17	0.561	1.726	0.302	0.604	0.658	0.480
HK1	15.71	0.205	13.33	0.163	2.38	0.262	0.20	0.262	0.457	0.729	-0.067	1.047	0.888
TWO1	19.10	0.071	14.95	0.184	4.15	0.197	1.97	0.197	2.162	0.223	1.768	0.294	0.259
TWO4	17.38	0.156	13.88	0.205	3.51	0.257	1.32	0.257	1.577	0.335	1.063	0.479	0.407
C666-1	12.42	1.266	10.30	0.841	2.12	1.520	-0.07	1.520	1.455	0.365	-1.585	3.001	1.682
Biological Replicate 2													
NP69	20.36	0.007	18.42	0.148	1.94	0.149	0.00	0.149	0.149	0.902	-0.149	1.109	1.005
HONE-1	22.49	0.382	15.61	0.035	6.89	0.383	4.95	0.383	5.330	0.025	4.560	0.042	0.034
SUNE-1	16.95	0.686	13.54	0.389	3.41	0.788	1.47	0.788	2.259	0.209	0.682	0.624	0.416
HK1	15.57	0.028	13.29	0.827	2.29	0.828	0.35	0.828	1.173	0.444	-0.483	1.397	0.921

TWO1	19.09	0.049	15.23	0.141	3.86	0.150	1.92	0.150	2.065	0.239	1.765	0.294	0.267
TWO4	17.68	0.679	14.25	0.049	3.44	0.681	1.50	0.681	2.176	0.221	0.814	0.569	0.395
C666-1	11.55	0.834	9.54	0.481	2.01	0.963	0.07	0.963	1.033	0.489	-0.893	1.857	1.173
Biological Replicate 3													
NP69	23.40	0.184	22.88	0.247	0.53	0.308	0.00	0.414	0.414	0.750	-0.414	1.333	1.042
HONE-1	22.49	0.382	15.54	0.127	6.95	0.402	6.43	0.403	6.828	0.009	6.023	0.015	0.012
SUNE-1	23.35	0.163	18.88	0.092	4.47	0.187	3.95	0.187	4.132	0.057	3.758	0.074	0.066
HK1	22.00	0.141	14.67	0.240	7.33	0.279	6.81	0.279	7.084	0.007	6.526	0.011	0.009
TWO1	19.89	0.523	16.50	0.346	3.40	0.628	2.87	0.628	3.498	0.089	2.242	0.211	0.150
TWO4	21.05	0.940	17.43	0.099	3.62	0.946	3.09	0.946	4.036	0.061	2.144	0.226	0.144
C666-1	18.84	0.156	16.08	0.014	2.76	0.156	2.24	0.156	2.391	0.191	2.079	0.237	0.214

BTF3			GAPDH		ΔC_T		$\Delta\Delta C_T$		$2^{-\Delta\Delta C_T}$ (upper)		$2^{-\Delta\Delta C_T}$ (lower)		FD
	Average C_T	SD	Average $C_{T,\ GAPDH}$	SD	ΔC_T	SD	$\Delta\Delta C_T$	SD	$\Delta\Delta C_T$ + SD	$2^{-\Delta\Delta C_T}$	$\Delta\Delta C_T$ - SD	$2^{-\Delta\Delta C_T}$	
Biological Replicate 1													
NP69	16.80	0.205	18.53	0.092	-1.73	0.225	0.00	0.225	0.225	0.856	-0.225	1.169	1.012
HONE-1	17.51	0.099	15.91	0.000	1.60	0.099	3.33	0.099	3.429	0.093	3.231	0.107	0.100
SUNE-1	14.06	0.332	13.97	1.315	0.09	1.357	1.82	1.357	3.172	0.111	0.458	0.728	0.419
HK1	14.62	0.601	13.54	0.163	1.08	0.623	2.81	0.623	3.428	0.093	2.182	0.220	0.157
TWO1	18.97	1.195	14.45	0.523	4.52	1.305	2.09	1.305	3.390	0.095	0.781	0.582	0.339
TWO4	15.25	0.021	13.88	0.205	1.37	0.206	-1.06	0.206	-0.854	1.807	-1.266	2.405	2.106
C666-1	12.32	0.049	10.39	0.714	1.93	0.716	-0.50	0.712	0.212	0.861	-1.216	2.323	1.592
Biological Replicate 2													
NP69	26.32	0.544	22.88	0.247	3.44	0.598	0.00	0.598	0.598	0.661	-0.598	1.514	1.087
HONE-1	19.95	0.530	15.54	0.127	4.41	0.545	0.97	0.545	1.510	0.351	0.420	0.748	0.549
SUNE-1	26.00	0.629	18.47	0.021	7.53	0.630	4.09	0.63	4.720	0.038	3.460	0.091	0.064

HK1	17.83	0.608	13.21	0.240	4.62	0.654	1.18	0.654	1.834	0.281	0.526	0.694	0.487
TWO1	21.22	1.987	15.23	0.141	5.99	1.992	1.33	0.542	1.867	0.274	0.783	0.581	0.428
TWO4	16.00	0.665	14.25	0.049	1.76	0.667	-2.91	0.667	-2.239	4.719	-3.572	11.897	8.304
C666-1	15.81	0.134	16.08	0.014	-0.27	0.135	-4.94	0.425	-4.51	22.790	-5.360	41.078	31.926
Biological Replicate 3													
NP69	29.85	1.315	22.88	0.247	6.98	1.338	0.00	1.338	1.338	0.395	-1.338	2.529	1.462
HONE-1	23.75	0.332	15.69	0.233	8.06	0.406	1.09	0.406	1.491	0.356	0.679	0.625	0.490
SUNE-1	25.80	0.587	18.47	0.021	7.33	0.587	0.36	0.587	0.942	0.520	-0.232	1.175	0.848
HK1	20.66	1.280	12.70	0.240	7.96	1.302	0.98	0.563	1.543	0.343	0.417	0.749	0.546
TWO1	23.23	0.856	15.13	0.346	8.10	0.923	1.12	0.923	2.043	0.243	0.197	0.872	0.558
TWO4	19.84	0.884	17.43	0.099	2.41	0.889	-4.57	0.889	-3.681	12.82	-5.459	44.056	28.411
C666-1	21.27	0.396	16.08	0.014	5.19	0.396	-1.79	0.396	-1.389	2.619	-2.181	4.535	3.577

UBA52			GAPDH		ΔC_T		$\Delta\Delta C_T$		$2^{-\Delta\Delta C_T}$ (upper)		$2^{-\Delta\Delta C_T}$ (lower)		FD
	Average C_T	SD	Average $C_{T,\ GAPDH}$	SD	ΔC_T	SD	$\Delta\Delta C_T$	SD	$\Delta\Delta C_T$ + SD	$2^{-\Delta\Delta C_T}$	$\Delta\Delta C_T$ - SD	$2^{-\Delta\Delta C_T}$	
Biological Replicate 1													
NP69	19.69	0.233	18.53	0.092	1.16	0.251	0.00	0.251	0.251	0.845	-0.251	1.190	1.015
HONE-1	15.18	0.368	16.61	1.478	-1.43	1.523	-2.59	1.523	-1.062	2.088	-4.108	17.247	9.665
SUNE-1	16.01	0.035	13.94	0.219	2.07	0.222	0.91	0.222	1.132	0.456	0.688	0.621	0.539
HK1	14.64	0.064	13.26	0.537	1.38	0.541	0.22	0.538	0.753	0.594	-0.323	1.251	0.922
TWO1	15.04	0.106	16.67	0.233	-1.63	0.256	0.07	0.256	0.326	0.798	-0.186	1.1389	0.968
TWO4	16.75	0.332	18.82	0.127	-2.08	0.356	-0.38	0.356	-0.019	1.013	-0.731	1.660	1.337
C666-1	14.05	0.813	10.30	0.841	3.75	1.170	2.59	1.170	3.760	0.074	1.427	0.374	0.224
Biological Replicate 2													
NP69	19.69	0.233	18.42	0.148	1.27	0.277	0.00	0.277	0.277	0.826	-0.277	1.211	1.018
HONE-1	16.36	1.110	19.34	1.103	-2.99	1.565	-4.26	1.565	-2.697	6.453	-5.820	56.497	31.473

SUNE-1	16.05	0.148	13.54	0.389	2.51	0.416	1.24	0.416	1.656	0.317	0.824	0.565	0.441
HK1	14.81	0.311	13.29	0.827	1.53	0.884	0.26	0.872	1.127	0.458	-0.617	1.534	0.996
TWO1	15.03	0.325	16.20	0.106	-1.17	0.342	0.48	0.342	0.817	0.568	0.133	0.912	0.744
TWO4	16.85	0.438	18.94	0.17	-2.09	0.470	-0.45	0.470	0.026	0.986	-0.927	1.892	1.439
C666-1	11.85	1.499	9.54	0.481	2.31	1.574	1.04	1.574	2.614	0.163	-0.534	1.448	0.806
Biological Replicate 3													
NP69	19.58	0.509	22.88	0.247	-3.3	0.566	0.00	0.566	0.566	0.675	-0.566	1.483	1.078
HONE-1	13.36	0.049	18.31	0.106	-4.95	0.117	-1.66	0.117	-1.538	2.904	-1.772	3.415	3.165
SUNE-1	17.17	0.064	18.47	0.021	-1.30	0.067	2.07	0.067	2.062	0.239	1.928	0.263	0.251
HK1	15.03	0.000	14.67	0.240	0.36	0.240	3.66	0.24	3.895	0.067	3.415	0.094	0.081
TWO1	16.40	0.120	16.50	0.346	-0.17	0.367	3.20	0.367	3.562	0.085	2.828	0.141	0.113
TWO4	18.75	0.000	17.43	0.099	1.32	0.099	4.62	0.107	4.714	0.038	4.516	0.044	0.041
C666-1	14.87	0.530	16.08	0.014	-1.22	0.531	2.08	0.531	2.611	0.164	1.550	0.342	0.253

FD: Fold difference; SD: Standard deviation. $2^{-\Delta\Delta C_T}$ is the relative expression of fold difference.

Appendix D. Sequence analysis of target genes. Multiple sequence alignment was conducted using ClustalW and visualized with MultAlin program. Paired-wise sequences with low consensus are within the boxed region.

1. Sequence analysis of *uS4 (S9)*.

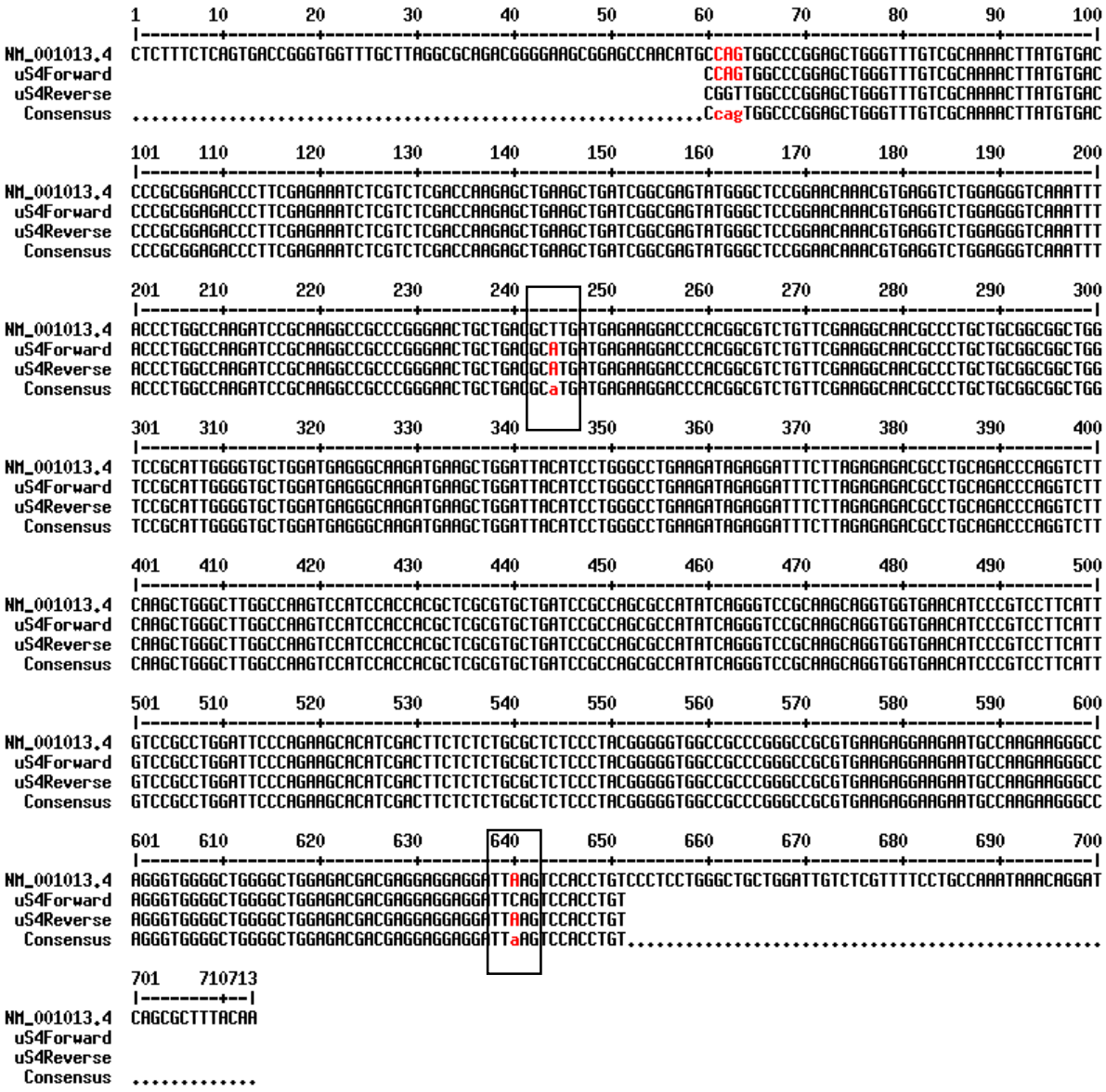

2. Sequence analysis of *eS8 (S8)*.

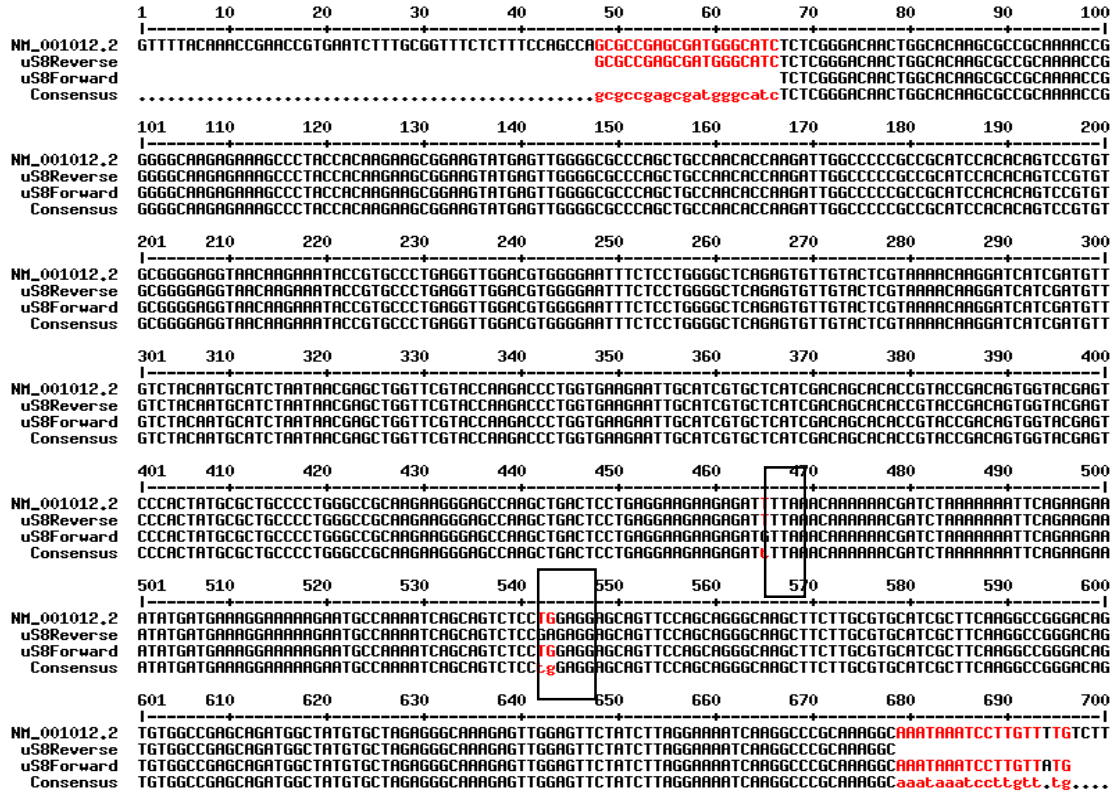

3. Sequence analysis of *eS31 (S27a)*.

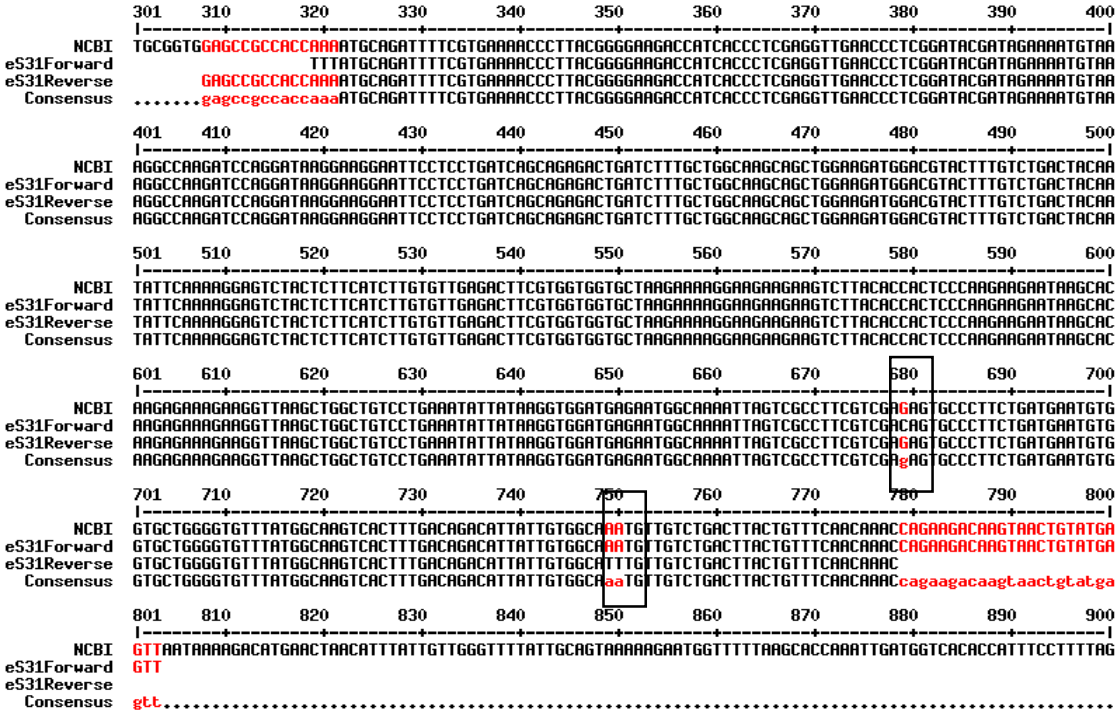

4. Sequence analysis of *eL6 (L6)*.

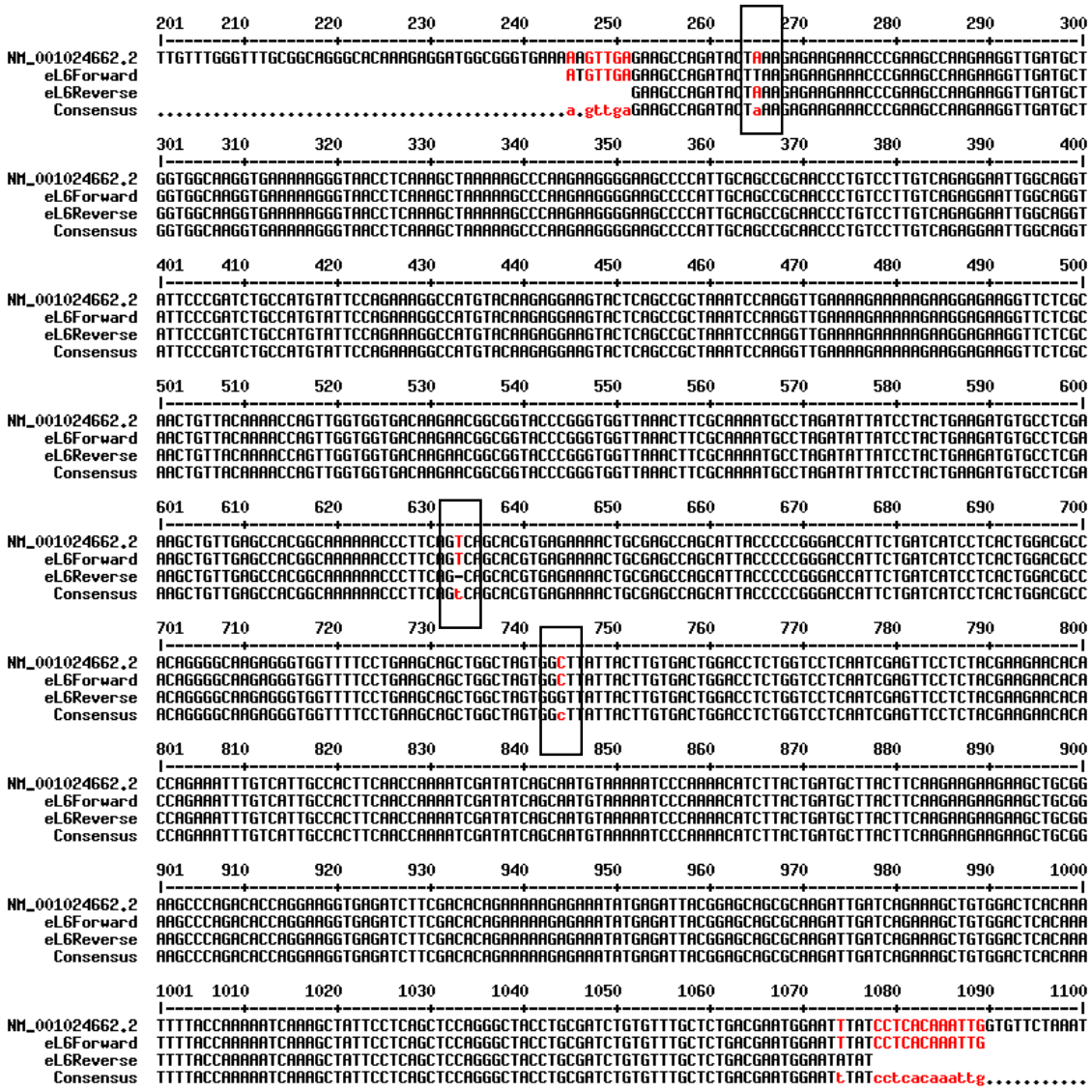

5. Sequence analysis of *uL14 (L23)*.

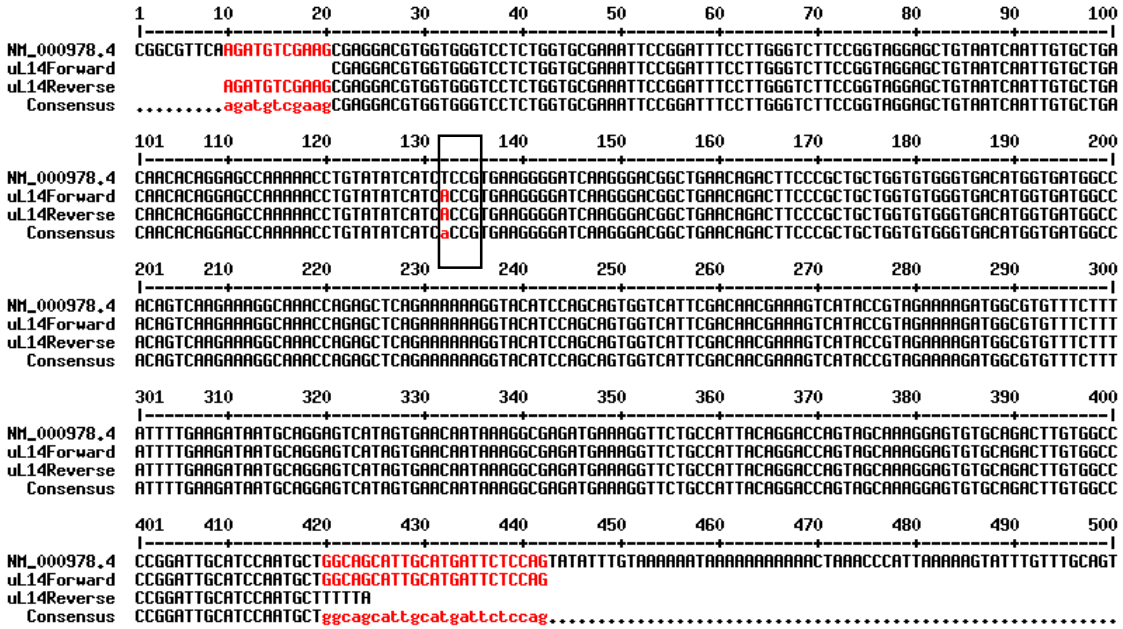

6. Sequence analysis of *eL18 (L8)*.

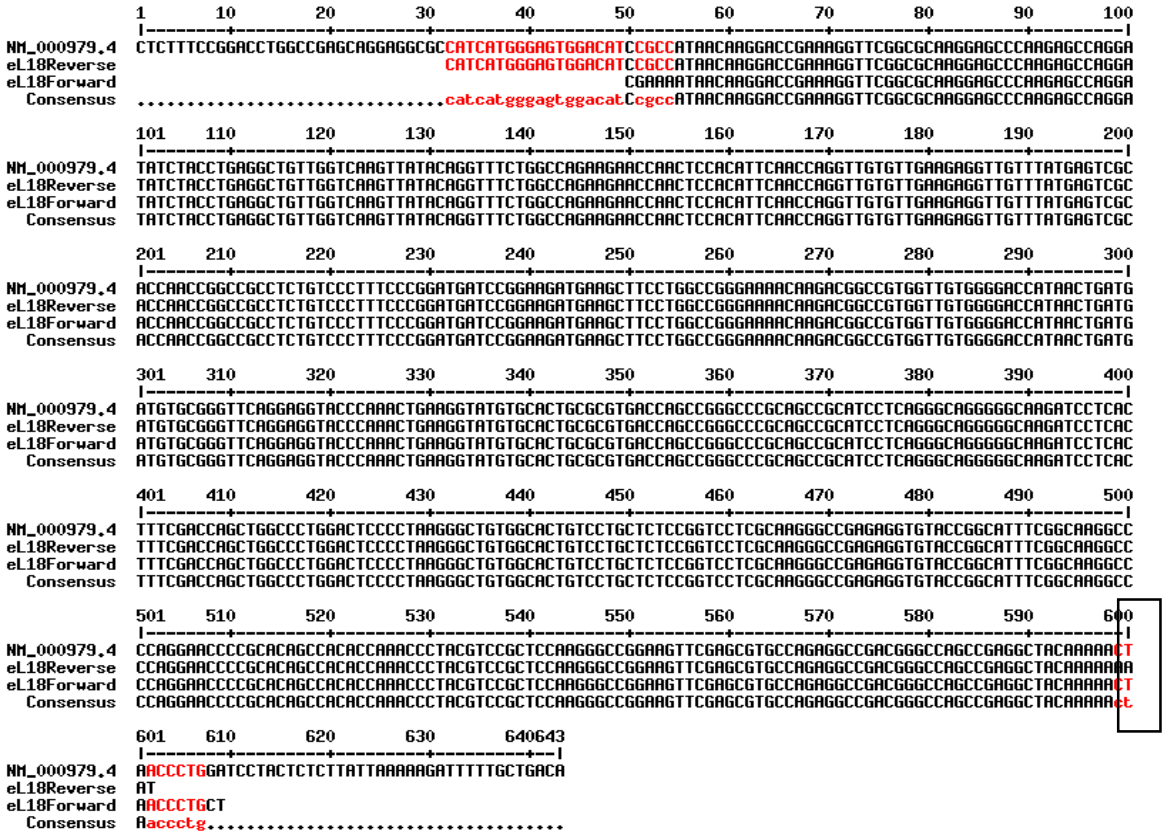

7. Sequence analysis of *eL24 (L24)*.

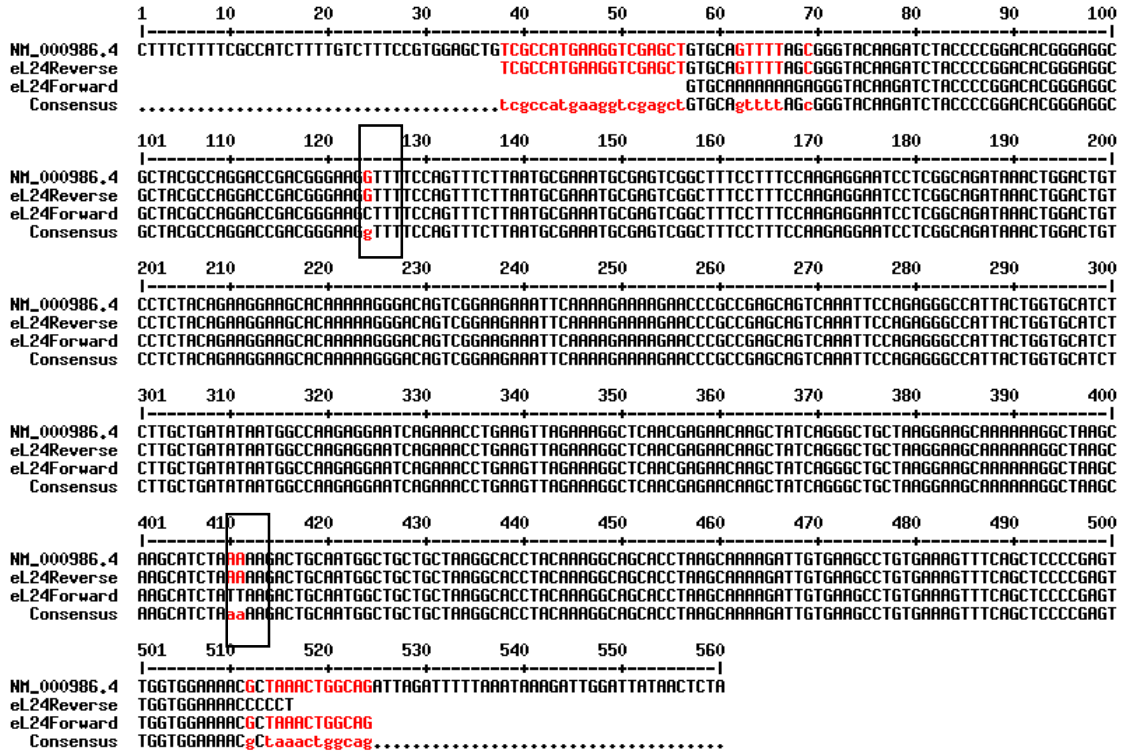

8. Sequence analysis of *eL30 (L30)*.

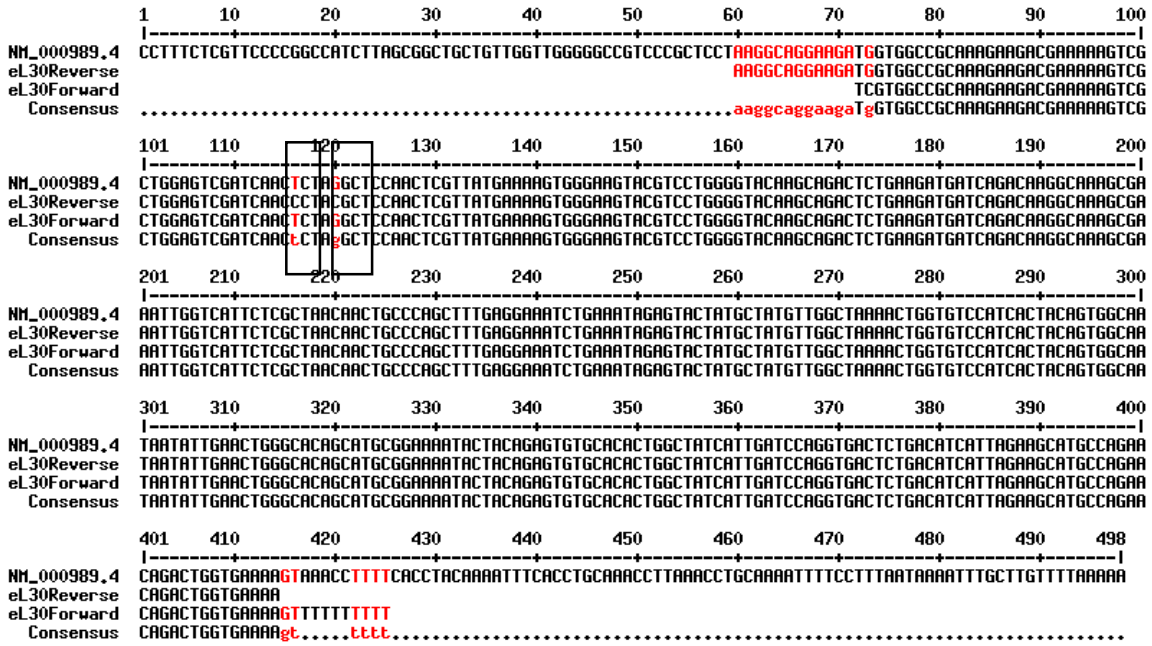

9. Sequence analysis of *NPM1*.

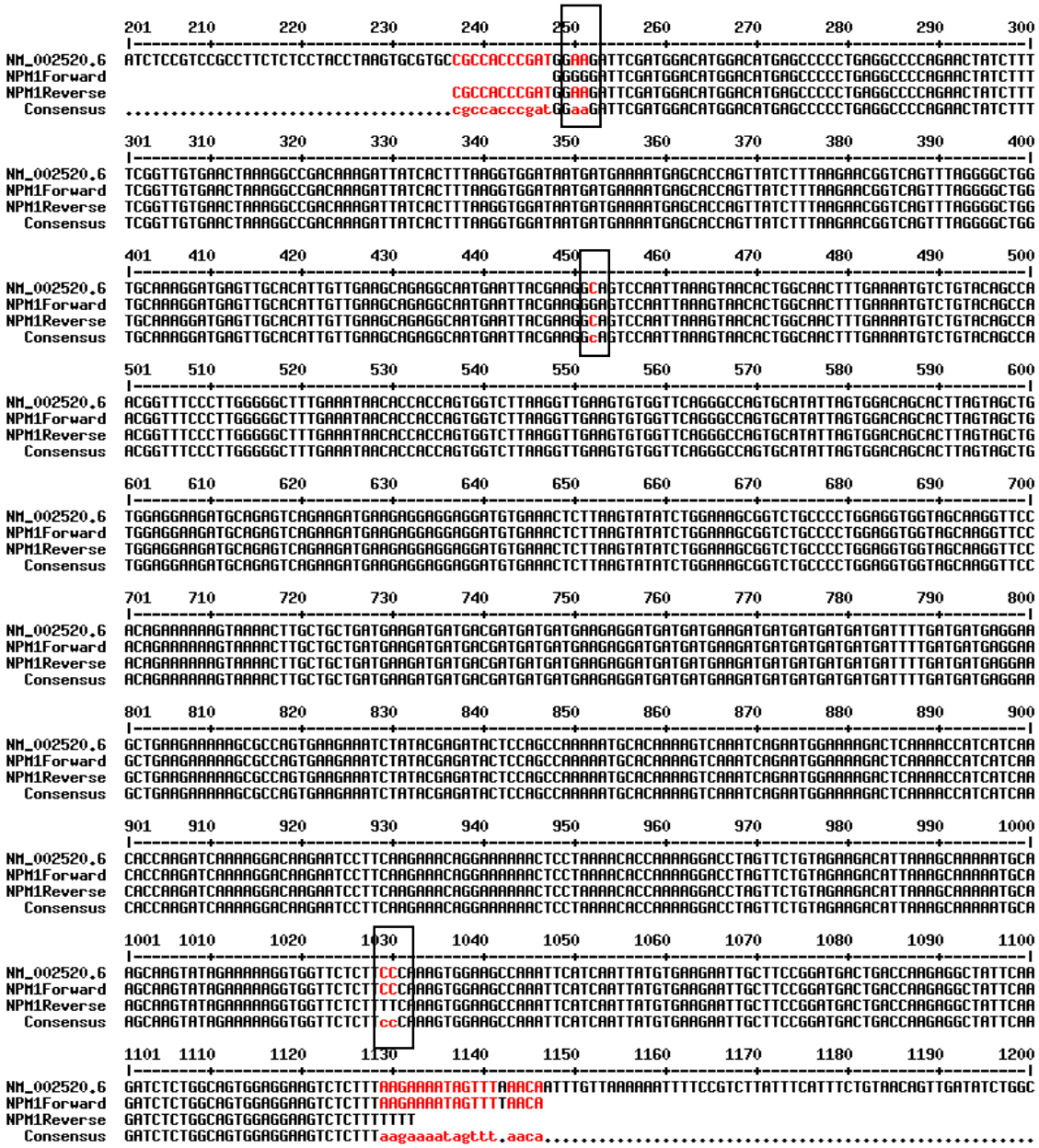

10. Sequence analysis of *BTF3*.

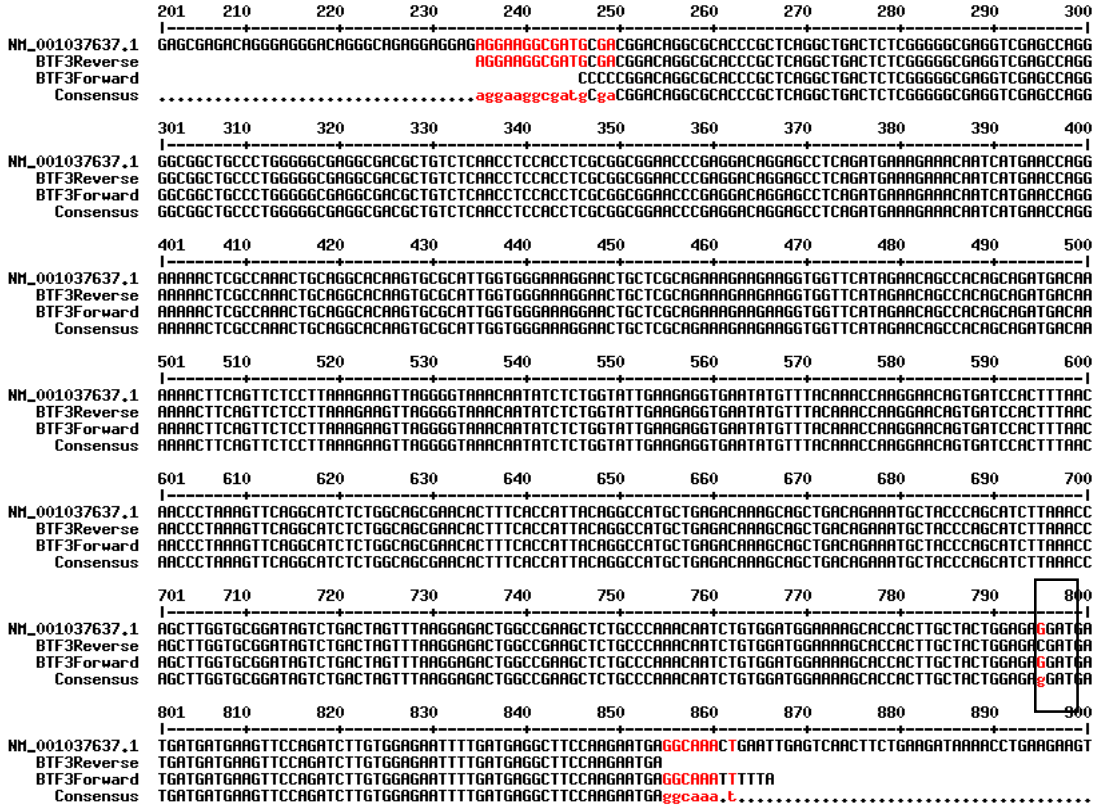

11. Sequence analysis of *UBA52*.

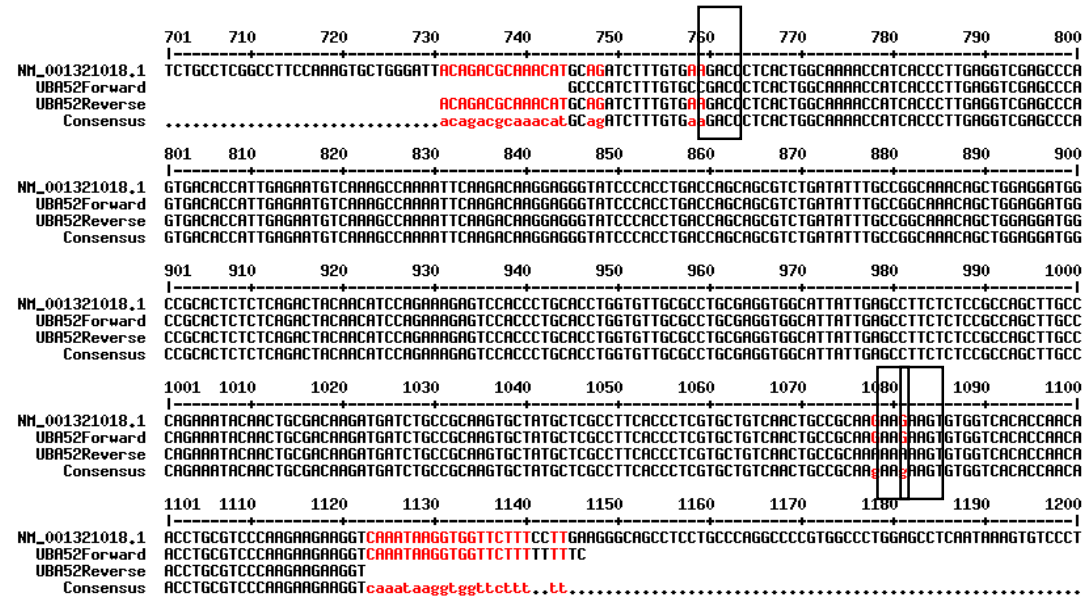

Appendix E. Normalized protein expression of uS4 (S9), eS8 (S8), eS31 (S27a), uL14 (L23), eL18 (L18) and NPM1 in six NPC derived cell lines, and NP69 in three biological replicates. The band intensities of each target protein within each cell line were normalized against that of the endogenous ACTB control. Mean band intensity and corresponding standard deviation were calculated and subsequently analysed with independent Student's *t*-test, in which *p*-values of <0.05 were considered statistically significant.

Target Protein	**Cell Lines**	**Normalized Band Intensity**			**Mean**	**SD**	***p*-value**
		BR1*	**BR2**	**BR3**			
uS4 (S9)	NP69	1.000	1.000	1.000	1.000	0.000	-
	HONE-1	3.562	1.883	2.612	2.686	0.842	0.013
	SUNE-1	4.654	1.511	2.260	2.808	1.641	0.065
	HK1	3.522	1.287	1.117	1.975	1.342	0.138
	TW01	2.068	1.873	1.448	1.796	0.317	0.006
	TW04	1.932	1.887	2.505	2.108	0.344	0.003
	C666-1	1.452	1.417	1.447	1.439	0.019	1.1E-06
eS88 (S8)	NP69	1.000	1.000	1.000	1.000	0.000	-
	HONE-1	0.600	1.225	0.872	0.899	0.313	0.303
	SUNE-1	0.547	0.403	0.728	0.559	0.163	0.005
	HK1	0.690	0.655	0.576	0.640	0.058	2.2E-04
	TW01	0.554	0.850	0.797	0.734	0.158	0.022
	TW04	0.624	0.880	1.244	0.916	0.312	0.332
	C666-1	0.594	0.464	0.438	0.499	0.084	2.4E-04

eS31 (S27a)	NP69	1.000	1.000	1.000	1.000	0.000	-
	HONE-1	2.505	2.564	3.667	2.912	0.655	0.004
	SUNE-1	3.109	1.777	3.812	2.900	1.034	0.017
	HK1	1.307	1.664	1.674	1.548	0.209	0.005
	TW01	1.943	3.376	3.168	2.829	0.775	0.007
	TW04	2.197	2.070	3.530	2.599	0.809	0.013
	C666-1	1.172	2.493	2.077	1.914	0.675	0.040
uL14 (L23)	NP69	1.000	1.000	1.000	1.000	0.000	-
	HONE-1	1.918	3.266	2.699	2.628	0.677	0.007
	SUNE-1	0.929	1.590	1.237	1.252	0.331	0.129
	HK1	2.060	2.058	1.786	1.968	0.158	2.2E-04
	TW01	2.357	2.770	2.077	2.401	0.349	0.001
	TW04	1.279	1.233	1.891	1.467	0.367	0.046
	C666-1	1.237	2.288	1.685	1.737	0.527	0.036
eL18 (L18)	NP69	1.000	1.000	1.000	1.000	0.000	-
	HONE-1	0.385	1.485	1.896	1.255	0.781	0.301
	SUNE-1	0.575	0.963	7.089	2.876	3.654	0.212
	HK1	1.293	1.467	2.701	1.820	0.768	0.069
	TW01	1.691	1.561	1.954	1.735	0.200	0.002
	TW04	0.896	1.283	3.914	2.031	1.642	0.169

	C666-1	0.000	0.073	0.306	0.126	0.160	3.5E-04
NPM1	NP69	1.000	1.000	1.000	1.000	0.000	-
	HONE-1	2.808	3.458	5.684	3.983	1.508	0.013
	SUNE-1	2.251	3.235	4.253	3.246	1.001	0.009
	HK1	1.683	2.278	3.087	2.349	0.705	0.015
	TW01	3.007	4.399	4.744	4.050	0.919	0.002
	TW04	3.640	4.931	9.651	6.074	3.164	0.025
	C666-1	1.161	2.124	2.796	2.027	0.822	0.048

*BR= biological replicate; SD= standard deviation

Appendix F. Normalized fold change in firefly luciferase activity for *in vivo* protein-protein interaction between NPM1 and ribosomal protein uS4 (S9), eS31 (S27a) and uL14 (L23) in TW04 cells.

	Transfection	pACT	pBIND	pG5*luc*	Average Normalized RLU*	Normalized SD	Induction of Firefly Activity[#]	p-value
Negative and positive controls	1	pACT	-	pG5*luc*	0.029	2.03E-04	-	
	2	-	pBIND	pG5*luc*	0.009	3.69E-04	-	-
	3	-	-	pG5*luc*	0.009	0.004	-	-
	4	pACT-MyoD	-	pG5*luc*	0.035	0.006	-	-
	5	-	pBIND-Id	pG5*luc*	0.023	0.011	-	-
	6	pACT-MyoD	pBIND-Id	pG5*luc*	5.536	0.678	-	-
uS4 (RPS9)-NPM1	7	pACT	pBIND	pG5*luc*	0.041	0.003	0.770	0.082
	8	pACT-uS4	pBIND	pG5*luc*	0.065	0.012	1.236	0.359
	9	pACT	pBIND-NPM1	pG5*luc*	0.047	0.003	10.884	0.206
	10	pACT-uS4	pBIND-NPM1	pG5*luc*	4.368	0.169	82.841	0.009
	11	pACT-NPM1	pBIND	pG5*luc*	0.065	0.014	1.238	0.395
	12	pACT	pBIND-uS4	pG5*luc*	0.046	0.002	0.873	0.153
	13	pACT-NPM1	pBIND-uS4	pG5*luc*	2.995	0.409	56.812	0.031
	14	pACT	pBIND	pG5*luc*	0.044	0.002	0.957	0.499
	15	pACT-eS31	pBIND	pG5*luc*	0.053	0.005	1.138	0.301

eS31	16	pACT	pBIND-NPM1	pG5*luc*	0.036	0.007	0.776	0.236
(S27a)-	17	pACT-eS31	pBIND-NPM1	pG5*luc*	0.052	0.005	1.129	0.138
NPM1	18	pACT-NPM1	pBIND	pG5*luc*	0.052	0.004	1.116	0.240
	19	pACT	pBIND-eS31	pG5*luc*	0.047	0.003	1.013	0.860
	20	pACT-NPM1	pBIND-eS31	pG5*luc*	0.058	0.009	1.260	0.146
uL14 (L23)-	21	pACT	pBIND	pG5*luc*	0.045	0.002	0.903	0.113
NPM1	22	pACT-uL14	pBIND	pG5*luc*	0.045	0.001	0.901	0.091
	23	pACT	pBIND-NPM1	pG5*luc*	0.052	0.005	1.037	0.686
	24	pACT-uL14	pBIND-NPM1	pG5*luc*	3.714	0.007	73.759	1.024E-04
	25	pACT-NPM1	pBIND	pG5*luc*	0.054	0.007	1.066	0.605
	26	pACT	pBIND-uL14	pG5*luc*	0.055	0.004	1.094	0.338
	27	pACT-NPM1	pBIND-uL14	pG5*luc*	3.203	0.008	63.596	1.805E-04

*RLU= relative luminescence unit

Induction of firefly activity was calculated by the division of the average RLU of all negative controls (transfection 7, 8, 9, 11, and 12 for uS4-NPM1 experimental set; transfection 14, 15, 16, 18, and 19 for eS31-NPM1 experimental set; transfection 21, 22, 23, 25, and 26 for uL14-NPM1 experimental set)

Appendix G. Normalized fold change in firefly luciferase activity for *in vivo* target interacting domain between NPM1 and ribosomal protein uS4 (S9) and uL14 (L23) in TW04 cells.

Interact-ion	Deletion Mutant	Trans-fection	pACT	pBIND	Average Normalized RLU	Normalized SD	Normalized Fold Change in Activity	*p*-value
uS4	uS4	1	pACT	pBIND	0.045	0.001	0.708	0.184
(RPS9)-	Δ 1-60	2	pACT-uS4/1-60	pBIND	0.082	0.005	1.292	0.186
NPM1		3	pACT-uS4/1-60	pBIND-NPM1	0.080	0.004	1.258	0.114
	uS4	4	pACT	pBIND	0.038	0.001	0.806	0.187
	Δ 1-120	5	pACT-uS4/1-120	pBIND	0.056	0.003	1.194	0.196
		6	pACT-uS4/1-120	pBIND-NPM1	3.208	0.246	68.773	0.017
	uS4	7	pACT	pBIND	0.048	0.003	0.903	0.246
	Δ 121-	8	pACT-uS4/121-194	pBIND	0.059	0.001	1.097	0.197
	194	9	pACT-uS4/121-194	pBIND-NPM1	0.050	0.003	0.941	0.455
	NPM1	10	pACT	pBIND	0.049	0.002	0.912	0.200
	Δ 1-107	11	pACT	pBIND-NPM1/1-107	0.059	0.001	1.088	0.192
		12	pACT-uS4	pBIND-NPM1/1-107	2.083	0.168	38.601	0.019
	NPM1	13	pACT	pBIND	0.046	0.004	0.833	0.316
		14	pACT	pBIND-NPM1/108-188	0.057	0.001	1.096	0.207

	Δ 108-188	15	pACT-uS4	pBIND-NPM1/108-188	0.057	0.002	1.080	0.112
	NPM1	16	pACT	pBIND	0.053	0.004	1.023	0.730
	Δ 189-294	17	pACT	pBIND-NPM1/189-294	0.051	0.004	0.977	0.752
		18	pACT-uS4	pBIND-NPM1/189-294	2.532	0.119	48.794	0.011
uL14 (L23)-NPM1	uL14	19	pACT	pBIND	0.045	0.003	0.883	0.206
	Δ 1-105	20	pACT-uL14/1-105	pBIND	0.057	2.798E-06	1.117	0.189
		21	pACT-uL14/1-105	pBIND-NPM1	0.047	0.002	0.915	0.156
	uL14	22	pACT	pBIND	0.045	0.019	0.997	0.941
	Δ 35-105	23	pACT-uL14/35-105	pBIND	0.046	0.002	1.003	0.955
		24	pACT-uL14/35-105	pBIND-NPM1	2.535	0.077	55.743	0.007
	uL14	25	pACT	pBIND	0.050	1.270E-04	1.048	0.205
	Δ 66-140	26	pACT-uL14/66-140	pBIND	0.046	0.002	0.952	0.304
		27	pACT-uL14/66-140	pBIND-NPM1	0.048	0.001	1.000	0.495
	NPM1	28	pACT	pBIND	0.046	0.005	0.927	0.517
	Δ 1-107	29	pACT	pBIND-NPM1/1-107	0.053	0.006	1.073	0.536
		30	pACT-uL14	pBIND-NPM1/1-107	0.046	0.002	0.914	0.134
	NPM1	31	pACT	pBIND	0.052	1.464E-04	1.070	0.223
	Δ 108-188	32	pACT	pBIND-NPM1/108-188	0.045	0.004	0.930	0.395
		33	pACT-uL14	pBIND-NPM1/108-188	0.048	0.003	0.985	0.413

	NPM1	34	pACT	pBIND	0.051	0.002	1.012	0.795
	Δ 189-	35	pACT	pBIND-NPM1/189-294	0.049	0.004	0.988	0.865
	294	36	pACT-uL14	pBIND-NPM1/189-294	2.942	0.020	58.880	0.001

Appendix H. Normalized fold change in firefly luciferase activity for *in vivo* investigation on the synergistic effect of NPM1 and ribosomal proteins uS4 (S9) and uL14 (L23) on MDM2 in TW01 cells.

Interact-ion	Trans-fection	pACT	pBIND	pCI	Average Normalized RLU	Normalized SD	Normalized Fold Change in Activity	*p*-value
-ve controls	1	pACT	pBIND	-	0.048	0.002	1.014	0.732
	2	pACT	pBIND-MDM2	-	0.046	0.004	0.980	0.873
	3	pACT-NPM1	pBIND	-	0.046	0.004	0.974	0.732
+ve control	4	pACT-NPM1	pBIND-MDM2	-	3.447	0.032	73.284	0.002
uS4 (RPS9)-NPM1-MDM2	5	pACT-uS4	pBIND-MDM2	-	0.045	0.002	0.977	0.590
	6	pACT-NPM1	pBIND-MDM2	pCI-uS4 (1:1:1)	1.544	0.176	32.831	0.026
	7	pACT-NPM1	pBIND-MDM2	pCI-uS4 (1:1:2)	0.990	0.125	21.047	0.030
	8	pACT-NPM1	pBIND-MDM2	pCI-uS4 (1:1:3)	0.399	0.048	8.476	0.032
uL14 (L23)-NPM1-MDM2	9	pACT-uL14	pBIND-MDM2	-	2.208	0.047	46.943	0.004
	10	pACT-NPM1	pBIND-MDM2	pCI-uL14 (1:1:1)	1.165	0.151	24.763	0.034
	11	pACT-NPM1	pBIND-MDM2	pCI-uL14 (1:1:2)	0.344	0.027	7.313	0.020
	12	pACT-NPM1	pBIND-MDM2	pCI-uL14 (1:1:3)	0.191	0.024	4.054	0.036